Modelling the atmospheric controls and climate impact of mineral dust in The Sahara Desert

Carolina del Carmen Cavazos Guerra

Department of Geography
University College London

Thesis submitted for the fulfillment of the degree of:

Doctor in Philosophy in Climate Science

Supervised by Prof. Martin Todd

I, Carolina del Carmen Cavazos Guerra confirm that the work presented in this thesis is my own. Where information has been derived from other sources, I confirm that this has been indicated in the thesis.

Acknowledgements

To Professor Martin Todd, whose expertise, understanding, and patience, added considerably to my experience as a graduate and as future researcher.

To the examiners Dr Richard Washington and Dr Nick Drake, for their wise comments during the revision process of this work and during the exam.

To CONACYT (Mexican Council of Science and Technology) for the awarded scholarship to pursue a PhD degree in a high ranked Department at UCL

To my parents Eusebio Cavazos and Maria Cecilia Guerra for their moral support towards this long journey.

To my loving husband Juan Antonio for all his support and patience all these years. To my dear in laws Soledad and Pascual for adopting me as a daughter.

To the dear friends I had the fortune to meet during those days of solitude in UCL: Chiara Ambrosino and Giovanni Scarso Borioli, Rotchana Prapainop. Mohammad Shamsudduha and Natasha Macbean. To Chris Knell, departmental computer manager.

To my dear Mexican friends either in UK or Mexico, for their support and keeping their friendship flourishing in spite of my common absences.

Abstract

Mineral dust aerosols play an important role in climate and the Earth's energy budget. The effect of dust on the radiative forcing is uncertain due to the complexity of particle properties and the complexity to quantify and discriminate preferential dust sources. This research considers the potential of two Regional Climate Models (RCM's): The Weather Research and Forecasting model (WRF-Chem) and the Regional Climate Model (RegCM3) both with an integrated dust module. Numerical sensitivity experiments are performed to quantify the ability of both models to simulate sources, the magnitude of dust emission, the transport in 3-dimensions and the subsequent impact on the radiative forcing. Particular emphasis is given to preferential source regions within the Sahara and Sahel in North Africa including the Bodélé Depression in Northern Chad. To account for the distribution of preferential dust source regions, soil texture characteristics were modified in dust source regions in RegCM3. As for WRF-Chem GOCART scheme, a new higher resolution erodible fraction map is tested. Moreover, the sensitivity of the results to the specification of aerosol optical properties to evaluate the impacts of optical characteristics on the radiative forcing was considered for the RegCM3. Finally, model outputs are compared to in-situ data: weather stations (WMO) and AERONET and satellite estimates: MODIS, MISR, OMI, CALIPSO and SEVIRI. Results show that both models represent the space/time structure of near-surface meteorology well. The tuning of preferential dust sources tested in this research provides a more realistic representation of local dust sources, emissions and resulting AOT. This suggest that in the absence of truly accurate soil maps at high resolution, further refinements to preferential sources map and its implementation in dust models can lead to useful improvements in simulation of dust processes and dust forecast accuracy.

Table of Contents

List of figures

List of Tables

List of Abbreviations

AEJ	African Easterly Jet
AI	Aerosol Index
AMMA	African Monsoon Multidisciplinary Analyses
AOT	Aerosol Optical Thickness
BATS	Biosphere-Atmosphere Transfer Scheme
BODEX	Bodélé Experiment
CALIPSO	Cloud-Aerosol Lidar and Infrared Pathfinder Satellite Observation
ECMWF	European Centre for Medium Weather Forecasting
GCM	Global Climate Model
GEOS	Goddard Earth Observing System
GES DISC	Goddard Earth Sciences Data and Information Services Center
GOCART	Goddart Chemistry of Atmospheric Radiation and Transport
IPCC	Intergovernmental Panel of Climate Change
LLJ	Low Level Jet
LWR	Long-wave Radiation
MISR	Multiangle Imaging SpectroRadiometer
MOSAIC	Model for Simulating Aerosol Interactions and Chemistry
MODIS	MODerate Resolution Imaging Spectrometer
NCAR	National Center for Atmospheric Research
NCEP	National Centers for Environmental Predictions
NOAA	National Oceanic ad Atmospheric Administration
OMI	Ozone Monitoring Instruments
RCM	Regional Climate Model
RegCM3	Regional Climate Model (version 3.0)
RF	Radiative forcing
SEVIRI	Spinning Enhanced Visible an InfraRed Imager
SWR	Short-wave Radiation
TAR	Third Assessment Report
TOMS	Total Ozone Map Spectrometer
WAM	West African Monsoon
WRF-Chem	Weather and Research Forecasting with Chemical Ensemble

1 Introduction

Over the last few decades, studies have shown the influence of aerosols (from natural and anthropogenic sources) on the atmospheric, terrestrial and hydrological systems, leading to a growing interest in the scientific community on climatic processes [*Forster et al.*, 2007; *Ramanathan et al.*, 2001]. Atmospheric aerosols along with clouds have the biggest control on the radiative energy budget of the Earth's climate system [*Albrecht*, 1989; *Hansen et al.*, 1997]. Mineral dust is the dominant natural atmospheric aerosol by mass [*Buseck and Posfai*, 1999] and plays an important role in the climate system. However, the contribution of dust particles to the radiative forcing (RF) is still uncertain [*Mahowald and Kiehl*, 2003]. Important aspects to consider in dust studies are: theabundance of natural sources (desertic and semi-desertic areas), the capability of dust particles to travelling thousands of kilometres [Prospero et al., 1981] and the complexity of optical and physical properties [*Sokolik et al.*, 2001]. Mineral dust interacts with climate in different ways: i) The direct effect due to the ability of dust particles to scatter, absorb and emit solar and thermal radiation [*Sokolik and Toon*, 1996]. ii) The indirect effect related to the interaction of dust with clouds (i.e. during cloud formation or controlling precipitation) affecting consequently the radiative budget [*Kaufman et al.*, 2005a; *Rosenfeld et al.*, 2001]. Finally, iii) A 'semi-direct effect', where the resulting changes in the radiative budget at surface and mid-level troposphere lead to the modulation of atmospheric dynamics [*Helmert et al.*, 2007; *Huang et al.*, 2006](see section 2.1).

Dust emission estimates for the present climate range from 1000–2150 Tg yr^{-1} [*Zender et al.*, 2004] and studies suggest that the increase in atmospheric dust concentrations are related to the increase in occurrence and intensity of droughts on a global scale. [*Prospero and Nees*, 1986]. The Sahara Desert in North Africa is the world's most important dust source alongside the Sahel with about ~50% of the total dust global mass [Middleton and Goudie, 2001], particularly from certain preferential sources or 'dust spots' like the Bodélé Depression in Northern Chad [*Todd et al.*, 2007]. However, estimations of dust loadings in the atmosphere over the Sahara Desert (as other global dust sources) are limited and uncertain. The shortage of long-term dust records in these regions is either a consequence of political or geographical factors [*Washington et al.*, 2006b]. These issues, beside the complexity to determine dust properties and to discriminate natural and anthropogenic dust emissions, represent a challenge to evaluate

radiative effect of dust globally [*Forster et al.*, 2007; *Yu et al.*, 2006]. Nevertheless, intensive field campaigns involving in-situ surface and aircraft observations have been conducted in recent times to increase our understanding on dust effects (see section 2.2) [e.g. *Myhre et al.*, 2003; *Redelsperger et al.*, 2006; *Todd et al.*, 2007]. In addition, surface based photometer instruments (i.e. the AERosol NETwork –AERONET-) provide information on aerosol loading and optical and physical properties [*Dubovik et al.*, 2000]. These measurements have been complemented with satellite observations which provide crucial information on dust distribution globally, most notably from the TOMS, AVHRR, MODIS, Meteosat and MISR instruments (section 2.2.1) [*Brindley and Ignatov*, 2006; *Herman et al.*, 1997; *Prospero et al.*, 2002; *Washington et al.*, 2003] Moreover, the combined use of satellite-borne lidar from the CALIOP sensor and passive radiometers offers better observations of the 3-dimensional distribution of mineral dust [*Berthier et al.*, 2006; *Liu et al.*, 2008].

Ultimately, the study of aerosol-climate interaction over the past, present and future requires coupled aerosol-chemistry climate models [*Le Treut et al.*, 2007]. Such models are designed to represent the dynamics the emission, transport and settling mechanisms along with chemistry interactions as a complement of ground based and satellite based information [*Tegen and Fung*, 1994]. In addition, the integration of dust simulations using Global and Regional Climate Models leads to a more accurate understanding of the RF caused solely by mineral dust. Regional Climate Models (RCM's) provide an important test bed for developing and testing aerosol processes modules for subsequent incorporation into GCM's [*Ghan and Schwartz*, 2007].

The present work is an effort to understand dust aerosol modelling of emission, transport and radiative effect over the Sahara Desert using two RCM's with different dust schemes. In order to improvedust simulations,sensibility analysis considers the optimisation of dust source regions within the model, known to be a key problem in dust modelling [*Sokolik et al.*, 2001]. The variability in the solar and infrared radiative fluxes and optical properties using different maps of dust activation sources are analysed and compared. Sensitivity experiments comprise an extended zone in the Sahara Desert, including a singular hot spot the Bodélé Depression. Finally, available ground-base and satellite records are used for comparative purposes.

2 MINERAL DUST OVERVIEW

This chapter provides a summary of the current understanding of atmospheric mineral dust and climate interaction. It includes the state of art in dust monitoring including ground and space-based remote sensing campaigns. In addition, an overview of climate models with the integration of dust schemes is presented. The importance of the Sahara Desert as the main dust source and the atmospheric mechanisms controlling dust production and transport are also included. Ultimately, uncertainties involving dust estimations and the effect on climate are considered.

2.1. Dust aerosols and climate

The atmospheric radiative budget represents the incoming and outgoing radiation fluxes into the climate system and is mostly controlled by clouds, tropospheric aerosols (natural or anthropogenic origin), Earth's albedo, atmospheric trace gases, and solar radiation [*Liao and Seinfeld*, 1998; *Satheesh and Moorthy*, 2005; *Yu et al.*, 2006]. The variation in the radiative fluxes is known as Radiative Forcing (RF). Thus, positive RF means a warming effect over the Earth's atmosphere, whilst negative RF represents a cooling effect [*Forster et al., 2007*]. The effects of radiative forcing vary depending on the surface, being more pronounced in continents than in the oceans due to the reflectance variability [*Sokolik and Toon*, 1996]. The dominant fraction of natural tropospheric aerosols burden over land corresponds to mineral dust (sea salt over ocean); especially close to the sources, mostly located at desert and semi-desert areas [*Prospero*, 1979]. Mineral dust interacts actively in the different Earth's systems. It includes atmospheric photochemistry [*Bian and Zender*, 2003], cloud formation from the availability of dust particles to act as cloud condensation nuclei (CCN) [*Demott et al.*, 2003] and nutrient transport [*Prospero et al.*, 1996]. Dust also plays an important role in the fertilisation of marine and terrestrial ecosystems (i.e. The Amazonian rain forest) by deposition resulting in modification of the earth's carbon budget [*Jickells et al.*, 2005; *Swap et al.*, 1992]. However, the main concern in atmospheric dust studies is related to the uncertainties about the interaction of dust particles to the atmospheric radiative budget [*Claquin et al.*, 1998]

Among the key properties that determine the effect of mineral dust particles on climate are: the particle size distributions and chemical composition of the individual particles [Alfaro et al., 1998]. Fundamentally, mineral dust at sources is formed by large particles (0.1 to 20 μm) and classified as: clay (< 2 μm), small silt (1 – 2 μm), large silt (10 - 25 μm) and sand (50 – 2000 μm) [*Buseck and Posfai*, 1999]. The amount of particles present, sorted according to size information relies on the particle size distribution N(r) [*d'Almeida and Schutz,* 1983]. This parameter also provides information about the efficiency and amount of dust particle emissions from sources. The dust chemical composition depends on source regions. Most particles are aggregates of different minerals. In some localities, the mineral content of dust particles may be formed of iron (Fe), which tends to reside on the particles' surface, while Ca, Mg, K, Al, and Si are an integral part of the particles [*Falkovich et al.*, 2001]. In the Northern Sahara, mineral dust composition is well mixed as a product of continuous deposition and uptake of material from the ground [*Rahn et al.*, 1976] and according to some studies, quartz, calcite and dolomite can be considered as the major tracers for atmospheric mineral dust [*Schutz and Sebert,* 1987]. In some cases the past morphology determines the mineral composition like the Bodélé depression where dust is dominated by fragmented fossil diatoms from the dry bed of the Lake Chad [*Todd et al.*, 2007]. In addition, other elements can be found in dust particles that are known to have substantial anthropogenic sources (e.g., Zn, As, Sb) [*Schutz*, 1989].

The magnitude of the radiative forcing of dust aerosol particles is still quite uncertain. Some studies based on observations and modelling, depict a cooling effect, which results in negative values of RF at the surfaces under the presence of dust layers. [*Haywood et al.*, 2003; *Miller and Tegen,* 1998]. Meanwhile, larger mineral dust particles are big enough to significantly absorb infrared radiation, thus acting as greenhouse gases, unlike other types of aerosols. As a consequence a heating effect reflects positive values of RF at the top of the atmosphere (TOA) [*Tegen et al.*, 2000]. The occasional mixing of dust with other water-soluble aerosol species (i.e. sulphates) changes substantially the optical properties of the sulphate aerosol. As a consequence, the magnitude of radiative effects on the mixed dust particle is modified [*Stier et al.*, 2007]. Since estimates of anthropogenic aerosols are more reliable than those of natural aerosols (especially over oceans and continental regions with complicated accessibility), there is an enormous inconsistency in climate information from both sources [*Kondratyev,* 1996]. The comprehension of the radiative properties of dust aerosol particles and climate interaction

requires information about particle size distribution, composition, abundance, hygroscopicity, surface properties, density, and refractive indices [*Pilinis et al.*, 1995].

However, due to the complexity that involves the reliability of the characteristics enlisted above, at present, it is complicated to estimate the overall uncertainty in the climate forcing caused by dust aerosols [*Ramanathan et al.*, 2001; *Yu et al.*, 2006]. Early estimates of the global mean direct radiative forcing by mineral dust vary in the range +0.09 to -0.46 W m-2 [*Haywood and Boucher*, 2000]. The Third Assessment Report (TAR), published by the Intergovernmental Panel of Climate Change (IPCC), reports that the radiative forcing (RF) of anthropogenic mineral dust lie in the range of +0.4 to –0.6 W/m^2 [*Ramaswamy et al.*, 2001]. This report did not assign a best estimate due to the difficulty to discriminate natural sources and those of anthropogenic origin, such as landuse practices [*Tegen et al*., 2002]. More recently, the Fourth Assessment Report (AR4), updated estimates of dust RF to -0.1 [± 0.2] W/m^2 after a re-evaluation concluded that the dust aerosol anthropogenic fraction is smaller than previously thought [*Forster et al.*, 2007]. These estimates reflect the uncertainty in total dust emissions and burdens and the range of natural and possible anthropogenic dust fractions. In addition, the current estimation corresponds solely to the direct effect and does not consider the indirect effect due to the deficiency of quantitative information available to approach it. Based on these grounds, the radiative effects of mineral dust and the existing uncertainties about them are disclosed in the following sections.

2.1.1. The Direct Effect

The direct effect depends on the optical and physical properties of the dust, such as scattering and absorption of solar and thermal radiation at the Earth's surface and top of the Atmosphere (TOA) (Figure 2.1a) [*Haywood and Boucher*, 2000; *Sokolik and Toon*, 1996; *Yu et al.*, 2006]. Scattering refers to the redirection of the radiation by atmospheric particles suspended in the atmosphere. The amount of scattering depends on the particles size, abundance, wavelength and depth of the atmosphere through which radiation is travelling [*Liou,* 2002]. Absorption refers to the direct interaction of a particle with the incoming radiation andaltering its electronic stateby vibration, rotation or a combination of all these. A good measure to determine how much the speed of light is reduced inside the particle is the refractive index (n) and it depends on chemical composition and particle mixing state [*Tegen,* 2003]. The single scattering albedo (ω) is used to determine the

efficiency of aerosols to scatter solar radiation compared to absorption. Hence, when ω = 1.0, the particle scatters all the light it intercepts, and ω = 0 if it absorbs all the light [*Jacobson,* 2001]. Saharan and Arabian dust particles make the single-scattering albedo as large as 0.8–0.9 because of the strong absorption of the direct solar radiation and the reflected radiation caused by bright surfaces [*Takemura et al.,* 2002]. Along with surface reflectance, ω determine the sign of direct radiative forcing [*Liao and Seinfeld,* 1998]. Thus positive forcing tends to exist over regions of high surface reflectance and low ω, whilst negative tends to exist over areas of low surface reflectance and high ω [*Haywoodand Shine,* 1995].

2.1.2. The Indirect Effect

The indirect effect is related to the interaction of aerosols with clouds and the subsequent affectation to the radiative budget [*Twomey,* 1977] (Figure 2.1.b). It is subdivided in two effects: i) The first indirect effect is related to the fact that dust particles act as Cloud Condensation Nuclei (CCN) and Ice Nuclei (IN) which modifies cloud droplets number concentration related to the formation of clouds of higher albedo (cloud albedo effect) leading to changes in cloud cover [*Kaufman et al.,* 2005a]. As a result, the short-wave solar radiation that reaches the Earth's surface is diminished [*Penner et al.,* 1994]. ii) The second indirect effect is associated to the increase in the cloud lifetime [*Lohmann,* 2006] and the effects on precipitation [*Teller and Levin,* 2006]. Some studies suggest that dust controls precipitation occurrence close to the sources [*Rosenfeld et al.,* 2001] although this evidence requires further research.

Some studies in the Sahara Desert suggest that African dust interacts with clouds over a large region, where dust particles can act as kernels for cloud formation [*Demott et al.,* 2003; *Lohmann et al.,* 2007]. In low clouds, such as cumulus and stratocumulus, water attaches to dust particles. Higher dust concentrations at surface can suppress rainfall and enhance drought conditions by dispersing water among many dust particles preventing droplets from becoming heavy enough to fall, resulting in more thin, low clouds and less rain [*Ramanathan et al.,* 2001; *Rosenfeld et al.,* 2001]. In high clouds, such as cirrus, cirrostratus, and deep convective clouds, there is some evidence that dust particles over wetter regions south of the desert provide surfaces for ice crystals to form around. The crystals grow rapidly, drawing moisture from surrounding cloud droplets.

They become heavier and eventually fall, generating more rain and reducing the total amount of high clouds [*Mahowald and Kiehl*, 2003].

2.1.3. The Semi-direct Effect

The semi-direct effect is associated to the radiative forcing on the surface and TOA caused by changes in the atmospheric structure (i.e. heating the air andreducing relative humidity) as a consequence of previously described effects (Figure 2.1.c). This effect has been attributed to the presence of absorbing aerosols [*Hansen et al.*, 1997]. As a response, a reduction in the surface temperature due to a cooling effect [*Miller and Tegen*, 1998] and heating in the troposphere might eventually modify the atmospheric circulation [*Ackerman* et al., 2000]. The semi-direct effects on RF are still quite uncertain. Consequently, it has been suggested that absorbing aerosols should be included in emissions controls because of their potentially large warming effect on climate [*Jacobson*, 2001]. This effect is just described, but not quantified in the last assessment report published by the IPCC, due to the high complexity to discriminate a semi-direct effect caused by a particular aerosol and modifications to the hydrological cycle. Additionally, it is still under debate whether the semi-direct effect is just an unidentified cloud feedback rather than a forcing [*Forster et al.*, 2007].

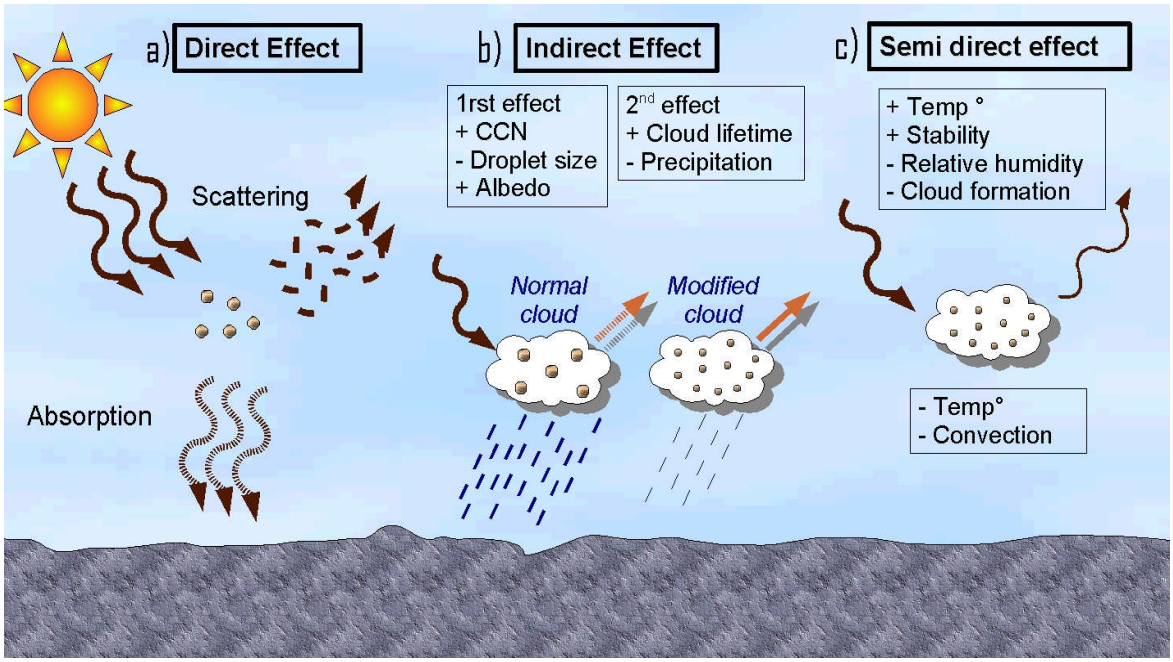

Figure 2.1: Radiative effects of mineral dust in the atmosphere

Based on these premises, global studies of mineral dust radiative forcing allow us to assess the extent to which mineral dust may mitigate or exacerbate climate change caused by radiatively active atmospheric constituents [*Zender et al.,* 2004]. To reduce current uncertainties in the radiative forcing of mineral dust, many challenges must be overcome [*Sokolik et al.,* 2001]. These challenges include proper integration of land surface and radiative properties of dust particles into coupled chemical atmospheric models and the integration of satellite and ground observations.

2.2 Mineral Dust Observations

The experimental measurement of mineral dust and radiative effects to date is limited.Nevertheless, the available information collected from dust studies is very valuable especially to determine dust physical and optical properties. This information is particularly valuable in numerical modelling studies and for calibration purposes of remote sensing instruments. Hence, constant monitoring is essential to improve global records for dust climatologies.

2.2.1 Satellite Observations

Several spacecraft based instruments to monitor the global dynamic of Earth's atmosphere have been developed in recent years [*King et al.*, 1999]. Satellite observations have provided crucial information of global distribution of mineral dust along other important trophospheric and stratospheric aerosols at different wavelengths (Table 2-1, Figure 2.2), most notably from instruments on board polar orbiting and geostationary satellites [*Prospero et al.*, 2002; *Yu et al.*, 2006]. Moreover, the combined use of satellite-borne lidar from the CALIOP sensor and passive radiometers offers better observations of the 3-dimensional distribution of mineral dust. For practical purposes, the aerosol optical properties are represented in terms of Aerosol Optical Thickness (AOT) [Power, 2003] being a well-known measure of atmospheric turbidity to represent the total amount of aerosol integrated along the air column. Other known qualitative indices are: Aerosol type, Aerosol Index (AI), particle size distribution (Nr), aerosol mass concentration.

Table 2-1: Instrumentation used for aerosol monitoring

MISSION	Coverage	Spatial Resolution	References
TOMS, TOMS-Earth Probe	1979–1992 1996 >	50 X 50 km 39 X 39 km	*[Herman et al., 1997]*
OMI	2004 >	13-24 km	*[Torres et al 2007]*
MODIS	Terra: 2000 > Aqua: 2002 >	bands 1-2 -> 250 m bands 3-7 -> 500 m bands 8-36 -> 1km	*[King et al., 1992]*
MISR	2000 >	275 m – 1.1 Km	*[Diner et al*, 1998, *Bothwell et al*., 2002]
MSG/SEVIRI [1]	2004 >	3 x 3 km	*[Schmetz et* al., 2002]
CALIPSO	2006 >	Horizontal: 1, 5, 40 km Vertical: 30, 60 m	*[Winker et al.*, 2007]

[1] All sensors provide global coverage except SEVIRI, due to it geostationary orbit over Europe/Africa

The Total Ozone Mapping Spectrometer (TOMS) is considered as the pioneer for qualitative detection of aerosols from space, due to its capacity for detection in the ultraviolet (UV) at 340,360 and 380µm [*Herman et al.,* 1997]. Retrievals from TOMS in the form of AI have been useful to track global transport of smoke and dust in extended areas [e.g. *Prospero et al.,* 2002; *Torres et al.,* 2002]. Some studies have use AI records from TOMS to depict long-term transport and to detect dust hotspots in the Sahara Desert [e.g. *Prospero et al.,* 2002; *Torres et al.,* 2002]. The Ozone Mapping Instrument (OMI), launched in 2004, continues the TOMS record for total ozone and other atmospheric parameters related to ozone chemistry and atmospheric aerosols [*Torres et al.,* 2007].The OMI is a high-resolution spectrograph that measures the upwelling radiance at the top of the atmosphere in the UV and visible (VIS) at 64 wavelengths (270–500 nm) [*Levelt et al.,* 2006]. Compared with the 6 bands of TOMS, the retrievals of AI at a higher resolution have a considerable reduction in noise levels with higher accuracy and precision compared with its predecessor (Figure 2.2.a).

As part of the NASA's Earth Observing System (EOS), The Multiangle Imaging SpectroRadiometer (MISR), launched in December of 1999 onboard of Terra spacecraft, retrieves AOT by nine cameras distributed at different angles in four wavelengths [*Bothwell et al.,* 2002]. Among the few limitations of the MISR are: the inability to acquire data in the dark side of the earth, limited spatial view due to the reduced swath (400km) and limited temporal resolution (a week to scan the exact location). Nevertheless, retrievals from MISR are quite valuable and confident [*Yu et al.,* 2006] (Figure 2.2.b). More recently, the MODIS instrument (Moderate Resolution Imaging Spectroradiometer) onboard Terra and Aqua spacecrafts, retrieves aerosol loads at a wider spectral range, high resolution and near daily global coverage which fulfil the limitations of MISR (Figure 2.2.c). The MODIS instrument is conformed by 36 spectral bands in the UV, visible (VIS) and thermal infrared (IF) spectral regions between 0.45 and 14.4 µm. *[King et al., 2003]*. Although AOT comparisons between MODIS and MISR have been generally good, the correlation between both sometimes can be low [*Prasad and Singh,* 2007]. While MODIS AOD retrieval algorithm works best for dense and dark vegetative regions, the MISR retrieval is generally less sensitive to surface type. However, the AOT retrievals from MODIS have improved to a greater extent over the last years. The data retrieval limitations with the VIS channels over regions with high surface reflectance

have been overcome with the implementation of the 'Deep Blue' algorithm [*Hsu et al.*, 2004].

The SEVIRI (Spinning Enhanced Visible and Infrared Imager), onboard the geostationary satellite Meteosat-8 (MSG), is equipped with 12 channels which operate in the VIS: 0.6, 0.8µm and High Resolution Visible (HRV), Near IR: 1.3µm, and IR: 3.4, 6.2, 7.3, 8.7, 9.7, 10.8, 12.0 & 13.4 µm. Channels operating in the IR observe thermal emission from Earth's surface and are less susceptible to the high albedo effect by deserts.(Figure 2.2.d). Furthermore, measurements in the IR make also possible night detection of dust loadings, although observations are more diffuse than day measurements. All the SEVIRI sensor bands operate at 3km resolution, except for HRV (1km), and acquired data every 15 minutes. The Dust Product is a qualitative measurement generated from the IR 8.7, 10.8 & 12.0 µm bands using the Eumetsat dust product algorithm [*Schmetz et al.*, 2002]. Some authors have attempt to quantify AOT by generating Look-Up Tables (LUT) with the radiative transfer model to create a relationship between the dust microphysical properties and Brightness temperature (BT) and BT difference (BTD). Studies suggest infrared window BTs at 11 µm show a quasi-linear relationship with dust optical thicknesses and the split window BT difference (BTD) between 11 µm and 12 µm shows a quasi-linear relationship with the particle radius [*Brindley and Ignatov*, 2006].

The Light Detection and Ranging instrument (LiDaR) is a practical device for observations of cloud cover and vertical aerosol layers based on light scattering measurement of a light pulse transmitted from one point either space or ground to other. A Lidar utilizes it own light source rather than solar energy (as the spectrometers do), that is scattered from the earth's surface [*Rees*, 1990]. The CALIPSO (Cloud-Aerosol Lidar and Infrared Pathfinder Satellite Observation) launched in late April 2006, combines an active lidar instrument with passive infrared and visible imagers representing an advance in the monitoring of aerosol and cloud vertical structure and optical properties [*Winker et al.*, 2007]. As part of the payload of CALIPSO, the CALIOP (Cloud-Aerosol Lidar with Orthogonal Polarization) utilizes three receiver channels: one measuring the 1064 nm backscatter intensity and two channels measuring orthogonally polarized components of the 532 nm backscattered signal (Figure 2.2.e). With a vertical resolution of 30-60 m and an horizontal resolution of 333 m profiles derived from CALIPSO provides, for the first time, a global picture of the profile of atmospheric scattering layers, due to the overpass

at a same region twice a day, once during the daytime and other during the night-time, with a revisit time period of the same orbit of 16 days [*Vaughan et al.*, 2004]. Each overpass of the CALIOP lidar is able to provide a quasi-instantaneous view of the vertical structure of dust plumes [*Liu et al.*, 2008].

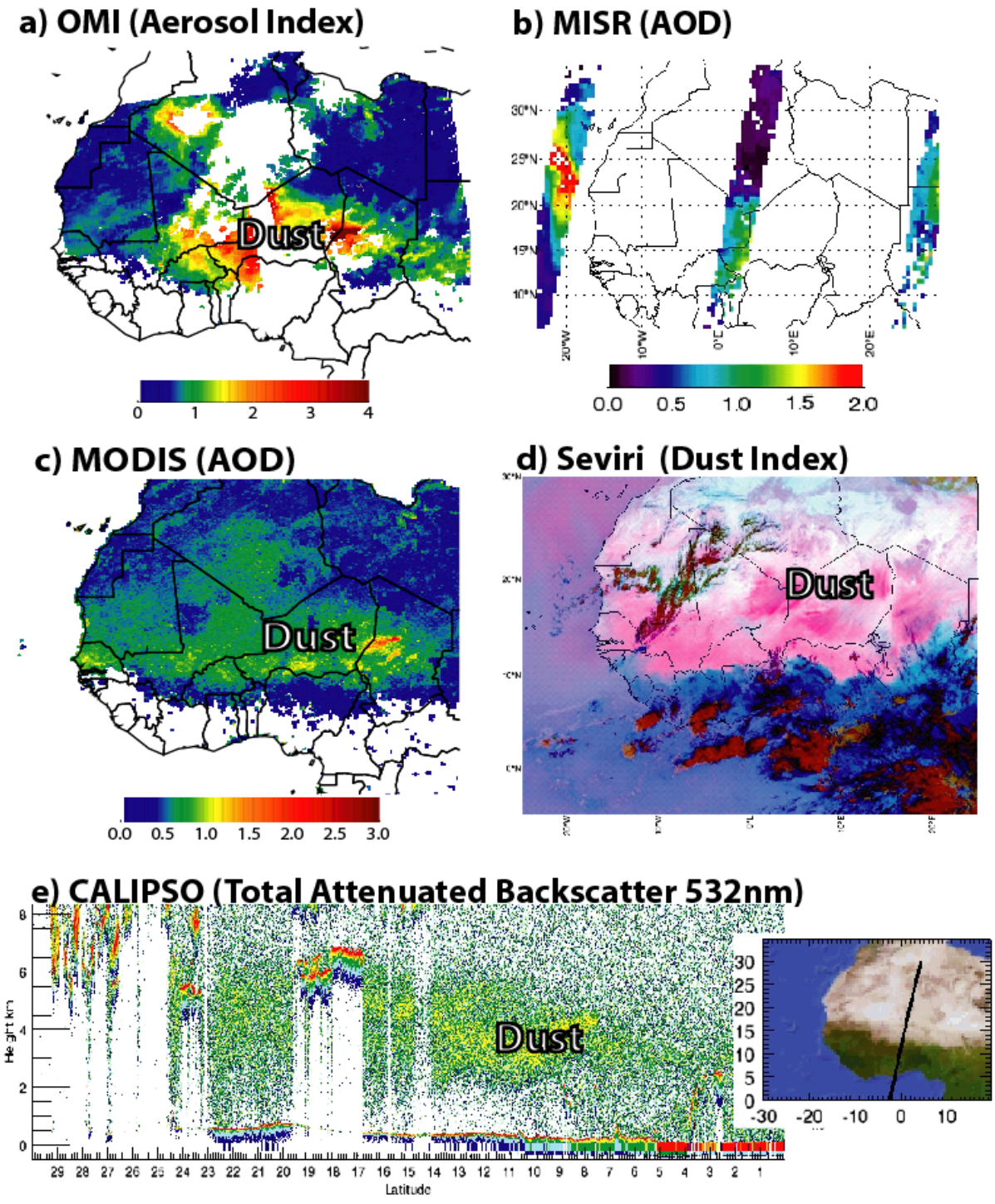

Figure 2.2: Aerosol retrievals from different satellites (see text)

The radiative energy is the main factor that controls Earth's climate. The radiative budget is the balance between incoming SW radiation and outgoing LW radiation emitted from the Earth. Therefore, monitoring of the ERB aids to understand the processes that govern the climate system variability. Table 2-2 shows missions designed for this purpose:

Table 2-2. Space-based platforms for radiative measuring

MISSION	Coverage	Products
ERB ERBE	1978-1987	Direct solar irradiance, reflected SW radiation and emitted LW radiation
CERES	1997	Direct solar irradiance, reflected SW radiation and emitted LW radiation
GERB	2002	SW and total radiation

CERES products include both solar-reflected and Earth-emitted radiation from the top of the atmosphere to the Earth's surface. CERES instruments were launched aboard the Tropical Rainfall Measuring Mission (TRMM) in November 1997 and on the EOS Terra satellite in December 1999. Two additional instruments fly on the EOS Aqua spacecraft since 2002. Multiple satellites are needed to provide adequate temporal sampling since clouds and radiative fluxes vary throughout the day.

The GERB instrument is one of the scientific instruments on board the European Space Agency's Meteosat Second Generation (MSG) satellite. It is expected to be operating for at least a five-year period. The purpose of the instrument is to accurately measure the Earth Radiation Budget (ERB): The measurements will be made of the whole Earth disc from geostationary orbit at 0°176N, 0°176E with a nadir resolution of 50km, in wavebands of 0.32 - 4.0 microns and 0.32 - 30 microns to cover SW and total radiation bands (LW achieved by subtraction of SW from total radiation). The instrument will accumulate images of the disc of the Earth every 15 minutes, providing the first consistent measurements of the hour-by-hour variation of clouds and simultaneous measurements of the radiation balance [*Harries et al.,* 2005].

2.2.2 Ground Based Observations

Ground based quantifications are used for dust measurements based on its optical properties or the composition of dust grains. The scarcity of long-term databases in a limited number of locations has lead to an ambiguous quantification of the radiative impacts of mineral dust. Furthermore, most of the sources of dust in the world (i.e Bodélé Depression) are located in regions where the absence of data is more a consequence of political or geographical factors [*Washington et al.*, 2006a]

A source for dust measurement is the Aerosol Robotic Network (AERONET), an optical ground-based aerosol-monitoring network and data archive. The organization of this network consists of identical automatic sun-sky scanning spectral photometers owned by national agencies and universities. This allows frequent measurements of atmospheric aerosol optical properties and precipitable water at remote sites, providing globally distributed near-real time data [*Dubovik et al.*, 2000; *Holben et al.*, 1998]. So far the AERONET network constitutes the most complete ground based global data for dust analysis. Retrievals from optical parameters are suitably integrated with satellite data for validation purposes. The number of stations is yet limited in North and West Africa, particularly in locations known to be key dust sources in the Sahara and Sahel (Figure 2.3.). Nevertheless, important long-term data have been obtained in recent years and have been quite helpful for comparative, validation and climatic purposes.

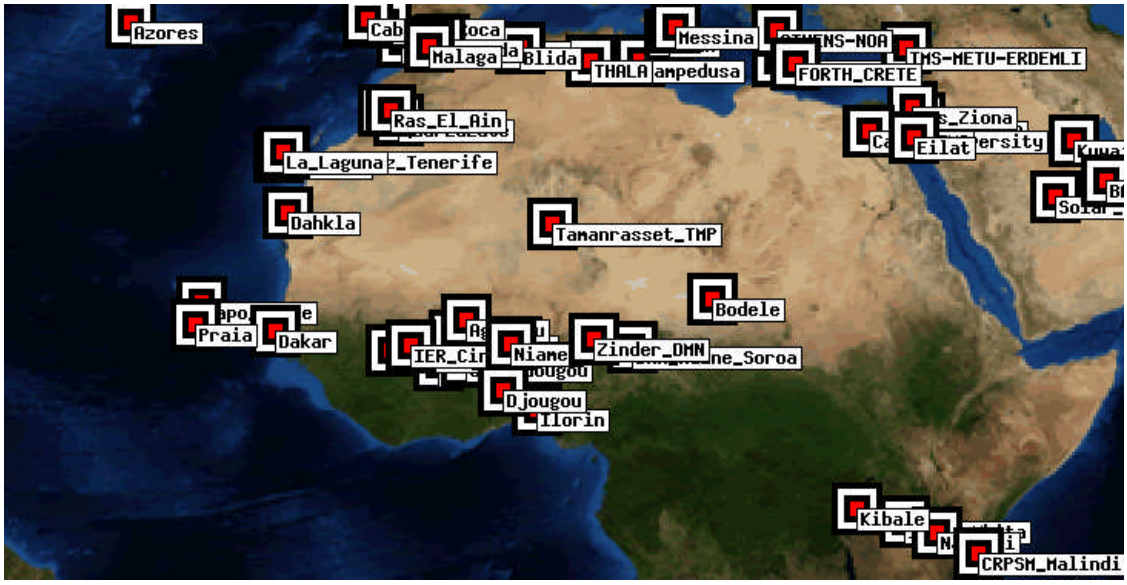

Figure .2.3: AERONET Stations located in North and West Africa. Source: aeronet.gsfc.nasa.gov

In the last few decades, several international multidisciplinary field campaigns close to major global dust sources have been organized. They include a wide range of measurements from ground base to aircraft observations (Table 2-3) and complemented with available datasets from satellite retrievals. The main goal of these observational experiments is to improve the knowledge about different aspects of the climate and radiative impact of aerosols loadings including dust from a regional perspective. In addition, the impact on ecosystems and the social-political context are analyzed to understand climate in a global prospect. The African Monsoon Multidisciplinary Analysis (AMMA) is an international integrated multidisciplinary project, which aims to understand to a better extent, the West African Monsoon (WAM) and environmental and socio-economical impacts of its variability [*Redelsperger et al.*, 2006]. More recently, the GERBILS (Geostationary Earth Radiation Budget Experiment Intercomparison of Longwave and Shortwave radiation) field campaign conducted in West Africa in June 2007 by the Met Office, aimed to understand the differences between modelled and observed radiation over the south-western Sahara [*Haywood et al.*, 2005].

Table 2-3: International campaigns with dust measurements included

Name	Location	Period	References
Saharan Dust Experiment (SHADE)	West coast of Africa	September 2000	[Tanre et al., 2003];
Puerto Rico Dust Experiment (PRIDE)	Roosevelt Roads, Puerto Rico.	June - July 2000	[Reid et al., 2003];
Asian Pacific Regional Aerosol Characterization Experiment (ACE-Asia)	Off the coast of China, Japan and Korea.	March - May 2001	[Seinfeld et al., 2004].
Bodélé Dust Experiment (BoDEx)	Chad	28 February - 13 March 2005	[*Todd et al.*, 2007];
African Monsoon Multidisciplinary Analysis (AMMA)	West Africa	LOP: 2001–2009 EOP: 2005-2007 SOP: 2006	[*Redelsperger et al.*, 2006];
The Saharan Mineral Dust Experiment (SAMUM)	Morocco	May-June 2006	[*Knippertz et al.*, 2007]
Geostationary Earth Radiation Budget Experiment Intercomparison of Longwave and Shortwave radiation (GERBILS)	West Africa	June 2007	Haywood et al., 2005

LOP: Long-term monitoring period
EOP: Enhanced Observed Period
SOP: Special Observing Periods

Although these campaigns have providedvaluable observational data, there exist human and economical limitations to achieve large temporal and spatial datasets to understand climate effects on the large term. Hence these studies need to be complemented with climate models to comprehend the mechanisms involved in dust production and long-term and higher scale effects.

2.3. Global Distribution of Dust Aerosols

Most of the dust sources are located in the subtropics and zones influenced by the descending limbs of the Hadley cells. These regions are distributed across a band of arid and semi-arid regions that extends from the west coast of North Africa, across the Middle East, and into central Asia [*Goudie,* 2001; *Goudie and Middleton,* 2006]. Although it is difficult to estimate global dust emissions, recent studies estimate that global dust emission rates fall within a range from less than 1000 to 3000 Teragrams (Tg) yr–1, and about 80% of the dust is from the Northern Hemisphere [*Tanaka and Chiba*, 2005]. The world's largest source of dust is the Sahara Desert in North Africa [*Prospero et al.*, 2002]. The recent estimates of dust emission from the Sahara Desert ranges from 500 to 1400 Tg yr–1, which contribute with around the 50% to 69% of the total global dust emission. [*Ginoux et al.*, 2001; *Zender et al.*, 2003a].

Large dust sources in the northern hemisphere include the Chinese and Mongolian deserts in East Asia (~11% of total emissions) [Laurent et al., 2005]. In addition, some important dust sources are located in the Arabian Peninsula which contribute to the dust transported and deposited in the East Mediterranean and the Arabian Sea [*Middleton*, 1986]. Some estimates of dust emission from the Arabian Peninsula to the total global dust emission range from 4% to 28% [*Tanaka and Chiba*, 2006]. Australia exhibits the greatest contribution of dust in the southern hemisphere, with estimates ranging from 2.5% [*Zender et al.*, 2003a] to 8% [*Miller et al.*, 2004] of the total dust emissions. Figure 2.4 shows an Aerosol Index (AI) five-year composite from the Ozone Monitoring Imager (OMI). The high values of AI in the desert regions (particularly the Saharan Desert) are caused mainly caused by mineral dust activity. The Bodélé Depression in Africa shows the highest value of AI. The most active sources in Asia are located in the Arab Peninsula, the western China (the Taklimakan desert) and the eastern China (the Gobi desert). High values of AI in some areas (i.e. Amazon and Central Africa) might indicate biomass burning, especially in zones with high vegetation areas.

Several studies have depicted that source regions are commonly located close to topographic features (i.e. Hoggar, Aïr and Tibesti mountains in North Africa) where dry valleys (*wadis*) and the paleo-drainage density is high, providing fine grained fluvial material for deflation [*Prospero et al*., 2002]. A particular dust source, the Bodélé depression in Chad, known as one of the dustiest places on earth, is an important spot for emissions in the Sahara Desert. This is due to the erodibility of the surface material and the erosive potential of the wind [*Todd et al*., 2007; *Washington et al*., 2006b]. A key feature for this region is the generation of the Bodélé low level jet [*Washington and Todd*, 2005] in the gap between the Tibesti and Enneldi mountains, which act as a wind tunnel enhancing deflation. The prevailing northeasterly wind direction of the winter provides perfect conditions for aerosol saltation, uplift and transport. It is estimated that this small area produces approximately 50% of the Saharan dust deposited in the Amazon in South America [*Koren et al*., 2006]. The Bodélé depression is the lowest part of the paleo-lake basin Mega-Chad. The lake last dried up some 5000 years BP [*Drake and Bristow*, 2006] leaving exposed extensive diatomite sediments. Today, these sediments cover an area of ~10,800 km^2 centred near 17°N, 18°E.

Other large parts of West Africa, between the 17-18°N and 8 -10°W, just between the south border of Algeria and Mali have been acknowledged as important dust sources [*Engelstaedter et al*., 2006]. Several studies have regarded the availability of deflatable material combined with the atmospheric variability in the form of heat lows to play an important role for dust emissions in this region [*Knippertz*, 2008]. However, the importance of the western African source region is much less understood due to the limited observations.

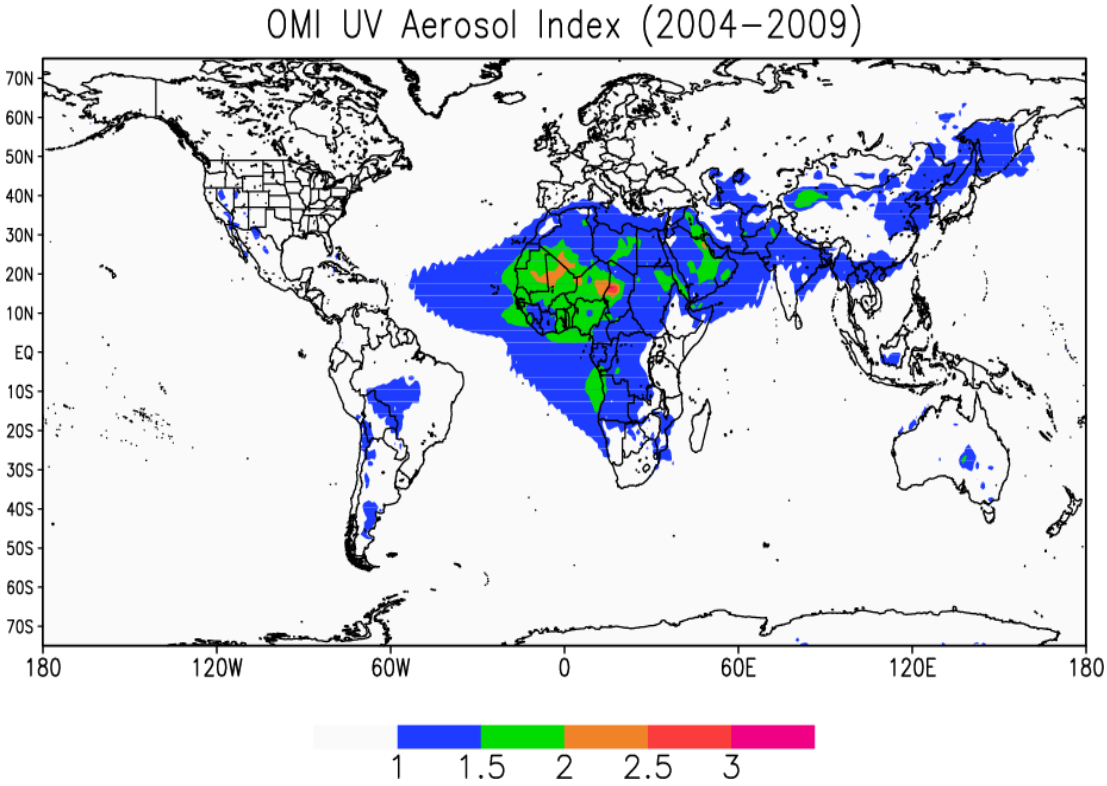

Figure 2.4: Aerosol Index global annual mean extracted from OMI. Source:Giovanni data system, NASA GES DISC.

2.3.1 The Sahara Desert

The Sahara Desert in North Africa is the world's largest desert (area ~7 million km^2), occupying approximately 10% of the African Continent [*Cooke et al.*, 1993]. The ecological and geomorphologic diversity is distinctive from other regions in the world. The Sahara Desert is characterized as one of the hottest regions in the world, with mean annual temperatures exceeding 30°C. In the hottest months, temperatures can rise over 50°C, and temperatures can fall below freezing in the winter [*Catalisano and Massa*, 1989]. The surface of the desert comprises large areas of sand dunes (which make up about one quarter of the total area), stone plateaus, gravel plains, *wadis*, and salt flats [*Cooke et al.*, 1993].

The geomorphologic and climatic features (rain scarcity, surface water, extreme day and night temperature and the constant wind), makes the Sahara Desert an inhospitable environment and the world's most important dust source [*Middleton and Goudie*, 2001]. Estimates of the global dust production suggest that approximately 50% of total mass loaded into the atmosphere is originated in the region of the Sahara and the Sahel (Figure 2.5). This region is increasingly vulnerable to the impact of climate change;

rainfall scarceness, prolonged drought and intensified landuse lead to enlarging desertification.

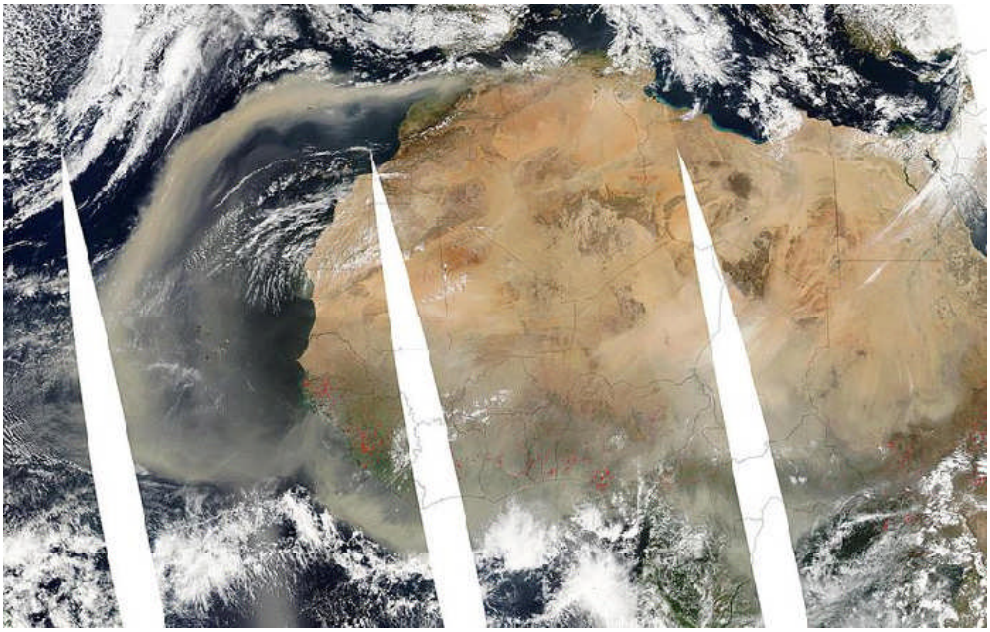

Figure 2.5: Dust plumes from the Sahara transported over the Atlantic. Source: modis-atmos.gsfc.nasa.gov

2.3.1.1. Climate

The Sahara's climate is conformed by a dry subtropical climate in the north and a dry tropical climate in the south. Climate in the North portion of the Saharan Desert is determined by the dynamic of Hadley atmospheric circulation [*Diaz and Bradley,* 2004]. The extension of the North African continental mass along with radiation and high albedos determines the intensity of Hadley cells that transport vertically air masses heated by solar insolation. A relatively simple overturning circulation accomplishes the energy transport in this region, with rising motion near the equator leading to a low atmospheric pressure at surface levels. As consequence of the mass balance, air masses experience poleward motion near the tropopause [*Palmen and Newton*, 1969]. Finally, the air cooled due to the conversion of latent heat, descends in the subtropics leading to an area of high pressure at surface levels: the subtropical high. Within the lower troposphere, surface air flows from the North African high pressure towards the lower pressure area prevailing over the ocean (Figure 2.6). This dry trade wind over the Sahara is often named *Harmattan* [*Kalu,* 1979].

The main climatic feature is the annual cycle of dry and rainy monsoon seasons resulting from the Intertropical Discontinuity (ITD) oscillations (Figure 2.6) [*Fontaine and Bigot,* 1993]. The ITD is defined as the interface between the cool, moist southwesterly monsoon flow and the warm, dry-laden northeasterly *Harmattan* flow [*Hayward and Oguntoyinbo,* 1987] and it can be identify about the 925 hPa.

During boreal winter (October-March), North Africa is dominated by the low level north-easterly*Harmattan* winds. (Figure 2.6.a). The *Harmattan* flow is influenced by day-to-day synoptic scale variability in the strength of the north-south pressure gradient across the region intensifying anticyclonic conditions notably controlled by ridging of the Libyan high [*Kalu,* 1979].

In boreal summer, atmospheric circulation in the Sahara Desert and the Sahel bound becomes more complex, dominated in a great extent bythe West African Monsoon (WAM) (Figure 2.6.b). It coincides with the crossing of the ITD to its northernmost location. The seasonal cycle of the WAM is closely linked to the energy balance in the Sahara [*Hall and Peyrille*, 2006; *Peyrille et al*., 2007]. The Saharan Heat Low (SHL) over the Sahara is a key element of the WAM. This region of high surface temperatures and low surface pressures covers the warmest and driest region of the Sahara [*Thorncroft and Blackburn*, 1999] and contributes to enhance meridional circulation [*Parker et al.*, 2005b]. Some authors have acknowledged this feature as the West African Heath Low (WAHL) due to the geographical location of the SHL in summer during the monsoon onset [*Lavaysse et al.*, 2009].

In response to the large-scale pressure gradient between the SHL and the Gulf of Guinea, the monsoon flow may penetrate deeply into the continent reaching the Sahel and favouring the appearance of convective systems and the beginning of the rainy season in Sahel (“monsoon onset”) [*Sultan and Janicot,* 2000]. In this period, MCS (Mesoscale convective Systems) are responsible for the rainfall generated towards the year in the tropics (12–16°N) [*Laing et al.,* 1999]. In this region, dry air and strong winds are transported westward across the tropical Atlantic Ocean within the Saharan Air Layer (SAL) (Figure 2.7). This layer is a mass of very dry, dusty air produced over the Sahara Desert at around 850-500mb height [*Karyampudi and Carlson*, 1988]. The SAL’s dry air is associated with a decrease in tropical cyclone in the Atlantic Ocean by inhibiting

updrafts in the storm, while its strong winds can substantially increase the vertical wind shear in and around the storm environment [*Dunion and Velden*, 2004].

The African Easterly Jet (AEJ) over West Africa is a central feature that plays an important role in the organization and propagation of MCS and dust across the African continent. The maximum mean wind speeds in the jet are usually located around 4°N—5°N. The jet is basically geostrophic and is formed due to the presence of surface temperature and moisture gradients from the cool waters in the Atlantic off the coast of Guinea and the Sahara, and the atmosphere responds by generating vertical wind shear to maintain thermal wind balance [*Cook*, 1999]. The height of the jet is determined by the level at which the surface-induced positive temperature gradient is replaced by the free atmosphere's negative temperature gradient (usually about a height of 4 Km or 650 mb) [*Thorncroft and Blackburn*, 1999]. The AEJ also contributes to the formation of the African Easterly Waves (AEW) (Figure 2.7), which is another fundamental synoptic feature over West Africa and Tropical Atlantic Ocean during boreal summer [*Burpee*, 1978]. These waves have an approximate duration of 3 to 5 days are formed west of 20°E on the south north ridges of the AEJ and propagate westward and can provide a favourable environment for generating rainfall especially over the Sahel [*Fink and Reiner*, 2003a]. These lows associated with the AEW formation produce winds to generate and transport dust (Figure 2.7).

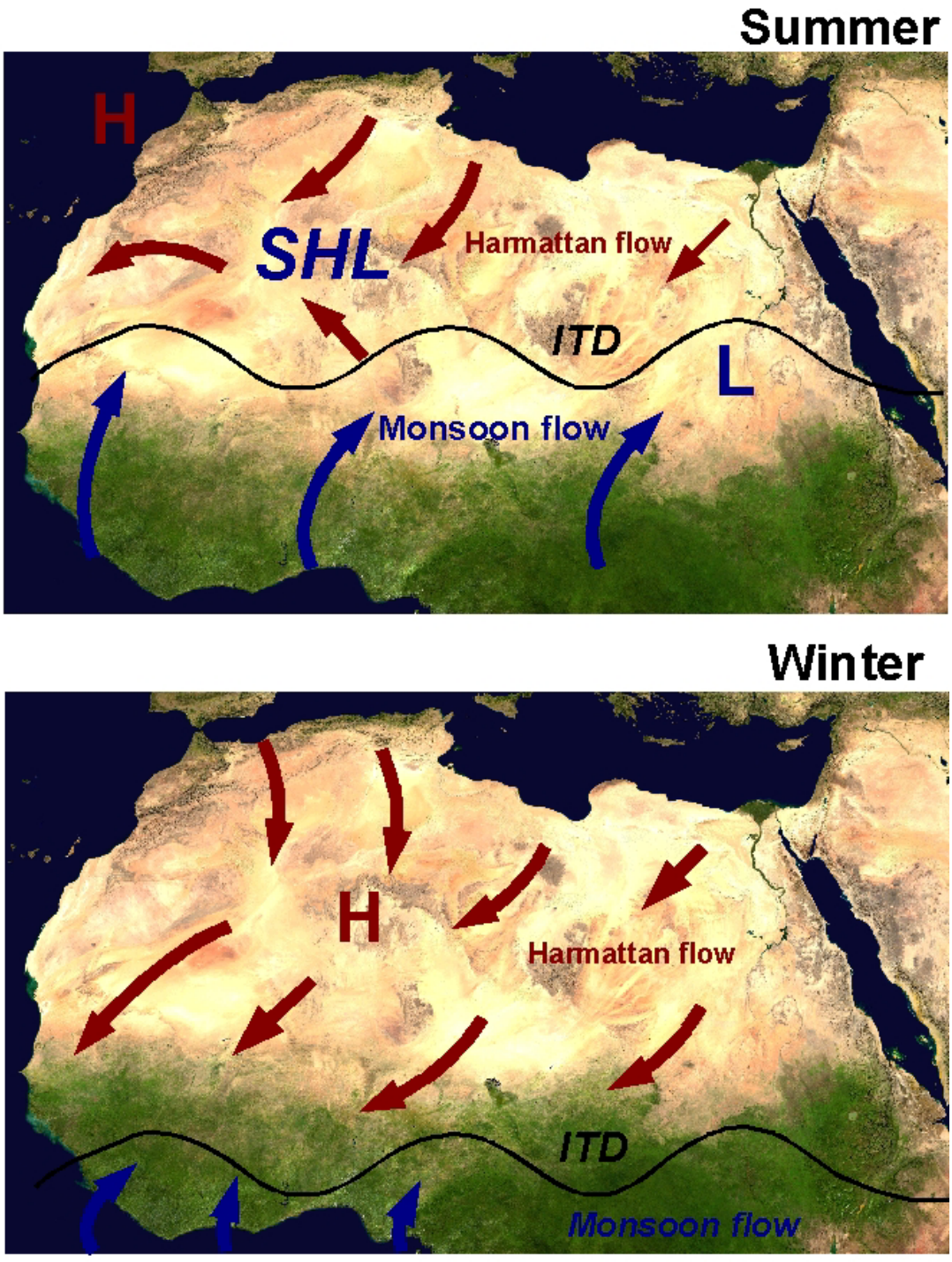

Figure 2.6. Schematic representation of atmospheric circulation in West Africa.

2.3.1.2. Dust outbreaks

The mechanisms that control dust mobilisation in the Sahara and the Sahel in West Africa are well delimited according to the annual cycle [*Engelstaedter and Washington*, 2007].

During dry season (December – May),the influence of the ITD in the Sahara and Sahel is minimal. Large dust mobilizations are controlled by wind intensity driven by several weather systems [*Washington et al.*, 2003] in addition to the suitable soil conditions. On a synoptic-scale and meso-scale, dust lifting is associated to strong near-surface and upper winds related to the formation of surface lows and cold outflows [*Thorncroft andFlocas*, 1997]. The dominant low-level north-easterly*Harmattan* winds, play the main role for dust lifting in some parts in the Sahara region (Figure 2.7.a). On a smaller scale, atmospheric dry convection is associated with the formation of dust devils in the Sahara. Dust devils are defined as dusty convective vortices with typical diameters ranging from 3 to 15 meters and lifetimes of only a few minutes [*Sinclair*, 1969; *Williams*, 1948]. Turbulence causes air to swirl upwards, carrying fine particles of dust with it especially around dry lakes or on the valley floor (Figure 2.7.b). Dust mobilisation by dry convection over the Sahara in West Africa prevail during the late spring, summer, and early fall due to the increase in solar heating. The resulting dry and strong winds transport large amounts of dust across the Sahara, which can be also transported up to 6 km in the Saharan atmospheric boundary layer (SABL) [*Gamo*, 1996].

In boreal summer, the factors related to dust mobilisation include systems at (i) synoptic scale: low pressure centres or cold breaks from middlatitudes, ii) meso-scale: cold fronts, density currents [*Knippertz et al.*, 2007; *Knippertz*, 2008], gustiness generated by mesoscale convective systems (MCS's) or density currents (*haboobs)* [*Cooke et al.*, 1993; *Sultan and Janicot*, 2000], turbulence induced by low level jets (LLJ) at the North-easterly harmattan flow [*Knippertz and Martin*, 2005] and North-south flanks of the ITD [*Flamant et al.*, 2007; *Karam et al.*, 2008] and iii) small scale: turbulence caused by dry convection due to surface heating [*Thorncroft and Blackburn*, 1999].

In summer, the ocurrence of MCS caused by monsoon flux displacement from near the Equatorial bell in a northwards direction to the Sahel and the Sahara brings precipitation to this area. Most precipitation evaporates before reaching the surface, and a pool of cold, dense air is generated sinking rapidly downwards. Such downward flow of cold air generated by evaporative cooling is often termed “gravity current” or “density current” [*Flamant et al.*, 2007]. These cold outflows originated by deep convective systems in the form of thunderstorms or squall lines cause gustiness just ahead of them favouring dust lofting on a meso-scale in the form of *Haboobs* [*Sutton*, 1931]. These phenomena are most likely to occur in the afternoon and evening before, or at the beginning of, the rainy season (Figure 2.7.c) [*Knippertz et al.*, 2007]. They can propagate at speeds on the order of 10 m s^{-1} over hundreds of kilometers, sometimes far away from the parent convective clouds [Freeman, 1952; Miller et al., 2008].

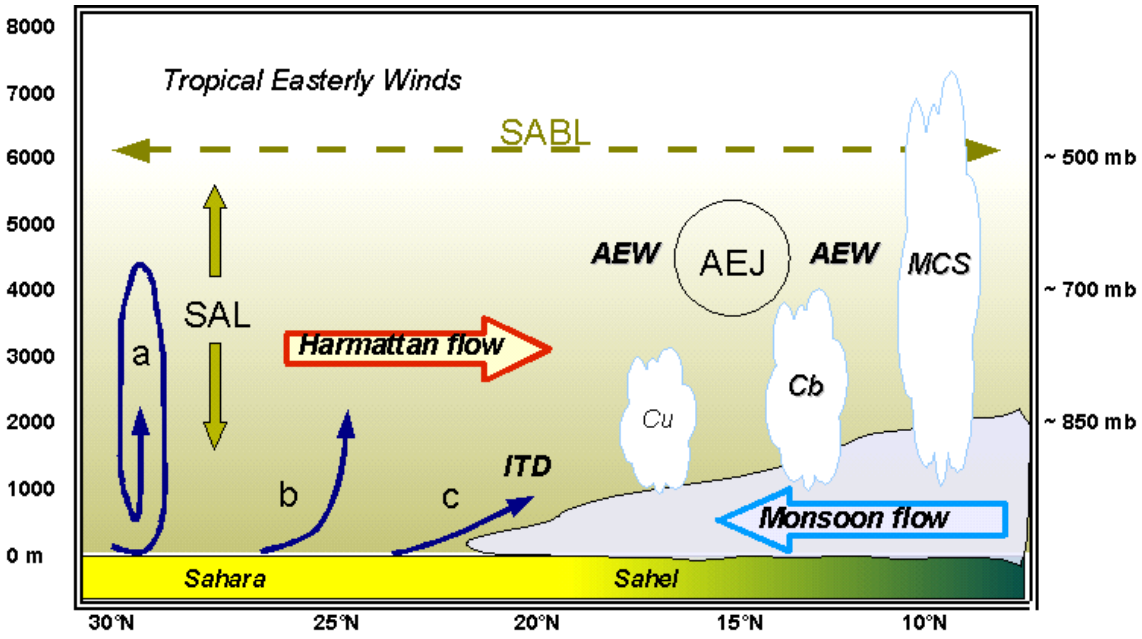

Figure 2.7: Vertical structure of atmospheric dynamics in West Africa. Blue arrows symbolize dust uplifting (see text).

Dust activation sources and transport patterns differ during boreal winter compared with summer outbreaks. The Bodélé depression in Chad is the most active dust source area in winter and early spring while West Africa becomes more active during summer [*Engelstaedter et al.*, 2003; *Washington et al.*, 2003]. Also, the retreat of the ITD southwards and the dominance of a northeasterly wind regime allow dust transport towards South America. On the other hand, dust aerosols emitted during summer in West

Africa tend to displace in an East-West direction towards the Caribbean islands [*Prospero et al.*, 2002].

Dust plumes from the Bodélé depression as a preferential source are transported in topographically constrained Low Level Jet (LLJ) features [*Todd et al.*, 2008b; *Washington and Todd*, 2005] and the LLJs to the north and south of the Aïr mountains [*Schepanski et al.*, 2007]. For the Bodélé Depression, the high dust emission frequencies are caused due to the erosive action on these readily erodible sediments of locally strong winds associated with the Bodélé Low Level Jet (LLJ) [*Todd et al.*, 2007]. This phenomenon is associated with the channelling effects of the Tibesti and Ennedi mountains, which rise around 2600m to the north, and 1000m to the east, respectively, above the Bodélé depression. The LLJ exhibits a pronounced diurnal cycle with a night-time (daytime) maximum (minimum) consistent with the inertial oscillation mechanism [*Washington et al.*, 2006b]. During the day, surface heating leads to a well mixed deep boundary layer which exerts a frictional retardation of the LLJ. Radiative cooling of the surface after sunset leads to a near surface temperature inversion and decoupling of the surface and low level winds, and initiates an inertial oscillation in which the LLJ accelerates through the night, until turbulent mixing starts again the following day. This process leads to a phase shift of the surface wind diurnal cycle with respect to that of the low level wind. At the surface maximum wind speeds are observed during mid-morning when turbulence mixes the momentum of the nocturnal LLJ down to the surface. At night decoupling of the surface and low levels leads to minimum wind speeds at the surface [*Todd et al.*, 2008b]. Many regions in the tropics experience a nocturnal LLJ phenomenon [*Stensrud*, 1996].

2.4. Mineral Dust Modelling

This section includes a brief description of Global Climate Models (GCM's) and their evolution to depict complex climate processes. Furthermore, the implementation of Regional Climate Models and the development of coupled chemistry climate models to simulate dust emissions and the climate feedback are discussed. Finally, the efforts made by different groups to improve dust-simulations from operational and forecasting model framework are included.

2.4.1. Global Climate Models

Global Climate models or Global Circulation Models (GCM) are mathematical representations of the complex interactions between atmosphere, hydrosphere, cryosphere, lithosphere and biosphere to understand and describe the complexity of the climate system [*Vallis*, 2006]. GCMs aim to describe climate behaviour by integrating a variety of fluid-dynamical, chemical, or even biological equations that are either derived directly from physical laws (e.g. Newtons Laws) or empirical equations [*Randall et al.*, 2007; *Randall and Wielicki*, 1997] The complexity of climate models has increased over the last 40 years due the computational progress that allows the inclusion of more components and processes (refer to Figure 1.2, AR4, *Le Treut et al* 2007), simulation lengths and spatial resolution. Ideally, climate models would simulate all of the physical, chemical and biological processes interacting in the global climate system on a computational grid and all the points were close enough to resolve every single mechanism (i.e. cloud formation or the influence of topographic features). However this is computationally impossible, even with today's fastest computers, and judicious simplifications and parameterisations (representation of processes occurring on smaller spatial scales than the model grid) must be considered. [*Le Treut et al.*, 2007; *Randall*, 1996].

Different approaches have been taken to evaluate climate feedbacks by GCMs. One approach involves 'offline' processing of model data using simplified (1D or 2D) climate models applied to mean model dataor repeated 3Dcalculations with the model radiation code run offline onmodel fields [e.g. [*Wetherald and Manabe*, 1988].The "offline" coupling, simulate thermodynamic terms for various energy sources. However, the configuration of these models does not permit simulation of feedbacks between air

quality and climate/meteorology and may result in an incompatible and inconsistent coupling between both meteorological and air quality models [*Zhang,* 2008]. Offline models are rather used for the development or improvement of the chemistry portion in a model code or for testing sensitivity analysis; hence feedback to meteorology is not essential [*Grell et al.,* 2005]. Currently, climate simulations including atmospheric aerosols with chemical transport have greatly improved. Some models are configured in the form of fully coupled "online" atmospheric models with coupled meteorology and chemistry. The online models are reliable because they provide radiative and cloud feedback from the chemistry to the meteorology and in turn update the dynamics and physics variables [*Zhang,* 2008].

The inclusion of dust aerosols in the coupled chemistry climate models is an important contribution to understanding the role of dust in the climate system [*Ghan and Schwartz,* 2007]. In essence, models with dust emission schemes consider soil characteristics and wind speed among other important parameters (described with more detail in further sections). A complete dust-modelling framework includes an atmospheric model, a land surface model, a dust model (emission mechanisms), a transport scheme and a deposition model as well as the direct and indirect radiative effects [*Tegen and Miller,* 1998]. A number of Global Circulation Models (GCMs) now incorporate active dust emission and transport schemes in which dust is a prognostic variable. For example, the Hadley Centre Models HadCM3 and HadGEM [*Bellouin et al.,* 2008; Woodward, 2001] and the European Centre HAmburg Model (ECHAM5) General Circulation Model [*Stier et al.,* 2005].

In addition, some global off-line chemical tracer models that include dust as a tracer have been developed: the Georgia Tech/Goddard Global Ozone Chemistry Aerosol Radiation and Transport (GOCART) [*Ginoux et al.,* 2001], the global chemical transport model from the Goddard Earth Observing System (GEOS-Chem) [*Bey et al.,* 2001] and the Dust Entrainment and Deposition (DEAD) model [*Zender et al.,* 2003a]. Furthermore, the incorporation of dust in forecasts has been shown to improve forecast accuracy [Perez et al., 2006]. Consequently, A number of experimental and operational dust forecasts systems have been developed at institutes around the world e.g. The Global Environmental Multiscale Model (GEM) [*Cote et al.,* 1998]; the Navy Aerosol Analysis and Prediction System (NAAPS) [*Christensen,* 1997; *Hogan and Brody,* 1993] The

European Centre for Medium-Range Weather Forecasts (ECMWF) [*Tompkins et al.*, 2005] and the UK Met Office [*Greed et al.*, 2008].

2.4.2 Regional Climate Models

Whilst GCM's are able to reproduce dust episodes caused by atmospheric disturbances at synoptic scale, some surface physical properties (i.e. terrain features) and small-scale atmospheric processes (i.e. those associated with dry convection) are still an issue for dust modellers. The development of high-resolution ensemble models able to recreate these processes has resolved partially these limitations. The inclusion of Limited Area Models (LAMs) in regional climate studies was originally proposed by *Dickinson* [1989] and *Giorgi, et al.* [1990]. This idea was based on the concept of one way nesting, in which large-scale meteorological fields from general circulation model (GCM) runs provide initial and time-dependent meteorological lateral boundary conditions (LBC) for high-resolution LAM simulations. The strategy underlying this technique for Regional Climate Modelling is that GCMs can provide the response of the global circulation to large-scale forcings, and nested LAMs or Regional Climate Models (hereafter RCM's) can account for the effects of local, sub-GCM grid scale forcing [*Giorgi and Mearns*, 1999].Given the localized nature of many dust sources and the spatial heterogeneity in dust properties, the high spatial resolution of Regional Climate Models (RCMs) can facilitate more accurate simulation of dust aerosol-climate processes. RCMs provide an important test bed for developing and testing aerosol processes modules for subsequent incorporation into GCMs [*Ghan and Schwartz*, 2007].

A number of RCM's with dust emission schemes have been developed over the last decade or so. These include the 'Lokal-Modell' online-coupled Multiscale Chemistry Aerosol Transport model with a dust emission scheme (LM-MUSCAT-DES) [*Heinold et al.*, 2007], the Regional Climate Model third version (RegCM3) [*Zakey et al.*, 2006], the Regional Atmospheric Modelling System (RAMS) [*Cotton et al.*, 2003], the DREAM model [*Nickovic et al.*, 2001], the Meso-NH [*Grini et al.*, 2006] and more recently, the implementation of a dust scheme for the Weather Research and Forecasting model (WRF-Chem) developed jointly by NCAR, NOAA, NCEP (FSL), AFWA, Naval Research Laboratory and Oklahoma University [*Grell et al.*, 2005]. Simulations by both global and regional models can lead to a better understanding of dust processes and their effects on the climate system. Nevertheless, considerable uncertainty in model estimates dust

emission and fluxes at global [*Zender et al.*, 2004] and regional scales [*Uno et al.*, 2006] is still present. Therefore, numerical simulation of dust processes needs to be improved.

Although most dust schemes apply more or less the same principle, different factors related to modelparameterisation and prognostics implemented for initialisation can produce quite different dust emissions and vertical fluxes even within the same regional model. Since it is very difficult to make representative measurements of emitted dust fluxes and all required land and atmospheric properties, development of physically based parameterizations of dust production remains a challenging problem. Even if high-quality local measurements of emitted dust fluxes could be made, the heterogeneity and temporal variability of land surfaces and meteorological fields make such measurements unrepresentative of the area- and time-average fluxes at the scales needed for input into regional and global models. Thus, not only do dust emission schemes rely on various assumptions, but also their implementation represent many challenges [*Darmenova et al.*, 2009]. As an example, a model intercomparison in the Bodélé depression made by *Todd et al* [2008a] showed significant biases between different regional models implementing the same dust emission scheme. An explanation to this regards on the fact that the actual saltation and sandblasting process of dust generation in the Bodélé depression is very complex due to the high content of diatomite sediments [*Warren et al.*, 2007; *Washington et al.*, 2006b]. Since soil maps do not consider regional sedimentation but rather an already established classification, the degree of uncertainties in emissions from this dust source are still an issue.

The following section addresses the particulars of two regional models with differences in the dust schemes used for experimentation in this work. The particulars of the emission, transport and deposition mechanisms implemented in both schemes (as in most dust models) are addressed in section 2.5.

2.4.2.1 WRF-Chem 3.1

The Weather Research Forecasting Model (WRF) is a next-generation mesoscale forecast model and assimilation system to advance both the understanding and the prediction of atmospheric structure with emphasis on precipitation systems. WRF is applied in a variety of areas including storm-scale research and prediction, air-quality modelling, wildfire simulation, hurricane and tropical storm prediction, regional climate, and operational numerical weather prediction [*Michalakes et al*., 2005]. It includes two different dynamic cores, the Advanced Research Version (ARW) and the Nonhydrostatic Mesoscale Model (NMM) [*Shamarok, et al* 2004]. WRF is suitable for a broad spectrum of applications across scales ranging from meters to thousands of kilometres. The WRF model is conformed by no hydrostatic, compressible flux-form equations; terrain-following hydrostatic pressure vertical coordinate and two-way interacting moving nested grids.

The WRF-Chem is a fully coupled online community model for the prediction and simulation of weather, dispersion, air quality, and regional climate. WRF-Chem may also be run offline for some chemical applications. WRF-Chem is currently used from hemispheric to local cloud-resolving scales.All transport is done by meteorological model [Grell et al., 2005]. The WRF-Chem contains different aerosol modules: i) A total mass aerosol module from GOCART and includes PM advection, transport, emission and deposition ii) The Modal Aerosol Dynamics Model for Europe MADE/SORGAM [*Ackerman et al., 1995*] and iii) The MOSAIC sectional model aerosol parameterization [*Zaveri et al., 2008*].

The GOCART dust modelis a simple scheme in which the vertical dust flux depends on a prescribed erodible surface fraction and fixed threshold friction velocity. This schemeisbased on*Ginoux et al.* [2001] and it is fully described in Section 2.5. It was conceived as an offline transport model driven by assimilated meteorological fields from the (GEOS) Data Assimilation System (DAS) GEOS-1 [*Schubert et al.,* 1993]. The GOCART module simulates dust along other major tropospheric aerosol components as a function of surface topographic depression, surface wetness, and surface wind speed. The WRF-Chem GOCART based scheme also implements various Goddard physical packages (i.e., CRM-based microphysics, radiation and land-surface hydrology processes)

as well as a real-time forecast system using Goddard Earth Observing System (GEOS) global analyses that have been developed at NASA [*Tao et al.*, 2009]. To this date though, there are some limitations with available schemes to simulate dust into the WRF-Chem and require more development. Although the dust scheme in the version described here (V 3.1.) is able to simulate emission, transport and deposition of dust particles, radiative feedback and cloud interactionhave not been coupled. Although modules available to simulating dust aerosols in the WRF-Chem are still quite under developing [*Ajjaji et al.*, 2008; *Grell et al.*, 2005], the meteorological and dynamical modules of the WRF-Chem are efficient to perform state-of-the-art atmospheric simulations including regional climate, and operational numerical weather prediction [*Michalakes et al.*, 2005].

2.4.2.2 RegCM3

The Regional Climate Model (RegCM3) with a dust module is a hydrostatic, sigma vertical coordinate model similar to the hydrostatic version of the Mesoscale Model (MM5). It was conceived for a wide range of applications at high spatial (20-80 km) and temporal resolution (1 hr). The latest model development is the implementation of aerosol modules in an attempt. This scheme allows the simulation of aerosols of anthropogenic origin [*Solmon et al.*, 2006] and those from natural sources such as mineral dust [*Zakey et al.*, 2006] to quantify the climate forcing. The mechanisms that control dust production, which include emission, transport and deposition processes, have been described by various authors [*Alfaro and Gomes*, 2001; *Marticorena and Bergametti*, 1995; *Shao*, 2000] and are included in most of models with a physical based dust scheme (view Chapter 2.5).

The soil aggregate size distribution is prescribed from a land surface map with 18 classes of natural land type that is interpolated onto the model grid, including the intensity of cultivation for each grid cell. This classification is a simplification of the classes used to define a wide variety of land surface, hydrological, and vegetation properties. The prescribed soil textures are defined as the percentage of three classes (clay, silt and sand) from the *Zobler* [1986] assessment of FAO (Food and Agriculture Organization) Soil Units and the USDA (United States Department of Agriculture) dataset of soil type, texture, surface slope and other properties. The land surface properties are provided by the Biosphere-Atmosphere Transfer Scheme (BATS) [*Yang and Dickinson*, 1996], including roughness length, soil moisture and vegetation cover fractions properties that are assigned parameters in the aerosol dust model. RegCM3 also contains a radiative

transfer scheme of the National Center for Atmospheric Research (NCAR) Community Climate Model (CCM3) described by *Kiehl et al* [1998]. Its predecessor (CCM2) accounted for the effects of H2O, O3, O2, CO2. The CCM3 is structured in the same way, but it includes new features such as the effect of additional greenhouse gases (NO2, CH4, CFCs), atmospheric aerosols, and cloud ice. This latest version of RegCM3 determines the radiative interaction of aerosol tracers over the shortwave solar wavelengths only [*Qian and Giorgi*, 1999].

2.5. Dust models parameterisation

As explained in previous sections, a dust-modelling framework includes an atmospheric model, a land surface model, a dust model (emission mechanisms), a transport scheme and a deposition model. This section includes a description of the conception ofthese mechanisms and the way they are integrated into models with particular emphasis in the dust schemes (WRF-Chem and RegCM3) used in this work.

2.5.1. Emission Mechanisms

Most of dust emission schemes include: surface meteorological conditions (surface wind speed and atmospheric stability) and surface physical properties (soil particle distribution, surface roughness, soil type, soil moisture and vegetation cover). Dust emissions schemes range from simple type schemes, in which the vertical dust flux depends on a prescribed erodible surface fraction and fixed threshold friction velocity (i.e. GOCART) to advanced, physically based schemes (i.e. RegCM3). In the latest, the surface characteristics are considered explicitly in the parameterizations of the threshold friction velocity, and horizontal and vertical fluxes [*Marticorena and Bergametti*, 1995; *Shao*, 2001].

In principle, dust uplift is boosted by the combination of strong winds, topographic features and material available for deflation. This happens when surface winds exceed the threshold velocity (e.g. ~10 ms^{-1} at 2m height for the Bodélé Desert, Todd et al., 2008b). An initial conception about how dust particles are released to the atmosphere was proposed by *Bagnold* [1935; 1937]. He suggested that dust particles are release to the atmosphere in three ways: i) the direct aerodynamic entrainment or suspension of particles. ii) Saltation bombardment (sand blasting) iii) aggregates disintegration (self-abrasion) (Figure 2.8.a). The aerodynamic entrainment is related to fine particles smaller than 50μm (silt and clay) able to be mobilised by turbulence and aerodynamic forces [*Shao*, 2000]. Fine particles like clay however, pose strong cohesive forces and tend to agglomerate which makes difficult simple mobilisation by suspension. Nevertheless, once in the atmosphere these particles are able to travel long distances [*Middleton and Goudie*, 2001]. The saltation and sandblasting processes in which saltating sand size soil aggregates (~50μm-500μm) break soil into smaller particles which are released into the atmosphere [*Grini et al*., 2002] are common process for mobilisation

of particles. Moreover, dust flux F should separately accounted in horizontal and vertical components.

2.5.1.1. Simple dust emission schemes

Bagnold, [1937] proposed dust mobilisation by relating the amount of sand moved to wind speed by saltation, where mass transport of sand is proportional to the third power of the friction velocity (u^*). Later, *Gillete and Passi* [1998], introduced a formulation with information of the parent soil size distribution included in a parameter *sp*(fraction of size group within the soil).In the simple physic parameterisation schemes, the vertical flux F (g cm^{-2} s^{-1}) of emitted mineral aerosols is parameterised in terms of u^*. Models based on this simple dust emission scheme include CFORS [*Uno et al.,* 2001], COAMPS [*Liu et al.,* 2003], DREAM [*Nikovic* et al., 2001], CARMA-MM5 [*Barnum et al.,* 2004] and GOCART [*Ginoux et al.,* 2001]. These models consider preferential sources (based on erodible fraction and a mass normalization) rather than individual soil particle properties. These preferential sources might be related to natural topographic depressions [*Ginoux, et al,* 2001], dry lake basins [*Engelstaedter et al.,* 2003], geomorphology [*Zender, etal* 2003], surface reflectance[*Grini et al.,* 2005].

In the GOCART dust emission scheme based on *Ginoux et al* [2001] used in WRF-Chem, a dust-source function is constructed as the probability of sediments accumulated in the topographic depression regions with bare surfaces [*Ginoux et al.,* 2001] and considering the surface roughness to delimit the ability for dust uplift between topographic lows and the surrounding [*Chin et al.,* 2002]. These locations correspond to regions where the erodable fraction area is higher than 30% particularly with an elevated proportion of sand.

On these grounds, the emission flux *Fp* for a size group *p* expressed as:

$$Fp = C\,S\,sp\,u^2_{10m}(u_{10m} - u_t) \quad \text{if} \quad u_{10m} > u_t$$

Where C is a dimensional, scheme-specific constant of proportionality equal to 1 μg s^{-2} m^{-5}, S is the probability source function, which is the probability of sediments accumulated at the topographic depression regions with bare surface; *sp* is the fraction of each size class within the soil; u_{10m} is the wind speed at 10m, and *ut* is the threshold

velocity of wind erosion, determined by particle size and surface wetness. Due to the uncertainties in the available soil texture data, a simple particle size distribution following *Tegen and Fung* [1994] is implemented. The fraction of clay is based on the assumption that erodible clay represents 1/10 of the total mass of emitted silt, and that of each silt subclass is assumed to be the same. The *sp* values are thus 0.1 for the class 0.1-1μm, and 1/3 for the classes 1-1.8μm, 1.8-3μm, and 3-6μm, respectively.

The source function *S* that conform the erodibility fractional map is the fraction of alluvium available for wind erosion. It considers the surface roughness to delimit the ability for dust uplift between topographic lows and the surrounding [*Chin et al.*, 2002] and it is represented as follows:

$$S = (z_{max} - zi \,/\, z_{max} - z_{min})^5$$

where S is the probability to have accumulated sediments in the grid cell *i* of altitude *zi*, and z_{max} and $z_{min}$are the maximum and minimum elevations in the surrounding 10 x 10 topography, respectively. Only land surface with bare soil is considered as possible dust sources. The bare soil surface map is obtained from the 1 x 1 vegetation data set derived from the advanced Very High Resolution Radiometer (AVHRR) data [*DeFries and Townshend*, 1994]. These locations correspond to regions where the erodable fraction area is higher than 30% particularly with an elevated proportion of sand (rather than a presentation of diatomite). In this work, a newest version from this erodible fractional map derived from AVHRR at a higher resolution 0.25° X 0.25° is used (Figure 4.1). One of the advantages of using this new map is that areas with high *S* are located near to Chicha and the extended area in the Bodélé Desert (a well known dust source). In the previous coarser map, erodable areas were rather located in a southwestern position. In addition, some mesoscalar features might now be visible compared with the 1°X1° degree version (View Annex A).

2.5.1.2. Physical based dust schemes

The advanced, physically based schemes proposed by several authors [e.g.. *Shao etal*, 1993, 1996; *Marticorena and Bergametti*, 1995; Alfaro and Gomes, 2001] offer physically based parameterisations of processes in order to provide amore realistic

representation of the emission processes. These schemes explicitly consider surface characteristics when calculating the threshold friction velocity (*u*t*) and the size-resolved horizontal (saltation) and vertical fluxes. In most models, threshold friction velocity (*u*t*) is controlled primarily by the local soil roughness length (*z0m*). It also depends on soil moisture (only dry surface can emit dust), particle radius, surface, temperature, and surface wetness [*Gillete et al* 1988; *Marticorena and Bergametti,* 1997]. Particle size distribution of dust emission flux is either prescribed or predicted from soil particle size. The size distribution of dust vertical flux can be calculated by first predicting the size distribution of the horizontal flux [*Grini and Zender*, 2004].

The physically based dust emission models can be broadly classified into energy-based [*Alfaro and Gomes,* 2001; Shao et al., 1996] and volume removal based [*Lu and Shao,* 1999; *Shao,* 2004]. The central difference is based on the linkage between dust emission and saltation. To date, a number of regional dust modelling systems have incorporated physically-based dust emission schemes (with various modifications): for instance, LM-MUSCAT [*Heinold et al.*, 2007], CEMSYS5 [*Shao,* 2004], CHIMERE-DUST [*Bessagnet et al.*, 2004], RegCM3 [*Zakey et* al., 2006] and MesoNH [*Grini et al.*, 2006]. For most of the above models, the parameterisation is based on *Alfaro and Gomes* [2001] and *Marticorena and Bergametti* [1995] in which the main steps are: the specification of soil aggregate size distribution for each model grid cell, the calculation of a threshold wind friction velocity above which wind stress leads to saltation processes, the calculation of the horizontal saltating soil aggregate mass flux, and finally the calculation of the vertical transportable dust particle mass flux generated by the saltating aggregates. For a full description of the equations, which parameterize these processes in the RegCM3 see Zakey et al. [2006] and see Table 1.

2.5.2. Transport Mechanisms.

The geomorphologic characteristics in certain regions depend on the transference of dust from erosive regions [*Shao,* 2000]. The knowledge of the lifetime of mineral dust in the atmosphere is critical for studies in radiative forcing caused by dust particles when traveling over an extended area [*Tegen and Fung,* 1994]. As a result, the importance of representing properly dust transport is critical for models. Fine particles like mineral dust (<20μm) can be transported easily once they are suspended [*Gillette and Passi,* 1988]. Once in the atmosphere, dust particles are displaced by convective processes, horizontal

and vertical turbulent diffusion or advection (Figure 2.8. b). As example, in some models (i.e. RegCM3) for transport, settling and scavenging processes, the tracers are considered as individual components. The tracer transport equation is described in *Solmon et al* [2006]. In this equation, the transport mechanisms (advection, horizontal and vertical turbulent diffusion and convective transport) are represented according to the equation used by *Qian et al* [2001]. WRF-Chem GOCART model transports four size ranges from 0.1 to 10 μ using a three-dimensional flux form semi-Lagrangian scheme [*Lin and Rood,* 1996] and considers advection, eddy diffusion and moist convection for transport [*Ginoux, et al* 2001].

2.5.3. Deposition Mechanisms

Mineral dust deposition is expressed in terms of deposition rate (g m^{-2} yr^{-1}). So far models have given a good representation about the processes involved in dust removal [*Ginoux et al*., 2001; *Mahowald et al*., 2005; *Nickovic et al*., 2001]. Deposition processes for mineral dust are purely mechanic and depend of the particle size and meteorological conditions. In principle, mineral dust is removed by wet (large-scale and convective rain) and dry (gravitational settling) deposition (Figure 2.8.c). Other turbulent processes might also be included. On global scale, the total dry and wet deposition are probably of similar magnitude [*Duce and Tindale,* 1991], though dry deposition dominates source regions because of large particle sedimentation [*Zender et al.*, 2003a]. Most models add of a size dependant particle gravitational settling term and a dry deposition scheme including turbulent transfer in the surface layer and surface interception as a function of land cover characteristic [*Zakey et al,* 2006] Dry deposition includes gravitational settling as a function of particle size and air viscosity [*Wesely,* 1989].

The efficiency of the wet deposition depends on many parameters such as particle size distribution, raindrop size distribution and the chemical characteristics of the particles. Treatment of in-cloud scavenging is very different among models. Some models treat dust particles are hydrophobic and do not include in-cloud scavenging, while others treat in-cloud scavenging. Wet deposition parameterizations used for dust modeling can be classified into four types based on their formulations: the first type calculates scavenging coefficient as a function of raindrop size distribution and particle–raindrop collection efficiency. The second type estimates scavenging coefficients as a function of a single variable such as precipitation rate (e.g. *Nickovic et al.,* 1966) or relative humidity (RH) [*Pudykiewicz,* 1989]. In the third type, an empirical relationship derived from direct

measurements of scavenging coefficients is used. Finally, for the estimation of large-scale dust deposition, scavenging ratio, which is different parameter for describing the efficiency of the removal process, is often used (e.g. *Tegen and Fung*, 1994).

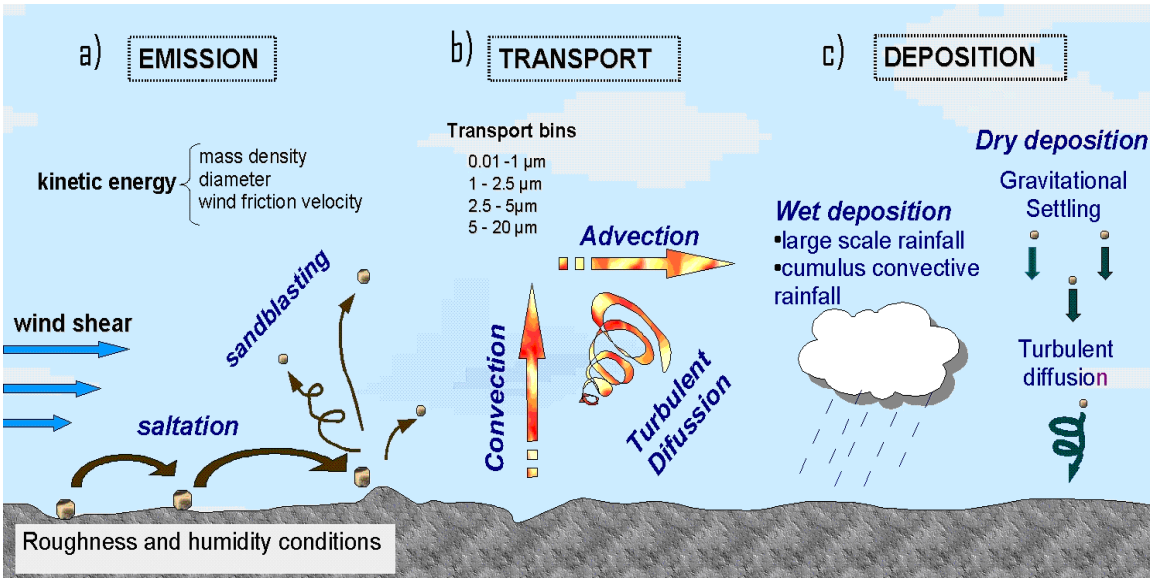

Figure 2.8: Physical processes related to dust mobilisation

3 Research Proposal

3.1. Thesis purpose and particular questions

The understanding of the atmospheric controls and climate impact of dust emissions in the Sahara Desert is still uncertain. A better comprehension of the dynamics of these processes and the identification of dust preferential sources is partly accomplished using observations from ground-based and space-based instruments. However, the simulation of sources, magnitude of dust emission, transport in 3-dimension and deposition from synoptic to a smaller scale relies on the ability Regional Climate Models to represent atmospheric aerosol processes. Hence, integration of these data to model outputs facilitates the evaluation and parameterisation of regional models describing such processes related to dust mobilisation. Nevertheless, some specific questions remain regarding particularly such processes in the Sahara Desert, which this work will address in the upcoming sections:

1. What are the existing uncertainties in RCM dust estimates over important dust sources in the Sahara Desert (i.e. the Bodele Dessert)
2. How model errorscan be reduced by the optimisation of initial model configuration (i.e. preferential sources and optical properties) in order to represent in a better extent:

a) Dust emission and vertical fluxes
b) Radiative impact (direct effect) during major dust outbreaks
c) Dust-generation mechanisms and impact in the atmospheric circulation.
d) Dominant transport trajectories and the implications to the seasonal cycle.

3. What are the limitations of satellite datasets for model validation and what are the latest efforts to offset these constraints.
4. To utilise the best available observational datasets taking advantage of recent field campaigns in the region.

To answer these questions a two-stream approach of: (i) model experiments and (ii) analysis of observational datasets are conducted for a number of carefully selected case studies. This is to demonstrate the implications of model optimisation in dust simulations and how observations can be used as a complement to expand our understanding of the effect of dust aerosols in the Sahara Desert.

3.2. Experimental design

The following sections provide an insight of each case and the particular objectives assessed. A summary of model configuration is shown in table 3-1.

3.2.1 Sensibility analysis by tuning of preferential sources

It is well known that most dust is emitted from preferential source regions [*Prospero et al.,* 2002; *Washington et al.,* 2003], often related to topographic depressions [*Zender et al.*, 2003b], fluvial sedimentary deposits or paleolake beds. Adequate representation of these sources has often been noted to be a problem for dust models.

As explained in section 2.5, dust emissions in the WRF-Chem GOCART scheme are triggered upon the source function *S* that conform the erodibility fractional map derived from AVHRR. In this research a new version from this erodible fractional map at a higher resolution 0.25° X 0.25° is tested (Figure 4.1). One of the advantages of using this new map is that areas with high *S* are located near to Chicha and the extended area in the Bodélé Desert (a well known dust source). In the previous coarser map, erodable areas were rather located in a southwestern position. In addition, some mesoscalar features might now be visible compared with the 1°X1° degree in previous version (View Annex A).

In the GOCART scheme used in WRF-Chem, a dust-source function is constructed as the probability of sediments accumulated in the topographic depression regions with bare surfaces [*Ginoux et al.,* 2001] and considering the surface roughness to delimit the ability for dust uplift between topographic lows and the surrounding [*Chin et al.,* 2002]. These locations correspond to regions where the erodable fraction area is higher than 30% particularly with an elevated proportion of sand. The dust emission scheme used by WRF-Chem with the GOCART module is based on *Ginoux et al* [2001] and it is widely detailed in section 3.2.1. For this research, a newest version from this erodible fractional map derived from AVHRR at a higher resolution 0.25° X 0.25° is used.

In counterpart, in this work RegCM3 uses another approach for preferential sources where a Dust Frequency Activation Source (DFAS) map is used to replace the default soil texture class map following *Cavazos et al.* [2009] (See section 3.3.2). In

RegCM3 all model grid cells in which the DSAF is greater than 1% were prescribed a soil texture class of the sand type. From a traditional point of view, large sand seas in North Africa are not considered as source regions of dust [*Goudie and middleton,* 1995]. However, previous simulations in RegCM3 have shown that in the dust emission scheme used by RegCM (*Marticorena and Bergametti*, 1995, herein M&B 1995) the net effect is that dust emission peaks for sand soils. The logic behind this outcome can be explained as follows: under the M&B scheme, the vertical flux of dust into the atmosphere results from the effect of sandblasting by large saltating aggregates (i.e. the vertical flux is a function of the horizontal flux). In desert regions with no vegetation and a uniform roughness length the saltation flux is essentially a function of the friction velocity in excess of the threshold friction velocity for saltation (*u*t*). M&B 1995 (Fig. 1) show that *U*t* is actually high for the fine grained (clay) soils and lower for coarser soils. However, *u*t* reaches a minimum for soil aggregates ~80um in diameter. Therefore a given wind speed the saltation flux will be highest for the silt sized aggregates and not for sand dominated soils. However, it is through the calculation of the vertical flux (from *Alfaro and Gomez*, 2001) that sand soils produce dust. First, the size distribution of the vertical dust flux is defined from 3 predefined log normal modes which are therefore independent of the size distribution of the soil. The logic here is that saltation can produce dust by releasing fine material from soils and from disintegration of the aggregates themselves. Second, the resulting vertical dust flux is derived from is a complex function of the kinetic energy of saltating aggregates and the binding energies of soil particles. There are many competing effects operating over the range of friction velocities and saltating aggregate sizes typically experienced, as described by *Alfaro and Gomes* [2001]. Most notably, although the *u*t* for saltation is higher for sand than silt sized soils the sandblasting u*t is lower, such that for vertical dust flux can occur at lower wind speeds for sandy sopils compared to silt soils. The net effect in our simulation is that dust emission peaks for sand soils. For that reason we chose to use this define preferential source regions.

3.2.2 Observational data

Different data from in-situ and satellite observations are used for all cases depending of availability during the analysed period (Table 3-1). This section describes a general overview of data sources and how they were used to validate model results.

Long term and daily means from operational data are used to define the initial boundary in the models. RegCM3 uses NCEP-DOE Reanalysis 2 data provided by the NOAA/OAR/ESRL PSD, Boulder, Colorado, USA, from *http://www.cdc.noaa.gov/*from 1979 to 2003, 2.5° x 2.5° at pressure levels. This dataset is an improved version of the NCEP Reanalysis I model that fixed errors and updated parameterizations of physical processes. In all cases three key parameters were analysed: sea level pressure (SLP), air temperature and wind speed at 925 hPa to define the meteorological patterns during each analysed case.

Meteorological observations were obtained from a number of WMO stations in the study domains. We selected those stations in the Saharan zone rather than the Sahelian zone further south, as we are primarily interested in model performance in the Saharan dust source regions. The reporting frequency varies between stations. At best the data is hourly although some stations report only at the 0600, 1200 and 1800hrs local time. Model estimates of near surface temperature, pressure and wind speed and direction are compared to the observations. Modelled aerosol coefficient extinction at the lowest level (attenuation of the light passing through the near surface atmosphere due to the scattering and absorption by aerosol particles) is compared to the observations of visibility from WMO stations located in areas near to dust sources. Previous studies have demonstrated a good correspondence of visibility and surface extinction at dusty sites [*Mahowald et al.*, 2007].

Ground base profiles of AOT at different wavelengths (440-1020 nm)from Sun photometer measurements from nine AERONET stations located in the modeldomains are used.

The spatial distribution of modelled AOT is also compared with a comprehensive set of satellite datasets providing information on atmospheric dust. These consist of (i) The European Organization for the Exploitation of Meteorological Satellites (EUMETSAT) dust product color-composite from SEVIRI available at a 15-minute

temporal resolution. The Dust Product is generated from the SEVIRI Brightness Temperature Difference (BTD) in three channels located at the infrared (8.7, 10.8, 12.0 μm) [*Legrand et al.*, 2001]. This spectral range allows retrieval of a qualitative dust product even over high albedo desert surfaces due to spectral different behaviour of airborne dust and surface at different wavelengths. Furthermore, measurements in the infrared make night observations possible, although the dust product is more diffuse than during daytime measurements and it is unlikely that dust close to the surface is identified at night. The SEVIRI dust product is a qualitative dataset useful to identify active dust sources [*e.g. Schepanski et al*, 2007]. (ii) Retrievals of the AOT from MISR which is onboard the National Aeronautic and Space Administration (NASA) Terra spacecraft with a local crossing time of 10.30hrs. MISR observes the Earth using nine cameras distributed at different angles in four wavelengths [*Bothwell et al.*, 2002], allowing an appropriate quantification of tropospheric aerosols. The spatial resolution is ~20km but the narrow swath limits the temporal resolution to around 1 week such that the spatial coverage is limited. (iii) Estimates of AOT were obtained from the qualitative OMI aerosol index (AI, *Torres et al.*, [1998]) using the algorithm proposed by *Christopher et al* [2008] based on a comparison of MISR and AI data (we used the regression equation for March in [*Christopher et al.*, 2008], their Figure 4). This regression equation was applied OMI AI at 13*24km resolution, daily at 13.30 local time. However, this relationship is sensitive to biomass burning aerosols and aerosol layer height [*Christopher et al.*, 2008] and in this case the relation results in a low bias in OMI-AOT estimates (see section 3.2). The space/time distribution of satellite AOT is evaluated both to determine mechanisms that contribute to dust emission and transport and analyse the agreement with the modeled dust emission. Model simulated AOT is obtained from integrating the extinction coefficient at 350-640 nm over the 23 vertical levels.

Modelled AOT (τd) is also validated in some cases with satellite estimates of MODIS-Aqua Collection 5.1 Level 2 (at 10km spatial resolution, daily at local noon) using the latest version of the Deep Blue algorithm, developed by *Hsuet al* [2004]. This latest processing algorithm derives aerosol properties from MODIS over land, providing estimates even over highly reflective desert surfaces.

Finally, several transects from the CALIOP Lidar Level 2 Vertical Feature Mask data product (VFM) are used to evaluate dust vertical structure with the dust layers predicted by the transport model in the form of light backscattered by aerosols with a high vertical resolution (30 m) [*Winker et al.*, 2007]. The VFM product describes the vertical

and horizontal distribution of cloud and aerosol layers observed by the CALIOP Lidar. Further details on CALIOP retrieval algorithms and data products are given in *Vaughan et al* [2004]. Although, initial retrievals from the CALIOP missed most parts of the analysed cases in this work, available transects covering the period 13 to 15th June 2006 acquired during both the daytime (local noon) and night-time (local midnight) portions of orbits are still useful to depict dust transport during two days period in a case to analyse dust mobilisation during the WAM onset.

3.3. Case study summary

3.31. Case 1: Model uncertainties in dust emissionsover the Bodélé Depression, Northern Chad during BoDEx (10-12th March 2005)

A key requirement of dust models is to simulate accurately the dust flux from regions where dust mobilisations are quite common. The ability of the WRF-Chem with the GOCART dust scheme to simulate dust emission and transport fluxes in the Bodele Depression (a very active dust source) is assessed.Results are compared to estimations from a recent model inter-comparison by *Todd et al* [2008a]as this case study represents a good platform to evaluatemodel efficiency.A large dust event from the Bodélé over 3-days from 10-12th March 2005 is analysed and coincides with the first in-situ data acquired form the region during the Bodélé Dust Experiment (BoDEx 2005; *Washingtonet al.*[2006]; http://www.geog.ox.ac.uk/research/projects/bodex/).

3.2.2.Case 2: Sensibility analysis of a major Saharan dust outbreak (6th–11th March 2006) with RegCM3

A major Saharan dust event of 6–11 March 2006, which produced some of the greatest dust emission in the last decade is investigated. The purpose of this analysis is to evaluate the ability of the RegCM3 to simulate dust mobilization over the Sahara desert by tuning preferential dust source regions. Additionally the sensitivity to optical properties is tested to quantify the model estimations of climate radiative impact of dust in the region. Results of this case study were published in the Journal of Geophysical Research [refer to *Cavazos et al* 2009]. The nature of experiments performed with RegCM3 is described in Table 5-1.

3.2.3. Case 3: Model characterisation of mechanisms controlling dust outbreaks in the WAM onset (6-11 June 2006)

Currently, models are more or less able to represent some of the dynamic mechanisms that favour dust emissions in the Sahara Desert (view section 2.3.). However, the parameterization of physical and dynamic components and limitations in model resolution,sometimes reproduce poorly shallow or deep convection and hence the efficiency to reproduce precipitation [*Wang and Seaman*, 1997]. Consequently, dust mobilisation in the model might not be induced near to areas affected by these processes. On the other hand, other atmospheric features involved in dust production during the monsoon season, such as the Saharan Heat Low (SHL) have not been well studied due to the reduced observations in the area. This analysis aims to evaluate and compare models performance (WRF-Chem and RegCM3) of mechanisms controlling dust outbreaks in the WAM onset (6-11 June 2006).

The period chosen for this experiment is part of the Special Operation Period Phase 1 (SOP1, 2006) from the African Monsoon Multidisciplinary Analysis (AMMA) during the monsoon onset (May-June) The period used for simulation agrees with observational campaigns during this period and availability of satellite measurements [*Lebel et al.*, 2009]. Dust simulations are made using two RCMs: RegCM3 and WRF-Chem. Both models used tuned preferential dust sources (section 3.2).

3.2.4. Case 4: Dust climate impact in the Sahara Desert in winter and summer 2006 and 2007

The Saharan dust cycle during a two years period is described using satellite remote sensing techniques and regional modeling. The purpose of this chapter is: (1) climatic features nvolved on the seasonal occurrence of dust outbreaks and compare with climatologies from satellite and ground base observations. (2) To evaluate the dominant transport trajectories on a seasonal basis and 3) Radiative forcing in the SW on the long term.

Table 3-1. Summary of experimental design and data validation (view text for detailed information)

Chapter	Simulation period	Model tested	Domain and resolution	Initial conditions	Satellite-based observations	In-situ observations
IV	5-9 Mar 05	WRF-Chem	12-24°E, 12-24°N 20km, 23z lev	NCEP Final Analysis (FNL from GFS), 1°X 1°.	AOT (τd) deep blue algorithm *Hsu et al* [2004]	Large-scale meteorological fields: (NCEP) reanalyses Bodélé Dust Experiment (BoDEx 2005): 2m height winds (converted here to 10m height) AOT(micro tops sunphotometer) at 'Chicha' (16.9°N, 18.5°E).
V	6-11 Mar 06	RegCM3.	21° N, 2.5° E 40 km, 23z levs	(NCEP/NCAR) Reanalysis Product at 2.5° x 2.5°	SEVIRI dust product AOT from OMI aerosol index and MISR	ERA-Interim re-analysis WMO stations: near surface temperature, pressure and wind speed and direction and visibility. AOT at different wavelengths (440-1020 nm) from nine AERONET stations.
VI	4-16 Jun 06.	WRF-Chem and RegCM3	20°W-40°E, 5–30° N. 30km. 23z levs	(NCEP/NCAR) Reanalysis Product at 2.5° x 2.5°	SEVIRI dust product AOT (τd) deep blue algorithm *Hsu et al* [2004] MODIS-Aqua Collection 5.1 Level 2. CALIOP Lidar Level 2	SYNOP database AOT at different wavelengths (440-1020 nm) from nine AERONET stations.
VII	Jan, Feb and Mar 06 and 07 Jun, Jul and Aug 06 and 07	RegCM3	40 km, 23zlevs	(NCEP/NCAR) Reanalysis Product at 2.5° x 2.5°	AOT from OMI aerosol index	Large-scale meteorological fields: (NCEP) reanalyses

4 Model uncertainties in dust emissions over the Bodélé Depression, Northern Chad during BoDEx (10-12th March 2005)

4.1. Introduction

The Bodélé depression corresponds to the extent of the paleo lake Mega-Chad, whose deposits account for the today's strong dust activity. Observations during the Bodélé Experiment (BoDEx) campaign in 2005 showed that dust generation in the Bodélé depression is very complex due to the prevalent diatomite sediments [*Washington et al.*, 2006b]. In this area, the processes of saltation and sandblasting occur where transport of sand sized quartz particles from the surrounding sand dunes is pronounced, largely at the northeastern end of the diatomite deposits where the dune density is highest. However, over most of this sediment of the Bodélé an unusual process of 'auto-abrasion' occurs; in which saltating diatomite aggregates themselves disintegrate into fine dust sized particles [*Warren et al.*, 2007]. Such complexity of dust generation mechanisms has yet to be parameterised in dust models. A key requirement of dust models is to simulate accurately the dust flux from regions where dust mobilisations are quite common representing a test of model reliability.

A sensibility analysis of wind dynamics and model dust flux estimates from the WRF-Chem with GOCART module is evaluated and compared to estimations from a recent model inter-comparison by *Todd et al* [2008a]. Experimental design of the WRF-Chem was arranged in accordance to the used in *Todd, et al* [2008a]. In the WRF-Chem model based on GOCART module, dust sources are prescribed based on topography characteristics and vegetation [*Ginoux et al.*, 2001]. The erodible fractional map is derived from AVHRR at a higher resolution 0.25° X 0.25° (Figure 4.1).

The parameters analysed correspond to driving winds, the processes of dust emission, resulting dust burden and transport. The model horizontal and vertical resolution, domain size, driving boundary conditions, land surface conditions, run duration, and dust physical were configured to be as more compatible as possible to those from *Todd et al* [2008]. Although the differences between models configuration mean the model outputs need to be carefully interpreted, the results provide an initial standard of

model uncertainty. Dust quantities were integrated over the size range of 0.1-10μm diameter to represent that component involved in long range transport. In the WRF-Chem version used in this work (3.1) AOT is not derived. However, for comparative purposes, a calculation of τd following the ratio: M/ τd = 2.7 g m−2, as estimated in several field experiments combined with AERONET measurements and models from *Koren et al* [2006].

Model output and observations are compared at three spatial scales. (i) Point quantities at Chicha (ii) Quantities averaged over an area that approximates the area of exposed diatomite sediment, defined by the grid cells lower than the 250m surface height contour in the study domain. (iii) Quantities averaged over the domain 14-21°N, 14-21°E, which covers the area from the northern point of lake Chad in the southwest to the Tibesti - Ennedi gap in the northeast (Figure 4.1), encompassing the dust plumes in their entirety.

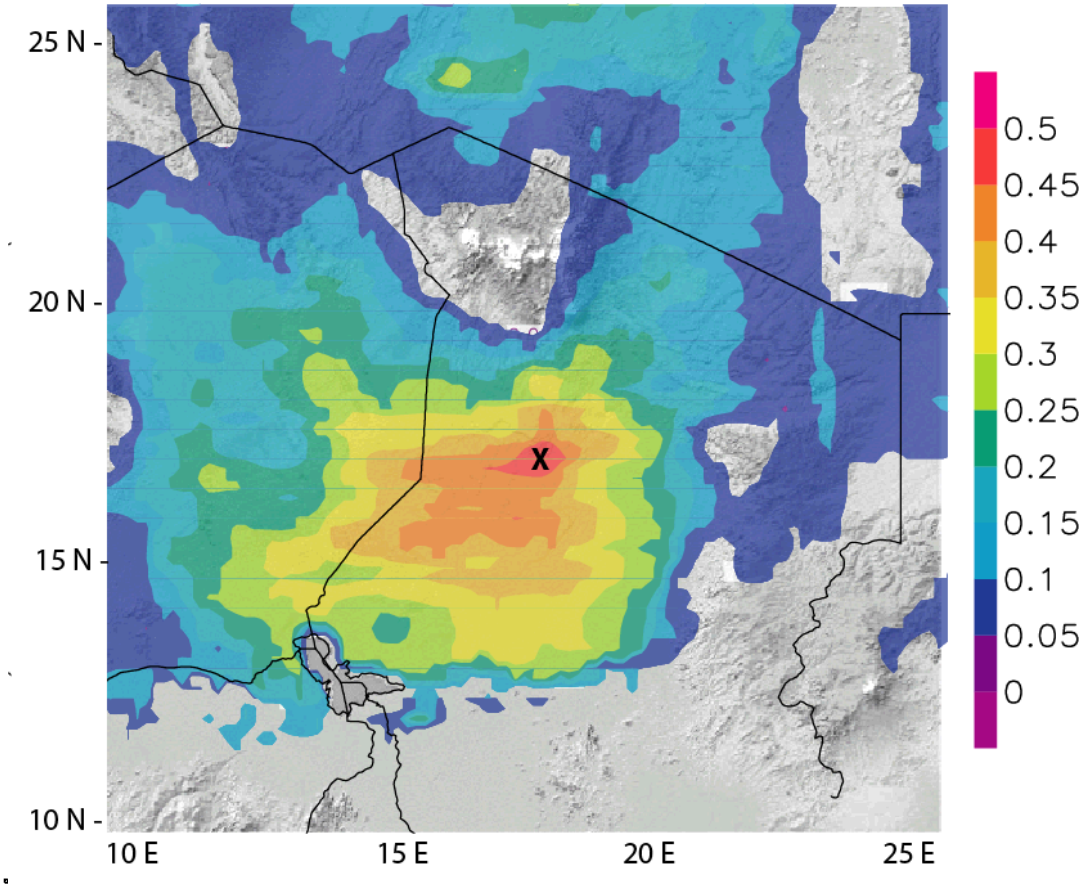

Figure 4.1: Fraction of erodible area used by the GOCART module (shaded), Chicha location (x). Map Source: Shuttle Radar Topography Mission (SRTM), NASA.

4.2. Synoptic Conditions

Climatic characteristics of the Bodélé Region are described on detail in *Washington and Todd* [2005] and *Todd et al* [2007]. Overall, in winter, North Africa circulation is dominated by the *Harmattan* winds, driven by north-south pressure gradient between the mean high-pressure ridge centred over Libya (the Libyan High) and the equatorial trough (Figure 4.2.a). The Bodélé Low level Jet (LLJ) is a key feature of the mean low-level atmospheric circulation over the Bodélé [*Washington and Todd,* 2005] which coincides with the north-easterlies' exit gap between the Tibesti and Ennedi mountains. From the analysis based on the ERA-40 reanalysis data, the Bodélé LLJ is embedded in the mean north-easterly *Harmattan* wind and is oriented NE-SW with a mean maximum of ~12m s^{-1}at 925hPa centred near 17°N, 19°E (Figure 4.2b). Mean wind speeds at 925hPa in excess of 11m s^{-1}extend over a large region from northern Chad to Lake Chad, a distance of some 1200km. The high wind speeds to the northwest of the Tibesti Mountains (centred near 22° N, 14° E) indicate a split in the Harmattan wind associated with the presence of the mountains. The north-easterly flow is channelled through the Tibesti-Enneldi gap (Figure 4.2.b) and the combination of a gap wind and downslope wind forcing acts to accelerate the LLJ by up to 50% [*Todd et al.*, 2008b]. Dust events occur when surface winds exceed the threshold velocity for dust emission (about 10m s^{-1} at 2m height, *Todd et al.*, 2008b) The large dust mobilisation corresponding for the period 10-12th March 2005 occurred when a blocking anticyclone over the northeastern Atlantic suddenly migrated eastwards and extended a pronounced ridge across North Africa, drawing an anomalously strong north-north-easterly flow across the Bodélé region (Figure 4.2.c). The structure and duration of this circulation pattern is quite typical condition for Bodélé dust events [*Washington and Todd*, 2005], resulting in pronounced dust emission over 3 days.

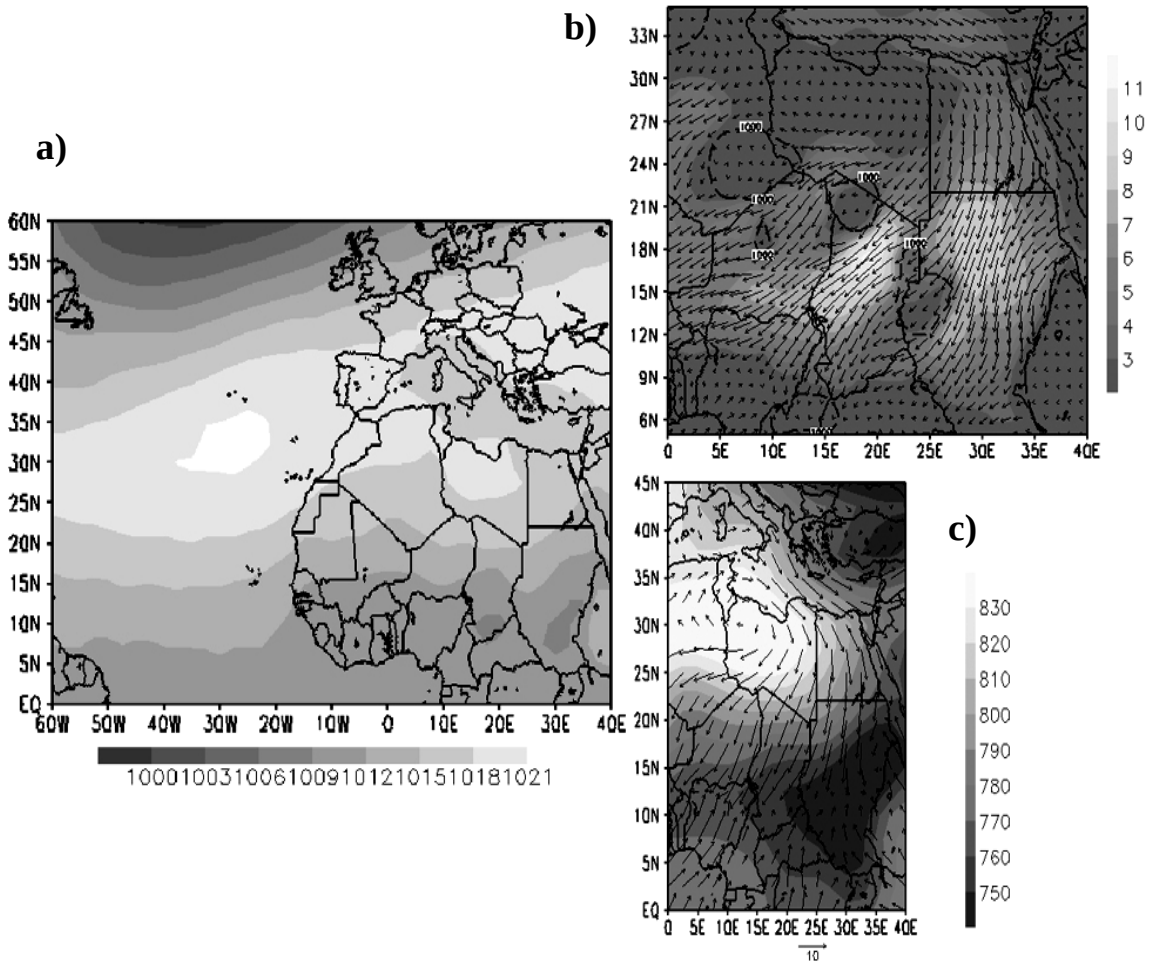

Figure 4.2: (a) Mean (1979-2001) winter season SLP (hPa) (b) Mean winter season 925hPa wind speed (m s-1) (c) SLP (hPa, shading) and 925hPa wind (m s-1, vectors) anomalies for 10-12th March 2005. Source: NCEP/NCAR Reanalysis Product at 2.5°x 2.5°x.

4.3. Model simulations and discussion

The next section evaluates briefly outputs of the WRF-Chem. Results are compared with those from models used in *Todd, et al,* [2008a]. Overall, the discussed results do not rank the model performance but rather highlight the degree of uncertainty in various aspects of model simulation.

4.3.1. Regional winds

The WRF-chem provides similar representation of the spatial structure of the LLJ and 10m height winds (Figure 4.3). Key features include a split jet north and south of the Tibesti Mountains with peak wind speeds located immediately south of Tibesti. This tunnelled winds flow over Chicha which an intensity up to 20 m s^{-1} (Figure 4.3, red cross).

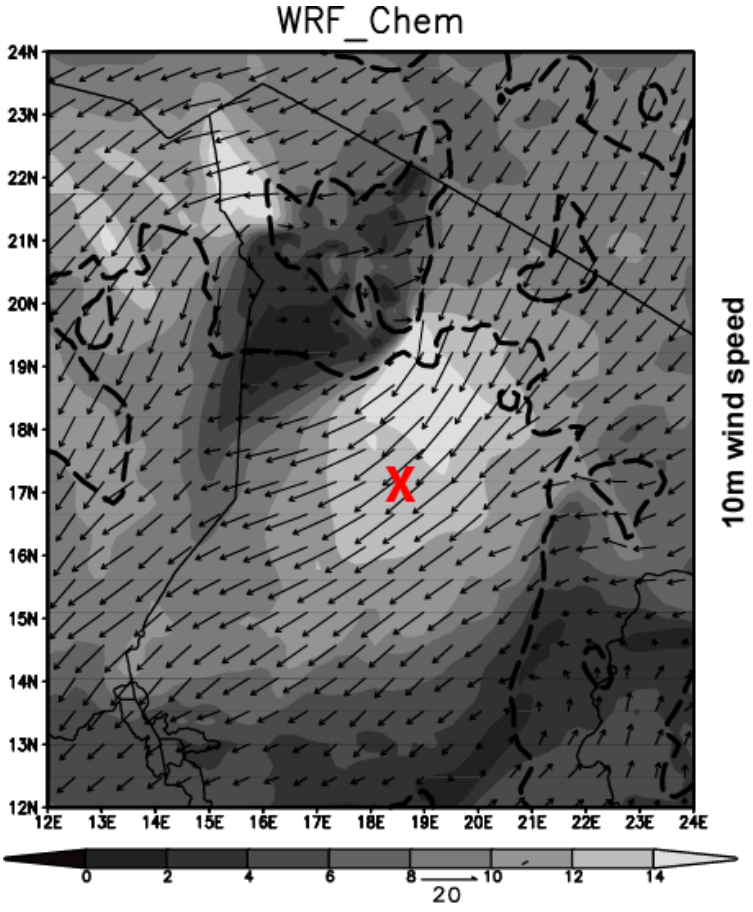

Figure 4.3: Model simulated 925hPa winds (vectors) and 10m scalar wind speed (ms^{-1}, shading) at 0900UTC on 10th March 2005. Red Cross indicates location at Chicha.

The model also simulates well the day-to-day variability (Figure 4.4.a), including the diurnal variability in a better extent than models used in *Todd et al* [2008a]. All models except RAMS-DPM have pronounced diurnal cycle in surface winds and LLJ but have smaller amplitude than observations (Figure 4a). Only WRF-Chem followed by the DREAM model captures the diurnal phase of wind speed maxima at 09.00UTC consistent with observations. All other models tend to produce the peak rather too early by ~3hrs typically. In these models the diurnal cycle of near surface wind speed is in phase with LLJ jet core such that downward mixing of nocturnal LLJ may not be well simulated. There does not appear to be a relationship between model horizontal or vertical resolution and the accuracy of near surface wind speed estimates.

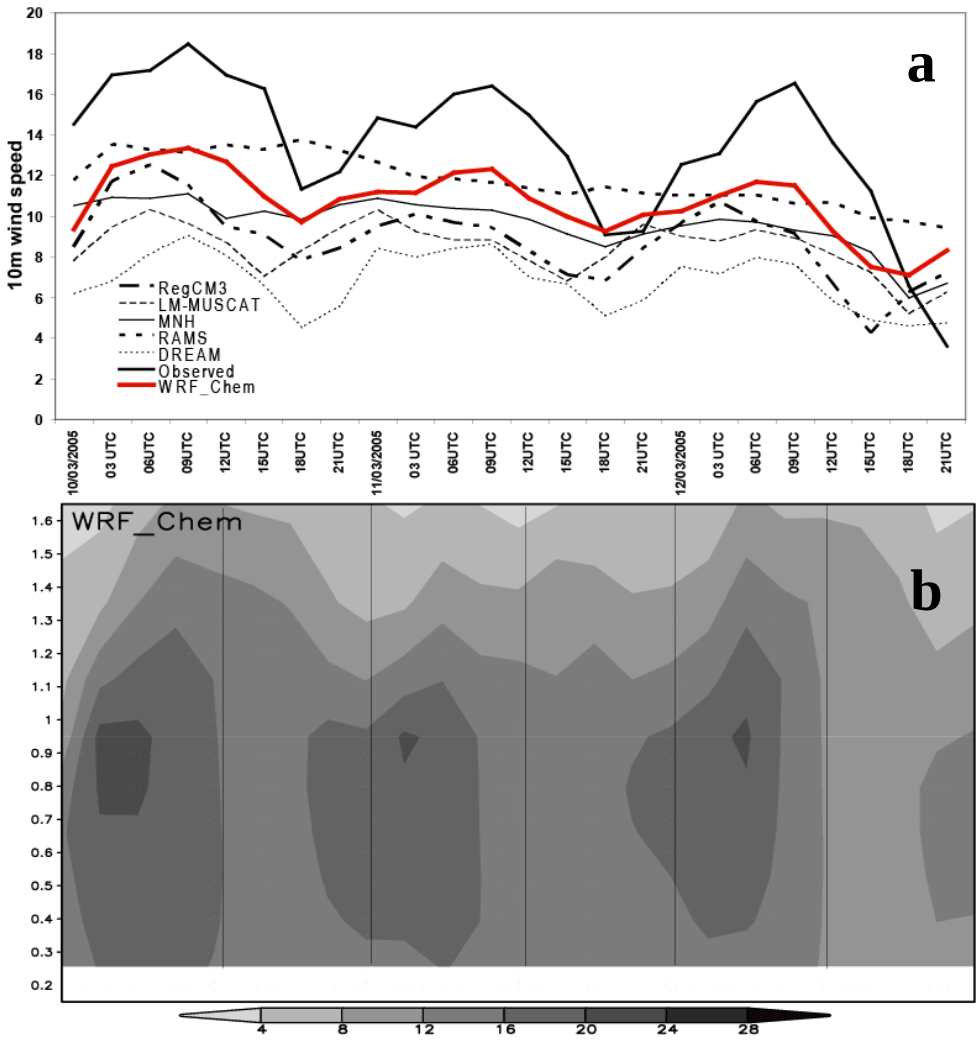

Figure 4.4: a) Time series of in-situ and model observations at 10 m height wind speed at Chicha (ms $^{-1}$). b) Timeseries of model simulated vertical profile of wind speed at Chicha (m s^{-1}).

WRF-Chem is able to represent the nocturnal LLJ maximum peak coincident with observations. It also shows a nocturnal LLJ maximum peaking at an elevation about 1000m at around 03.00UTC and with a similar structure and magnitude to those shown in *Todd et al* [2008a] (Figure 4.4.b). At this height where the LLJ is located, the peak wind speed reaches up to 25m s^{-1} on the 10^{th}, likely to be slightly lower that the real LLJ wind speeds.

Todd et al. [2008b] undertook a sensitivity study of the MM5 mesoscale model for near surface and boundary layer winds over the BoDEx period. They note that there is a factor of ~2 variation in mean and peak wind speeds over the BoDEx period using MM5 under various configurations. Simulated winds are most sensitive to the model Planetary Boundary Layer (PBL) scheme and vertical resolution in the lowest 200m. 10m wind speeds from the models in the present study lie within the range simulated using the MM5 model in *Todd et al* [2008b]. Under an optimised configuration (PBL scheme, 15 vertical levels in lowest 1000m with lowest level at 2m, z_o=0.001m) MM5 estimated that surface wind speeds and phase are close to observations. This suggests that improved representation of the surface and low level winds responsible for emission and transport of dust in these models would be possible with careful configuration. Overall, the WRF-Chem just underestimates 10m mean height winds by 12% whereas for other models used in *Todd et al* [2008a], the percentage varies between 13-50% (Table 4-1).

Table 4-1: Models Results from mean 10-m height wind speed

Variable/ Quantity	**Averaging time period**	**Averaging area**	**WRF_ Chem**	**Range of model results by *Todd et al.* (2008a) (1)**
10m height wind speed (m s^{-1})	10/3/05-12/03/05	14-21°E, 14-21°N	7.63	4.98-8.34
10m height wind speed (m s^{-1})	10/3/05-12/03/05	Chicha	10.56	6.78-11.73

(1) LM-MUSCAT, Meso-NH, RAMS-DPM, DREAM

4.3.2. Dust emission and transport

The spatial structure in dust emission estimates (Figure 4.5) from WRF-Chem is broadly comparable with those estimates by RAMS-DPM, LM-MUSCAT and RegCM3 with emission restricted to areas of low elevation close the Bodélé Depression. The WRF-Chem produces emissions in known dust preferential sources, which represent well the aerial extent of the localised outcrops of diatomite sediment. These features are identified as the dust sources regions in satellite observations [i.e. *Prospero,* 1990, *Engelstader et al*, 2007], although not in precisely the same location [view *Todd et al* , 2008a; Figure 6]. In the model intercomparison, these emissions are activated by saltating sand particles via the *Marticorena and Bergametti* [1995] emission parameterisation. In the GOCART module, saltation bombardment approximated by an expression similar to the empirical formula developed by *Gillete and Passi* [1988] and modified by *Ginoux et al.* [2001]. This parameterization is similar to the one used in LM-MUSCAT, hence a similitude in spatial distribution in emissions. The emissions for WRF-Chem and LM-MUSCAT largely come from regions north of 17°. In this model, (as for GOCART) preferential dust sources are parameterised to ensure that areas of high dust productivity are co-located with enclosed topographic depressions including the Bodélé depression [*Tegen et al.*, 2006].

Dust emitted from the surface is transported in the low-level northeasterly winds. As a result, the model simulates NE-SW oriented dust plumes, which have the fundamental characteristics of the observed data (Figures 4.7 and 4.8). Thus, despite small-scale differences in the location of dust source regions the coherent northeasterly LLJ results in dust plumes that are generally good representations of reality. Nevertheless, the WRF-Chem and most models used in the intercomparison produce a tongue of high atmospheric dust loadings extending to the north of the main NE-SW oriented plume, close to the Chad-Niger border north of about 17°N. Satellite estimates of AOT do not show elevated AOT values there (Figures 4.8). The time evolution of the dust plumes shows rapid transport to the southwest in all cases, with the dust transported in distinct diurnal “packets” in most cases. The speed of propagation for dust transport to 14°E (the longitude of Lake Chad) is around 12h for WRF-Chem. For other models time differs between about 9 h for Meso-NH to about 15 h for DREAM.

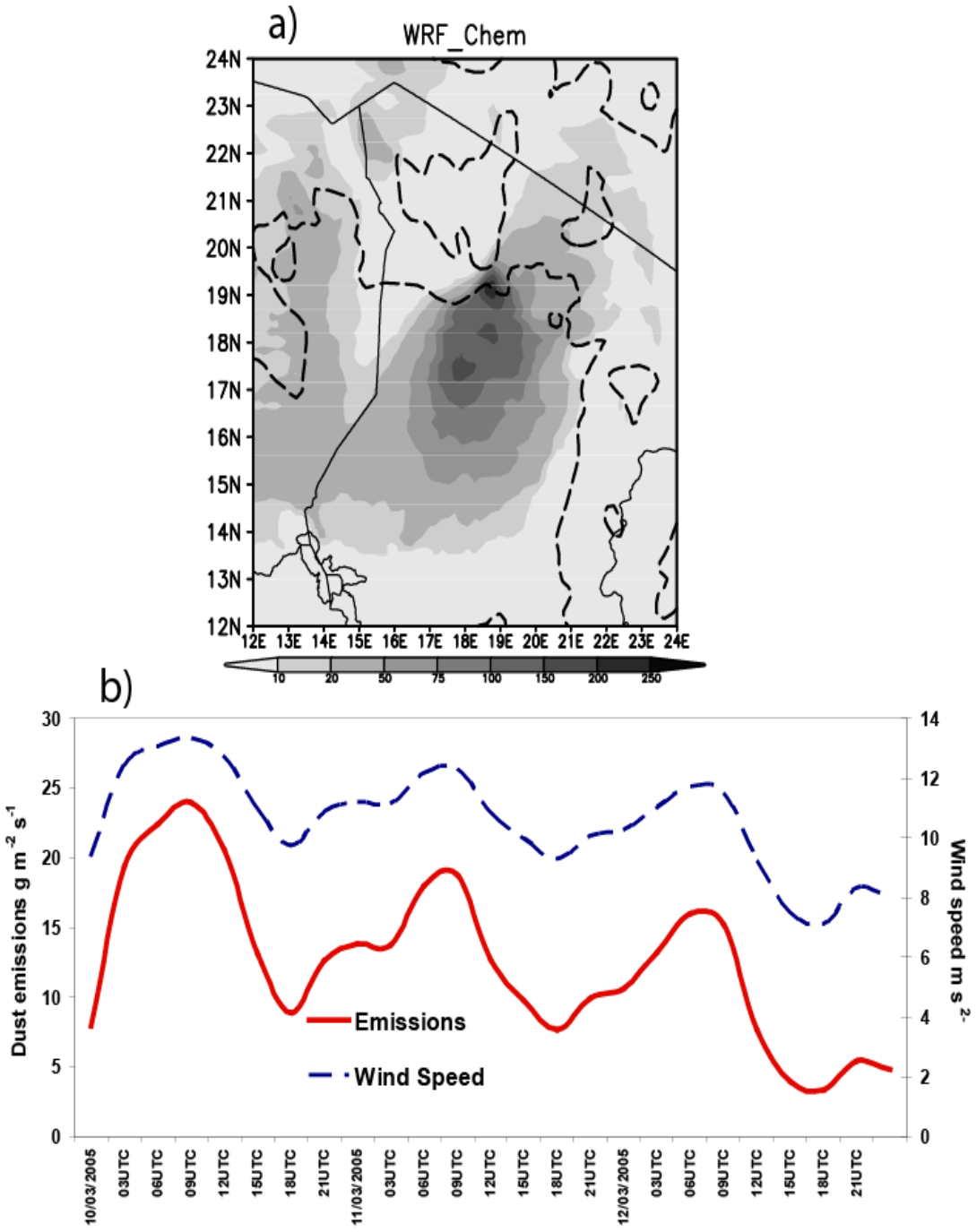

Figure 4.5: Model surface dust emissions, a) Mean rate 10-12 March 2005 (g m-2 day-1). Dashed lines represent the 500-m and 1000-m surface elevation. b) Timeseries at the location of Chicha (17°N, 18.5°E).

At the location of Chicha, dust emission matches the diurnal cycle of near surface winds, such that the WRF-Chem and the models evaluated in *Todd et al* [2008a] do simulate a diurnal 'pulsing' of emission (Figure 4.5b). Mean emission from WRF-Chem and the models used in the intercomparison (Table 4-2) show an approximately two-three-fold range in mean and peak dust emission at the location of Chicha and averaged the wider domains. Estimates of total emission from the area approximately co-located with the exposed diatomite within the Bodélé depression itself were calculated from the product of the mean emission rate over the area less than 250m elevation (which approximates the diatomite location) and the area of diatomite (10,800km^2) derived from MODIS surface reflectance data. Over the three days 10-12th March 2005, the WRF-Chem estimate is 2.3Tg, falls in the range of model estimates by *Todd et al.* [2008a]. In their model intercomparison, the estimates range between 1.4Tg for RegCM3 to 3.6Tg for RAMS-DPM (Table 4.2). *Todd et al.* [2007] estimated the total dust flux from the Bodélé during the 3-day dust event of 10-12th March 2005 using a simple relationship of surface wind speed and vertically integrated dust flux relationship derived empirically from observations at Chicha, then scaled to the entire area of diatomite sediment. Their estimate was 3.54Tg, which falls at the upper end of the range of model estimates. It should be noted, however, that the models do not all show peak emission be collocated with the region <250m height (Figure 6). The equivalent figures for the entire domain (12-21˚E, 12-21˚N) for the WRF-Chem is 27.04Tg, whereas the estimates in *Todd et al.* [2008a] range from 21.1Tg for RegCM3 to 42.5Tg for RAMS-DPM (Table 4-2). The DREAM estimates are highest as it produces the largest area of dust emission.

Table 4-2: Models Results, dust emissions

Variable/ Quantity	Averaging time period	Averaging area	WRF_Chem	Range of model results by Todd, et al. (2008a) (1)
Peak emission ($gm^{-2}s^{-1}$)	12.00UTC 10/3/05	Chicha	$1.90*10^{-4}$	$3.38*10^{-3}$-$5.92*10^{-4}$
Peak emission ($gm^{-2}s^{-1}$)	12.00UTC 10/3/05	14-21°E, 14-21°N	$4.77*10^{-4}$	$2.58*10^{-4}$- $5.61*10^{-4}$
Mean emission ($gm^{-2}s^{-1}$)	10/3/05-12/3/05	Chicha	$1.19*10^{-3}$	$4.1*10^{-4}$- $1.38*10^{-3}$
Mean emission ($gm^{-2}s^{-1}$)	10/3-05-12/3/05	14-21°E, 14-21°N	$2.6*10^{-4}$	$1.39*10^{-4}$-$2.81*10^{-4}$
Total emission (Tg)	10/3-05-12/3/05	Area of diatomite	2.3	1.4- 3.6
Total emission (Tg)	10-3/05-12/3/05	14-21°E, 14-21°N	27.04	21.1- 42.5

(1) LM-MUSCAT, RegCM3, RAMS-DPM

Mean dust concentration in the lowest model layer show a wide range between the WRF-Chem and the models used for comparison. Over the study domain the dust concentration from the WRF-Chem presents values up to 10000 μm m^{-3} (Figure 4.6a). At Chicha (17˚N, 18.5˚E) dust concentration at the lowest level ranges from 2000 to 8000 μm m^{-3} during the studied period from the 10-12 March 2005 (Figure 4.6b). These results fall into those from *Todd et al.* [2008a]. In the model intercomparison, for the simulated domain, the MESO-NH has the highest mean values, up to 30,000μm m^{-3} and DREAM the lowest, about one tenth of that of MESO-NH. At Chicha, model mean dust concentration values range over about one order of magnitude from 2100 (DREAM) to 25,200μg m^{-3} (Meso-NH) (Table 4.3). Similar values are estimated over the region with elevation <250m. In most models dust concentration at Chicha shows the diurnal pulsing and peaks at 09.00UTC on the 10th March when RAMS simulates the highest value of 78,000ug m^{-3} (Figure 4.6b). For WRF-Chem, this maximum diurnal pulse is shown earlier (06.00 UTC) with a maximum value of 7254 μm m^{-3}. In-situ observations at Chicha are limited but a maximum value of 9900μg m^{-3} at 2m height was observed at 10.00UTC on the 11th (Figure 4.6b). Observed dust concentrations therefore lie towards the lower end of the range simulated in the dust models. Caution must be exercised in comparing the models due to the varying heights of the lowest model layers. As noted above dust emission fields were not available from Meso-NH and DREAM. However, as MESO-NH produces the highest dust concentration of all models it is likely to have the highest emission. This may be related to the soil data used whereby the soil texture is set to 100% sand across the entire domain 14°N-17°N.

The time-mean column dust mass at Chicha for the WRF-Chem is 3.44 g m^{-2} that falls in the estimations by other models from 1.91g m^{-2} in RegCM3 to 24.5g m^{-2} in RAMS-DPM (Table 4-3) representing a 12-fold difference between models. At Chicha, the time distribution of dust mass is similar to most models with a peak between 09.00 and 12.00UTC on the 10th March and subsequent decline (Figure 4.7b). Estimates based on in-situ data from *Todd et al.* [2007] fall towards the lower end of the model range closest to the estimates by WRF-Chem followed by the RegCM and DREAM model. However, the significant diurnal variation in the in-situ data is barely distinguished in the WRF-Chem timeserie. On the spatial averaged domain mean column integrated dust mass for the three days period, WRF-Chem shown values of 2.78 gm^{-2} (Table 4.3). Estimates from other models show about a 15-fold difference in mean column dust mass between RegCM3 and RAMS-DPM spatially averaged (0.77 and 11.61 gm^{-2} respectively).

Table 4-3: Models Results, dust concentration and mass flux

Variable/ Quantity	Averaging time period	Averaging area	WRF Chem	Range of model simulations by Todd, et al. (2008a) (1)
Lowest level dust concentration ($\mu m\ m^{-3}$)	10/3-05-12/3/05	Chicha	4671	5400-26000
Column integrated dust mass (gm^{-2})	10/3-05-12/3/05	Chicha	3.44	1.91-24.5
Column integrated dust mass (gm^{-2})	10/3-05-12/3/05	14-21°E, 14-21°N	2.78	0.77-11.61
Dust mass flux				
Net westward dust flux at 16°E (Tg day^{-1})	10/3/05-12/3/05	14-21°N	1.86	0.36-10.05
Net westward dust flux at 12.5°E (Tg day^{-1})	10/3/05-12/3/05	14-21°N	0.51	0.26-1.84

(1) LM-MUSCAT, RegCM3, RAMS-DPM

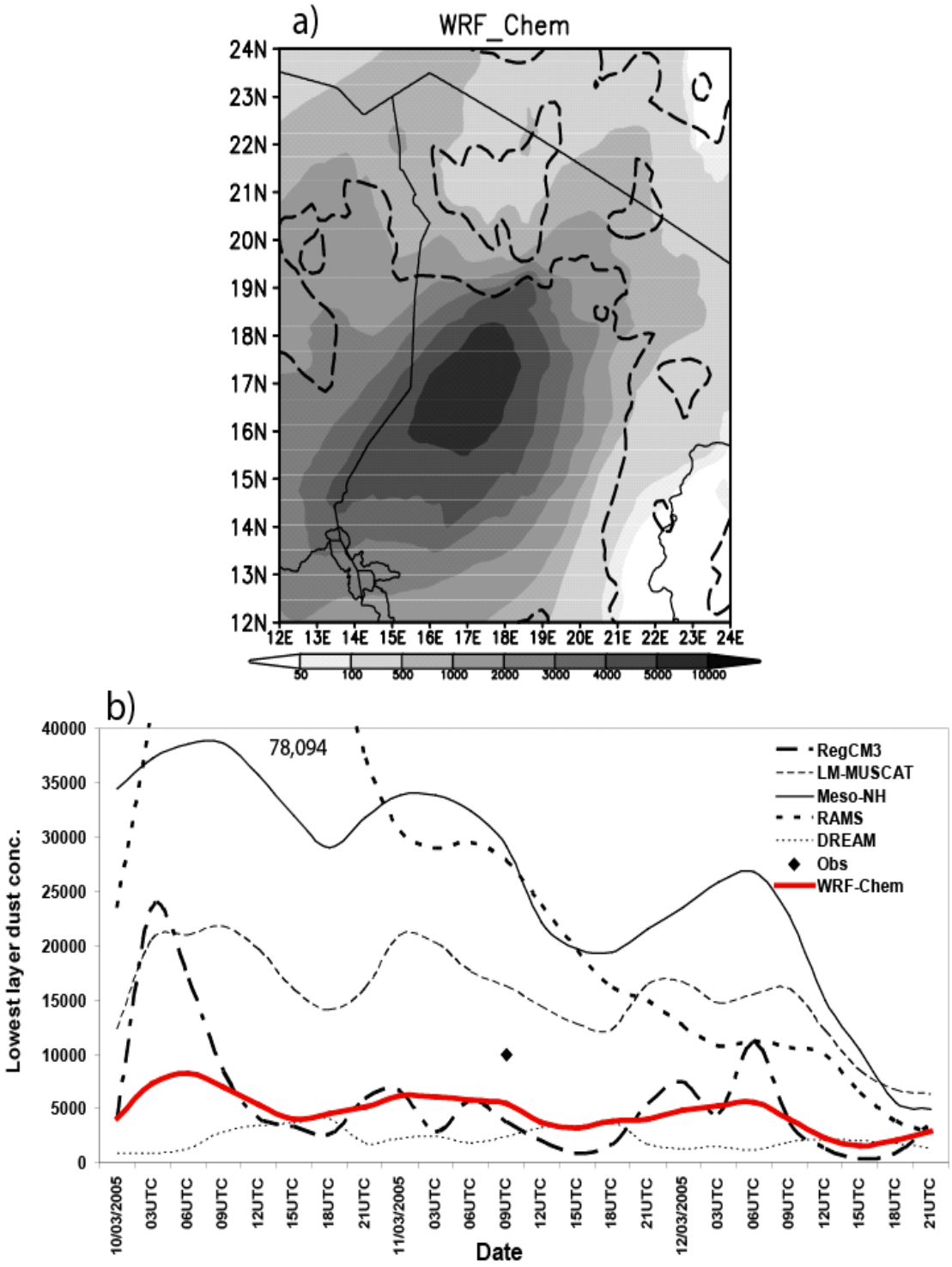

Figure 4.6: Model simulated concentration in lowest layer (µg m^{-3}). a) Mean 10-12th March 2005. Dashed lines represent the 500-m and 1000-m surface elevation. b) Timeseries at the location of Chicha (17°N, 18.5°E).

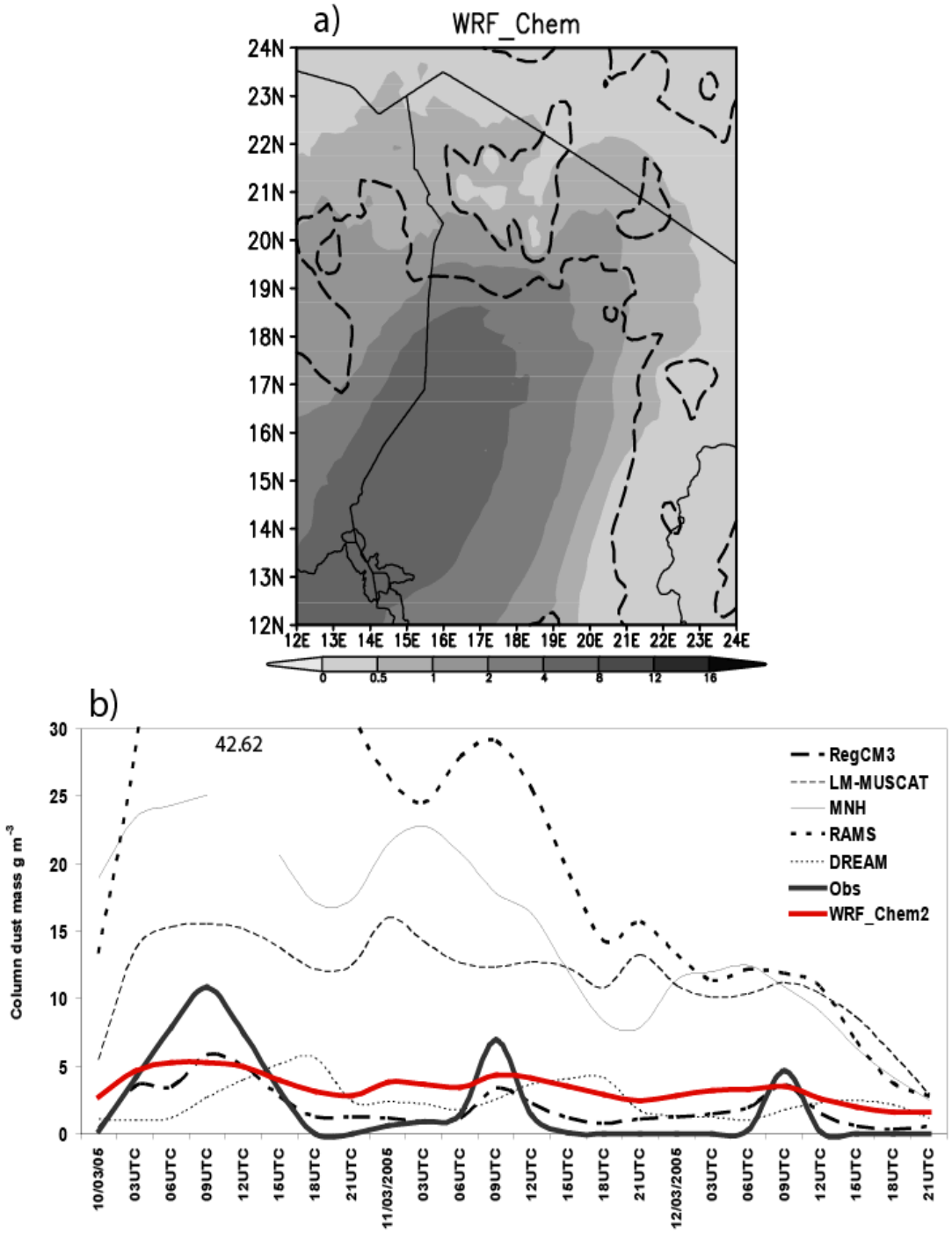

Figure 4.7: Model vertically integrated dust mass (g m^{-2}). a) spatial mean 10–12th March 2005. b) Timeseries at the location of Chicha.

4.3.2. Aerosol Optical Depth

At this stage for the present study, the direct integration of Aerosol optical Depth (τ) in the WRF-Chem GOCART scheme is still not possible. Nevertheless, for comparative purposes, we do calculate τ following the ratio: $M/\tau = 2.7\ g\ m^{-2}$, as estimated in several field experiments combined with AERONET measurements and models from *Koren, et al.* [2006].

There is a good agreement between the estimated AOD from the WRF-Chem model and AOD estimate from Deep Blue satellite algorithm regarding spatial structure at 12.00 UTC for the 10 and 12th March (Figure 4.5). The spatial structure agrees very closely to the models used in the model intercomparison (see figures 10 and 11, *Todd, et al* [2008a]). However, there is an approximately seven-fold range in simulated AOT at all spatial scales MESO-NH estimates the highest AOT and RegCM3 the lowest, the WRF-Chem estimation falls in the middle range of these estimates. Satellite estimates of AOT from the Deep Blue algorithm applied to SeaWifs and AI from OMI data indicate the distinct dust NE-SW oriented plumes. Although the location of the dust plume in the WRF-Chem seems to agree with the observed AOD, the areal extent of the plume might be slightly overestimated. Whilst the dust plume in the Deep Blue extents North up to 17˚N for both 10 and 12 March 2005, the estimated AOD in WRF-Chem extends up to 18˚N and 19˚N. Nevertheless, this overestimation does not have the same extent as MESO-NH and LM-MUSCAT, where high values of AOD are seen covering a large portion of the border of Chad and Niger up to 20˚N. The spatial structure is particularly well represented by RegCM3 and RAMS-DPM. We should be aware of potential errors in the Deep Blue aerosol product but the Aerosol Index product [*Herman et al.*, 1997] from the Ozone Monitoring Instrument (OMI, not shown) presents a very similar spatial structure to the Deep Blue AOT.

A quantitative comparison of AOT is problematic as the Deep Blue algorithm saturates at a maximum AOT of 3.0. At Chicha limited observations of AOT were made during the afternoons of on 11th and 12th March. On both days the decline in wind speeds after midday was such that transport exceeded local emission (which ceased in early afternoon) and AOT declined rapidly. Overall, the combined in-situ and satellite observations indicate slight overextension Northwards of dust plume by the WRF-Chem,

an overestimation of AOT by MESO-NH and LM-MUSCAT and underestimation by RegCM3.

Previous studies have clearly indicated substantial long-range transport of dust from the Bodélé [*Koren et al.* 2006]. The impact of this on climate and remote ecosystems will depend on the mass flux from the region. Here, we derive the mass flux of dust from the region estimated by each model from the product of the wind speed and dust concentration in each model layer, summed over the atmospheric column. Dust transport is dominated by a westward flux in the *Harmattan*north-easterly flow such that in the vertical integration at levels where the zonal wind component is eastward the dust flux is considered to be negative. This net flux is summed over the latitude range 14-21°N. Therefore, the result represents the net westward export of dust mass from the entire region towards West Africa. Estimates of westward dust flux over the 3-day period leaving Chad at 16°E in the WRF-Chem is 1.86 Tg day^{-1} whereas estimates in the model intercomparison range widely from 0.35Tg day^{-1} from RegCM3 to 10.05Tg day^{-1} from RAMS-DPM (Table 4-3). *Koren et al.* [2006] estimate the long range dust flux from the Bodélé by identifying dust plumes from MODIS satellite imagery and determining their average dimensions after one day when the plume lies to the west of lake Chad. The dust mass within the plume was then derived from the product of plume area and column integrated dust mass, estimated from the satellite MISR-derived AOT. The average plume mass over the period October 2003 to October 2004 was estimated at 0.77Tg day^{-1}. Assuming these 'one day old' plumes identified from MODIS/MISR are centred on 12.5°E then the equivalent estimates in WRF-Chem is 0.51 Tg day^{-1}. This amount lies within the model intercomparison estimates (0.26, 1.84 and 0.49Tg day^{-1} from the RegCM3, LM-MUSCAT and DREAM models, respectively). As such, the 'observational' estimates of *Koren et al.* [2006] lie within the model range, although it is not know to what extent the dust event of 10-12th March 2005 is typical of the those in the period studies by *Koren et al*. (2006).

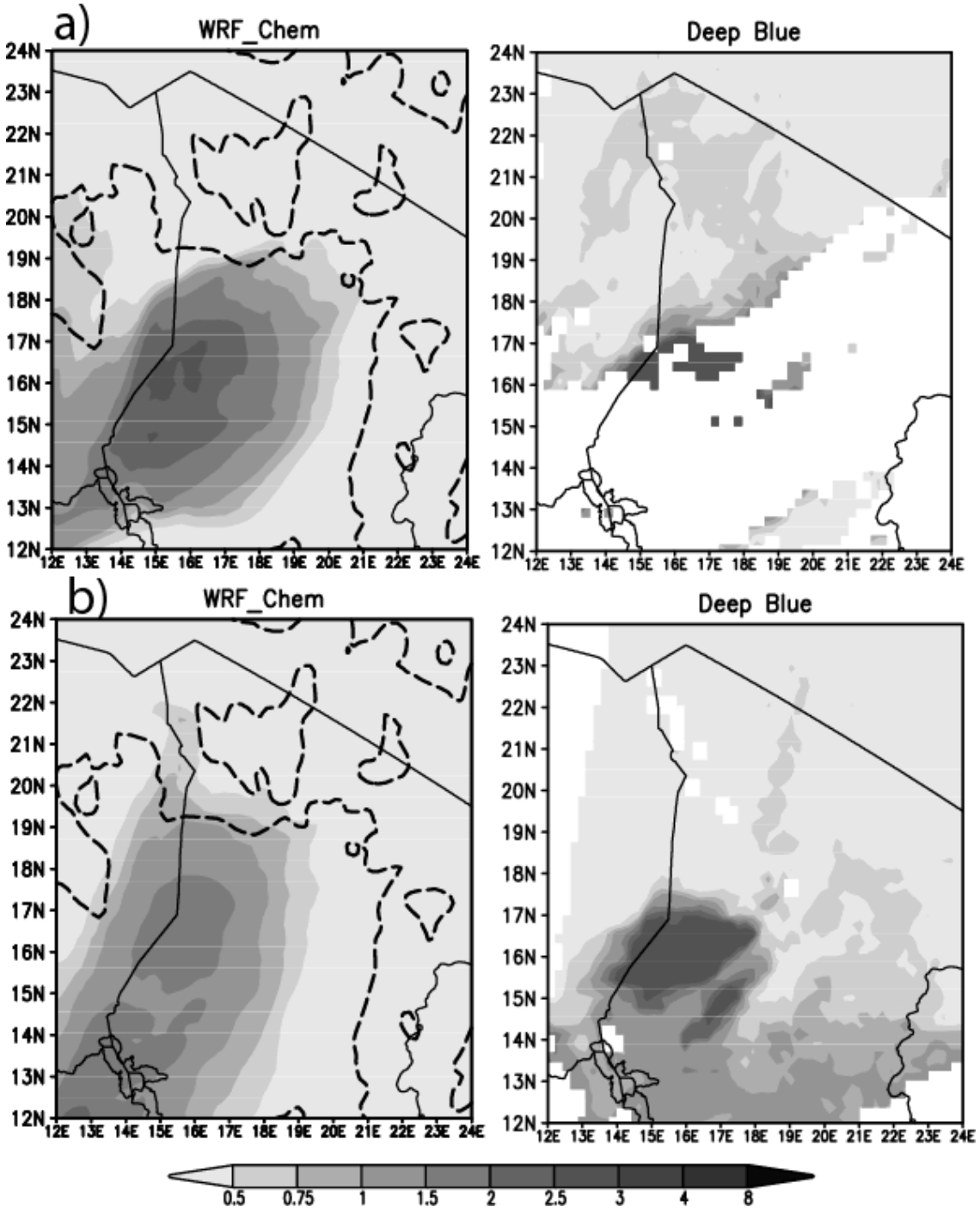

Figure 4.8: AOT estimated by WRF-Chem and Deep Blue satellite algorithm, a) 12.00UTC on 12 March 2005. b) 12.00 UTC on 12 March 2005.

4.4. Summary

In this section the performance of WRF-Chem model with a GOCART module was evaluated. The winds dynamic and model dust flux estimates over the Bodélé depression, Northern Chad were compared to estimations from a recent model inter-comparison by *Todd et al* [2008a]. To date, there is not documented information of dust emissions in North Sahara using WRF-Chem with the GOCART scheme at regional scale. Thus, this is the first time an evaluation of this nature was performed. Preferential sources were built using an erodible fractional map following the calculated source function *S* after *Ginoux et al.* [2001] and using a bare soil surface from the AVHRR at a high resolution 0.25° X 0.25°. Previous studies with the GOCART scheme at global scale [i.e. *Ginoux et a.l,* 2001; *Chin et al.,* 2002] use the AVHRR 1° X 1° bare soil surface map gives good results in large previously documented dust sources [i.e. *Prospero,* 2002; *Washington et al.,* 2003, *Schepanski, et al* 2008]. However, preferential sources derived from the previous coarse bare soil map within the Bodélé are missed particularly for Chicha (See Annex A). This is the first time that this bare soil surface database at high resolution was implemented to produce the erodibility map within the GOCART module.

Results show that WRF-Chem is able to calculate near surface wind speed more accurately than models used in *Todd et al.,* [2008] and it is the only model to depict diurnal cycle of winds. However, as in the model intercomparison, WRF-Chem underestimates wind speeds when compared with observations with a difference of 1.5-fold. These differences are greater during the early morning maxima, coincident with the phase shift of the diurnal cycle of the LLJ but the wind speed minima do not differ substantially. This is a quite positive advance compared with the model simulations in *Todd, et al.* [2008a] where models underestimated wind speed by up to 50% and the phase shift between the diurnal cycles of the LLJ and surface winds is not well resolved. In a comparable study of dust models over Asia, *Uno et al.* [2006] noted that for most locations wind speed observations lie within the range of model results.

Given that in the WRF-Chem GOCART dust scheme the dust flux is proportional to the third power of friction velocity, pulses of dust emissions do coincide with pronounced surface and lower level winds in the diurnal cycle. Nevertheless, small errors in wind speeds result might derive in large dust flux uncertainties. On the other hand, as dicussed in *Todd et al.* [2008a] the representation in models with highest wind speeds do

not produce the highest fluxes highlighting the importance of surface factors such as soil texture and surface roughness. The model generally shows good representation of Bodélé dust plumes over the period 10-12th March 2005 with emissions prominently generated in the Bodélé region. However, at local scale the sources of dust emission are spatially more widespread, relative to observations. This variation is not at greater than those shown by RAMS-DPM and LM-MUSCAT in the model intercomparison. The degree of model uncertainty reported for here is actually very similar to the range of mean emission and typical dust concentration from nine models compared for two dust events over all of East Asia by *Unoet al*. (2006). For sub-regions within East Asia the range is about one order of magnitude. This is somewhat greater than the uncertainty associated with model estimates of long-term mean global dust emission [*Zender et al.,* 2004], suggesting that model over and underestimation in various regions may cancel out to a certain degree.

There is a clear need for further research into other source regions in the Sahara, and elsewhere. This should include identification of the key preferential dust source regions, observation of the dust emission processes and determination of the associated soil characteristics at a resolution higher than that available from existing soil data sets. The inclusion of the geomorphological erodibility factor to account as preferential emission source into the WRF-Chem represents a good proxy to perform sensitivity test in areas well know as dust 'hot spots'. Although other satellite-derived estimates of surface roughness are available [e.g., *Marticorena et al.,* 2004] used in LM-MUSCAT and RAMS-DPM, dust models tend to rely on maps of soil texture (from which the dry soil size distribution is derived) with questionable accuracy in remote regions of the Sahara desert. There is a clear requirement for improved soil texture data for the Sahara that can resolve features like the diatomite deposits in the Bodélé depression. The results here demonstrate that the model dust emission is strongly associated with sandy soils such that the emission scheme itself may require modification in preferential source regions with similar characteristics to the Bodélé. It is important to determine to what extent the Bodélé is unusual among the source regions of the Sahara in this regard.

5 Sensibility analysis of a major Saharan dust outbreak (6th–11th March 2006) with RegCM3

5.1 Introduction

It is well known that most dust is emitted from preferential source regions often related to topographic depressions, fluvial sedimentary deposits or paleo-lake beds [*Prospero et al.*, 2002; *Washington et al.*, 2003]. Adequate representation of these sources has often been noted to be a problem for dust models. In this study, the performance of the Regional Climate Model third version (RegCM3) with an active dust scheme is evaluated.A major dust event of 6-11th March 2006 is analysed as a test case and described by *Slingo et al.* [2006], which produced some of the greatest dust emission in the last decade. Results of this work were already publish in the Journal of Geophysical Research (see *Cavazos et al* 2009).

5.2 Model configuration

The domain used for this simulation comprises most of North Africa centred on 21° N and 2.5° E (Figure 5.1), with horizontal resolution of 40 km and 23 vertical layers. The model was integrated over the period of 4-11th March 2006. A number of experiments were performed with RegCM3. The nature of these experiments is described in Table 2. In EXP2 a new data source on dust activation developed by *Schepanski et al.* [2007] is used (Figure 5.1). In this new data source or Data Source Activation Frequency map (hereafter, DSAF), active dust sources are identified from satellite imagery from the SEVIRI sensor on board the Meteosat Second generation (MSG) satellite.*Schepanski et al.* [2007] identified discrete dust plumes using the SEVIRI dust product and tracked these back to their source regions from successive 15-min SEVIRI imagery. By analyzing SEVIRI dust product data over the period March 2006 to February 2007 a data set of Dust Source Activation Frequency (DSAF), aggregated on a monthly basis at 1 degree resolution was produced. In EXP2 all model grid cells in which the DSAF is greater 1% were prescribed a soil texture class of the sand type. A total of 1587 additional grid cells with 100% sand were introduced to the default soil map. In both EXP1 and EXP2 dust is radiatively active.

In addition, the sensitivity of the results to the specification of aerosol optical properties is considered. In recent years there has been considerable discussion of the optical properties of mineral dust aerosols with observational studies indicating that dust is less absorbing at visible wavelengths than previously thought [e.g., *Kaufman et al*., 2001].

The shortwave radiative forcing (RF) sign is determined to a great extent by the Single Scattering Albedo values (*wo*) and represents the light scattering properties of mineral dust in the atmosphere. In the default configuration of RegCM3 the *wo* values are those defined in the OPAC (Optical Properties of Aerosols and Clouds) database [*Hess et al.*, 1998]. These values are rather lower than some more recent simultaneous remote and in situ observations suggest. According to the latest report of the Intergovernmental Panel of Climate Change (IPCC) [Forster et al., 2007], the single scattering albedo (*wo*) of pure dust at a wavelength of 0.67 mm is predominantly in the range 0.90 to 0.99, with a central global estimate of 0.96. To test the sensitivity to *wo*, a further experiment was conducted (EXP2b) identical to EXP2 except that the *wo* is increased on average +0.02 in the visible wavelengths (200–700 nm) for each one of the 4 bin sizes and in accordance with the more reflective aerosol type of *Helmert et al*. [2007].

Table 5-1: Model configuration

Experiment	**Description**
EXP-ND	The no-dust experiment in which the dust module is disabled
EXP1	The dust module is activated and the default soil map is used
EXP2	same as EXP1 except that soil texture is modified to represent preferential dust source regions.
EXP2b	Same as EXP2 but single scattering albedo (ωo) is modified as follows (default EXP1 values in parenthesis). (i) wavelength 0.35-0.64μm, ωo= 0.96 (0.94), 0.9 (0.88), 0.82 (0.80), 0.72 (0.70) for 4 dust size bins 0.1-1.0, 1-2.5, 2.5-5, 5-20μm diameter, respectively. (ii) wavelength 0.64-0.7μm, ωo= 0.99 (0.97), 0.91 (0.89), 0.88 (0.86), 0.77 (0.75) for 4 dust size bins.

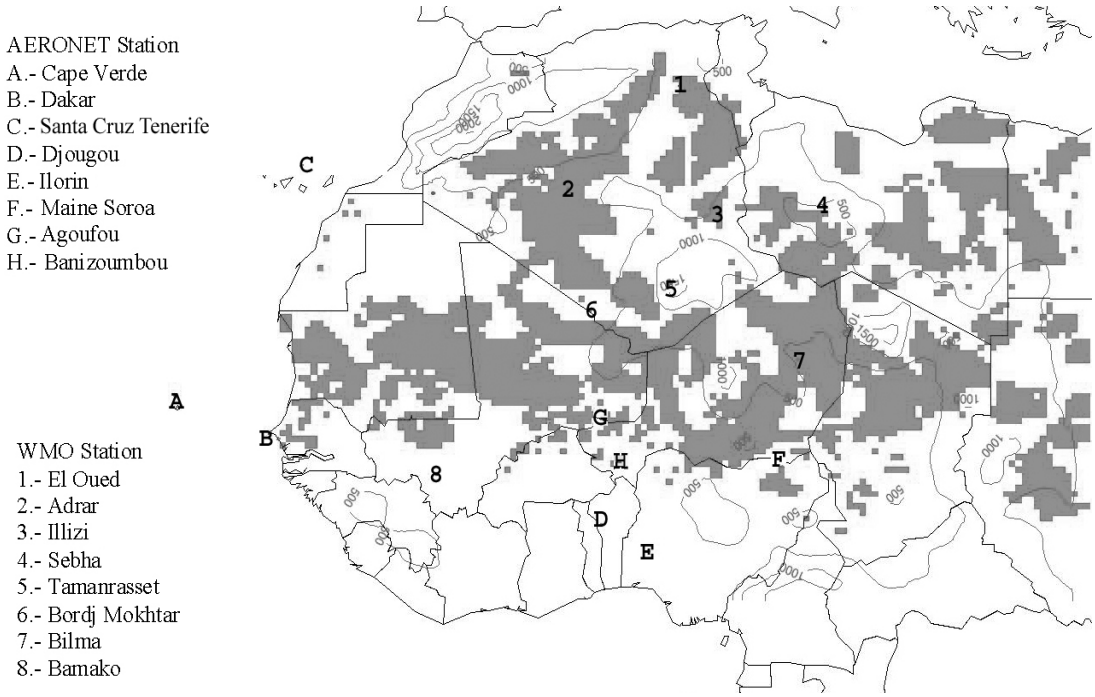

Figure 5.1: The model study domain. Surface elevation (m) is represented with contours. Locations of WMO (numbers) and AERONET stations (letters) used in this study are shown. Shading represents the areas where soil texture was adjusted using *Schepanski et al.* (2007) for EXP2.

5.3 Results and discussion

5.3.1. Synoptic conditions during the March 2006 event

Extreme dust events in many parts of the world are associated with synoptic scale atmospheric circulation changes. In the Sahara Desert, during winter (October to April), the low level circulation is dominated by persistent dry north-easterly winds, commonly named Harmattan wind [*Kalu,* 1979]. The *Harmattan* is driven by the pressure gradient between the subtropical high (with a mean ridge over Libya) and the equatorial trough (Figure 5.2a). The spatial structure of north-easterly wind velocity is influenced not only by the large scale pressure gradients but also locally by pronounced topographic features which act to channel the flow resulting in acceleration, mostly notably to the south of the Tibesti mountains over the Bodélé depression in northern Chad and to the north and south of the Aïr mountains of Niger [Engelstaedter and Washington, 2007; Schepanski et al., 2007; Todd et al., 2008b] .

Dust events are relatively infrequent in most parts of North Africa and they occur in winter when the synoptic scale circulation results in enhanced low level winds. The

large dust event of 6-11th March 2006 was characterized by rapid anti-cyclogenesis over the northwest Saharan region associated with an anomalous cold outbreak from the mid latitudes, which generated an anomalously strong northerly flow over the region. Recent studies [*Milton et al.,* 2008; *Tulet et al.,* 2008] describe this same large dust event highlighting the intensity of the dust emission, the horizontal and vertical transport and the effect that dust might have itself on atmospheric dynamic. The evolution of phenomena is represented in the Figure 5.2(b-e). Prior to the start of the dust event on the 5th March an intense cyclonic system developed over southern Europe and propagated eastward. By the 6th of March, the mid-latitude atmosphere in the European-Atlantic sector features an anomalous ridge-trough pattern with the trough centred over south-central Europe extending south over Libya (Figure 5.2b) and the ridge over the Eastern Atlantic, off the Iberian peninsular extending over Northwest Africa (Morocco and Algeria). This structure led to an anomalous northerly flow over northern Algeria from the 5th March onwards. Cold air advection causes large-scale negative temperature anomalies of ~10˚C over large parts of North Africa, enhancing anticyclogenesis. A striking feature of the atmosphere during this event is the very large ageostrophic component of the wind anomalies. As the mid-latitude low-pressure centre moved eastward, the ridging high extends south-eastward to cover most of the Sahara by the 8th March. At this time the northerly low level wind anomalies are centred over the central Sahara in the Libya-Chad sector. After the 9th March the positive pressure and wind anomalies declined.

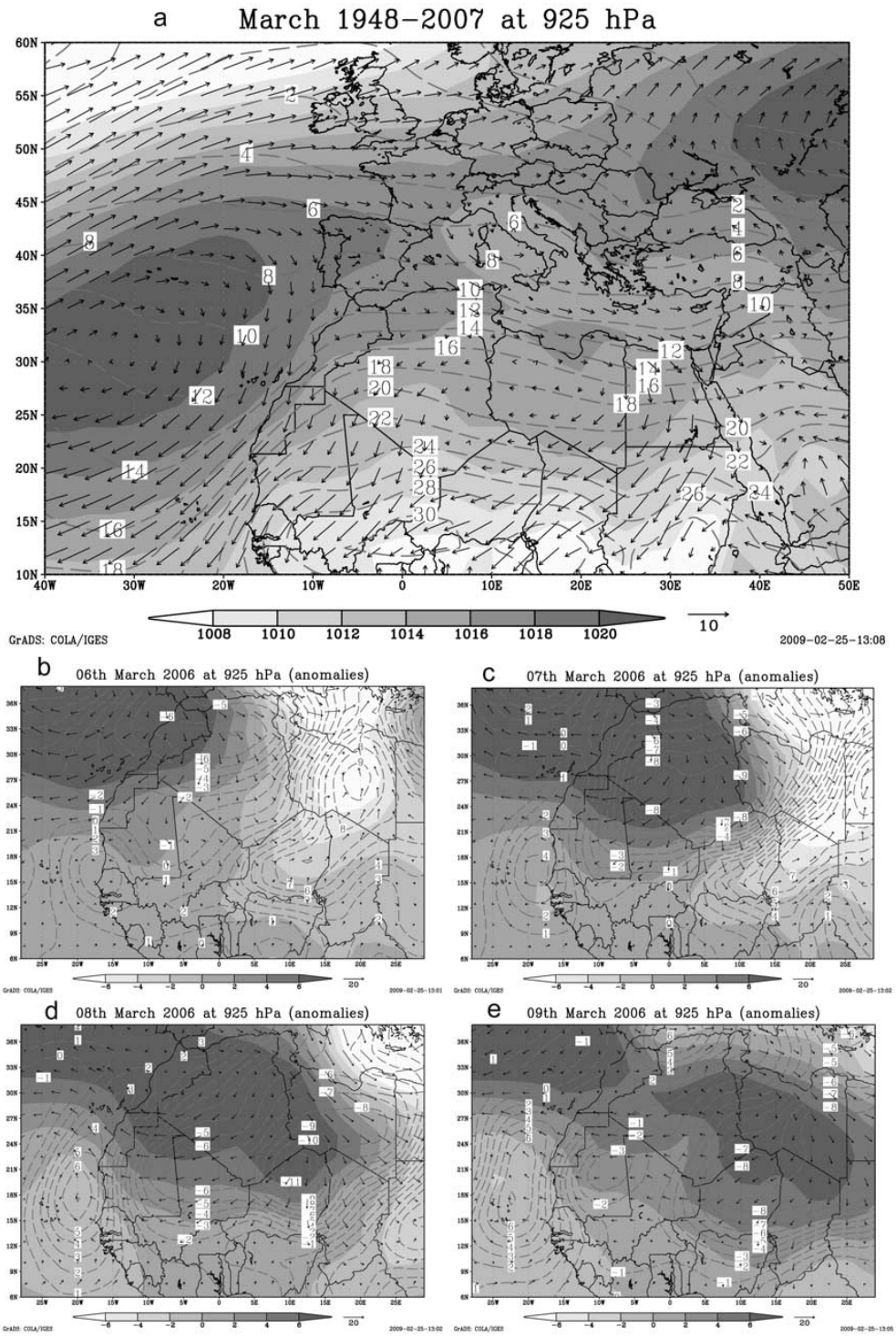

Figure 5.5.2: Atmospheric circulation pattern over the model domain, specifically sea level pressure (mb) (shaded) and 925hpa winds (vectors): (a) long term mean for March (b)-(e) anomalies on 6th-9th March 2006, respectively. Source: NCEP/NCAR Reanalysis Product at 2.5° x 2.5°

Synoptic weather station observations clearly depict the characteristics of the cold surge across the Sahara. At most stations the event is evidenced by a (i) pronounced drop in temperature (Figure 5.3) of up to 10˚C (ii) rapid shift to a northerly wind (Figure 5.4)

(iii) wind speed pulse during which time the velocity increases and declines rapidly over a period of about 24 hours (Figure 5.5) (iv) a decline in surface pressure prior to the wind speed maximum followed by an increase typically of about 15hPa (Figure 5.6). The southward propagation of the cold surge can be tracked from station to station from the timing of the wind speed maximum (Table 5.2). For example, the event was detectable over El Oued, northern Algeria at 1800UTC on the 5th March at the southern extremity at Bamako in southern Mali at 0900UTC on the 8th. In each case the wind speed maximum is coincident with a minimum in observed visibility (Figure 5.7), indicating a clear association of the wind and dust front features. The wind/dust front is followed by a sustained rise in surface pressure indicating that it occurs at the leading edge of the cold high-pressure surge.

5.2.2. Evaluation of model simulation

The model simulates reasonably well many key features of the meteorology. Most notably, the timing of the southward propagating northerly wind burst is well represented with respect to the station observations (Table 3, Figures 5.4 and 5.5). However, a systematic underestimation of wind speeds is evident by up to 50% in most cases. *Todd et al.* [2008b] tested the sensitivity of low-level and near-surface winds in the Bodélé region of northern Chad using the MM5 model and found that simulated winds are most sensitive to the choice of PBL scheme and vertical resolution. It is logical to conclude that the underestimation of LLJ wind speeds in RegCM3 results in part from limitations in the PBL scheme and vertical resolution. Day-to-day temperature anomalies are generally well represented in terms of timing and magnitude (Figure 5.3). In absolute terms the maximum temperatures are generally to within ±2˚C, but errors in night-time minima are larger. Notably, overestimated night-time minima at some locations by up to 5˚C (e.g. at Bilma) may be a result of an inability to resolve the fine structure of turbulent mixing of heat in the near surface layers [*Todd et al*, 2008b]. At other stations there is a slight under estimation of night-time minima which may be due to the absence of dust aerosol interaction with LW radiative flux. Overall, however, the model represents the space/time structure of the synoptic forcing reassuringly well even down to local scales.

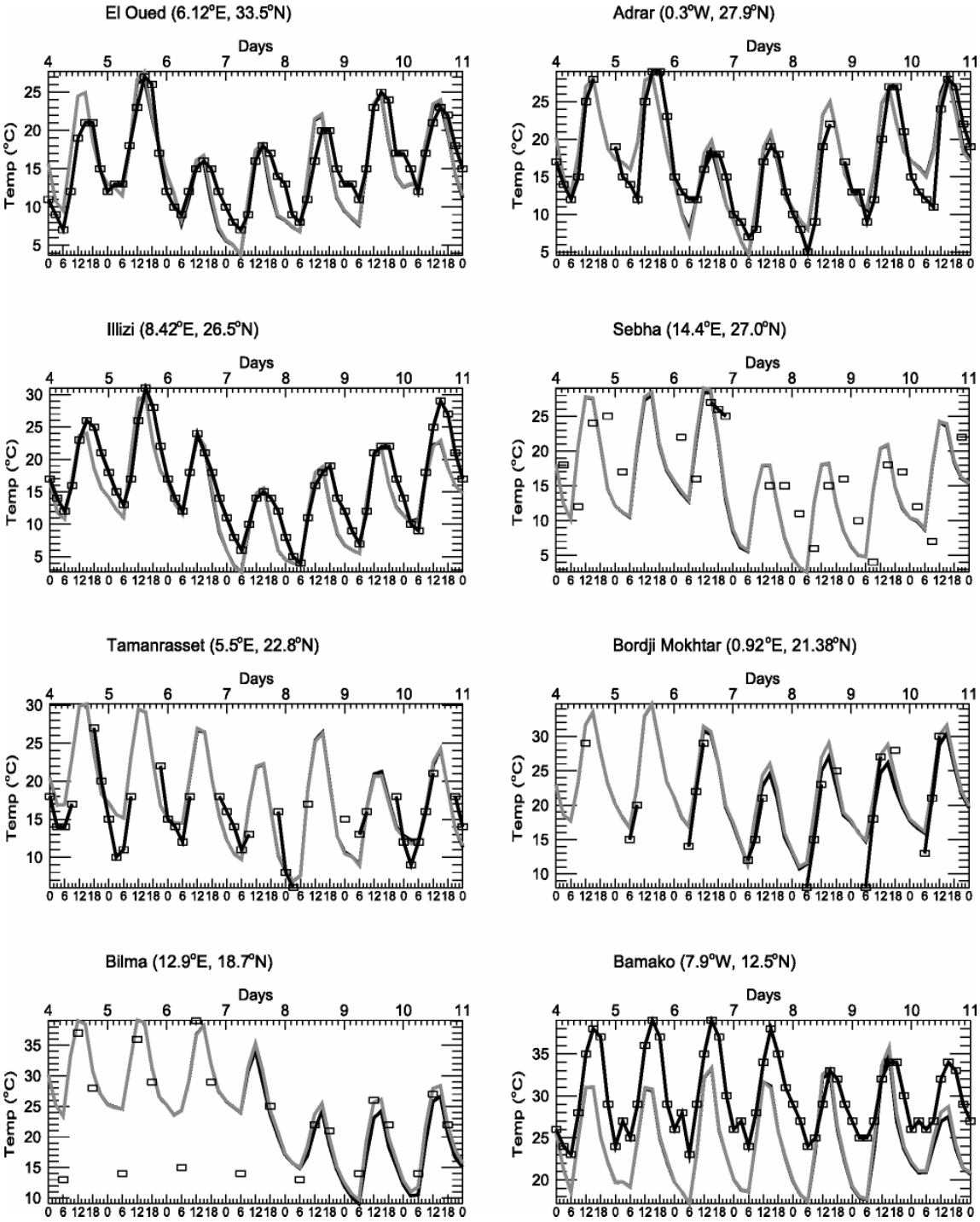

Figure 5.3: Time series of 2-m temperature (°C) at the location of the WMO stations from observations (squares) and RegCM3 experiments, EXP1 (gray solid curve) and EXP2 (black solid curve).

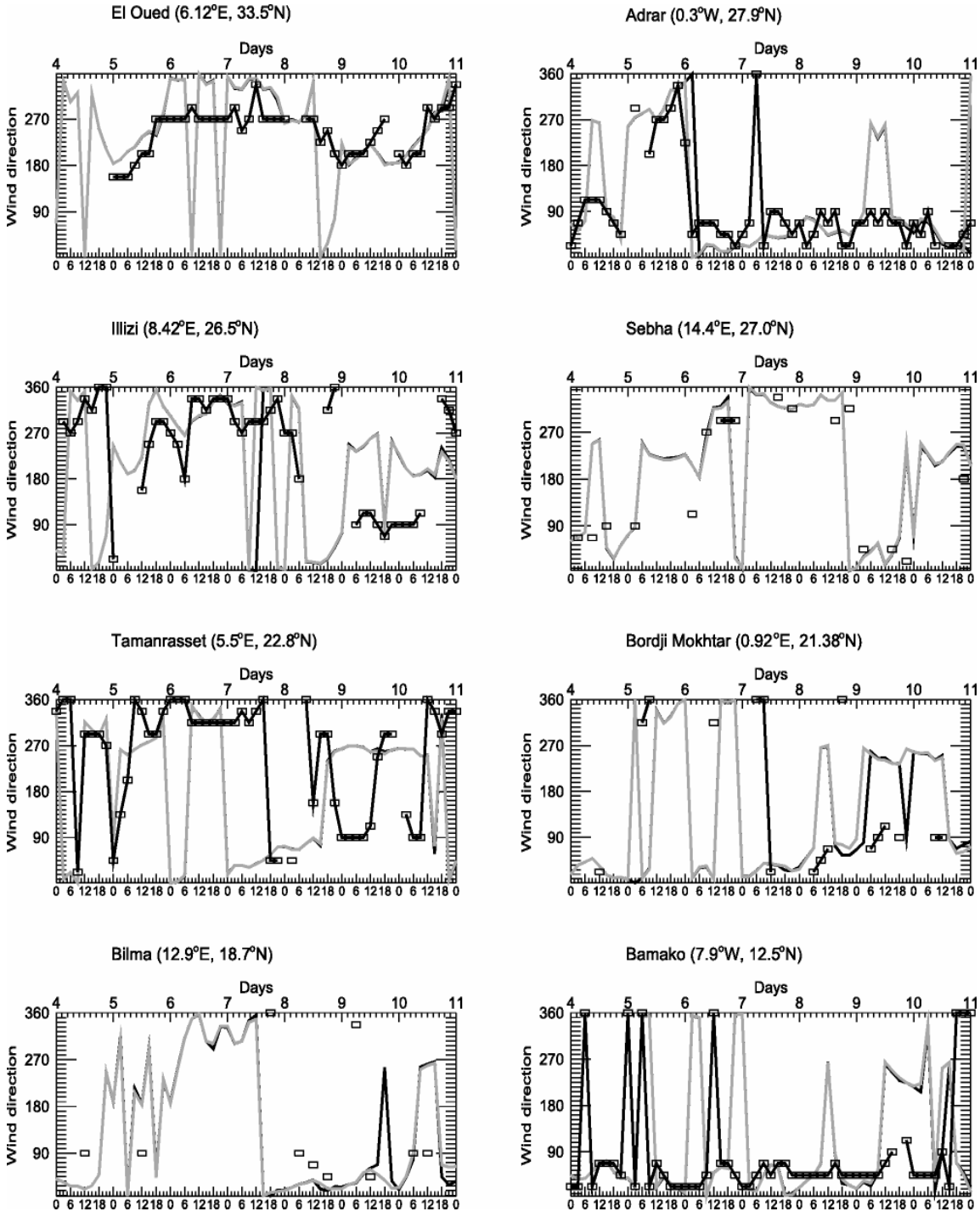

Figure 5.4: Time series of 10-m wind direction (degrees) at the location of the WMO stations from observations (squares) and RegCM3 experiments, EXP1 (gray solid curve) and EXP2 (black solid curve).

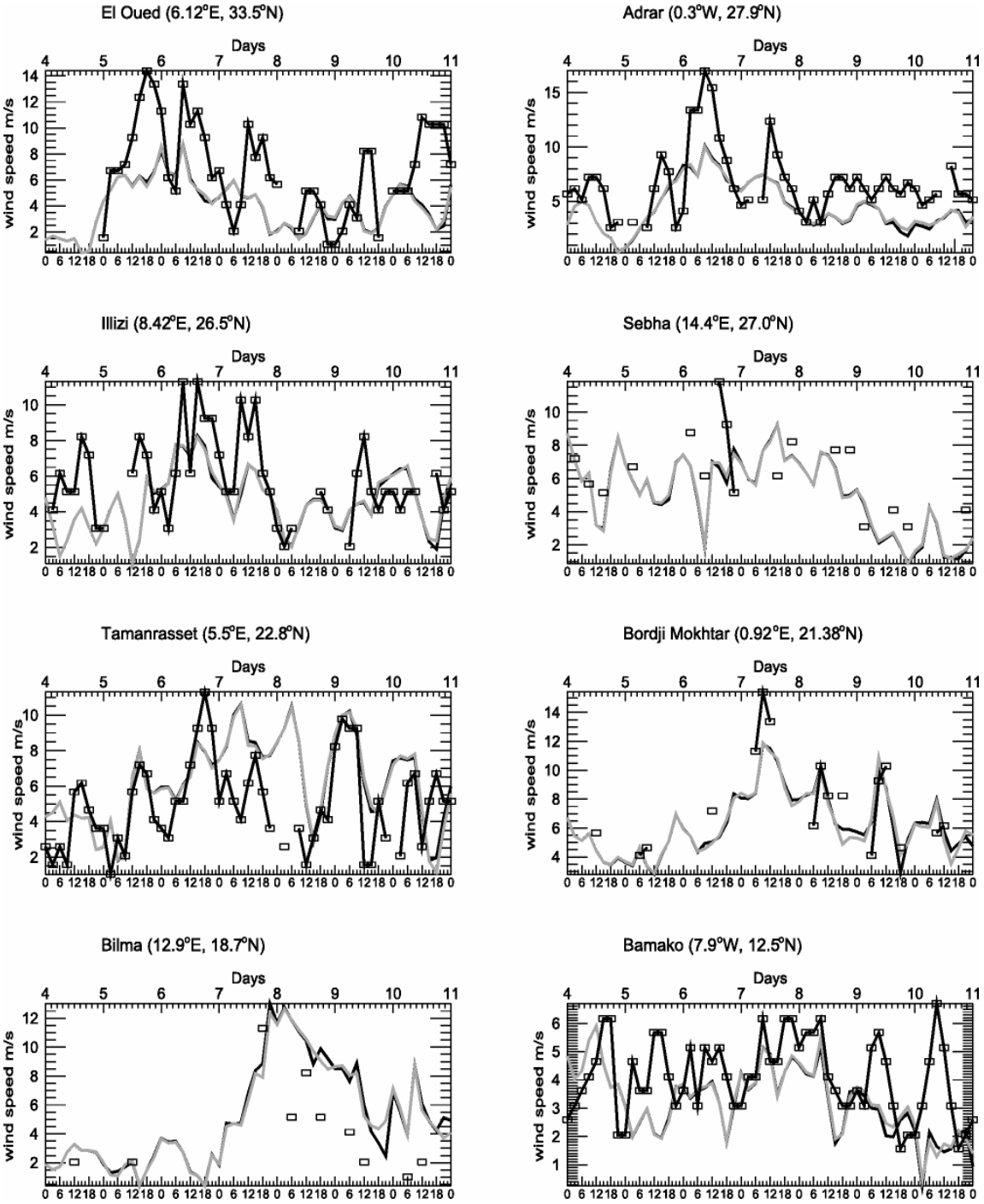

Figure 5.5: Time series of 10-m wind speed (m s_1) at the location of the WMO stations from observations (squares) and RegCM3 experiments, EX P1 (gray solid curve) and EXP2 (black solid curve).

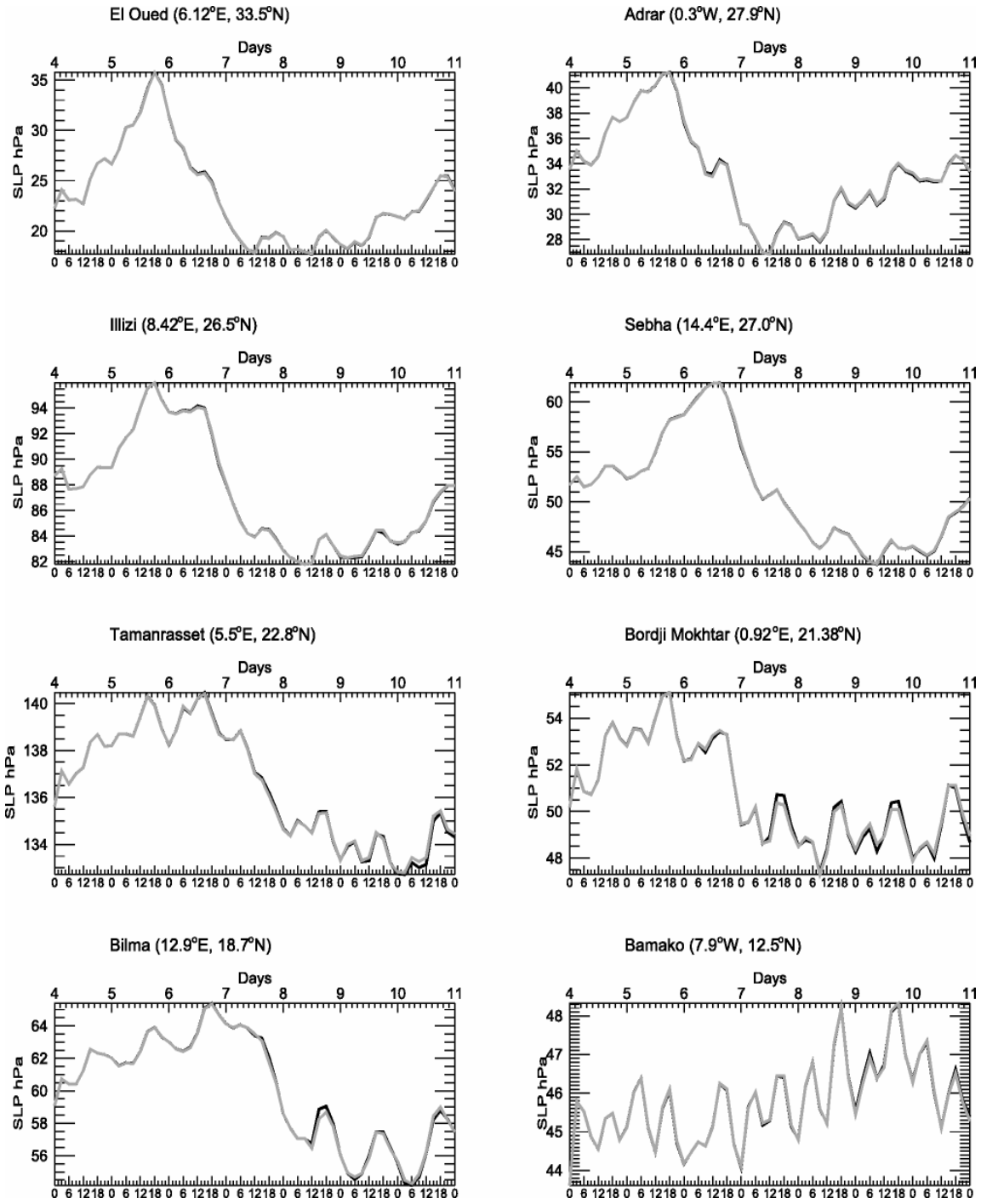

Figure 5.6: Time series of surface pressure anomalies (hPa), with respect to study period mean from observations at the location of the WMO stations. RegCM3 experiments, EXP1 (gray solid curve) and EXP2 (black solid curve).

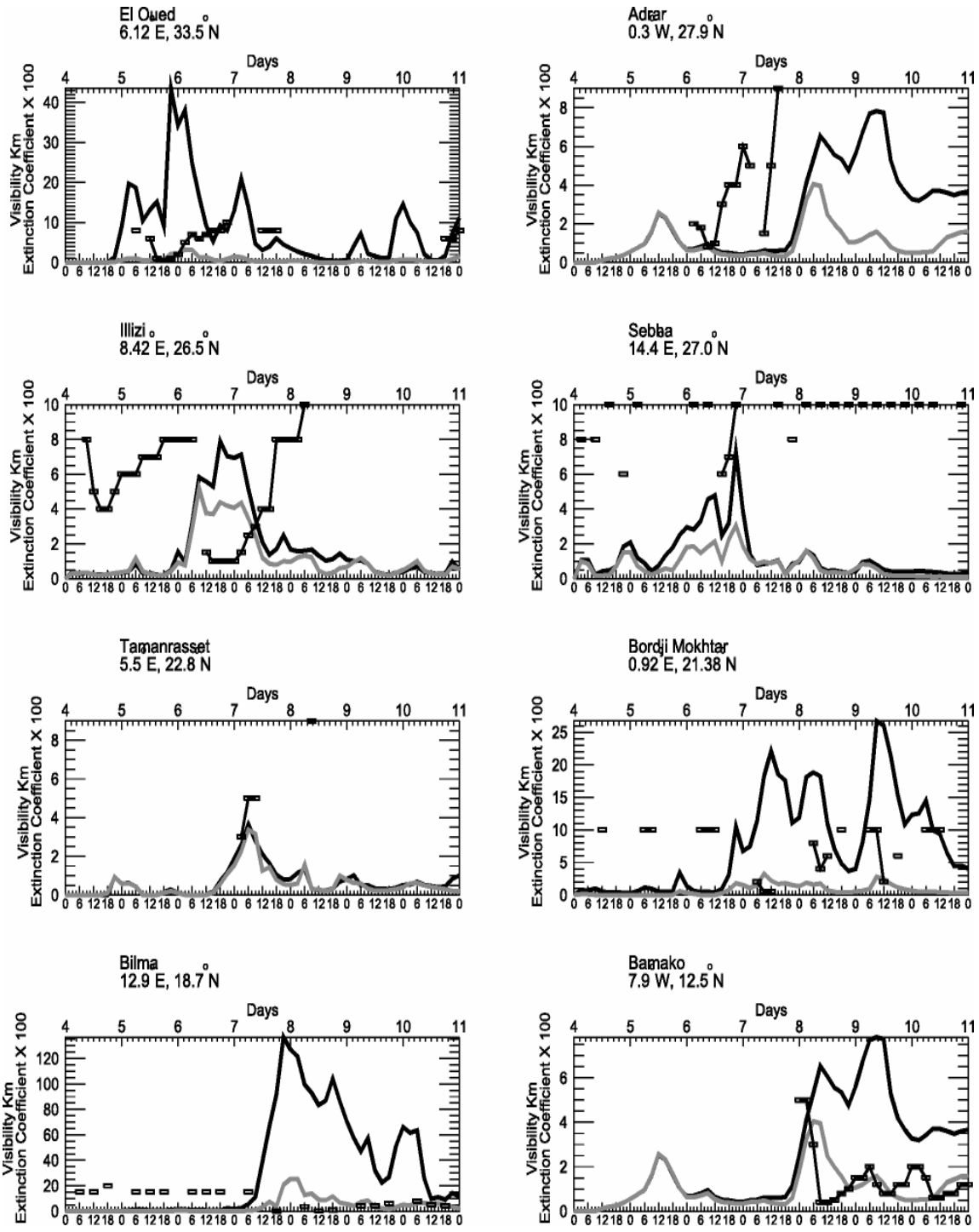

Figure 5.7: Time series of visibility (kilometers) at the location of the WMO stations from observations (squares) and modeled aerosol extinction coefficient at the lower level from RegCM3 experiments, EXP1 (gray solid curve) and EXP2 (black solid curve). Note inverted scale for visiility

Table 5-2 Timing of near surface wind speed maximum

WMO Station	Country	Location	Time (UTC) and date of observed wind maximum	Time (UTC) and date of modelled wind maximum
El Oued	Algeria	33˚ 30'N, 06˚, 07'E	1800 5th March	0900 6th March
Adrar	Algeria	27˚ 53'N, 00˚ 17'W	0300 6th March	0300 6th March
Illizi	Algeria	26˚ 30'N, 08˚ 25'E	0900 6th March	1500 6th March
Sebhah	Libya	27˚ 01'N, 14˚ 23'E	1200 6th March	1500 7th March
Tamanrasset	Algeria	22˚ 49'N, 05˚ 28'E	1800 6th March	0900 7th March
Bordj Mokhtar	Algeria	21˚ 22'N, 00˚ 55'E	0900 7th March	0900 7th March
Bilma	Niger	18˚ 41'N, 12˚ 55'E	1800 7th March	0600 8th March
Bamako	Mali	12˚ 32'N, 07˚ 57'W	0900 8th March	0900 8th March

With regard to dust emission and transport the satellite products show extensive dust mobilization across the Sahara desert during the study associated with the northerly wind outbreak (Figure 5.8). The dust front is first apparent at the extreme north of the domain over north-central Algeria at 2100UTC on the 5th March (not shown). The dust front propagates south to extend in a 'V' shape across southern Algeria by 1200UTC on the 6th (feature A in Figure 5.8a). This structure is partly a result of blocking by the Hoggar Mountains. By 1200UTC on the following day the cold surge and dust plume has propagated south and east, vigorously activating other dust sources, notably on the south-western flanks on the Hoggar mountains, northern Mali, north-western Mauritania, the Ténéré desert and the Tchigai Plateau of northern Niger, immediately to the west of the Tibesti mountains of northern Chad (features A-E, respectively, in Figure 5.8b). The dust front has similarities with those activated by density currents generated by evaporative cooling of air over the Atlas mountains documented by [*Knippertz and Fink,* 2006]. On the 8th March the active sources were located generally east of 5˚E and were dominated by sources close to the Algeria-Mali-Niger border point, to the southwest of the Aïr Mountains, the Tchigai plateau and the Tibesti-Ennedi gap of northern Chad, including the Bodélé Depression south of the Tibesti (feature A-D, respectively, in Figure 5.8c). By the 9th March strongly active emission was restricted to flanks of the Air mountains and especially the Bodélé Depression region (features A and B, respectively, in Figure 5.8d). By this time however, dust from the previous days had been transported to the south and west creating a vast plume of dust covering the Sahelian latitudes ~10-15˚N extending

from the Atlantic Ocean at ~25˚W to central Chad at ~20˚E. Throughout the period of this 4-day dust event the role of topography in modulating dust emission and transport is pronounced. Back-tracking dust plumes in sequential SEVIRI images shows the source regions to be localized and commonly located close to topographic features (Hoggar, Aïr and Tibesti mountains) where wadis and the paleo-drainage density is high, providing fine grained fluvial material for deflation. Dust plumes from such sources are transported in topographically constrained Low Level Jet (LLJ) features most notably the Bodélé LLJ [*Todd et al.*, 2008b; *Washington et al.*, 2006b; *Washington and Todd*, 2005] and the LLJs to the north and south of the Aïr mountains [*Schepanski et al*, 2007].

Simulated AOT from experiments EXP1 and EXP2 are shown in Figures 5.9 and 5.10 respectively. It is of interest to determine the extent to which the model simulates these localized dust sources accurately. Overall, both model experiments represent well the dominant features of the event. Specifically, (i) the pronounced dust emission over much of the Sahara (ii) the northwest to southeast evolution of dust source activation over the period, from northern Algeria on the 6th to parts of Niger and eastern Chad on the 7th and 8th (iii) the transport of dust to the south and southwest over the Atlantic/Sahel sector by the 9th March. However, it is clear that EXP2 provides a much more realistic representation of the key localized source regions evident in the SEVIRI imagery (Figure 5.8). Most notably, in EXP2 dust emission from the southern flanks of the Hoggar mountains on the 7th (feature A in Figure 5.8a), the Tchigai plateau on the 7th-8th (Features E in Figure 5.8b and C in Figure 5.8c) and the regions to the north and south of the Aïr mountains on the 8th-9th (feature A in Figures 8c and 8d) match very closely with SEVIRI. In EXP1 dust emission from these regions is largely absent. Emission from the Bodélé depression is more realistically extensive in EXP2. Both experiments show an extensive area of emission over central Mauritania on the 7th March, which is probably overestimated relative to SEVIRI. There is some indication from SEVIRI that dust is transported further south (to ~10ºN) from the 8th onwards, than is represented in the model. For example the dust plume covers Burkina Faso in SEVIRI but in the model the plume is located north of 13.5°N due to the influence of easterly winds which prevent propagation of the plume further south. It is likely that the model has an error in the circulation here. Overall, EXP2 has a higher mean AOT by about a factor of two when compared against EXP1.

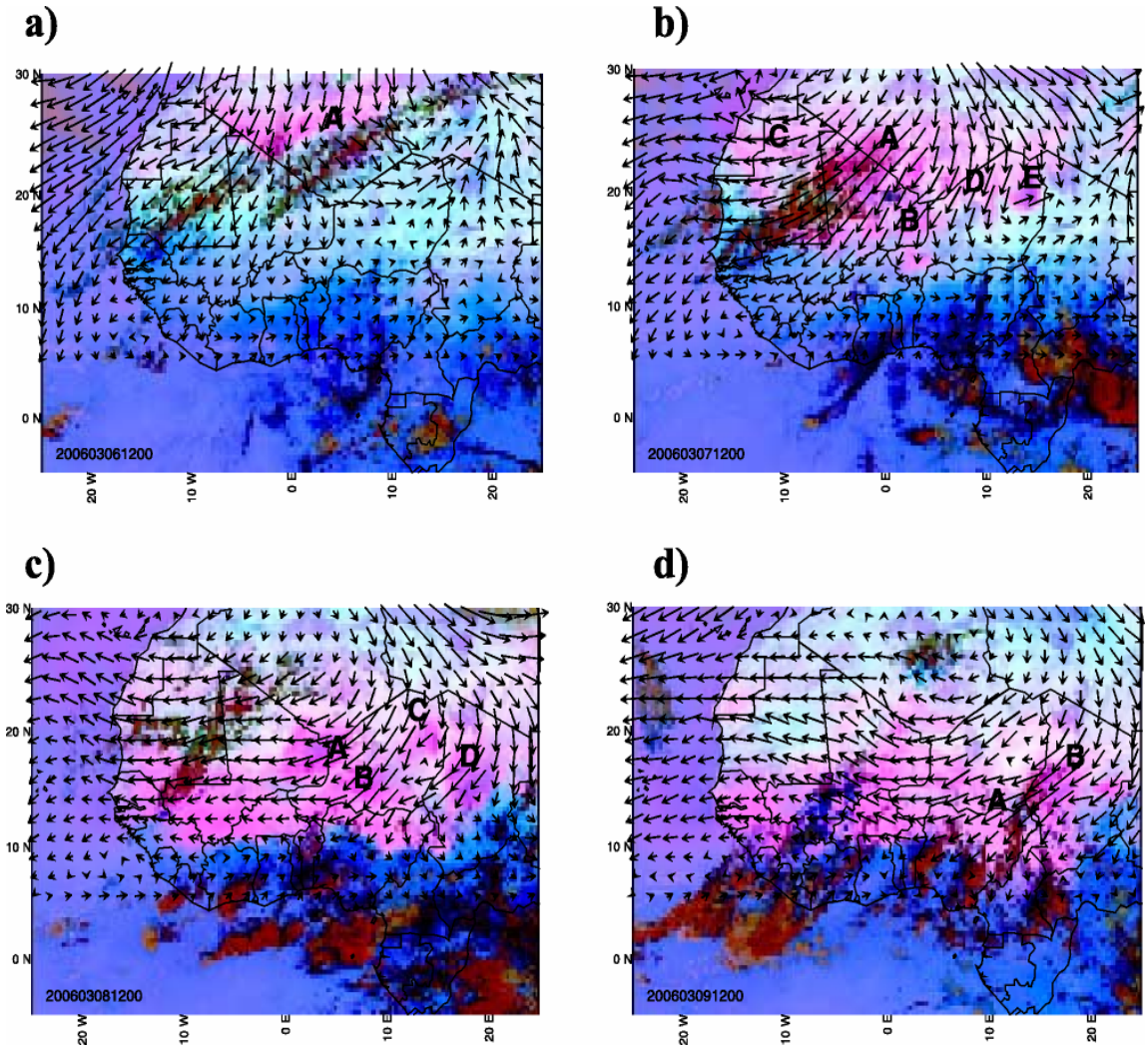

Figure 5.8: SEVIRI false color dust product imagery at 1200 UTC each day over the study period. Pink tones indicate dust. RegCM3 EXP1 925-hPa wind vectors are overlaid. Letters are explained in the text.

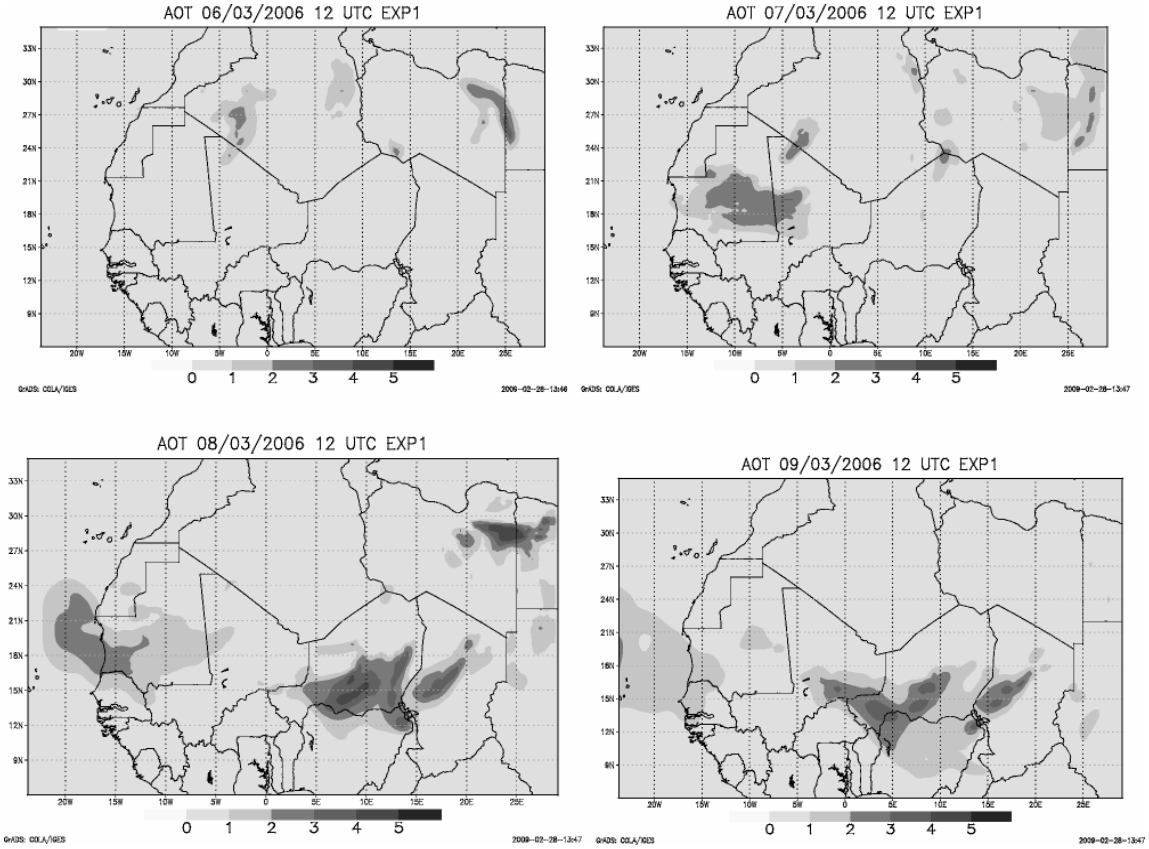

Figure 5.9: Model simulated AOT at 1200 UTC each day over the study period from EXP1.

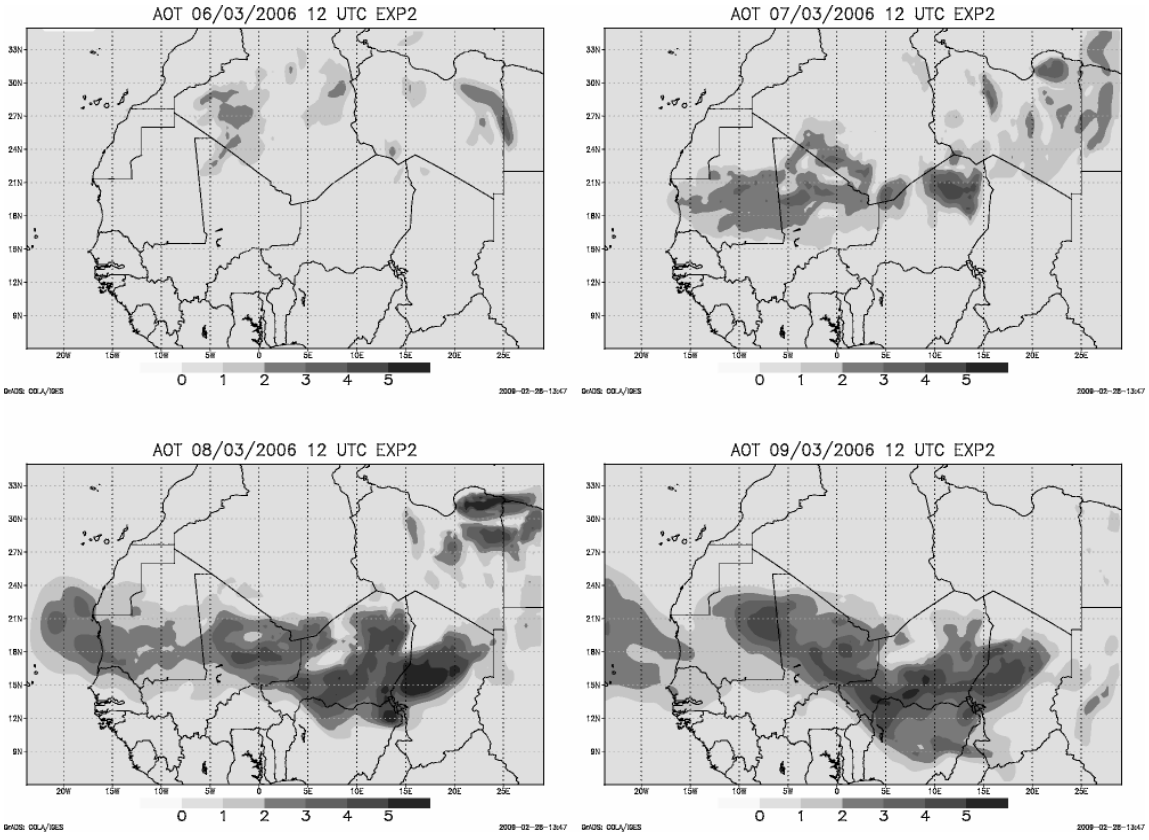

Figure 5.10: Model simulated AOT at 1200 UTC each day over the study period from EXP2.

The OMI-AOT and limited MISR AOT observations (Figure 5.11) serve to confirm all the key dust plume features identified from SEVIRI mentioned above. It is evident that in a qualitative sense EXP2 represents these features more comprehensively than does EXP1, illustrated by a stronger spatial correspondence between model AOT and satellite AOT (Figure 5.11 and 5.12). However, in EXP2 AOT is clearly overestimated relative to MISR by about a factor of 2 (Figure 11). The model overestimation relative to OMI-AOT is even higher (Figures 11, 12). However, it should be noted that there is a considerable underestimation of AOT by OMI compared to MISR (Figure 5.12a), suggesting that the relationship used to derive the former from the latter [*Christopher et al.*, 2008] is not especially robust for this case study period. It should be noted also that MISR underestimates AOT relative to the AERONET observations by a factor of ~2 and that model AOT is broadly in line with that estimates from AERONET (see below).

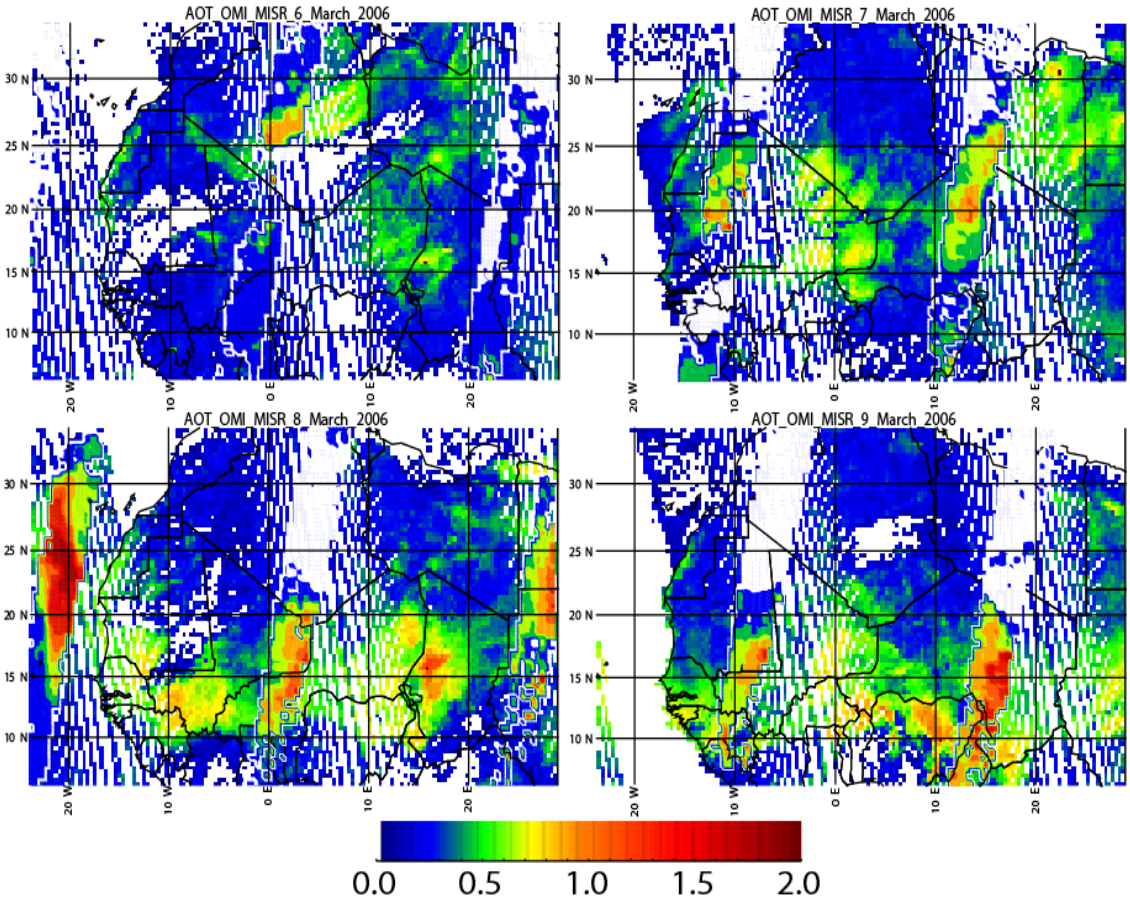

Figure 5.11: Estimated AOT for OMI at 1330 local time each day over the study period, 6–9 March 2006. MISR AOT at 1045 local time is overplotted

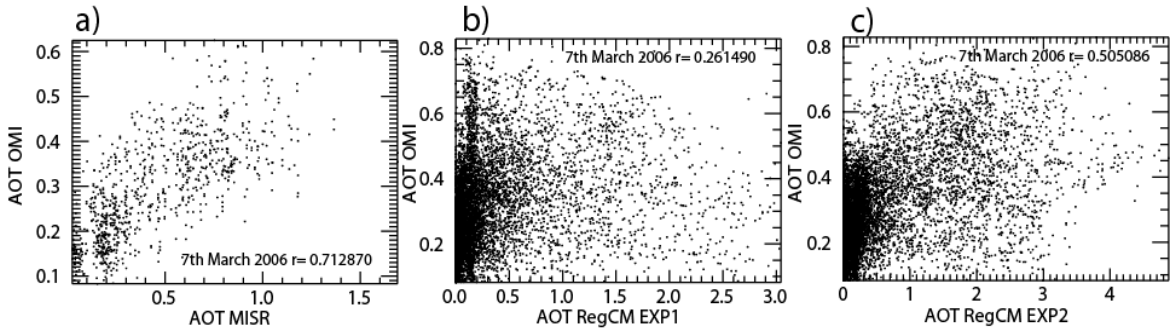

Figure .5.12: Example AOT scatterplot for 1200 UTC on 7 March over model domain. (a) MISR AOT versus OMI AOT, (b) AOT EXP1 versus AOT estimated OMI-AOT, and (c) AOT EXP2 versus OMI-AOT.

Quantitative evaluation of model AOT using AERONET sun photometer data is largely limited to the locations in the Sahelian sector (Figure 5.1) such that the observations tend to reflect long range dust transport from the Sahara rather than local dust emission. The only Saharan site at Tamanrasset is at a relatively high elevation in a region of complex topography and so it is not strongly influenced by local dust emission (AOT values observed did not exceed 0.2) therefore it was not considered in this study. The correspondence between modeled and observed AOT (Figure 5.13 and Table 5-3) is variable between stations, indicating that some transport pathways are well simulated and others not. Overall, there is no clear evidence of systematic model overestimation of AOT, whilst MISR and especially OMI-AOT underestimate relative to AERONET. There is a particularly close correspondence between observed and modeled AOT at the sites Maine Soroa (12.02˚E, 13.21˚N), in southeast Niger, Dakar (16.95˚W, 14.39˚N) on the Atlantic coast of Senegal and Capo Verde (22˚W, 14.39˚N). Maine Soroa lies directly downwind of the both the Ténéré desert in northern Niger (including the Tchigie Plateau) which was active on the 7th-8th March and the Bodélé depression to the north east, active 8th-9th March. Dust transport to Maine Soroa takes in excess of 12 hours from both source regions. As such, the timeseries of observed AOT show elevated values on the 8-10th March with peak values (AOT>4.0) on the 9th. SEVIRI imagery indicates that the major dust plumes pass Maine Soroa primarily at night so that the observed AERONET AOT values do not indicate the magnitude of the dust peak. The time evolution of AOT is well simulated in both EXP1 and EXP2, with EXP1 resolving the magnitude better on the 8th and 10th , whereas EXP2 captures the peak values on the 9th. A previous study of the Bodélé Depression region[*Todd et al.*, 2008b] indicated that the default RegCM3 configuration rather underestimated dust emission from this region, such that we might expect the dust emission in EXP2 to be rather more realistic than in EXP1. At Dakar, the time evolution of dust transport is well captured by the models with dust emitted from

Mauritania-Mali region reaching the site on the 8th, peaking on the 9th and declining thereafter. EXP2 estimates the magnitude of AOT far better than EXP1. Further west at Capo Verde the AERONET station shows elevated AOT on the 8th, peaking on the 9th, a pattern very closely represented by the model, especially EXP2. Although dust advection over the eastern Atlantic is well represented at these sites, further north the model under-estimates the magnitude of AOT at Tenerife, although the time evolution is reasonably accurate.

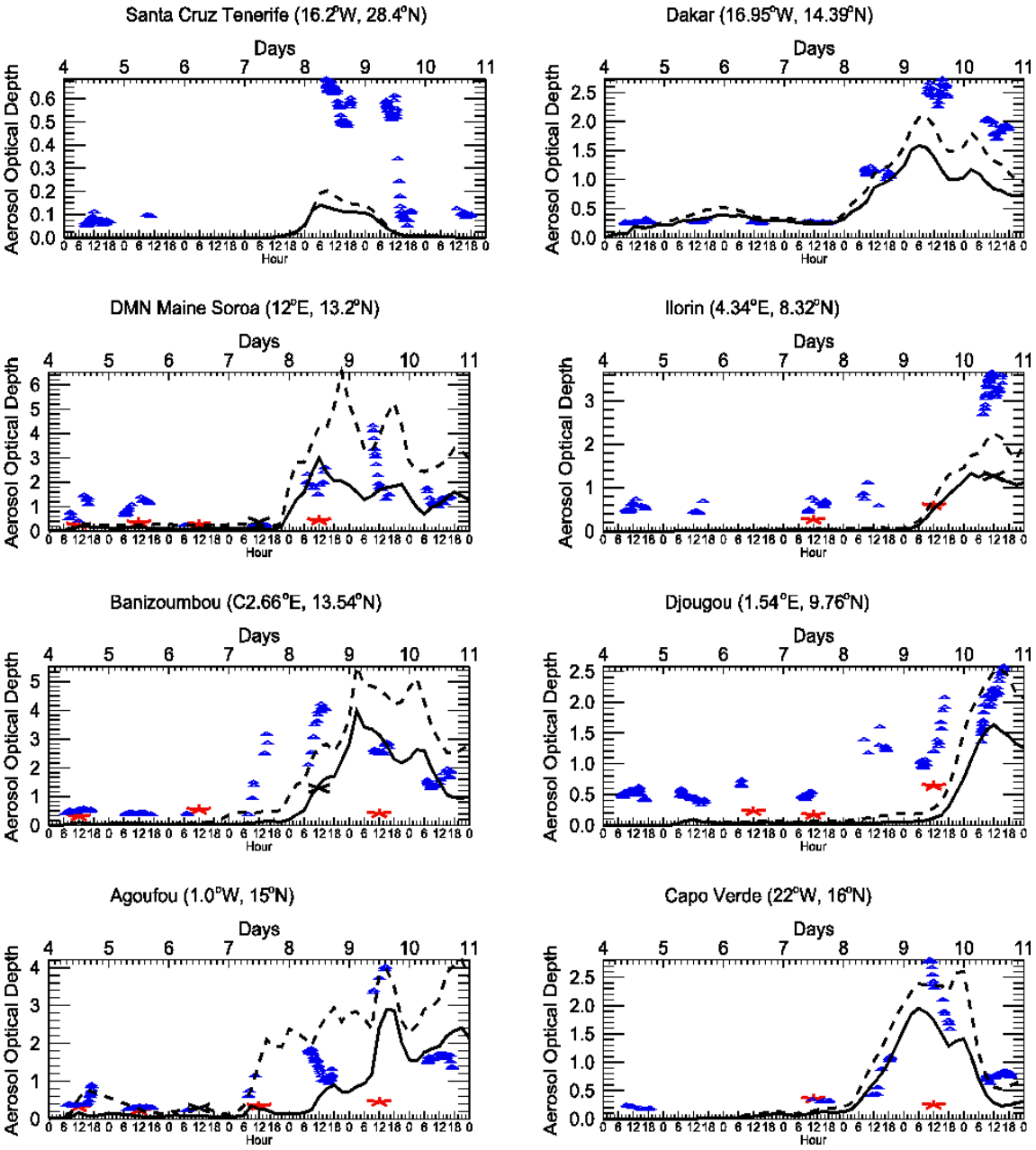

Figure 5.13: Time series of observed and model simulated AOT at the locations of the AERONET Sun photometer stations: 440 nm AOT from AERONET (triangles), AOT from EXP1 (dotted curves), AOT from EXP2 (black solid curves), coincident MISR-AOT (crosses), and OMI-AOT (asterisks) observations.

Table 5-3: Correlation analysis of AOT from AERONET stations simulations

Aeronet station:	**EXP1**	**EXP2**
Santa Cruz Tenerife	0.438	0.44
Dakar	0.77	0.829
DMN Maine Soroa	0.78	0.72
Ilorin	0.731	0.732
Banizoumbou	0.765	0.756
Djougou	0.66	0.73
Agoufou	0.656	0.62
Capo Verde	0.52	0.54

For the Sahelian sites, the closest correspondence occurs at the northernmost station of Agoufou (1.5˚W, 15.3˚N) where enhanced atmospheric turbidity begins on the 7th, peaks on the 9th before declining to background levels on the 12th. The models capture this pattern well, especially for the EXP2 in which the maximum peak observed of AOT (>4) on the 9th coincides with that of the site. At other Sahelian sites, however, the observed AOT is less well represented. At Banizoumbou (2.66˚E, 13.54˚N) and Djougou (1.54˚E, 9.76˚N) elevated AOT evident on 7th and 8th March is not apparent in the model which shows dust only from the 9th onwards. Analysis of the SEVIRI imagery shows that this model error is due to dust emission in southern Niger, north of Banizoumbou on the 7th and the subsequent southward advection. This particular dust source is not resolved in EXP2, indicating an omission in the dust plume identification by *Schepanski et al.* [2007]. The AERONET stations located further south at Ilorin (4.3˚E,8.3˚N) and Djougou (1.5˚E, 9.76˚N) identify the southward transport of dust towards the Gulf of Guinea reaching Ilorin on 10th March, peaking on the 11th and then slowly declining with elevated AOT values (>1.0) persisting until 16th March. The model generally underestimates the magnitude of AOT in this southern zone indicating either excessive dust deposition rates, errors in the southward circulation or the influence of non-dust aerosols (i.e. biomass burning) in the AERONET observations. However, we can assume that the observed AOT values are largely caused by desert dust rather than biomass burning and urban/industrial aerosol as the Angstrom coefficients (α) are below 1.0, indicative of large dust particles [*Dubovik et al.,* 2002]. Model error in the circulation is suggested also by comparison of model AOT and satellite imagery (Figures 5.8-5.11). It is interesting to note that the limited comparison available between the satellite products and surface based AERONET AOT indicates that MISR and OMI-AOT substantially underestimate the elevated AOT

values during the dust event at almost all the AERONET sites. As such, the apparent overestimation of model AOT relative to MISR-OMI (Figures 5.9-5.11) may partly reflect this. Overall, it is reasonable to conclude that EXP2 better resolves dust source regions than EXP1 and provides a more representative estimate of the space/time distribution of dust and AOT.

It is well known that Saharan dust is advected by the planetary scale circulation and transported many thousands of km around the globe [*Swap et al.*, 1992]. The impact of this on climate and remote ecosystems will depend on the mass flux along with the optical and physical properties of the dust from the emitting region [*Liao and Seinfeld*, 1998]. Previous attempts have been made to quantify the mass flux from observations [*Kaufman et al.*, 2005b; *Koren et al.*, 2006]. Here, we derive the mass flux of dust from the region estimated by RegCM3 from the product of the meridional and zonal wind speed and dust concentration in each model layer, summed over the atmospheric column. Dust transport is dominated by a southwestward flux in the Harmattan northeasterly flow such that in the vertical integration calculation at levels where the zonal wind component is eastward or the meridional component is northward the dust flux is considered to be negative. The net westward zonal and southward meridional components are derived. The net flux of dust exported southward from the Sahara to the West African land regions, determined from the meridional component at 15°N averaged over longitudes 15°W-25°E and is 1.67 (2.5) Tg day^{-1}, for EXP1 (EXP2), which may have implications for the Sahelian and equatorial African ecosystems. The westward net flux leaving the west coast of Africa over the Atlantic Ocean is determined from the zonal component at 15°W over the latitude range 0-30°N. For the 5 day period 6-11th March the flux is 1.05 (1.65) Tg day^{-1} for EXP1 (EXP2). *Kaufman et al.* [2005b] use a similar method to estimate the mass flux of dust from North Africa based on the product of mean monthly MODIS satellite estimated AOT and NCEP reanalysis 850hPa winds. Using their method applied to RegCM3 model 850hPa wind speed and AOT the flux for 6-11th March 2006 is 1.8 (2.7) Tg day^{-1} for EXP1 (EXP2), which is about 1.5 times higher than that derived using the full vertical distribution of winds and dust mass. [*Kaufman et al.*, 2005b] estimate the dust flux leaving West Africa at 15°W over the latitude range 0-30°N during winter months of 2001 to be about 0.3Tg day^{-1}. Our estimates of mass flux during the March 2006 event highlight the importance of these major events to total mass flux.

5.2.3. Model simulation of dust radiative impact.

At present, the RegCM3 model only determines the aerosol impact on shortwave (SW) radiative fluxes. The SW radiative forcing (RFSW) is determined at the surface (SFC) and top of the atmosphere (TOA) (Figures 5.14 and 5.16). Associated temperature anomalies are determined from the difference between the results of EXP1 and EXP2 and the control run ND without active dust (Figure 5.15). At the height of the dust event at 12UTC on 8 March RFSW(SFC) peaks at around -550 W m-2 (-650 W m-2) downwind of the major dust source over the Bodélé Depression for EXP1 (EXP2) (Figure 5.14). The peak domain averaged RFSW(SFC) is -71 W m-2, -128 W m-2 and -123 W m-2 for EXP1, EXP2 and EXP2b (wo values increased), respectively, indi¬cating how the RFSW(SFC) is far more sensitive to the areal dust emission than the range of optical properties in these experiments. The domain averaged RFSW(SFC) normalized by AOT is comparable for the three experiments (-139 W m-2, -151 W m-2 and -132 W m-2 per unit AOT, for EXP1, EXP2 and EXP2b, respectively). These are close to that estimated during the SHADE experiment over the Atlantic off the coast of west Africa (-129 Wm^{-2}) [*Haywood et al.*, 2003]. Compared to field observations at single sites at Niamey, southern Niger these results are very close to the -130Wm^{-2} obtained by [*Fouquart et al.*, 1987] but higher than the observed impact of ~100 Wm^{-2} per unit AOT reported by *Slingo et al.* [2006]. Our results are somewhat lower than those obtained in a similar model study by *Helmert et al.* [2007] over the southern Sahara for aerosols with varying optical properties (-220 to -196 Wm^{-2} per unit AOT).

The magnitude of reductions in daytime maximum air temperature between the day prior to and during the dust event agree well with station observations (Figure 5.3) and are often in excess of 10˚C. These temperature anomalies result from a combination of horizontal and vertical temperature advection and diabatic heating (consisting of radiant fluxes and surface heat fluxes, which are dominated by sensible heat flux). Given the strength of the northerly wind anomalies (Figures 5.3b and 5.8) and the $RF_{SW(SFC)}$ it is likely that both advective and diabatic heating contributions are substantial. We can estimate the magnitude of each of these components by comparing the temperature simulated by RegCM3 experiments with active dust to the control run (ND), for grid cells where cloud differences are minimal. The effect of the $RF_{SW(SFC)}$ is to reduce daytime surface temperatures, by more than 8˚C (10˚C) in EXP1 (EXP2) where aerosol loadings

are highest (Figure 5.15). Temperature anomalies directly attributable to $RF_{SW(SFC)}$ exceed 5˚C across much of the dust plume region. The daytime maximum temperature anomaly normalized by AOT averaged over the domain for grid cells where AOT>0.5 is about 2.5˚C per unit AOT in both EXP1 and EXP2, slightly higher than the value of 2.1 - 2.2 ˚C per unit AOT derived by *Helmert et al*. [2007].

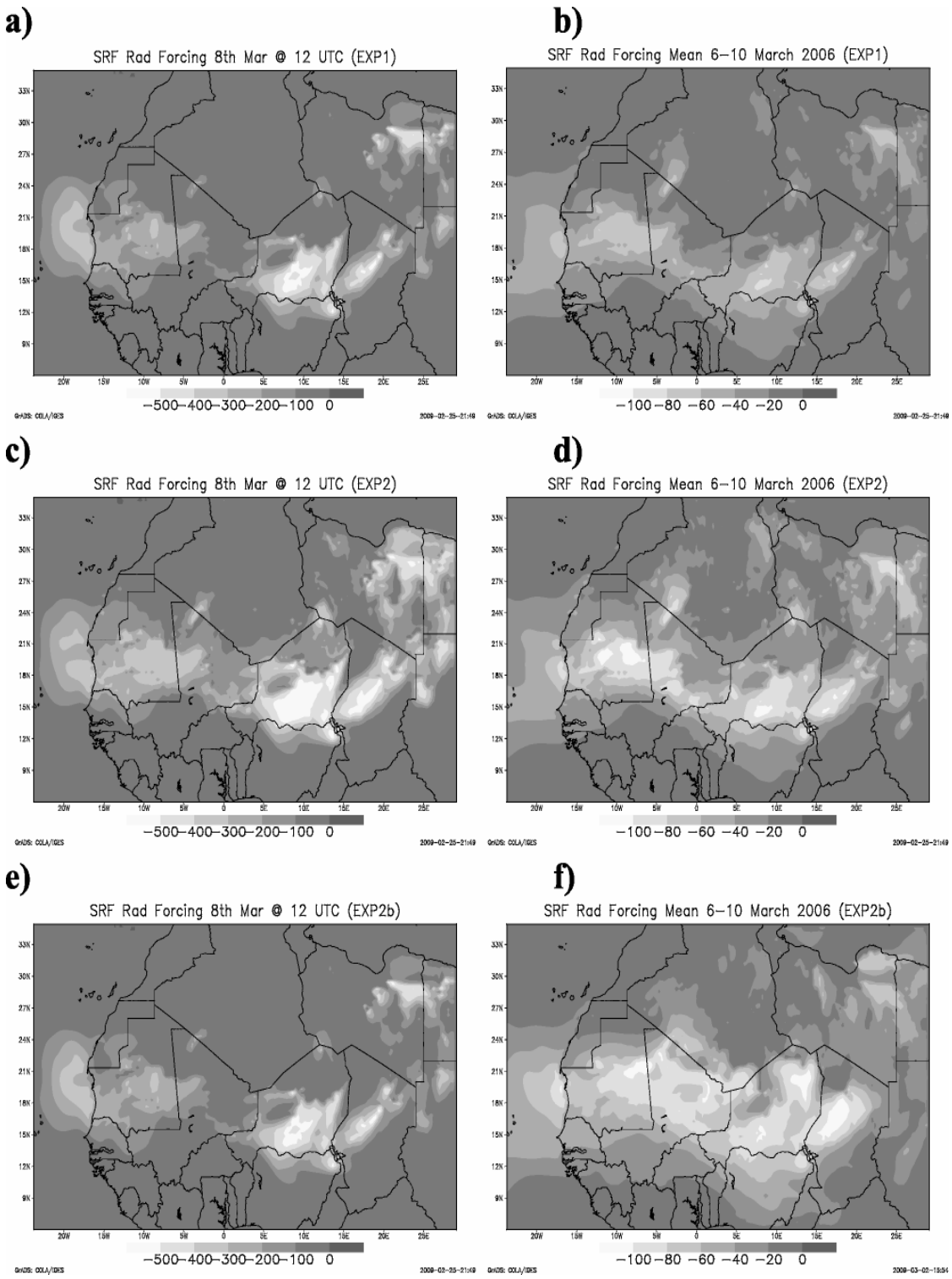

Figure 5.14: Shortwave radiative forcing at the surface (W m2). (a) Mean (6–10 March 2006) EXP1, (b) instantaneous 1200 UTC March 8 EXP1, (c) as in Figure 5.14a but for

EXP2, (d) as Figure 5.14b but for EXP2, (e) as in Figure 5.14a but for EXP2b, and (f) as in Figure 5.14b but for EXP2b.

The RF_{SW} at the top of atmosphere associated with aerosols is a function of the aerosols loading, optical properties, size distribution, and surface albedo. $RF_{SW(TOA)}$ is strongly negative over areas where the aerosol load is high and surface albedo is low (Figure 5.16). This is most notable over the Atlantic Ocean off the coast of Mauritania and over northern Nigeria and southern Niger where the instantaneous $RF_{SW(TOA)}$ has a minimum of about -180 Wm^{-2}. Over the Sahara itself $RF_{SW(TOA)}$ is positive, with instantaneous peak values in excess of +60 Wm^{-2} over parts of Niger and Chad in particular, as the dust aerosols produce an effective decrease in the planetary albedo over the bright desert surfaces (Figure 5.16). The effect of the higher aerosol ωo in EXP2b results in a lower $RF_{SW(TOA)}$ i.e. more negative over dark surface and less positive over bright surfaces (Figure 5.16). Nevertheless, the fundamental distinction in the sign of the $RF_{SW(TOA)}$ between dark and bright surfaces (along 15°N over land) remains in EXP2b. The aggregate effect of this complex spatial structure in $RF_{SW(TOA)}$ simulated by RegCM3 is negative when averaged over the domain, and the magnitude increases over the study period to peak at -16, -27, and -33 Wm^{-2} for EXP1, EXP2 and EXP2b, respectively, at 1500UTC on the 9th March as the dust plume shifts from the desert regions to darker surfaces in the south of the domain (not shown). The space/time averaged $RF_{SW(TOA)}$ is -4.7, -7.6, -9.15 Wm^{-2} for EXP1, EXP2 and EXP2b, respectively. The space/time average normalized $RF_{SW(TOA)}$ is ~-10 Wm^{-2} per unit AOT in both EXP1 and EXP2 whereas this value increases to -12 Wm^{-2} for EXP2b. Clearly these averaged figures are particular to the domain specified here. Over the darker land surfaces of the Sahelian zone model simulated instantaneous peak $RF_{SW(TOA)}$ normalized by AOT are ~-80 to -40 Wm^{-2} per unit AOT for both EXP1 and EXP2, respectively (not shown). At the location of Niamey, Niger the value is -40 Wm^{-2}, roughly consistent with the observations from the GERB (Geostationary Earth Radiation Budget experiment) and CERES (Clouds and the Earth's Radiant Energy System) instruments [*Slingo et al.*, 2006].

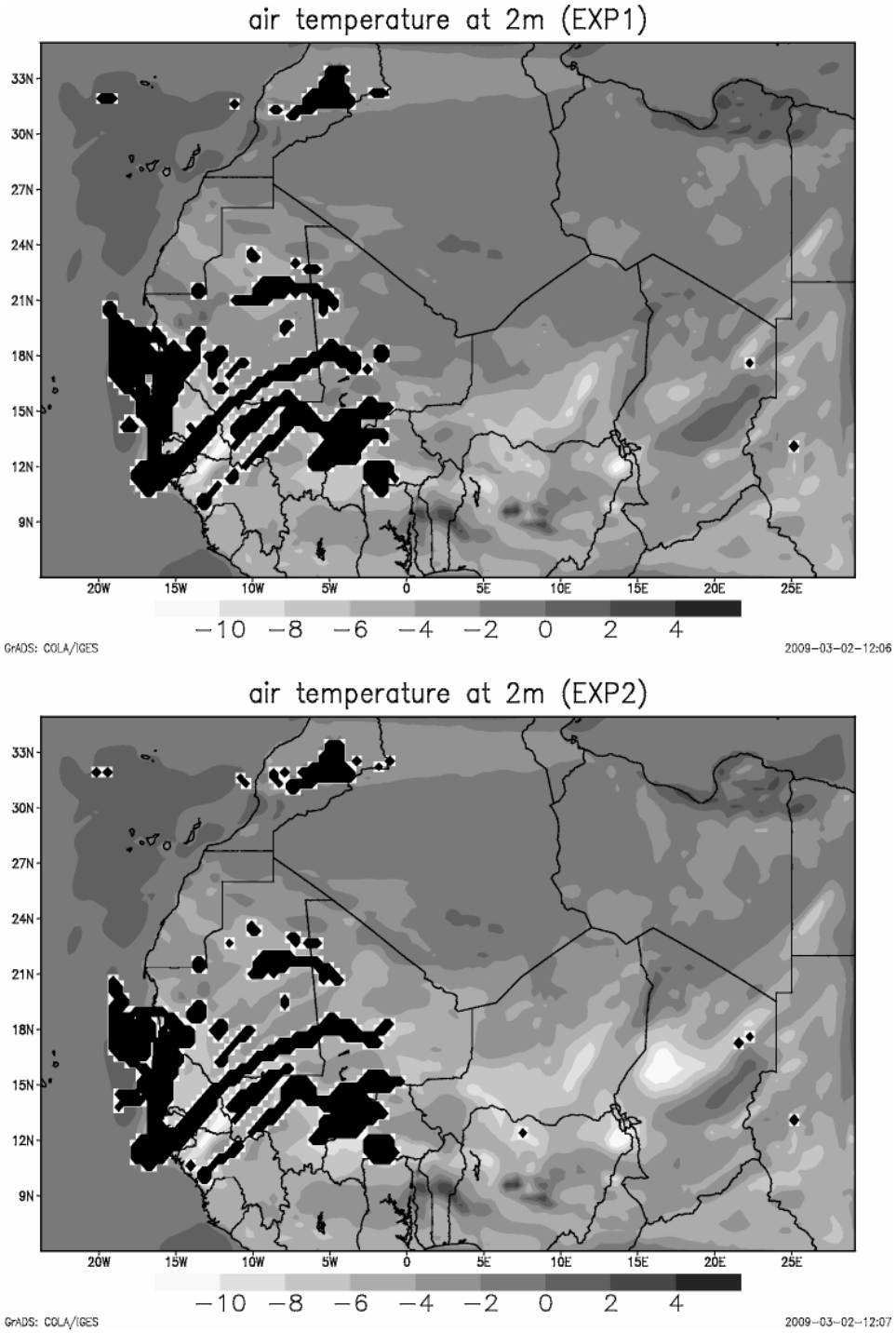

Figure 5.15: The 2-m temperature anomalies (°C) for 1200 UTC 8 March: (top) EXP1-ND and (bottom) EXP2-ND. A black mask is created when cloud fraction is greater than 20%.

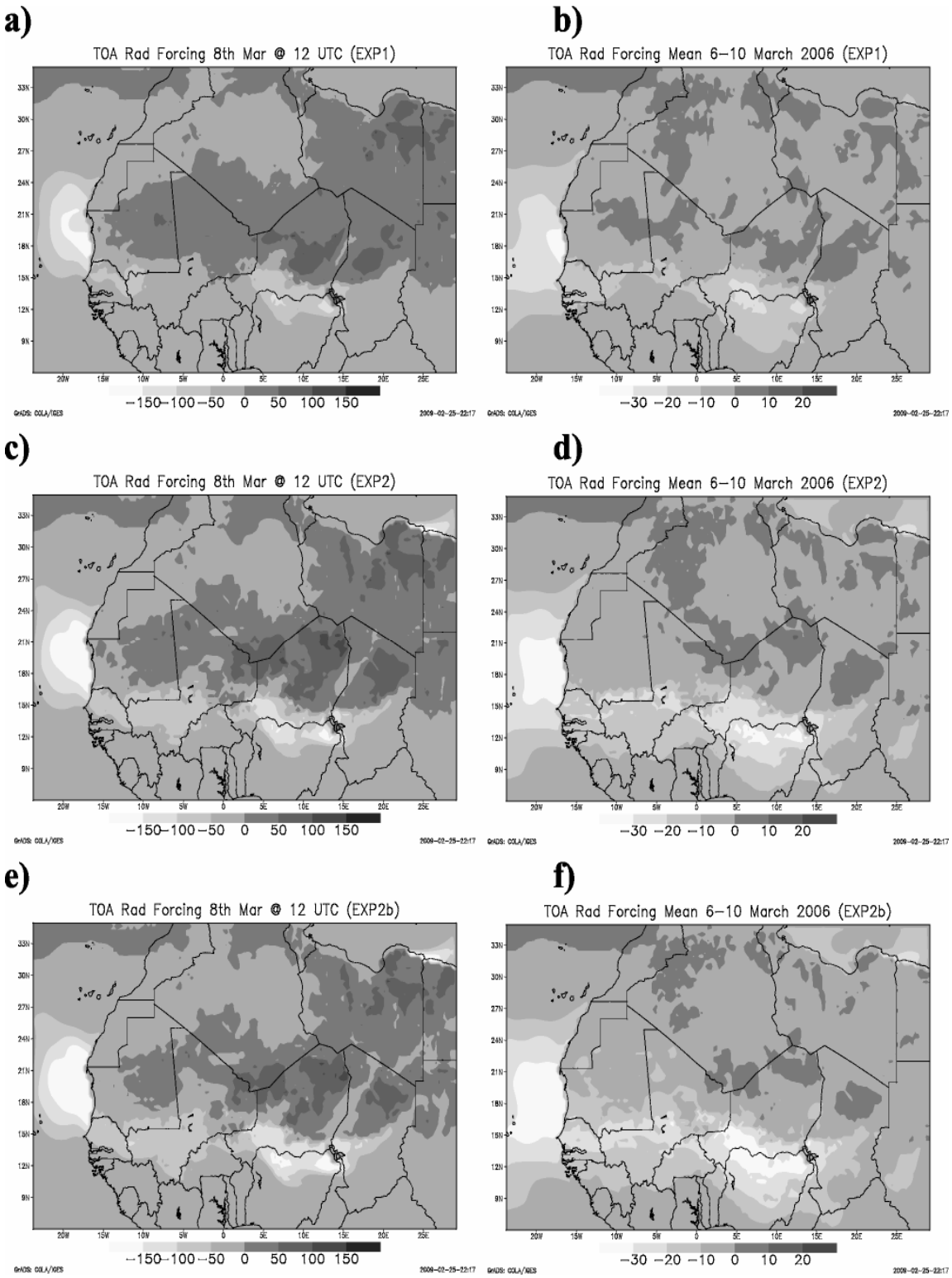

Figure 5.16: Shortwave radiative forcing at top of the atmosphere (Wm2). (a) Mean (6–11 March 2006) EXP1, (b) instantaneous 1200 UTC March 8 EXP1, (c) same as Figure 16a but for EXP2, (d) same as Figure 16b but for EXP2, (e) same as Figure 16a but for EXP2b, and (f) same as Figure 16b but for EXP2b.

This spatial structure in $RF_{SW(TOA)}$ simulated by RegCM3 with positive forcing over desert regions and negative forcing over dark surfaces is consistent with model simulations by *Perez et al*. [2006] but contrasts with those of *Helmert et al.* [2007] and *Myhre et al*. [2003] who document a consistently negative $RF_{SW(TOA)}$ even over bright surfaces. Even with the aerosol ω_o modified to represent the more highly reflective aerosols the $RF_{SW(TOA)}$ remains positive over bright surfaces (EXP2b). As such it is likely that the disparity between EXP2b and the simulations of *Helmert et al* [2007] is likely to result from differences in surface albedo over the desert regions. In RegCM3 the albedo is typically around 0.33 over desert (Figure 5.17) similar to those observed from the ERBE (Earth Radiation Budget Experiment) satellite sensor obtained from the NASA Langley Research Center Atmospheric Science Data Center (not shown), in contrast to values of ~0.2 in *Helmert et al*. [2007]. As such, the results of these modeling experiments illustrate how important it is to specify accurately not only the optical properties of aerosols but also the surface albedo.

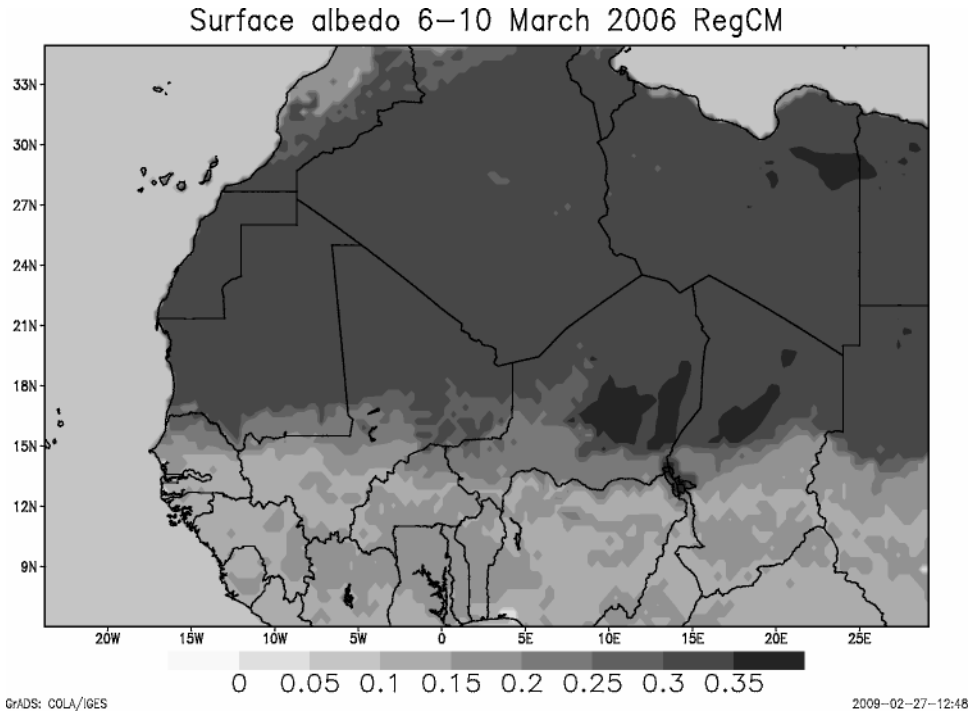

Figure 5.17: Time-averaged surface albedo values from RegCM.

5.3. Summary

This study has evaluated the ability of the RegCM3 regional climate model with active dust module to simulate the large Saharan dust event of 6-11th March 2006. This event was undoubtedly one of the most dramatic dust events ever recorded, with multiple source regions across the entire Sahara desert activated. The resulting dust plume extended for thousands of kilometres across the Atlantic and the west African sector. Dust activation was associated with strong winds at the leading edge of an explosive cold surge. The dust/wind front propagated south and southeast forms northern Algeria over a period of about 3 days. The RegCM3 model represents reasonably well many of the key features of the meteorology of the cold surge, although for dust studies it is interesting to note that near surface wind speeds are substantially underestimated. In this regard, the model might benefit from higher vertical resolution, especially in the boundary layer and alternative boundary layer parameterization to improve representation of turbulent fluxes in the lowest layers. Despite surface wind speed errors dust mobilization in the model is extensive. However, when using the predefined soil textures and hence aggregate size distributions, a number of active dust sources are not well reproduced by the model. Accurate description of soil characteristics in remote, poorly observed regions, is a widely acknowledged problem in dust modelling, and one which has been previously addressed through specification of preferential dust source regions. In this case we apply a new dust source activation map defined from SEVIRI observations to define all those model cells which are 'potential' dust sources [*Schepanski et al.*, 2007].

The results show a clear improvement in terms of the space/time structure of dust emission and transport. Quantitative comparison of modelled AOT is problematic due to lack of observations over the Sahara. Nevertheless, for the present work, there is considerable qualitative and quantitative evidence that the experiment with revised soil characteristics provides improvements in estimated AOT. The modified soil characteristics increases simulated AOT by about a factor of about two, which is not unreasonable given the rather low dust loading reported for RegCM3 in a model intercomparison project by *Todd et al.* [2008a]. The results suggest that in the absence of truly accurate soil maps at high resolution, further refinements to the dust source activation map and its implementation in dust models can lead to useful improvements in simulation of dust processes and may lead to improved dust forecast accuracy. However, further evaluation of long term model runs is required. In addition, the recent

development of techniques to measure aerosol properties over bright-reflecting surfaces (i.e. the Deep Blue algorithm on SeaWiFS and MODIS instruments [*Hsu et al.*, 2004]), will provide a solid evidence of the accuracy of models.

Estimates of shortwave radiative forcing are derived and highlight the substantial cooling effect dust events can produce at the surface, with a normalized RF of about -132-149Wm^{-2} per unit AOT. At the top of atmosphere the SW RF is sensitive to surface albedo with a domain average of about -10Wm^{-2} per unit in this study. The top of atmosphere SW RF is positive over desert surfaces even for highly reflective aerosols due to the high surface albedo in the model. It must be borne in mind that the modelled albedo does not represent the true spatial variability of surface albedo over the Sahara. Clearly the absolute magnitude of model simulated RF depends also on AOT and with the revised soil texture dataset the RF is about twice the magnitude simulated using the default model configuration. Unfortunately, the model does not reproduce radiative forcing in the long wave spectrum. As a consequence the magnitude of the absorbing pattern on the infrared can not be evaluated. Accordingly, further work is required to improve the soil datasets in dust models, as well as surface albedo, boundary layer meteorology and the specification of dust physical and optical properties as previous studies have indicated. These are likely to vary between different source regions across the Sahara such that further field studies are required to constrain our estimates of these parameters in model simulations.

6 Model characterisation of mechanisms controlling dust outbreaks in the WAM onset (6-11 June 2006)

6.1 Introduction

The efficacy of the models to simulate dust emissions during the onset of the African monsoon season is still a matter of debate. The existing limitations in ground based observations in remote areas in West Africa determine the reliance on numerical models to represent the various atmospheric mechanisms at different scales that influence the generation of dust outbreaks. The associated weather systems include atmospheric disturbances from synoptic and meso-scale such as strong *Harmattan* surges, cold breaks, Mesoscale Convective Systems (MCS's) and density currents to small scale such as turbulence by dry convection due to surface heating. Some atmospheric processes like those associated with large scale wind regimes (i.e. *Harmattan*) or small-scale atmospheric processes (i.e. dry convection) are partially resolved by the high-resolution ensemble models [*Giorgi and Mearns*, 1999; *McGuffie and Henderson-Sellers*, 2001]. However, dust emissions associated directly with the formation of MCS requires a more complex approach in physical parameterisations due to the assumptions used by models. Furthermore, the dust mobilized and transported in the Central West Sahara regions related to the presence of the Saharan Heath Low (SHL) has not been studied in detail. Thus the correct representation of the Saharan heat low in numerical models is crucial for modelling the West African monsoon and dust dynamics. The aims of this section include: (1) The evaluation of model performance to simulate dust emissions and transport during monsoon season using prescribed preferential sources, and (2) to evaluate model uncertainties in dust originated close to MCS and to discuss the effect of prescribed convective schemes on models.

6.2 The AMMA experiment (7-15 June 2006).

The period considered in this experiment is part of the Special Operation Period Phase 1 (SOP1, 2006) from the African Monsoon Multidisciplinary Analysis (AMMA) during the monsoon onset (May-June). A comprehensive description about the AMMA field campaign is well documented in *Redelsperger et al.* [2006]. The detailed

methodologies used for this section are described in Section 3.2.3. Configuration used for experimentation in both models is detailed in Table 6.1.

Table 6-1. Model configuration used for experimentation

Model name	WRF-Chem	RegCM3
Reference	[*Grell et al.*, 2005]	*Zakey et al*. [2006]
Boundary conditions	NCEP Final Analysis (FNL)	NCEP reanalysis
Domain	5°-30°N, 20°W-40°E	5°-30°N, 20°W-40°E
Dust-radiative feedback?	No	Yes
Simulation period	04-15th June 2006	04-15th June 2006
Horizontal resolution	30km	30km
Vertical levels	40	23
Height of lowest layer	40m	40m
PBL and surface schemes	Yonsei University (YSU) Scheme, Noah Scheme	[*Holtslag and Boville*, 1993]
Emission scheme [a]	[*Ginoux et al.*, 2001]	U^{*3} (MB 95)
Soil texture data	12 texture classes based on FAO [*Zobler*, 1986]	12 texture classes based on FAO [*Zobler*, 1986] and USDA data [*Dickinson et al.*, 1993], soil textures are prescribed for preferential source region
Number of dust bins	Total 5 size bins	4 size bins for dust transport derived from 3 log-normal dust emission modes
Dust particle size range	0.1 –10 µm	0.1-20µm diameter

[a]U* is the wind friction velocity and MB95 refers to Marticorena and Bergametti [1995].

Figure 6.1 shows the preferential dust sources (shading) used by both models and the location of AERONET and WMO stations used for validation purposes. The preferential dust sources were extracted using different methodologies as explained in section 3.2.3. In the GOCART scheme implemented for WRF-Chem, adust-source function is constructed as the probability of sediments accumulated in the topographic depression regions with bare surfaces in the form of an erodibility map (Figure 6.1.a). RegCM3 uses another approach for preferential sources. In this experiment, the model is configured following the methodology as in *Cavazos et al* [2009].

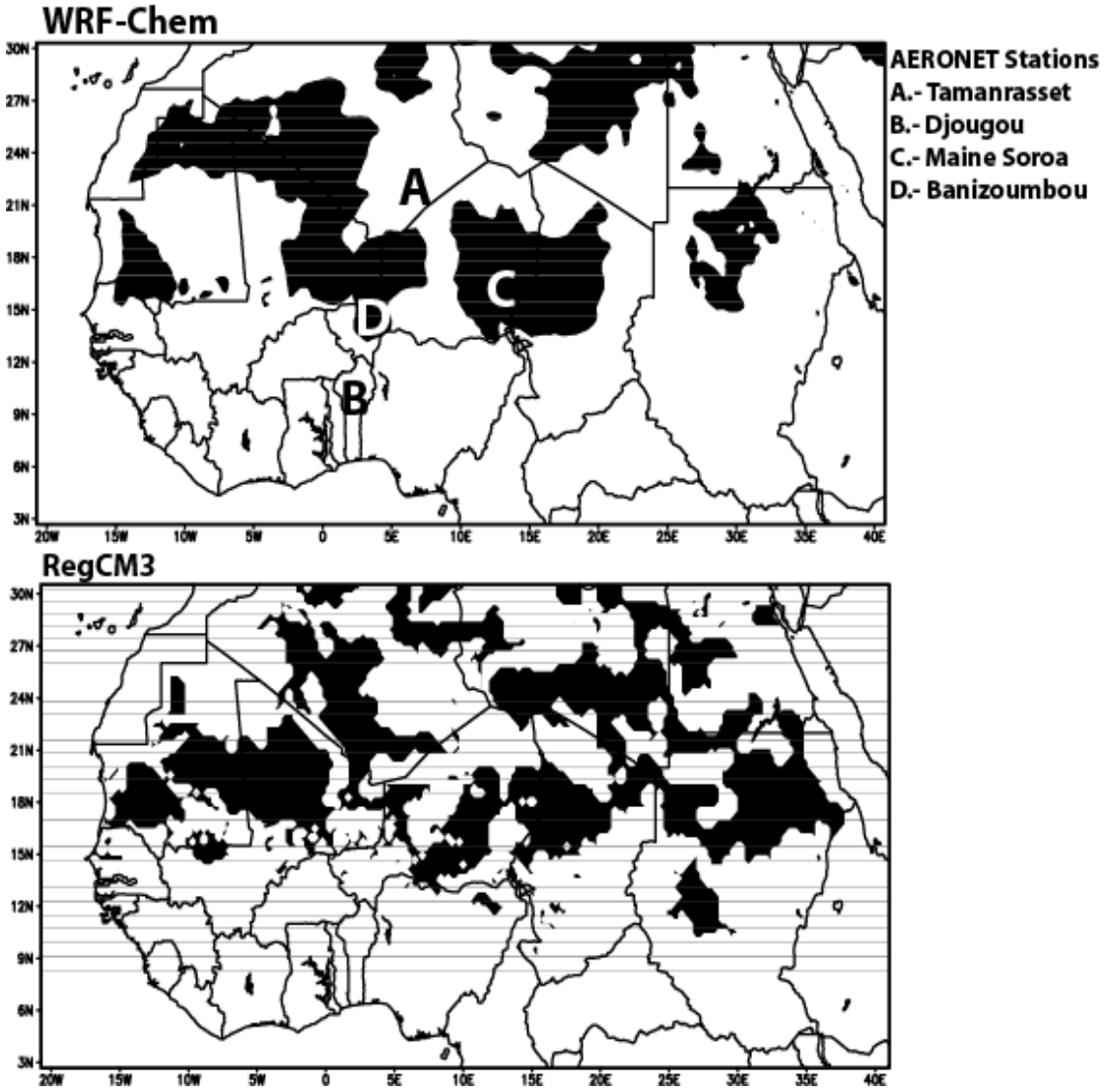

Figure 6.1; Area used as a model domain and location of AERONET stations (letters) used for validation. Shading represents the preferential dust sources used in the simulations (view text).

6.3 Results and discussions

The next sections show the results from both observational data and model simulations of the weather situation for June 2006 and the particular atmospheric features for the analyzed period that favour dust emissions towards the Sahara and Sahel. In addition, dust simulations are compared against satellite and ground-based observations to estimate model efficiency to finally determine uncertainties in simulations.

6.3.1. Mean monsoon conditions (June 2006)

Meteorological data from the ERA-Interim re-analysis were processed to describe the atmospheric circulation over the Sahara and the Sahel for June 2006 coinciding with the monsoon onset over West Africa. This is to depict the mechanisms that created favourable conditions for dust uplifting during this period. The Sea Level Pressure (SLP) for June 2006 (Figure 6.2) shows the prevalent influence of both the subtropical Azores high in the Atlantic and the Libyan high south of the Mediterranean controlling low-level circulation north of the equatorial beltbetween the 25°N and 35°N. The pressure gradient between the mid-latitude ridge from the Libyan high drives the northeasterly flow in the form of *Harmattan* winds, which converges with the southerly winds from the monsoon flow further south around the 15°N, near the Equatorial belt. The convergence line between both flows corresponds to the Intertropical Discontinuity (ITD). The typical values of water vapor mixing ratio (wvmr) for the moist monsoon flux (12 g Kg^{-1}) and the *Harmattan* flow (8 g Kg^{-1}) are used to characterise the limits of the ITD in the reanalysis data (Figure 6.2 brown contour).

The reanalysis also depicts the existence of several low-pressure centres along the Sahara and the Sahel (Figure 6.2) with an east-west propagation. These low centres, in the form of Sudano-Sahel depressions, are associated to the activity of African Easterly Waves (AEW) which are formed next to the flanks of the African Easterly Jet (AEJ) at around the 650hPa [*Cook, et al.,* 1999]. In turn, the AEJ is associated to the strong surface temperature and moisture gradient between the monsoon and the Harmattan flow and plays an important role in the organisation and propagation of MCS's which generate the rainfall over the Sahel [*Fink and Reiner,* 2003b]. At the surface, the tropical trough formed in Sudan moves north to form a closed low at about 18°N. *Flamant et al* [2007] observed that the occurrence of these depressions in the area is widespread from May to June [*Flamant et al.* 2007]. Further west, the borders of Niger and Chad are also

dominated by a low-pressure area -the monsoon trough- located around the 16°N. In august, the monsoon trough reaches its mature phase and reaches the 20°N and the Tibesti Mountains resulting in the occurrence of rainfall in the Sahel [*Saha*, 2009] Finally, there is an area of low pressure inducing strong cyclonic circulation in West Central Africa between the borders of south Algeria, eastern Mauritania and northern Mali known as the Saharan Heat Low (SHL). Some authors have acknowledged this area as the West African Heath Low (WAHL) [e.g. *Lavaysse et al.* 2009, *Knippertz,* 2008] due to the geographical location of the SHL during the monsoon onset. Northerly winds from the Harmattan flow are deflected and tunnelled between the Atlas and the Hoggar mountains. Subsequently, this flow encounters the advected moist air coming from the monsoon inflow feeding the SHL [*Knippertz*, 2007]. The heat low over the Sahara contributes to the strength of the monsoon trough [*Thorncroft and Blackburn*, 1999] and contributes to enhance meridional circulation [*Parker et al*, 2005]. Additionally, northwesterly winds from the mid-latitude ridge off the cost of Mauritania penetrate to the continent and are deflected around the 15° W and keep feeding the low level circulation in West Central Africa.

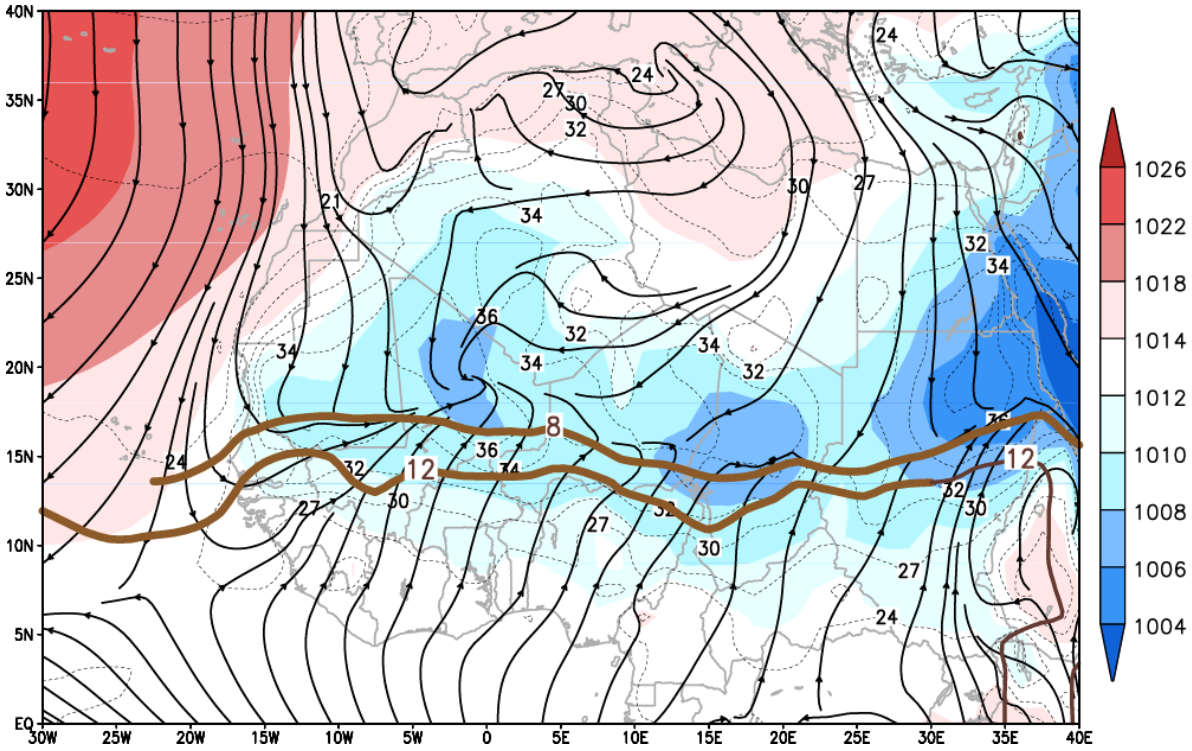

Figure 6.2: Atmospheric circulation over North Africa for June 2006. SLP (mb) (shaded), 10m winds (streamlines), temperature (contours) and wvmr g/Kg^{-1} at 925 hPa(brown contour). Source: ERA-Interim Re-analysis product 1.5 X 1.5.

6.3.2. Synoptic situation 7th to 12th June 2006

Part of the meteorological situation during the period under analysis has been detailed in *Flamant et al.* [2009]. These authors focussed their study in dust emissions from the Bodélé and Sudan regions from 9th to 14th June 2006. Additionally, *Knippertz* [2008] evaluated observations of dust mobilizations at the northwestern borders of the Sahara at the lee of the Atlas Mountains in southern Morocco for the period 6th to 12th just at the end of SAMUM 2006 campaign. In this research, the synoptic conditions for both periods are evaluated from re-analysis data and numerical modelling to provide a more detailed depiction of the propagation of low-pressure centres as one of the mechanisms involved in dust moilisation across the entire domain. The meteorological situation is depicted at 06UTC since this is the approximate time when the nocturnal monsoon flow and low level winds are strongest in this region [*Parker et al* 2005]. Accordingly, a Hovmoller analysis of the SLP and water vapor mixing ratio (wvmr) from the WRF-Chem simulations (Figure 6.4) and spatial distribution of wind components (Figure 6.5) are presented. Both diagnostics highlight the typical values of wvmr for the moist monsoon flux (12 g Kg^{-1}) and the *Harmattan* flow (8 g Kg^{-1}), which corresponds to the position of the ITD into the model.

In essence, the re-analysis products (Figure 6.3) show the retreat of the anti-cyclonic circulation around the Libyan High (North border between Libya and Egypt) from the 9th June 2006 00UTC. The *Harmattan* flux is reduced and moves back up to 30°N and is also deflected to the west. This pattern is also reflected in the Hovmoller analysis of SLP (Figure 6.4a). Nevertheless, part of the northeasterly winds from the Harmattan flux continues moving southwards and is channeled across the Tibesti and Eneldi Mountains (Figure 6.5) crossing the Desert of Bodélé, North of Chad on the 10th and 11thJune. The synoptic analysis also shows the development of several well-developed tropical troughs across the Sahara and the Sahel developed initially south Egypt and North Sudan on the 7th (Figure 6.3a), which propagated on a westward direction reaching the border with Chad around the 20°E with a length between the 10°N and 20°N by the 9th June (figures 6.3 and 6.4). By the same period, the mid-latitude ridge extending on the east flanks of the Atlas Mountains around the 5° W (Figure 6.4.b) retreats completely northwardly. Likewise, the Azores High (over 30° W) reduces its influence over Northwest Africa from the 8th June (Figure 6.3). This allows the inclusion of other disturbances the subsequent days.

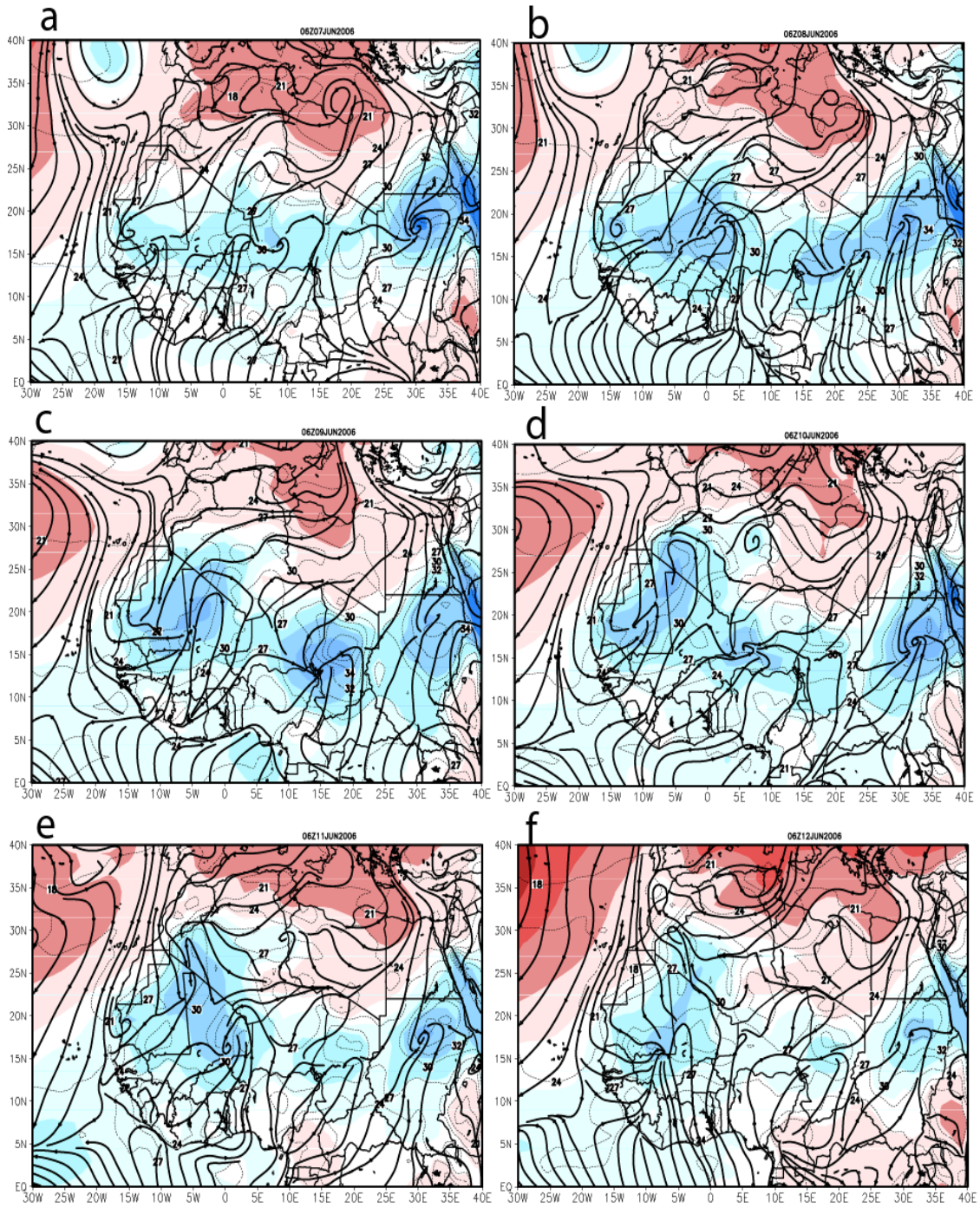

Figure 6.3: Atmospheric circulation over the model domain. Sea Level Pressure (mb) (shaded), 10 m winds (streamlines), temperature (contours). (a) 7th, (c) 8th, (d) 9th, (e) 10th, (f) 11th, (g) 12th June 2006 at 06UTC. Source: ERA-Interim Re-analysis product 1.5 X 1.5

The incursion of low-pressure circulation induces the development of a several Mesoscale Convective Systems (MCS) around 15°N 18°E during the period under study (Figure 6.6). TheseMCS's are often associated with large-scale atmospheric circulation such as the AEW to form a squallline at their leading edge [*Diongue et al.*, 2002] and are accountable mechanisms to produce winds to generate and transport dust [*Jones et al.*, 2004]. These squall line appear intermittently in the SEVIRI images as an elongated feature appearing on the 9th and 11th June crossing a long extent of south Algeria (Figure 6.6.c-d). It is now well established that they provide most of the annual rainfall in this area. Westerly winds move towards West Africa (Figure 6.5) crossing Niger and Mali at the northerly flanks of the ITD, which reaches its northernmost position around the 15°N (Figure 6.4). This might indicate the intrusion of moist air from the monsoon flow in this area. Further west, winds from the cyclogenesis originated in East Mali converge with Northerly winds apparently deflected from the Ahaggar Mountains in the South Algerian border.

The strength of wind speed at West Sahara in Mauritania, is reduced drastically compared with the previous day. This is caused by the west displacement of low pressure generating a cyclonic circulation. Moist air triggered by the daytime heating and topography seems to be advected by the monsoon flow causing moist convection and precipitation in this airmass. Strong evaporation in dry midlevel air generates extended cold pools and *haboob* dust storms [*Knnipertz,* 2006].In the reanalysis data, the temperature at the centre of the heat low in the borders between south Algeria, Mali and Mauritania oscillates around the 36° C. This represents an increase of 2°C and 3°C compared with the previous day. This increase might reflect the formation of an elongated low-level thermal depression, the Sahalan Heath Low (SHL), which is directly related to a decrease in surface pressure [*Lavaysse et al.*, 2010]. This feature is also seen in the cross section (Figure 6.4.b). In addition, wind speed is dramatically reduced (Figure 6.5) in the center of the heat low. The impact of the intra-seasonal variability on the low-level circulation and on convection isparticularly significant over the Sahel [*Flamant et al.*, 2007; *Parker et al.*, 2005a]. These lows associated with the AEW formation produce winds to generate and transport dust. As noted by *Knippertz and Fink* [2008], the SHL often takes the form of a zonal elongated heat trough rather than a circular low, depending

on the season. By the 12th, the SHL reduced its intensity (Figure 6.3) and is slightly retreated southwards (Figure 6.4.b).

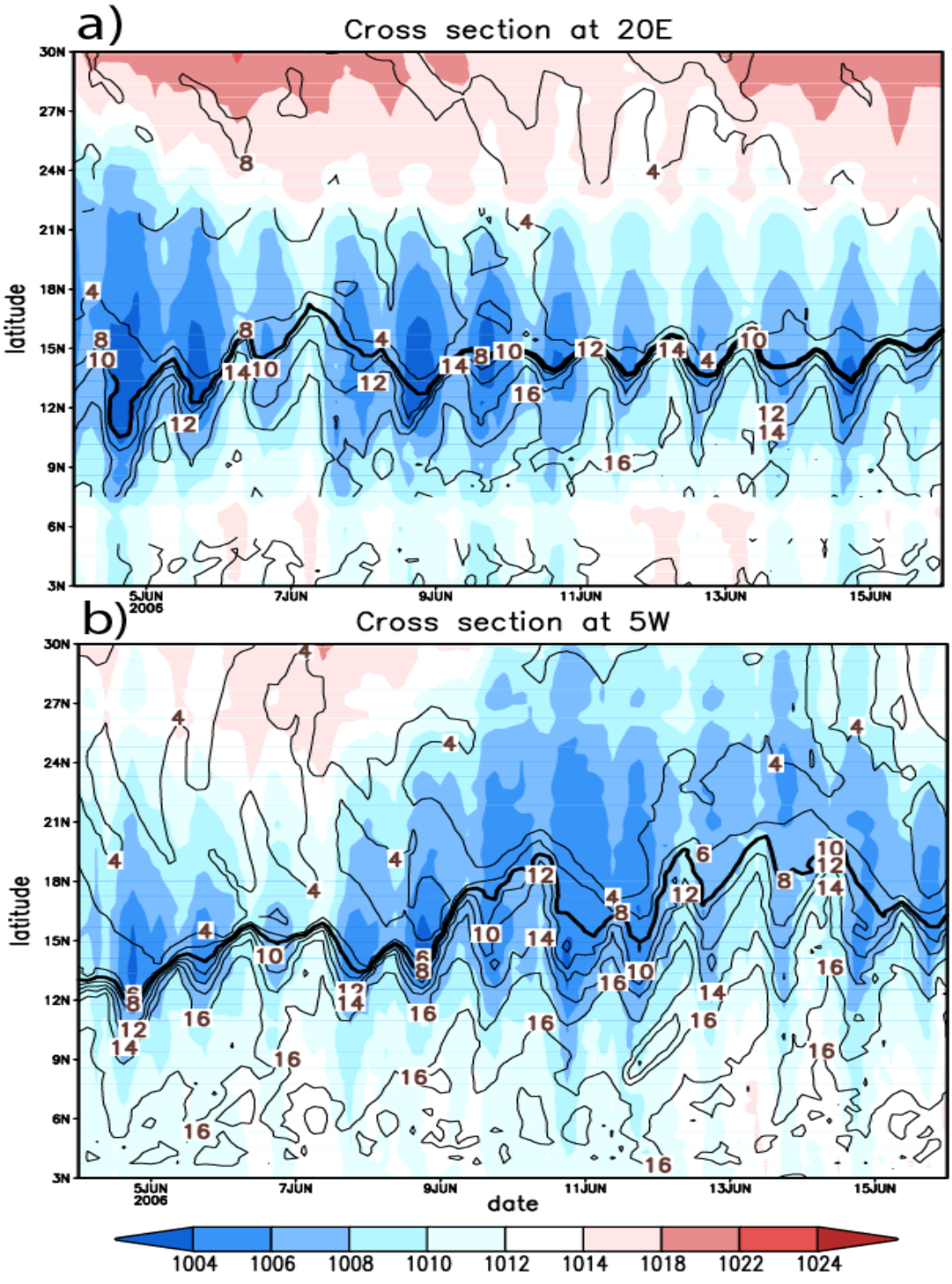

Figure 6.4: Hovmoller diagram showing WRF-Chem model simulations of SLP mb (color) and the wvmr g/Kg-1 (contour) at 925 hPa at (a) 20°E and (b) 5°W.

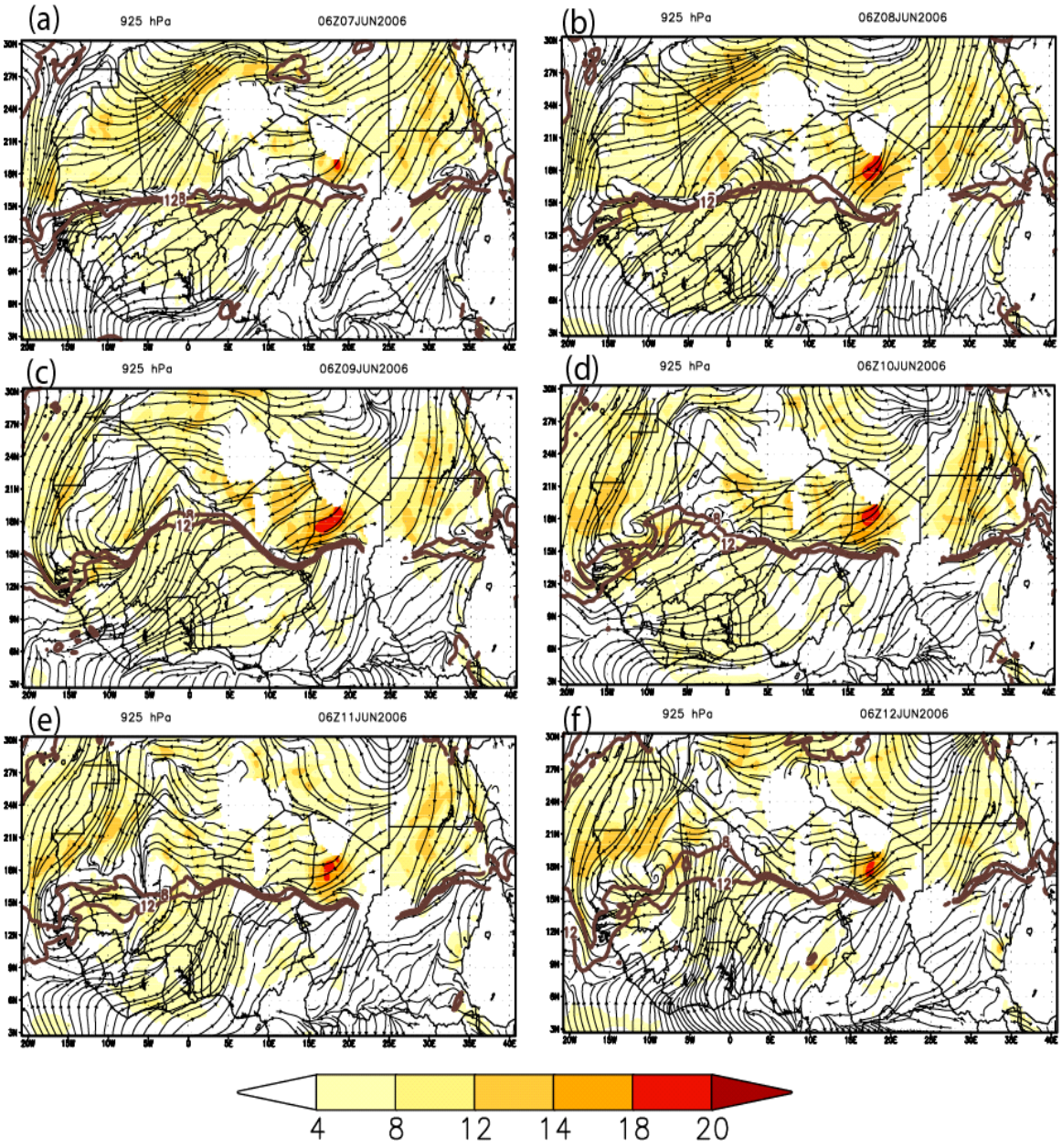

Figure 6.5: WRF-Chem simulations showing the wind direction (streamlines), wind speed m/s (color) and wvmr g/Kg^{-1} (brown contours)a't 925 hPa on the (a) 7th, (b) 8th, (c) 9th, (d) 10th, (e)11th and (f) 12th June 2006 at 06UTC.

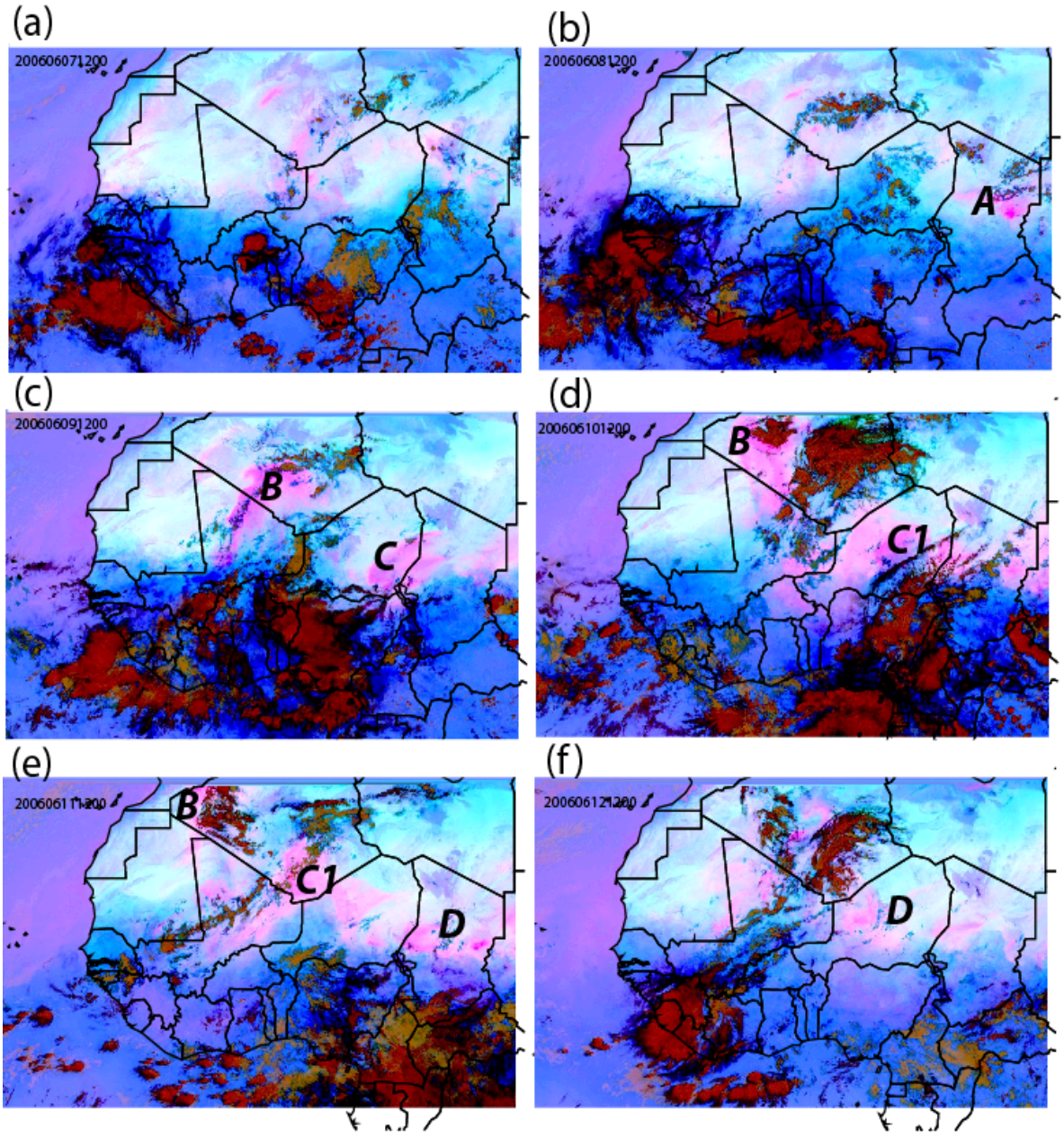

Figure 6.6: SEVIRI false colour dust product imagery at 1200 UTC each day over the study period. Pink tones indicate dust.

6.3.3. Dust model simulations and observational data

The Aerosol Optical Thickness (AOT) derived from MODIS Deep Blue product (Figure 6.7) and the SEVIRI false color imagery (Figure 6.6) denote continuous dust emissions along the Sahara belt during the period 7th to 12th June 2006. A detailed analysis to characterise late spring dust emissions transport using multi-platform observations by *Flamant et al* [2009], indicate that numerous dust sources over the Bodélé and West Sudan region were active. These general patterns agree in a good extent to dust simulations made with WRF-Chem and RegCM3 (Figure 6.8 and 6.9 respectively) for these regions.

Several atmospheric mechanisms at different scales are responsible for atmospheric dust release during this period. Although the prevalence of the strong *Harmattan* winds was reduced as seen in the meteorological analysis in the previous section, it influence is large enough to generate discrete dust outbreaks in North Africa. As seen in the SEVIRI imagery, dust plumes are originated in a prominent zone along the Libyan-Chad border (Figure 6.6 letters A, C and D), which are also seen in model simulations (Figures 6.8 and 6.9). On the 8th June, the northeasterly wind (up to 18m s^{-1} in the model) is channelled between the Tibesti and the Eneldy, mobilises dust in Bodélé Depression, North Chad (Figure 6.6 letter A).

High dust emissions in this area are favoured due to the material available to be deflated and the change in the LLJ diurnal cycle. Eventually, the dust plume moves westwards and mixes with a new dust plume formed in early hours on the 9th June (not shown). By midday, the plume is transported to the borders of Niger and Chad (Figure 6.6 letter C) and according to the MODIS Deep Blue composition, AOT values as high as 4 are registered in this area (figure 6.7). This peak in the AOT is also registered in the nearest AERONET station at DMN Maine Soroa (Figure 6.10) reaching AOT values at high as 3.5.

On the same day, a MCS in the form of a squall line in the borders between Algeria and Mali advances in a northwest direction, which is clearly seen in Figure 6.6.c. letter B. This feature favours the generation of the low-level cold outflow in the form of gravity current or *haboob* caused by this convective system. This cold outflow is an efficient mechanism for dust uplifting as seen in the same figure where a big dust plume

is developed along the whole extension of the squall line. This dust mobilised through this late mechanism appears to be missed in both models. Although some dust is fairly simulated in southeast Algeria dominated by MCS's on the 9th and 10th June, the simulations might be driven entirely by the strong low-level winds along the north and west flanks of the Hoggar as suggested by the strength of the modelled wind (Figures 6.8 and 6.9). Coincidentally, this region is characterised by a complex distribution of dust sources[*Prosperoet al.*, 2002] as seen in Figure 6.1. Over the next two days (10 and 11th June 2006), a large dust plume is observed west of Niger (Figure 6.6.d-e letter C1) near to a large MCS's around the 10°E and 10°N. Analysis from the SEVIRI imagery in early hours on the 10th (not shown) suggests that part of this dust plume might be a consequence of the dust mobilised the previous day and transported from the Bodélé Depression near the borders between Chad and Nigeria (around the 15°E) (letter C). Likewise, the westwards displacement of this MCS's might have contributed to the development of *haboobs* and hence favouring the mobilisation of more dust, which is transported on the 11th all the way through Niger and Mali (Figure 6.6 letter C1).

At this stage, the dust plume forms an elongated structure with a sharp leading edge at the north border of the ITD which is also seen in the MODIS Deep Blue product (Figure 6.7.e) with AOT values as high as 3 in the south borders of Algeria. These values agree to those in the nearest AERONET station (Tamanrasset 5.5°E, 22.8°N), which shows continuing dust emissions with the highest AOT by the 11th June (Figure 6.10). However, high cloudiness prevents the AERONET photometers to measure AOT, hence measurements on the 10th are missed. In this instance, both models fail to produce significant AOT values due to their failure to represent the MCS and hence the following mechanisms to trigger dust.

The west displacement following this elongated feature might be related to the presenceof the cooler more stable monsoon further south, forcing the hotterand drier Saharan air to ascend as high as 4 km which is in turn caught in the AEJ circulation and transported over Nigeria and Mali. The late assertion can be confirmed from the vertical dust distribution at the edge of a MCS seen in the CALIPSO profiles in subsequent days (section 6.3.5). Models depict the elongated dust transport across the Sahel at some extent, particularly for the WRF-Chem (Figure 6.8.e) and in less degree in the RegCM3. This can also be confirmed in the nearest AERONET station (Figure 6.10. Banizoumbou, West Niger).

Modelled AOT values suggest the presence of dust from the 9th at early hours in the morning. This is caused by the daytime PBL development that follows the nocturnal LLJ as key mechanism that resultsin a diurnal cycle in the uplift and vertical transport ofdust [e.g. *Chaboureauet al.*, 2007]. The diurnal dust 'pump' appears to be represented in the WRF-Chem and in a lower degree by the RegCM, which seems to underestimate AOT. A possible explanation for this underestimation is that the modelled dust transported to this area on the 10th was produced entirely by the strong northeasterly winds when actuality the total dust transported to this area might be a consequence of the dust mobilized by both the influence of the *Harmattan* and due to the presence of density currents. This latest mechanism is caused by the presence of MCS at the edge of the IDT as suggested in the SEVIRI composition (Figure 2.6.d letter C1). By the 11th and 12th of June, more dust is mobilised and transported from the Bodélé Depression (Figure 6.6. e-f, letter D) and it is clearly depicted by both models.

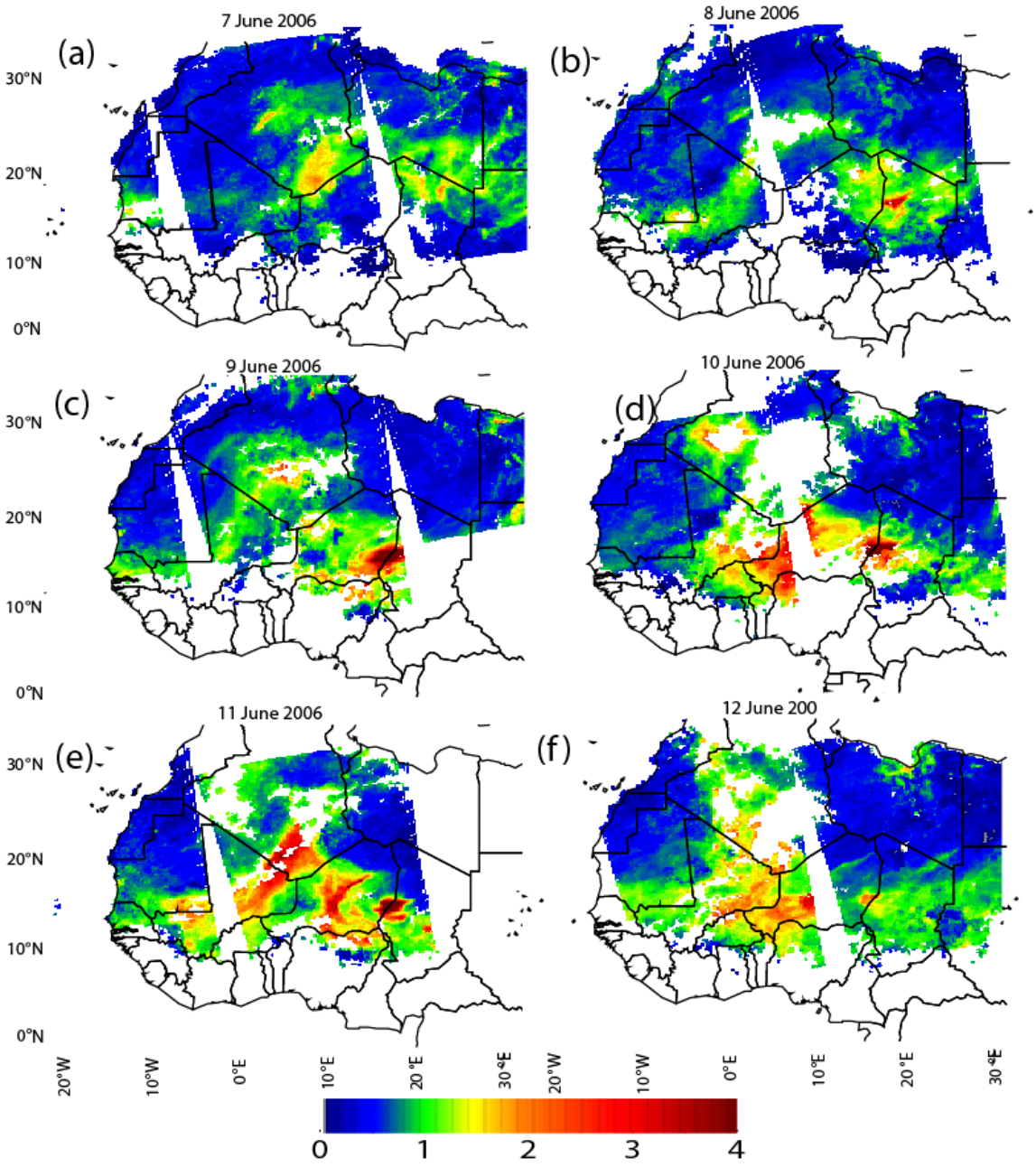

Figure 6.7: Daily MODIS Deep Blue Aerosol Optical Thickness (AOT) product over North and West Africa from 6th to 14 June 2006, around 13 UTC.

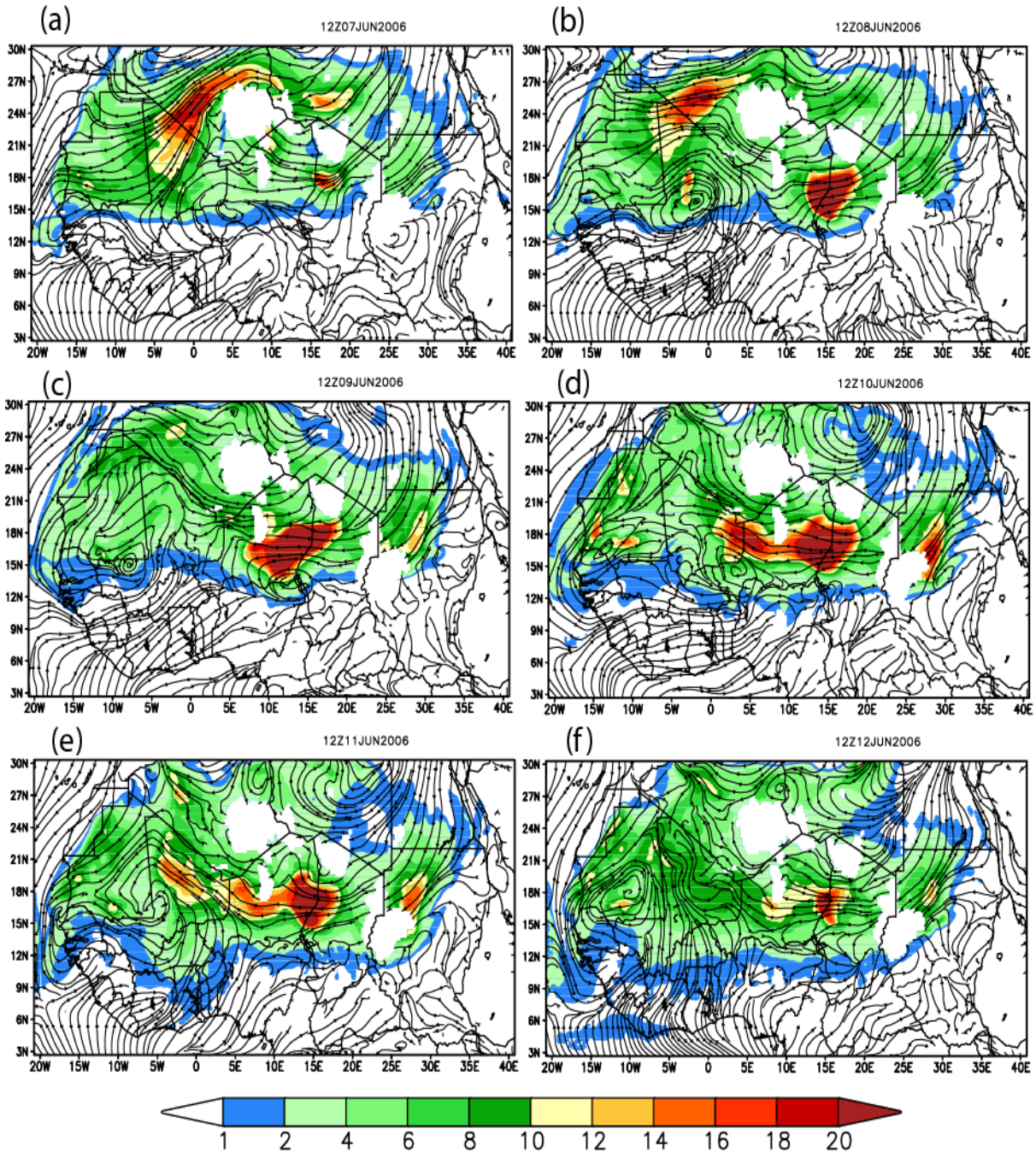

Figure 6.8: WRF-Chem Model simulated vertical integrated dust mass (g m^2) from 7th to 12 June 2006 at 1200 UTC. Wind direction (streamlines) at 925mb is shown.

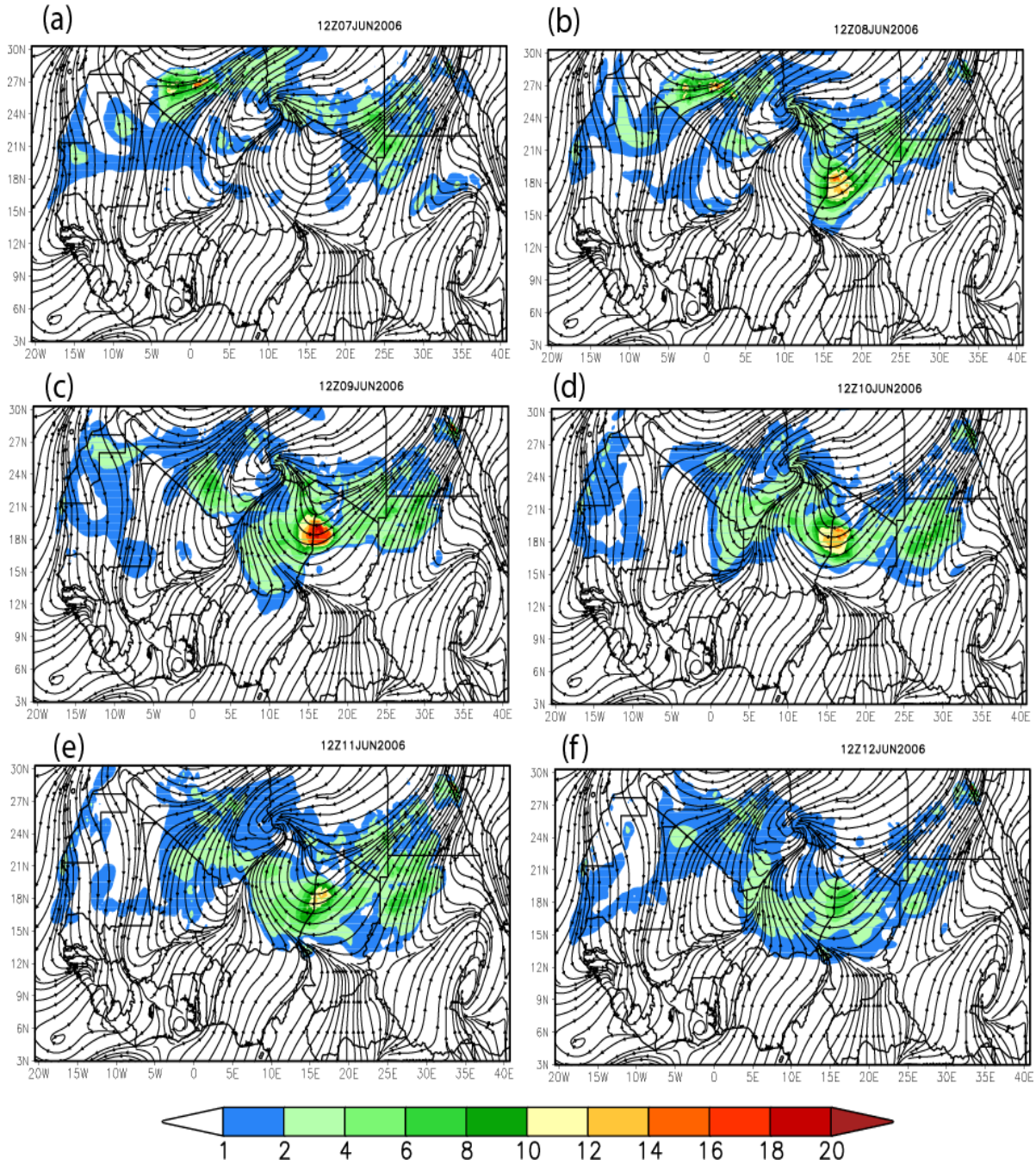

Figure 6.9. RegCM3 Model simulated vertical integrated dust mass (g m2) from 7th to 12 June 2006 at 1200 UTC. Wind direction (streamlines) at 925mb is shown.

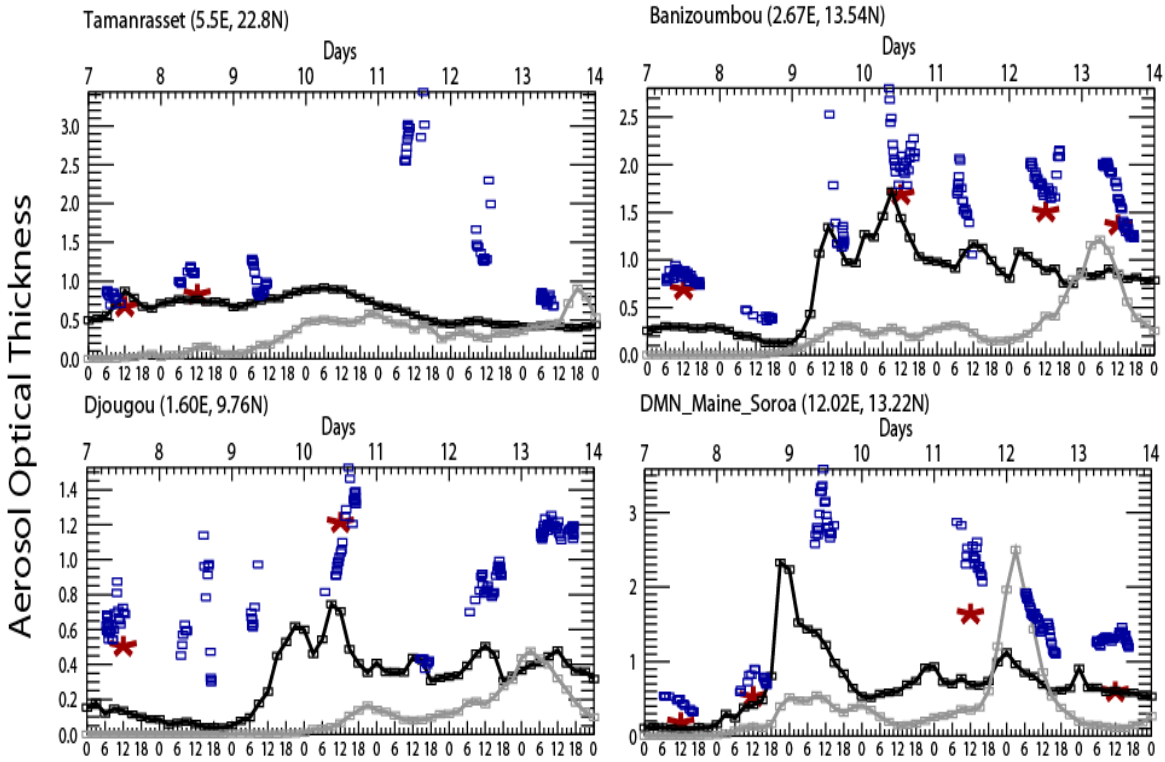

Figure 6.10: Time series of observed and model simulated AOT at the locations of the AERONET stations: 440 nm AERONET-AOT (blue squares), MODIS-AOT (asterisks), RegCM3-AOT (grey curve) and estimated WRF-Chem AOT after *Koren et al* [2006] (black solid curve).

The averaged surface dust emissions (Figure 6.11) for entire period (7^{th} -12^{th} June 2006) show that in the WRF-Chem model, dust is generated in a great extent in the Bodélé Depression around the 18ºN and 18ºE (among the Enneldi and Tibesti Mountains). Average estimations of dust emissions during the period under analysis are equal to 200 g m^{-2} d^{-1}. In the RegCM3 model, several dust hotspots are well depicted in a lower degree than in the WRF-Chem but yet, values as high as 180 g m^{-2} d^{-1} can be spotted at Chicha (around the 18ºN and 17ºE). Model estimates are close to those shown by *Todd et al.* [2008] in a model inter-comparison (~250 g m^{-2} d^{-1}) from a winter case in the Bodélé Region.

The nature of the recurrent dust emissions from the Bodélé Depression has been well documented by different authors [i.e. *Washington et al.* 2006, *Koren et al*. 2006, *Todd et al*. 2007]. Dust lifting is activated due to pronounced diurnal pattern of low-level winds associated to the downward transfer of momentum from the nocturnal LLJ to the surface due to turbulent mixing after solar heating starts. Consequently, the maxima wind speed few hours after sunrise is affected and high dust emissions are triggered. Although dust emissions are more recurrent during the winter-spring time, these sources are still active at the monsoon onset.

Other areas particularly active during the monsoon onset are located in North Sudan (20ºN and 30ºE), extending from the western flanks of the Ethiopian highlands west to the plateaus of western Sudan and eastern Chad (Ennedi plateau). The Sudanese sources have been reported to be particularly active in May–July by several authors [*Flamant et al.*, 2009; *Prospero et al.*, 2002]. Clear examples are regions near the Nubia Desert in northern Sudan where the topography is mainly characterized with dense drainage channels like *wadis* likely to provide fluvial sediments. *Engelstaedter et al* [2006] described these Nubian dust sources as active in the summer between April and August with highest values at the eastern Sudanese coast in June and July as shown in the WRF-Chem where average emissions exceed the 100 g m^{-2} d^{-1}. Although RegCM3 does not produce emissions in the late area, it produces dust emissions near the Nuba Mountains in South Kordofan, Sudan. This region is characterised by the abundance of lake sediments and alluvial deposits providing enough material to be deflated as depicted by *Prospero et al.* [2002].

Other sources with considerable dust emissions by both models during the period under study are located over Libya. In a study focussed on dust deposition over this area, *O'Hara et al.[2006]* describes thatvariations in deposition rates, particle-size and bulk mineralogy, indicate that the deposited dust is of multiple origins. Based on prevailing winds and likely surface conditions, the main source areas for the medium–long distance sediments are the Libyan Desert (eastern Libya and Egypt), the Ahaggar region of southern Algeria (Erg Edeyen), and the Chotts and Grand Erg Oriental/Occidental of southern and central Tunisia and Algeria. The WRF-Chem does not discriminate particular sources and dust emissions extents to the 50 g m^{-2} d^{-1}. On the other hand, RegCM3 spotted two particular areas around the 25ºN where dust emissions where higher (up to 100 g m^{-2} d^{-1}). One source is indeed located over the eastern Libyan Desert and other over the north region of Marzuq. These areas are located in low-lying regions and are characterised with a number of drainage features, particularly several *wadis* which act as dust sources under the influence of the northerly winds resulting from the edges of strong anticyclone circulation from the Libyan high (Figure 6.2).

The time average emissions in the region near the SHL around the 25-27ºN and 0ºE at the southwest flanks of the Plateau of Tademait indicate high emissions during the period under study. However, the magnitude of emissions is lower for the WRF-Chem with values around 60 g m^{-2} d^{-1} for the whole period whereas in RegCM3 exceeding the 150 g m^{-2} d^{-1}. This area is characterized topographically by the presence of *ergs* (dune fields, sand seas)and *Hammadas* (barren, rocky desert landscape) as well as drainage systems and topographic gaps [*Stone*, 1967], hence the erodable material is available for dust lifting.

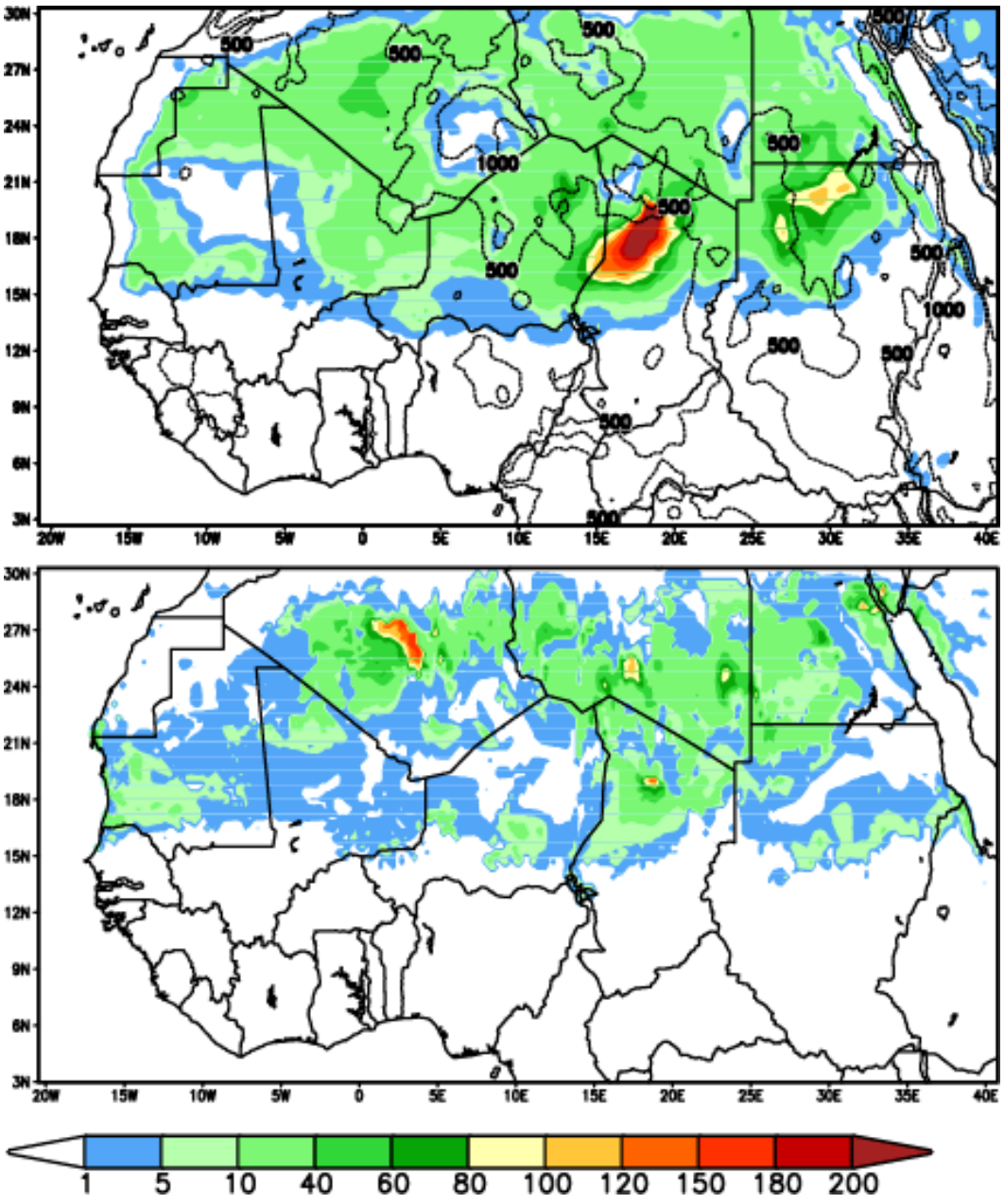

Figure 6.11: Model simulated mean rate of surface dust emission 07-12 June 2005 (g m^{-2} d^{-1}). WRF-Chem (top) and RegCM3 (bottom). Dashed lines represent the 500-m and 1000-m surface elevation.

6.3.4. Vertical cross sections (13 to 15th June 2006).

This section analyses the modelled vertical structure of dust plumes during 13th-15th of June. This period coincides with the first observations from the CALIOP sensor on board the CALIPSO satellite. These measurements in turn allow the evaluation of the model efficiency to simulate dust at the edge of the ITD and to determine transport along the whole Saharan Boundary Layer. The Level 2 Vertical Feature Mask data (VFM) and the Total Attenuated Backscatter (TAB) product at 532 nm acquired from a mid-day overpass and a mid-night overpass are chosen due to the strategic location at the time of the pass. (Figures 6.13 to 6.15). Daytime attenuated backscatter retrievals suffer with extreme noise due to contamination by solar background [*Mcgill et al.*, 2007]. However, daytime comparisons are still presented to demonstrate the importance of the increased signal noise of CALIPSO during daytime measurements (comparing with nighttime).

In the night overpass on the 13th June, a big cumulonimbus convective system is developed in Algeria extending from the 20°N to 30°N. This feature is seen in the SEVIRI composition (brown features), causing elevated cloudiness at about 8 km from the surface (figure 6.13.a1). According to the VFM mask and the TAB products, a big dust plume extents along the whole orbit, which might suggest that dust is being lifted probably due to the formation of density currents originated at the edge of this system. However, this dust plume is not clearly detailed in the SEVIRI image. Although, measurements in the infrared make night observations possible for this platform, the dust product is more diffuse than during daytime measurements and it is unlikely that dust close to the surface is identified at night. Nevertheless, from the dust column integrated product in the WRF-Chem experiment, a big dust plume is originated around the 17-19°N and 1°E, just at the south flanks of the Adrar Mountains. This depiction also agrees at some extent to the VFM Calipso features although due to the high cloudiness in this are it is not clear where exactly this dust plum is originated. The images suggest that the plume is elevated in the limits of the ITD which is demarked by the wvmr values between the 8 and 12 g/Kg suggesting the light dry dusty air mass is transported over the moist dense monsoon flow and it is elevated to the upper regions of the SBL (around the 6 km).

Another interesting dust feature is seen the same day at midday in the SEVIRI image (14:09 UTC CALIPSO orbit), which is well depicted by the VFM and TAB

products (around 20°N and 13°W) (Figure 6.13-b2,c2). An elongated dust plume appears to be transported in a westwards direction off the coast of Mauritania, which is also registered in the nearest weather station in Nouackchott, Mauritania (not shown). From VFM and TAB features, it would be suggested that most of this dust plume is just being transported from the east and not generated in the area. Nevertheless, some dust located very close to the surface around the 19°N and 12°W in Central Mauritania would indicate punctual emissions, which would be a confirmation of the dust plume being generated in the model in this region. Vertical transport is in turn modulated by the monsoon flow, which allows the ascending of the dusty light mass air (Figure 6.13.d2).

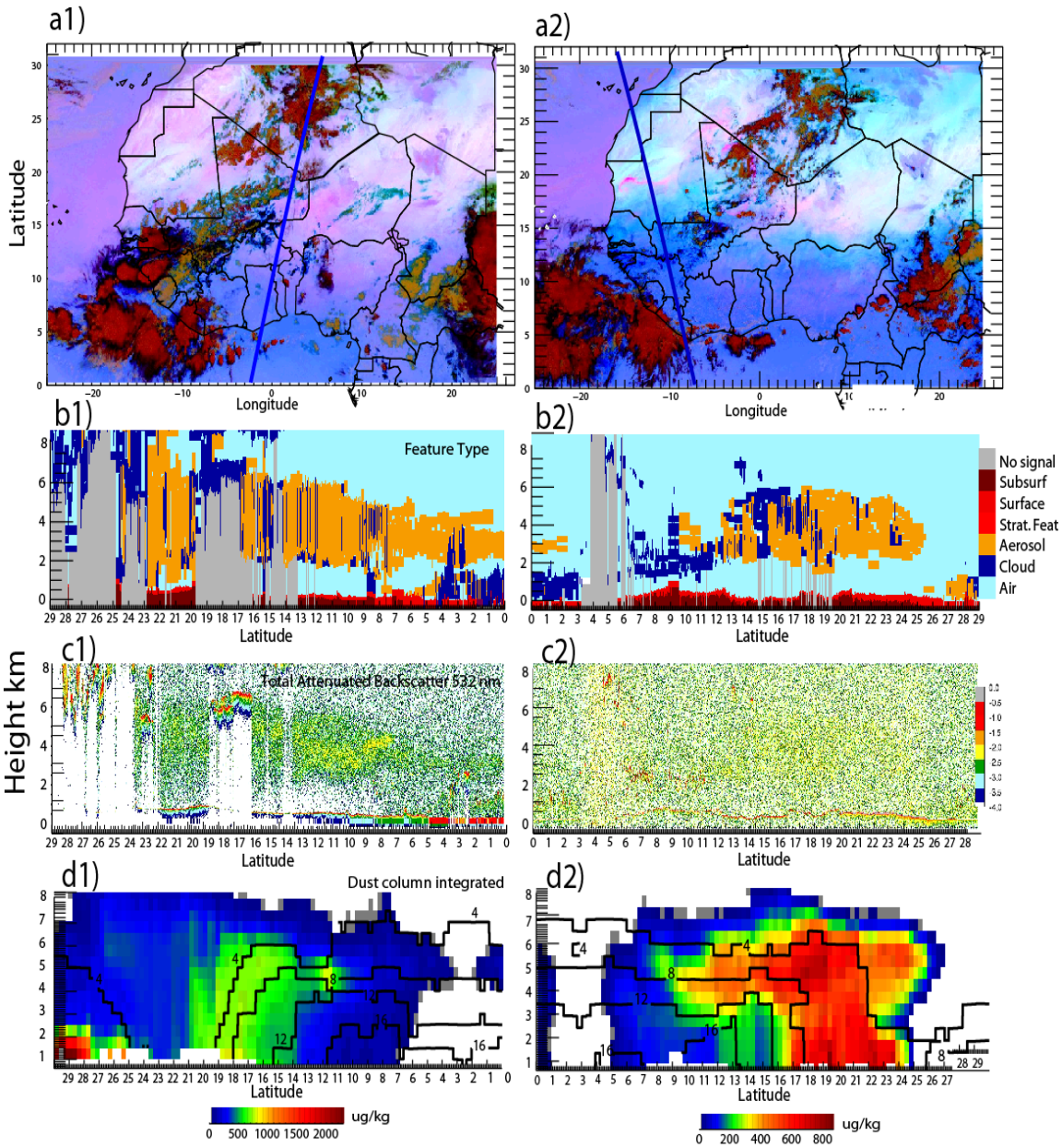

Figure 6.12: (a's) SEVIRI false colour dust product imagery on the 13th June 2006. Blue line indicates the CALIPSO track. (b's) CALIOP VFM product. (c's) CALIOP Total Attenuated Backscatter product $10^{-3}km^{-1}sr^{-1}$ (d's) WRF-Chem simulations showing the dust column

integrated cross section ug Kg^{-1} (color) and water vapor mixing ratio in g/Kg^{-1} (contours). (1's) night-pass at 01:37 UTC and (2's) day-pass at 14:09 UTC.

The next day (14th June), intense cloudiness in Algeria, Mali and Mauritania indicating the presence of several MCS's in the form of squall lines are featured during night-time (around the 02:20 UTC). Although the SEVIRI composition does not distinguish clearly the dust mobilised in the comprising the 10°W and 20°N, the CALIOP VFM and TAB profiles suggest that dust mobilisation occurs at the ITD and might be related to the presenceof the cooler air monsoon, forcing the hotterand drier Saharan air to ascend and favoring dust particles uplift. (Figure 6.14-b1,c1). This feature is well represented by the model (figure 6.14.d1). For the daytime orbit (around 13.00 UTC), the MCS's formed on previous hours disappear (Figure 6.14.a2) and the dust lifted in the central part of Algeria around the 27°N might be rather a consequence of either, the strong *Harmattan* wind or due to gustiness enhanced by deep convection due to the intense heating in this area. A similar feature can be seen further south around the 15°N. Both emissions seem to be well represented in the model, which might effectively suggest these are isolated plumes, generated by the same mechanism (Figure 6.14.d2). However, near to the equator, the VFM profile shows some features that might indicate dust, although it is not clear whether it is dust being transported and deposited or if the feature might be rather related to biomass burning in this region (Figure 6.14.b2-c2).

Finally, on the 15th June there are some notable features to discuss. The VFM profile (00.30 UTC) suggest a massive dust mobilisation around from the 15 to 21°N near the Hoggar Mountains, which is also well represented in the model (Figure 6.15.d1). There is good agreement in the high at which the dust is lifted (around the 6 km) for the model and the observations. It is possible that the prevailing nocturnal downslope flow in the form of a LLJ help to lift dust in this area although it is not clear in the SEVIRI composition due to the limitations of this satellite for measuring during night-time. During daytime, a massive dust plume is well depicted in the CALIPSO VFM and ATB profile (12.04 UTC). This dust plum appear to be originated near the Bodélé Depression around the 16°N and 17°E (Figure 6.15.a2) and it is well depicted in the model (Figure 6.15.d2).

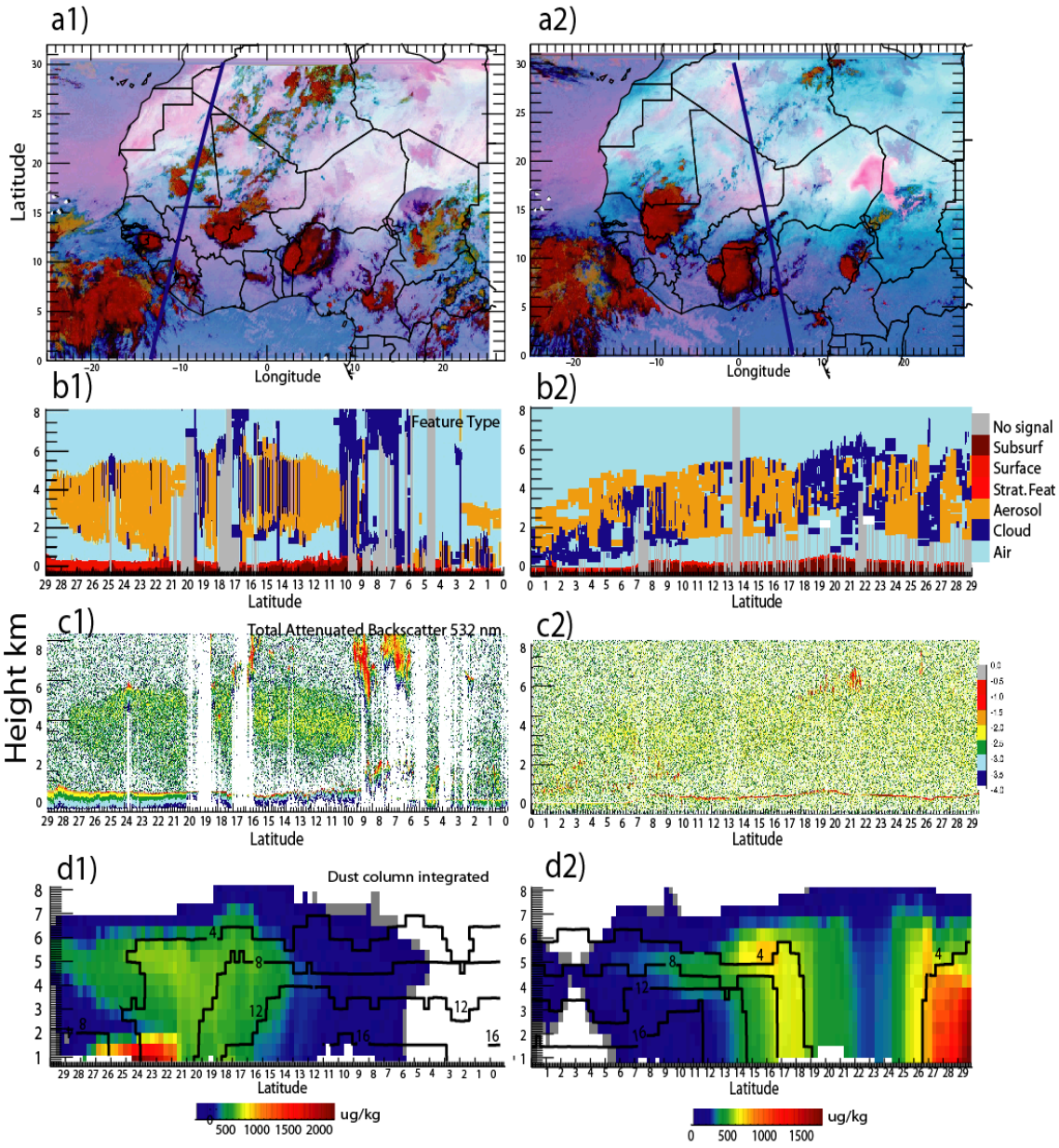

Figure 6.13: (a's) SEVIRI false colour dust product imagery on the 14th June 2006. Blue line indicates the CALIPSO track. (b's) CALIOP VFM product. (c's) CALIOP Total Attenuated Backscatter product $10^{-3}km^{-1}sr^{-1}$ (d's) WRF-Chem simulations showing the dust column integrated cross section ug Kg^{-1} (color) and water vapor mixing ratio in g/Kg^{-1} (contours). (1's) night-pass at 02:20 UTC and (2's) day-pass at 13:00 UTC.

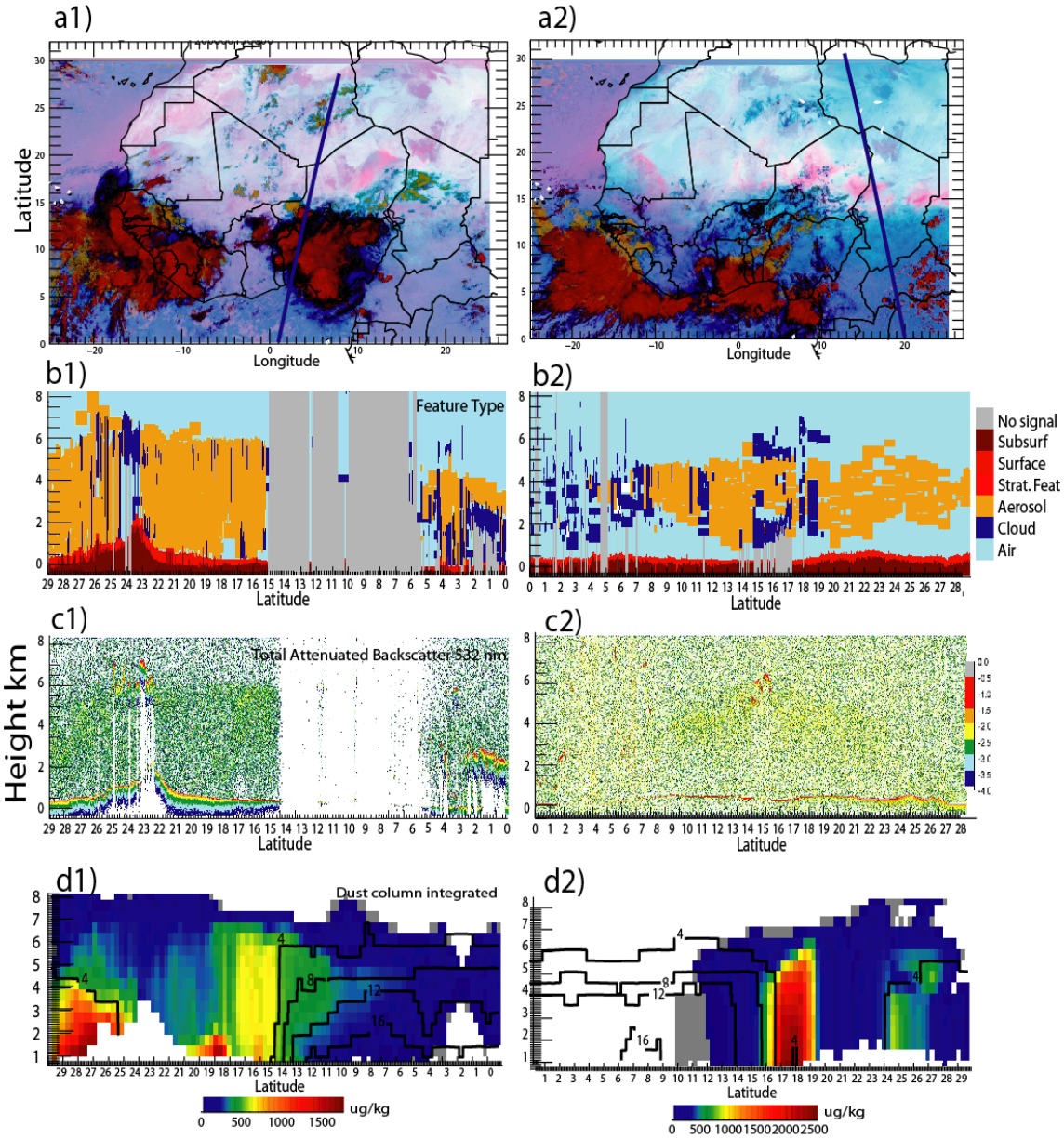

Figure 6.14: (a's) SEVIRI false colour dust product imagery on the 13th June 2006. Blue line indicates the CALIPSO track. (b's) CALIOP VFM product. (c's) CALIOP Total Attenuated Backscatter product $10^{-3}km^{-1}sr^{-1}$ (d's) WRF-Chem simulations showing the dust column integrated cross section ug Kg^{-1} (color) and water vapor mixing ratio in g/Kg^{-1} (contours). (1's) night-pass at 01:24UTC and (2's) day-pass at 13:43UTC.

6.4Summary

The model efficiency of the WRF-Chem and RegCM3 to simulate dust emissions and transport from preferential dust sources was evaluated in a particular period (7^{th} to 15^{th} June 2006) within the framework of the AMMA Special Observing Period (SOP) in North Africa [*Redelsperger et al*., 2006]. The spatial distribution from the ERA-Interim re-analysis data and model simulations confirm the development of small and meso-scale atmospheric processes related to the activation of dust sources in North Africa during the monsoon onset. It included the effects (i.e. strong gradient in moisture and temperature) modulated by the pressure gradients between the northesterly dry light *Harmattan* flow and the advected southerly moist monsoon flow into the Sahara-Sahel, which delimit the position of the ITD. The re-analysis also depicts the development of several low-pressure centres (Sudano-Sahelian depressions) associated with the progress of AEW, which are in turn related to the evolution of the AEJ in the upper atmosphere over North Africa.

Both models (RegCM3 and WRF-Chem) perform reasonably well representing these low-pressure centres with an east-west propagation along the Sahelian belt.The results also depict the position of SHL, in West Central Africa between the borders of south Algeria, Mauritania and northern Mali, which is known to play a key role in the West African monsoon system (Parker et al., 2005). Dust emissions within the models are mainly induced by the strong winds resulting from the *Harmattan* flow from the anticyclonic circulation. Both models represent adequately the day-to-day variability in emissions in the Bodélé Depression (a well known dust source) and other dust sources in Libya, Sudan and North Algeria. Emissions over these regions are conditioned in a great extent by the variability in the strength of the northeasterly LLJs and the availability of erodable material to be deflected (i.e. *wadis* and drainage systems). However, areas dominated by deep moist convection in the form ofMeso-scale convective systems (MCS's) leading to the formation of density currents or *haboos*favoring dust lifting at the limits of the MCS as seen in the SEVIRI images are not well defined with the same magnitude in model simulations. The main concern is the physical assumptions used by physical parameterizations schemes in models. The comparative analysis between observations from CALIPSO and WRF-Chem simulations demonstrate the model efficiency to simulate dust at the edge of the ITD and to determine transport along the whole Saharan Boundary Layer.

7 Dust climate impact in the Sahara Desert in winter and summer 2006 and 2007.

7.1. Introduction

One of the ultimate challenges to understand the climate effects of the dust cycle is the accurate representation of dust emissions and long-term transport. A few number of studies showing the potential of the RegCM3 model to describe climate impact of dust on a seasonal scale have been done in the past [i.e. *Konare, et al.,* 2008, *Solomon, et al* 2008]. Nevertheless, there are yet some constrains to resolve such as the accurate description of soil characteristics and hence aggregate size distributions that are incorporated into the emission and transport schemes. As a result, a number of active dust sources are not well reproduced by the model [*Todd, et al* 2008a, *Cavazos et al* 2009]. This issue is a widely acknowledged problem in dust modelling especially in remote, poorly observed regions such as extended regions in West Africa and is been previously addresses through the implementation of preferential dust source regions into the dust model with a considerable improvement in dust emissions [i.e. *Tegen et al* 2002]. In chapter, model estimates of long-term dust climate effects in the Sahara Desert are achieved using a dust source activation map defined from SEVIRI observations to identify all those ‘‘potential’’ active sources following *Schepanski et al.,* [2007]. From the dust model estimates, the next aspects are evaluated: i) model climatic features involved on the seasonal occurrence of dust outbreaks ii) the dominant model dust plumes trajectories and (3) the radiative forcing in the SW on the long term (the RegCM version used in this research does not take into account the effect of LW emissivity and scattering of dust).

7.2. Dust Sources

For model experimentation, a Dust Source Activation Frequency map DSAF from *Schepanski et al.* [2007] is used to replace the default soil texture class map used by RegCM3 (see chapter 3.2. for more details). The implementation of preferential sources into the model results in more realistic dust emissions in areas known to be active dust hotspots in accordance to the results shown by *Cavazos et al.* [2009]. A short climatology

depicting winter months: January, February and March (hereafter JFM) and for the onset and peak of the monsoon season: June, July and August (hereafter JJA)) is evaluated from NCEP reanalysis data and model simulations. This short period of two years is chosen on grounds of data availability from ground-base and satellite measurements and because the DSAF map was formulated from MSG SEVIRI satellite data since 2006. Figure 7.1 shows the domains used for experimentation including all model grid cells in which the DSAF is greater than 1% and prescribed as soil texture class of the sand type. A total of 1606 for JFM and 2319 for JJA additional grid cells with 100% sand were introduced to the default soil map. The preferential sources added for the JFM period (Figure 7.1.a), tend to depend on the topographic characteristics such as basins, ephidentrial lakes or other sources with material available to be erode and wind thresholds [*Engelstaedter et al,* 2003] enhanced by strength of the *Harmattan* flow. Some active sources in winter due to the above factors include the Bodélé depression of northern Chad and extended areas across North Africa such in Libya and Sudan. Other active areas include vast regions in Niger and Mali (Figure 7.1.a). In addition, large portions of South Algeria (south of the Air Mountains and the Hoggar Mountains), Mali and Mauritania are also depicted as important dust sources in the DSAF map. For the DASF map during summer (Figure 7.1.b), the Bodélé Depression as well as other eastern sources remain as active dust hotspots although not with the same strength as in winter [*Prospero et al*., 2002, *Koren et al.,* 2006]. Although average wind speeds are reduced across these regions, some heaviest dust-loadingsin a prominent zone along the Libyan–Chad border during this season have been registered. *Washington et al.,* [2003] established that dust sources correspond very closely with a maximum in near- surface convergence, suggesting that convection is an important process initiating dust storms in this region. Additionally, some areas south Niger and Mali are activated by the influence of summertime southwesterly monsoon flow as described in previous works [i.e. *Flamant et al*., 2007, *Bou Karam et al.,* 2008]. The increase of DSAF in Central West Saharan desert including large portions of Mauritania, Mali and south Algeria Dust might represent active dust sources triggered by the formation of cold pools or density currents related to deep moist convection [*Knippertz et al*, 2006].

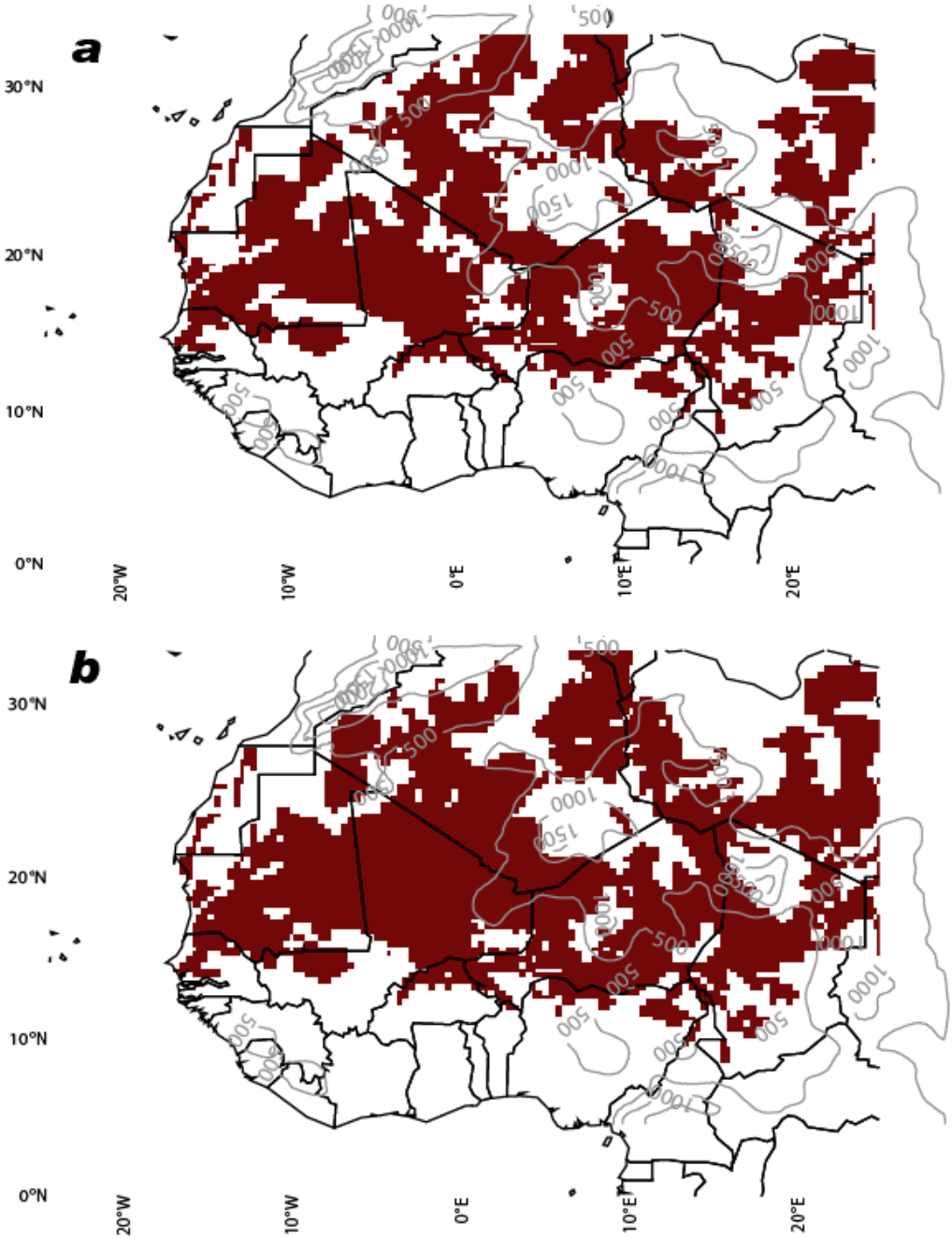

Figure 7.1: Model Domain with the DSAF map from *Schepanski et al* [2007] (color). a) JFM 2006- 2007 and b) JJA 2006-2007.

7.3. Results and discussions

Different mechanisms controlling atmospheric circulation in the Sahara and Sahel are responsible for dust outbursts. This section depicts the long-term means of the atmospheric components during winter and summer for 2006 and 2007. In addition, results from model dust emissions and the validation with observations are analysed. Finally the climate feedback and the future implications of dust mobilisation on the long term in the Sahara are discussed.

7.2.1. Climatology and dust mobilisations for JFM 2006-07

The long-term averages of SLP in mb, temperature and wind vectors from the ECMWF ERA-Interim reanalysis data corresponding to JFM 1989 to 2009 (Figure 7.2) show that the low-level circulation is influenced in a great extent by mid-latitude weather with predominance of northerly winds. There is a strong presence of the Azores High, which is associated with the Sahara Desert and the Mediterranean Basin's climate (~1022mb). The subtropical high is extended to the East where the influence of Libyan high drives the *Harmattan* wind, which brings strong north-easterly flux along the southern border of the Sahara. These winds are intensified at about 15°N due to the strong large-scale pressure gradient further south. In addition, winds strength in some regions might be intensified due to some regional topographic features causing a channelled effect and resulting in flow acceleration. As an example, strong winds in northern Chad in the form of the Bodélé LLJ with speeds up to 16 ms^{-1} in winter are caused by the topographic channelling South of the Tibesti Mountains and the Enneldi Mountains [*Washington and Todd,* 2005]. Other topographic features having the same effect are the North and South of the Air Mountains in Niger as observed by *Engelstaedter and Washington* [2007]. The horizontal temperature gradient (Contours Figure 7.2) shows a well-distributed linearity of the isotherms with relatively low values North Africa (~18 °C) due to the reduction in solar heating and the influence of cold air advected from higher latitudes. Meanwhile, higher temperatures are observed towards the Equator due to the influence of southerly warm moist air from the Guinean Gulf.

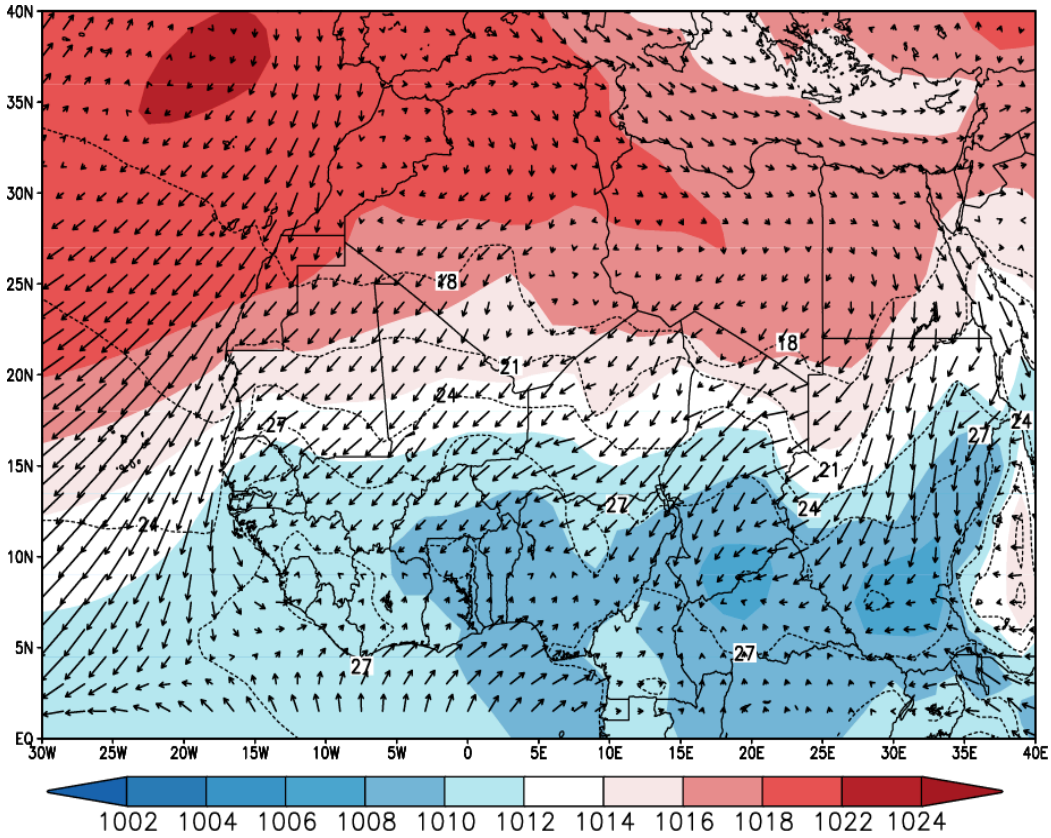

Figure 7.2: Meteorological components for January, February and March 1989-2009. SLP (shaded), air temperature (contours) and 10m wind direction (vectors). Source: ECMWF ERA-Interim.

Over the particular period of JJA 2006-2007, simulations show extensive dust mobilisation in the form of high AOT values in several regions across the Sahara and the Sahel belt between the 10 and 20°N (Figure 7.3). The regions with high AOT coincide with satellite observations during the same period. As seen in the climatologies, the increase of the mean northeasterly low-level flow or *Harmattan*, which dominates North Africa in winter in combination with particular topographic configuration are related to the activation of dust sources over Central Sahara. Dust plumes from these sources are transported in topographically constrained low level jet features, most notably the Bodélé LLJ around the 18°N-18°E where the northeasterly flow is channelled through the Tibesti-Ennedi gap and the combination of a gap wind and downslope wind forcing acts to accelerate the LLJ. Other area influenced by LLJ's is seen north and south of the Air mountains around the 15-18°N and 8°E. The nature of the LLJ's as key feature of low level atmospheric circulation has been described previously by several authors [i.e. *Washington et al.*, 2006; *Todd et al.*, 2008, *Schepanski et al.*, 2009]. The regions affected by this feature are well represented in the model and observations with AOT values as high as 2.In a comparatively basis, model simulations and satellite observations from MODIS and MISR suggest that JFM 2007 is more active than 2006 whereas AOT-OMI

values remain relatively constant for both years. An interesting feature seen in OMI is that there is a region with AOT values exceptionally high in the borders between Mali and Mauritania (18°N and 5° W) compared against the other platforms. Although the model represent in some degree high values of AOT along this latitudinal belt, it does not emphasize exceptional high AOT values in such region.

For the domain average time-series, AOT from OMI is used for comparison. The reason for this is that the AOT-OMI dataset is larger and more complete than the rest of the platforms. Hence the averaged AOT is more realistic and does not contain as many gaps in information as those from MODIS or MISR. The modelled and observed AOT spatial averages time-series (Figure 7.4) at midday follow similar pattern for the three months period and suggesting the presence of several episodes of large dust mobilisations with approximate duration of about 5 days particularly for February and March. Some studies have analyzed the occurrence of these large dust mobilisations in this area during February and March 2006 [e.g. *Slingo et al*. 2006, *Cavazos et al* 2009], which might be caused by cold air advection from middlatitudes causing large-scale drop in temperature over large parts of North Africa, enhancing anticyclogenesis. The constant ridging high might lead to the developing of cold surge propagating southwardly across the Sahara, which favors extensive dust mobilization across the Sahara desert associated with the northerly wind outbreaks as observed in *Cavazos et al.,* [2009]. These authors analysed a large dust mobilisation during early March 2006 related to this phenomena, which is clearly represented in the modelled and observed AOT spatial averages time-series (Figure 7.4). In this analysis the model seem to particularly overestimate maxima AOT with values as high as 1.7 at midday. Although AOT observations from OMI present the highest averaged value during the same period, values do not exceed the 0.75. It has to be appointed that the time series just represent modelled and observed AOT values at midday in order to make it more comparative with AOT MODIS daily retrievals. On the other hand, the model fails to represent dust emissions over Northeast Libya detected by all the satellite platforms, particularly for 2006. Overall, dust plumes in the simulations and observed data are transported to the south and west creating a vast plume of dust covering the Sahelian latitudes ~10°-15°N extending from the Atlantic Ocean at 25°W to 20°E.

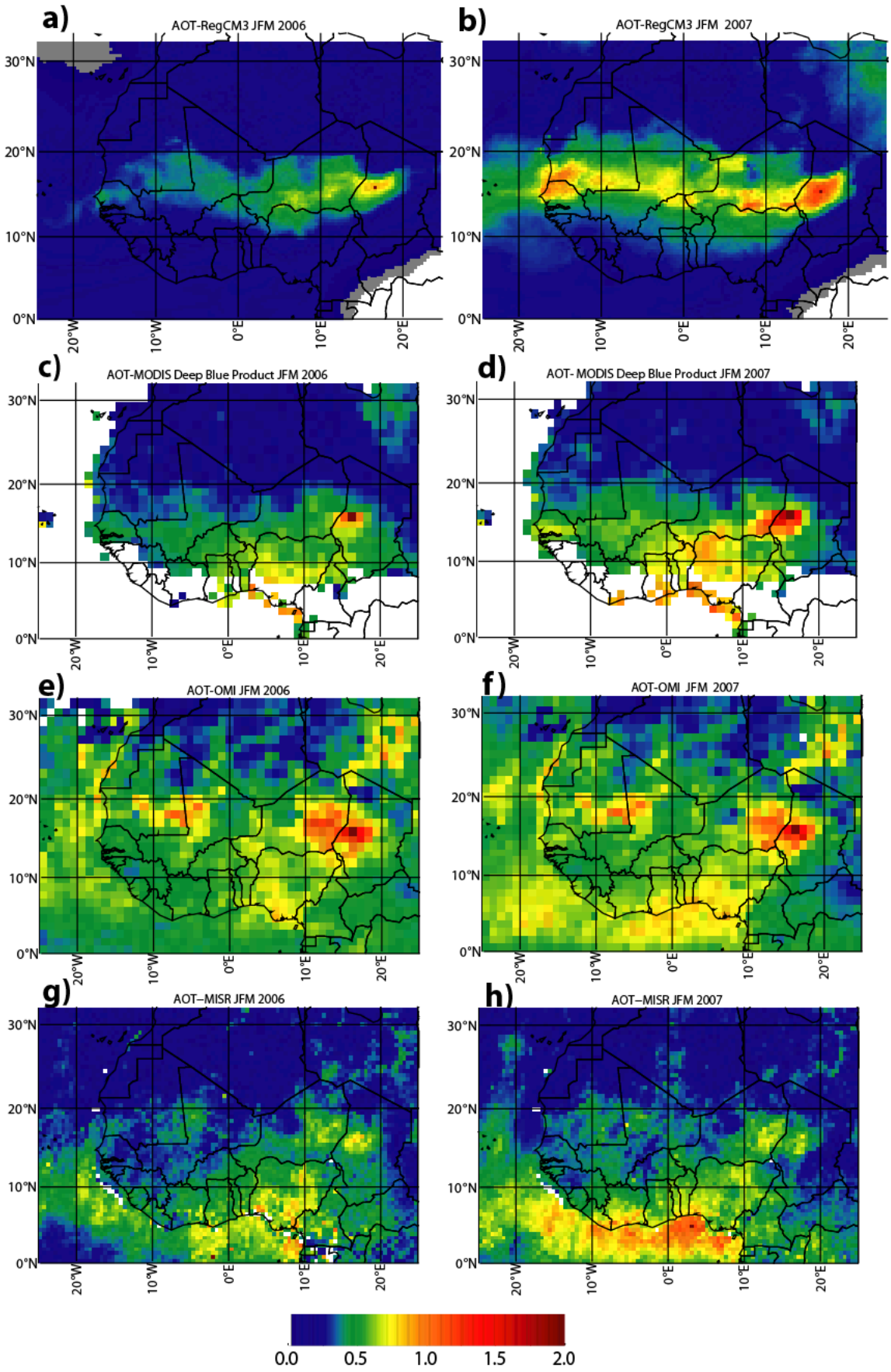

Figure 7.3: Mean AOT values at midday for JFM 2006 and 2007. (a-b) AOT-RegCM3, (c-d) AOT-MODIS. (e-f) AOT-OMI. (g-h) AOT_MISR. Data source: Giovanni online data system, NASA GES DISC.

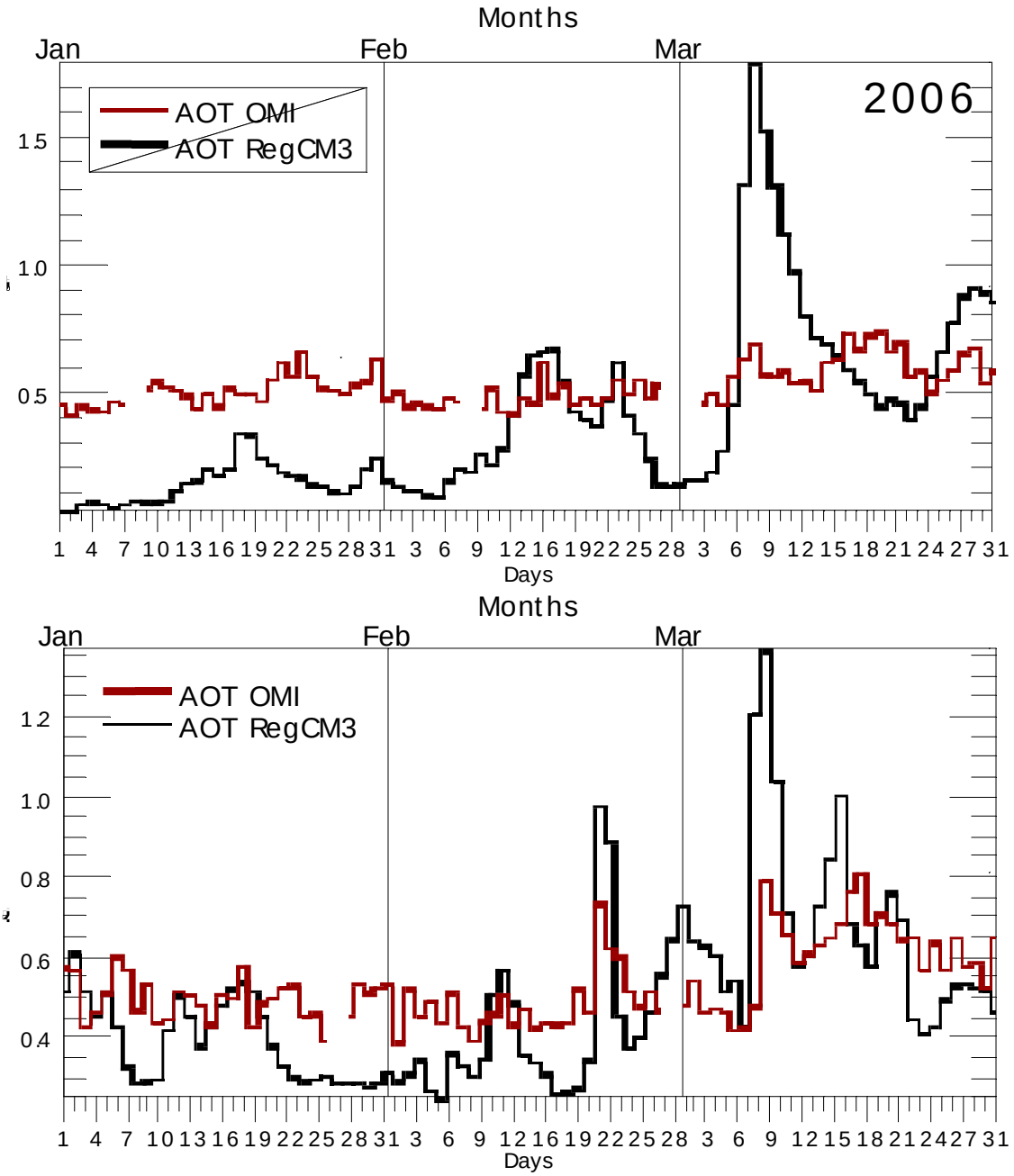

Figure 7.4: Domain averaged (10°N-30°N and 15°W-20°E) timeseries for AOT-RegCM3 and AOT-MODIS on JFM 2006 and 2007.

7.2.2 Climatology and dust mobilisations for JJA 2006-07

During the summer months coinciding with the occurrence of the West African Monsoon in West Africa, the anticyclonic circulation regime, which dominates the subtropics in winter, retreats further north and hence northerly winds strength influence is less effective [*Cook*, 1999]. The maximum heating in the North African land mass in summer (June, July and August) creates a surface temperature and moisture gradient from the Gulf of Guinea and the Sahara (Figure 7.5). This heating favours the presence of heat lows in areas where the atmospheric pressure drops with the subsequent lifting of isobaric surfaces and divergence of air aloft [*Knippertz and Fink*, 2008]. The persistent low pressure in the form of the Saharan Heat Low (SHL) over Algeria, Mali and Mauritania is clearly seen in the atmospheric components (Figure. 7.5), where the area dominated by the SHL shows the highest average surface temperature into the domain (~36 °C). Some authors (i.e *Knnippetz*, 2008) attribute the increase in outburst in this area due to the intense turbulence created by the increasing convection.

Meanwhile, the northwards displacement of the ITD above the 15ºN belt (~ 1008mb) favours the formation of several tropical troughs. This regime is produced due to the incursion to the Saharan belt of south-easterly monsoon flux coming from the Guinean Gulf (Figure 7.5) and the northeasterly dry wind. In addition, the African Easterly Jet plays a dominant role in formation of Mesoscale Convective Systems (MCS) at the south boundaries from the Sahara associated with synoptical-scale African Easterly Waves [*Diedhiou et al.*, 1999]. The cyclonic flow of the easterly wave extends along the 15ºN, but with even stronger winds. Significantly, south-westerly flow at this level is able to transport dust from the local Saharan area far northward to the western Mediterranean. [*Guerzoni et al.*, 1997; *Nickovic and Dobricic*, 1996].

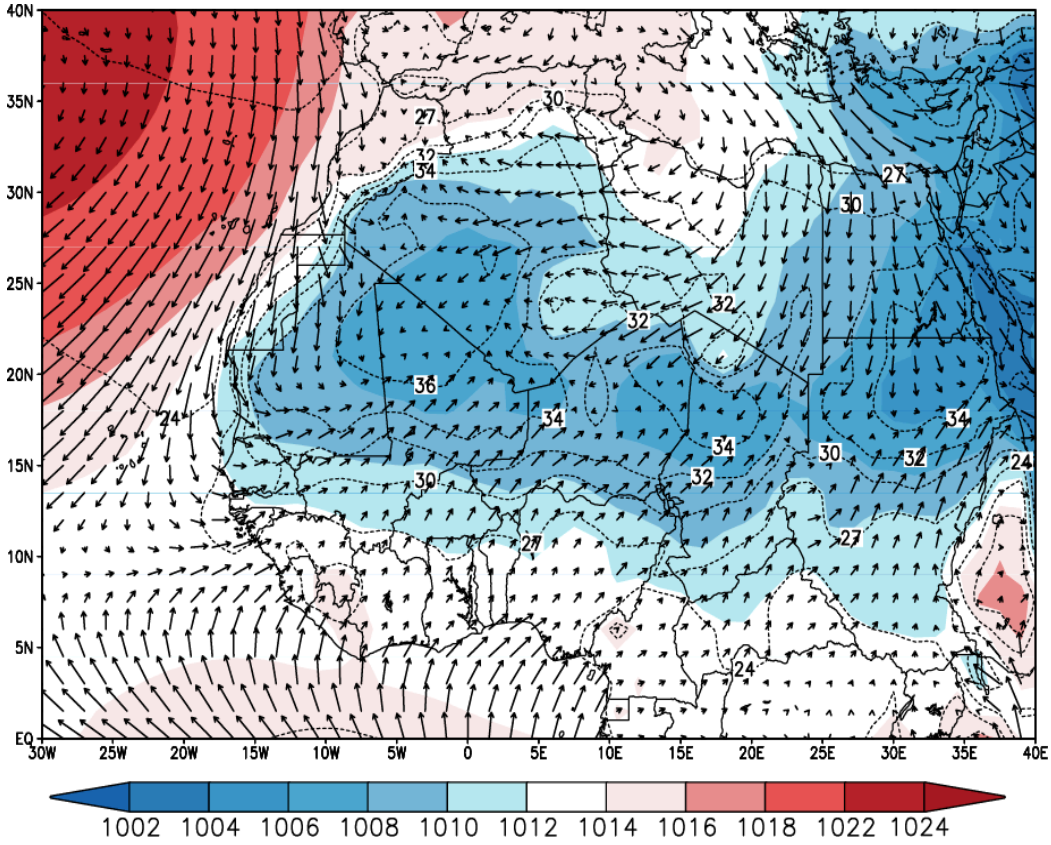

Figure 7.5: Synoptic components for June, July and August 1989-2009. SLP (shaded), air temperature (contours) and wind direction (vectors). Source: ECMWF ERA-Interim.

The late spring and early summer is arguably the period when the dust mobilization over West Africa is the largest [*Engelstaedter and Washington*, 2007]. For the two year simulated period, several atmospheric mechanisms influence dust mobilisation. On one hand, the prevailing high pressure over Tunisia and Libya leads to an increase of anticyclonic easterly winds in the form of the *Harmattan* wind of about 10 m/sec turning in this area, leading an increment of the dust pumped to the air column. This feature is represented in the observed AOT in satellites, particulary for OMI and MISR (Figure 7.6, e-f, g-h) with AOT values in excess of 1 are clearly seen over the area influenced by this phenomena. A primary maxima source includes the Bodélé Depression, which presents the highest AOT values (up to 2) although not at the same magnitude as in the JFM period. The interannual comparison between both years, suggest that AOT values from the satellite compositions are higher for 2006 than 2007 (Figure 7.6). Although AOT model estimates are relatively close to those observed values for the 2006 period, estimates for the next year are rather overestimated in the areas of maximum dust production. This might indicate that the model is overestimating dust emissions for this particular year in spite of using the same DSAF map and the same configuration for both years. These results would suggest that the inclusion of predefined sources on a long-term

analysis in a period where dust emissions are not linked completely to wind dynamics might be less efficient. AOT retrievals from all platforms also depict high values over a large region extending the central regions in Mali and Mauritania coinciding with the location of the Saharan Heat Low. The model captures quite accurately the location of these relatively high values. It is also suggested that dust transport follows an eastern direction. AOT values over a large region in south Algeria, Mauritania and Mali exceed the 1.5 in the model showing some agreement with those values by the OMI, whereas over this same region the observed AOT in MODIS do not exceed the 0.8. In this late case, the representation of dust emissions in the form of AOT in the MODIS satellite can also be misrepresented. One explanation to this is that close to these sources, substantial amounts of dust are present in the lowest atmospheric layers (below 1 km), which present difficulties for satellite retrieval and may be undetected in the MODIS data. On counterpart, the AOT- MISR also seems to show some agreement with simulated and observed AOT from OMI. However, the magnitude of averaged AOT is reduced due to the limited narrow swath in MISR, which would dismiss important emissions in certain regions on a daily basis.

Another matter to consider is that averages correspond to observations at midday for both observed and modelled AOT. This fact is particularly important when dust emissions occur near the limits of the ITD close to the Saharan-Sahelian belt. In this region the pressure gradient facilitates the formation of low-pressure centers or tropical troughs in the form of MCS's. In turn, the development of these MCS favors the formation of density currents or cold pools, which occurs regularly in mountainous regions in northern Africa late sprint and early summer. Behind a MCS a washout of particles behind leads to an increase in wet deposition, which suggests a residence time shorter that the dust generated during winter conditions. Hence, some of the actual dust emitted during the period is not well represented in the climatologies. A positive outcome from modelled AOT compared against observed values from OMI is that the spatial average estimates depict periods with large emissions. Figure 7.7 depicts two important periods with large dust emissions for 2006, especially during June 2006. The nature of this 5 days period with continuous dust emissions was analyzed in Chapter 6. Results for 2007 in the MODIS are rather low whereas the model demarks several important dust mobilisations.

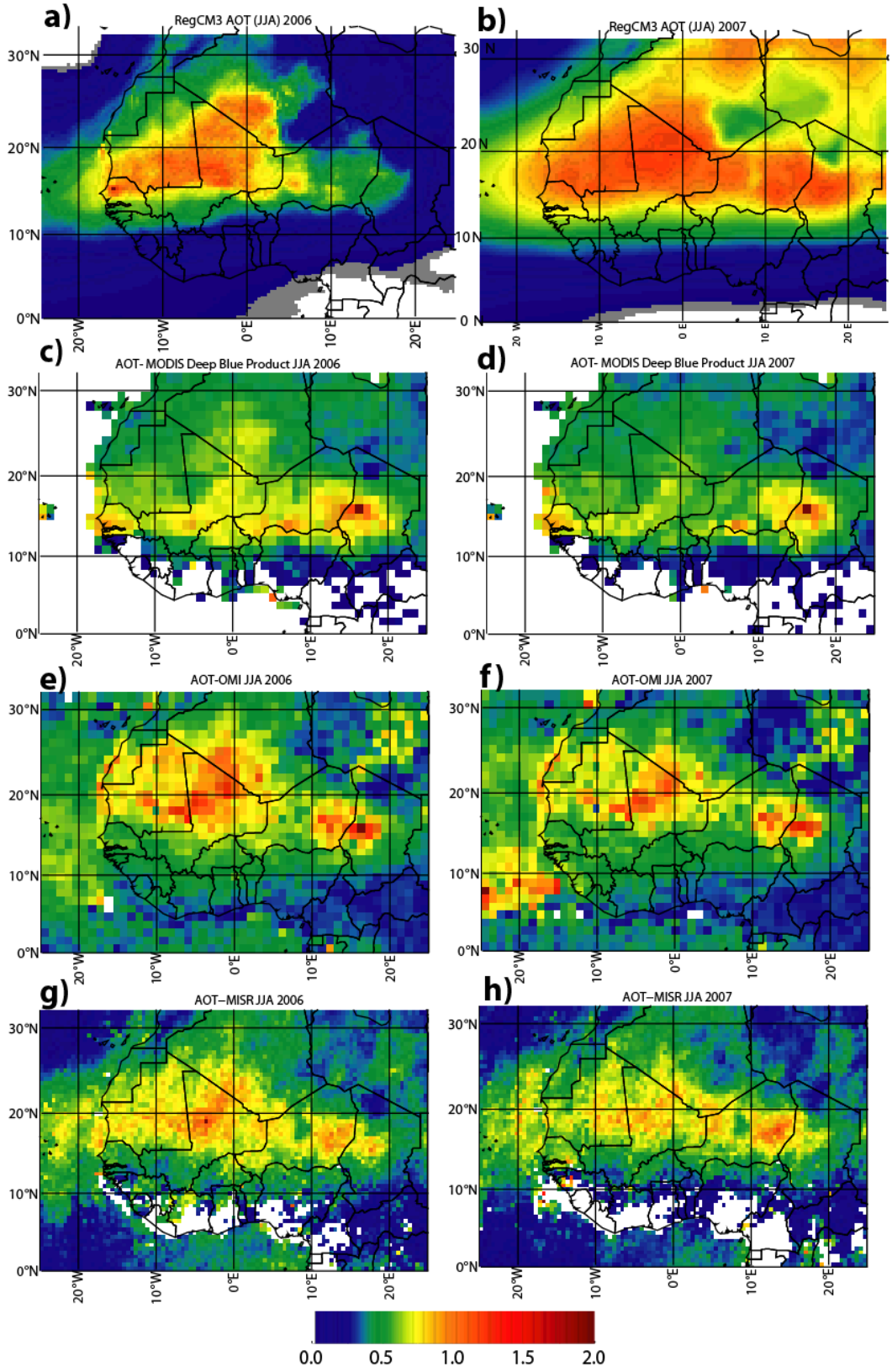
a)
RegCM3 AOT (JJA) 2006
b)
RegCM3 AOT (JJA) 2007
c)
AOT- MODIS Deep Blue Product JJA 2006
d)
AOT- MODIS Deep Blue Product JJA 2007
e)
AOT-OMI JJA 2006
f)
AOT-OMI JJA 2007
g)
AOT–MISR JJA 2006
h)
AOT–MISR JJA 2007
30°N
20°N
10°N
0°N
20°W
10°W
0°E
10°E
20°E
0.0
0.5
1.0
1.5
2.0

Figure 7.6: Mean AOT values at midday for JJA 2006 and 2007. (a-b) AOT-RegCM3, (c-d) AOT-MODIS. (e-f) AOT-OMI. (g-h) AOT_MISR. Data source: Giovanni online data system, NASA GES DISC.

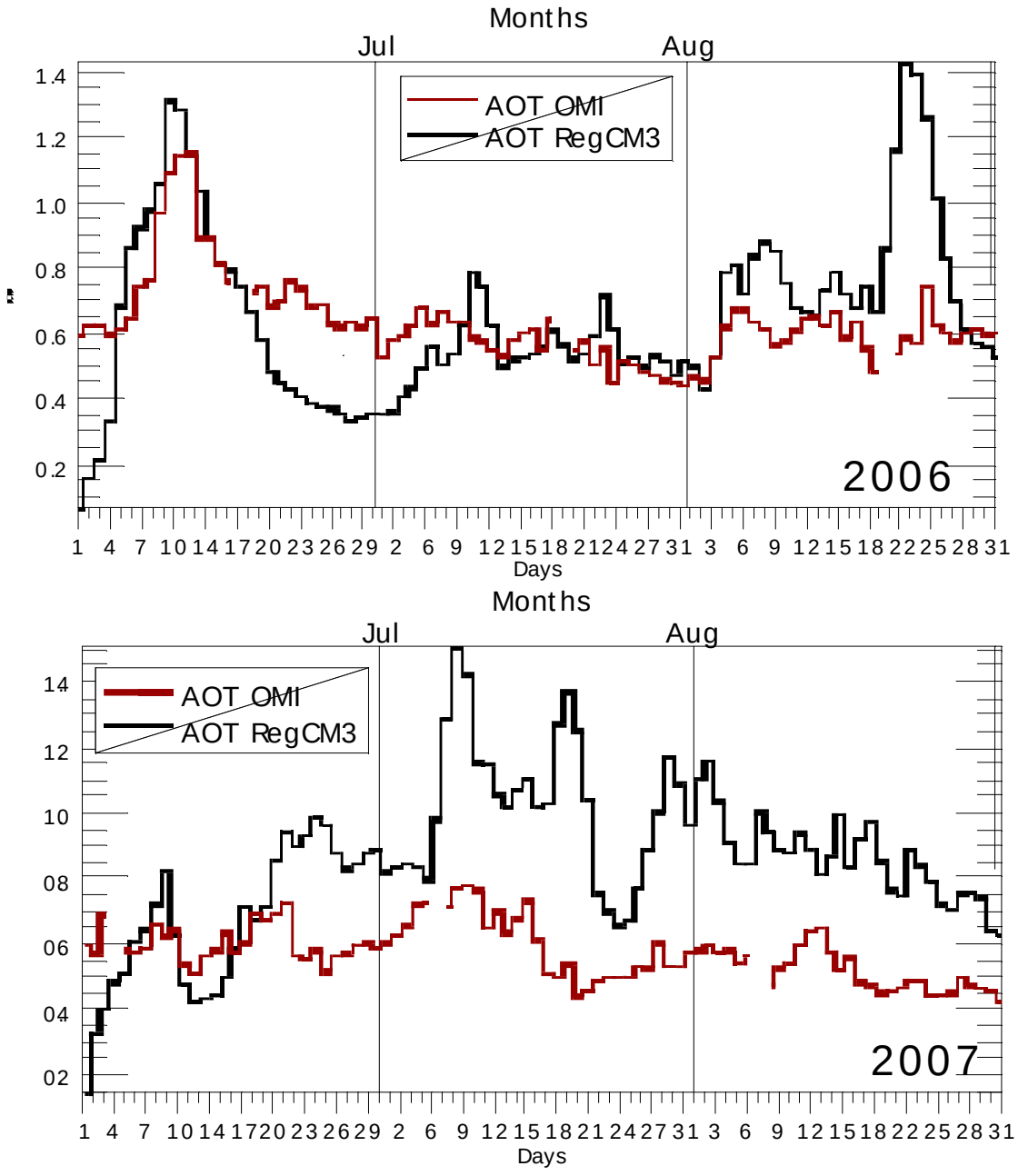

Figure 7.7: Domain averaged (10°N-30°N and 15°W-20°E) timeseries for AOT-RegCM3 and AOT-MODIS on JJA 2006 and 2007.

7.2.3. Long-term model simulation of dust radiative impact

The Short Wave Radiative Forcing (RF_{SW}) is determined at the surface (SFC) and top of the atmosphere (TOA) (Figure 7.8). The RegCM3 model version used in this analysis only determines the aerosol impact on short-wave (SW) radiative fluxes. Nevertheless, some efforts are being made to introduce the total RF from both SW and LW radiation fluxes in further versions of the RegCM model. In general terms, the maximum forcing is produced over areas of maximum dust loading. In the time averaged $RF_{SW(SFC)}$ for JFM, values vary from 0 to a maximum RF of about -100 W m^{-2}. The domain averaged$RF_{SW(SFC)}$ at midday is -60W m^{-2} whereas the $RF_{SW(SFC)}$ normalised byAOT is -85.39 W m^{-2} . The maximum forcing is located downwind of themajor dust source over the Bodélé Depression (Figure 7.8.a) in the borders between Chad and Niger. The domain averaged normalized byAOT for the Bodélé Depression (15-20°E, 15-20°N) is -92 W m^{-2}. On the other hand, for the JJA 2006-07, the $RF_{SW(SFC)}$ ranges from 0 to up -100 W m^{-2}(Figure 7.8.b).

During this period the Bodélé Depression as well as a large extended area in Central West Africa conforming Mali, Mauritania and South Algeria peak high values up to -90 W m^{-2} whereas a small region in Central Mali around 20°N reaches a maximum of 100 W m^{-2} (Figure 7.8.b). The time/space averaged$RF_{SW(SFC)}$ at midday normalized byAOT is -74 W m^{-2} whereas the domain averaged normalized byAOT for the area in Central West Africa characterised by the highest dust loadings (-10-5°E, 15-28°N) reaches the -75 W m^{-2}. These value are larger than reported in GCM estimates due to the higher horizontal resolution used here leading to more locally resolved dust loads. For the whole region however, the averaged surface forcing is consistent with those reported in previous works [*Konare et al.*, 2008; *Miller et al.*, 2004]

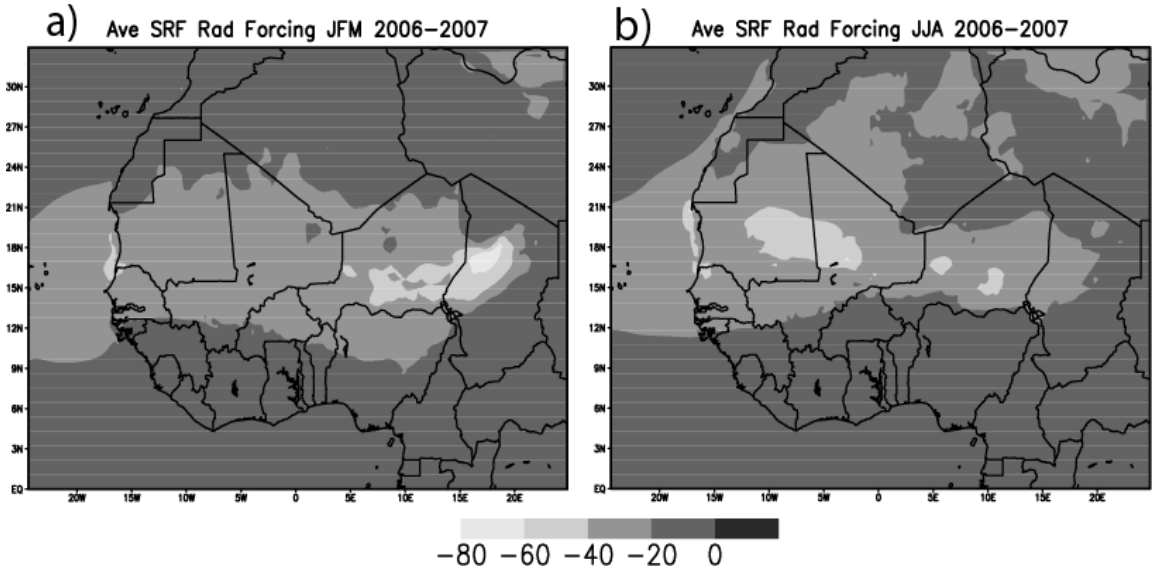

Figure 7.8: Average radiative forcing (W m^{-2}) at surface. a-c) JFM 2006-07, b-d) JJA 2006-07.

The magnitude of the air temperature decrease on a temporal scale is in agreement with areas characterized by the presence large dust plumes during the periods under study. The temperature anomalies result from a combination of horizontal and vertical temperature advection and diabatic heating (consisting of radiant fluxes and surface heat fluxes, which are dominated by sensible heat flux). Given the strength of the northerly wind patterns for both periods (Figures 7.2 and 7.5) and the RFSW(SFC) (Figure 7.8) it is likely that both advective and diabatic heating contributions are substantial. It is possible to estimate the magnitude of each of the radiant components by comparing the temperature simulated by RegCM3 experiments with active dust to a control run with the dust scheme deactivated (ND), for grid cells where cloud differences are minimal. The effect of the RFSW(SFC) is to reduce daytime surface temperatures with anomalies exceeding the -2 °C for both periods where aerosol loadings are the highest (Figure 7.9 and 7.10).

For the JFM period, the temperature anomalies directly attributable to RFSW(SFC) exceed -5°C across much of the dust plume region in the Bodélé Depression for both years (2006-07). For the JFM 2006, the cooling effect at surface is rather located in the area near the Bodélé Depression with a decrease in air temperature around the -4°C. Nevertheless, the cooling effect is greater on a spatial scale in 2007, where negative anomalies are well extended across the entire Sahel (Figure 7.9.b) with anomalies around the 5°C. The cooling effect is greater for the JJA period (7.10). The spatial area with the greatest reduction in temperature corresponds to the extended area in Central West Africa

(around -9°C). From the synoptic analysis (Figures 7.2), the air temperature in this area reaches its maximum heating of the lower troposphere leading to a subsequent lifting of isobaric surfaces and divergence of air aloft (Knnipetz and Fink). However, the analysis of the dust experiment against the no dust control experiment shows a considerable reduction at the surface temperature caused by the increase in dust activity in the area. As for the winter period JFM, the bigger reduction on a spatial scale is bigger during 2007 than the previous year. These results are consistent with those found with general circulation models simulations which showed a surface cooling under the dust layer [*Miller and Tegen*, 1998].

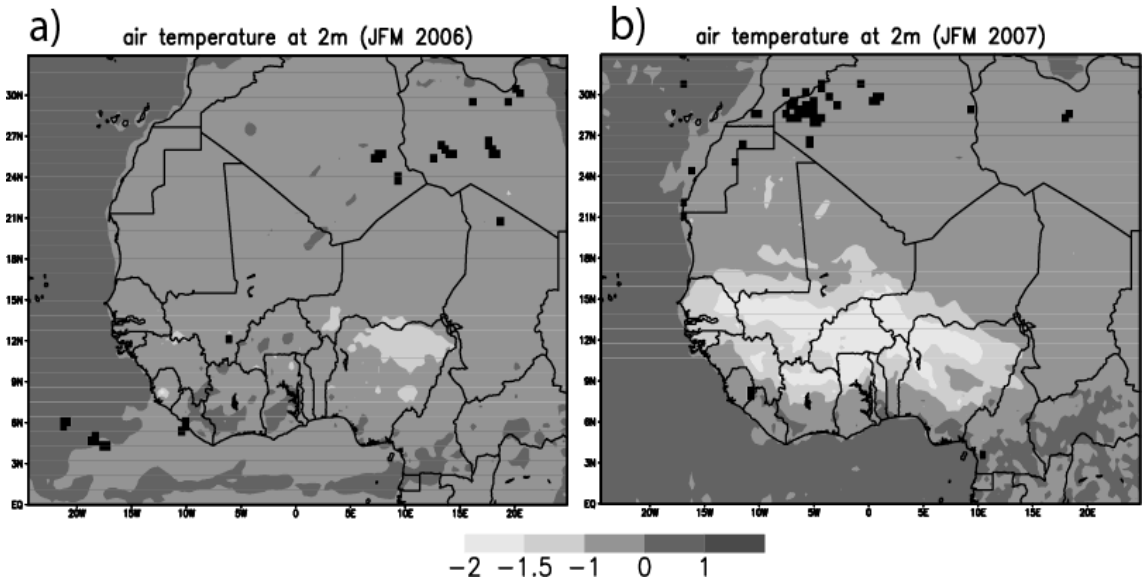

Figure 7.9: Time averaged 2 m temperature anomalies (C) for the JFM period a) 2006 and b) 2007. A black mask is created when cloud fraction is greater than 20%

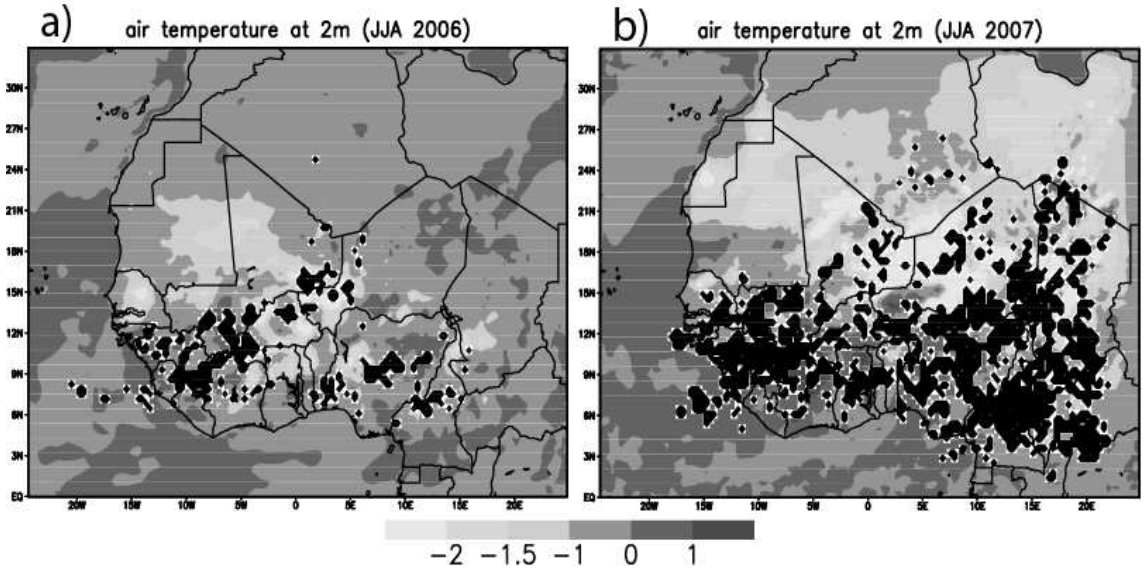

Figure 7.10: The time averaged 2 m temperature anomalies (C) for the JJA period a) 2006 and b) 2007. A black mask is created when cloud fraction is greater than 20%.

The $_{RFSW}$ at the top of atmosphere associated withaerosols is a function of the aerosols loading, opticalproperties, size distribution, and surface albedo. $RF_{SW(TOA)}$is strongly negative indicating a general cooling of the surface/atmosphere systems induced by the dust load (Figure 7.11.c-d) over areas where the aerosol load ishigh and surface albedo is low (Figure 7.12). On a regional scale, these figures vary considerably.The RFSW(TOA)is more effective off the eastern Atlantic close to the Mauritania coast around the -35 W m^{-2}, with an optical depth up to 2, for both periods due to the low albedo of water. However, the magnitude of the forcing is bigger spatially for JJA. This is attributed to the big dust loading transported off the continent over the Atlantic in an easterly direction (Figure 7.6). This magnitude of forcing is consistent with that of *Li et al.* [2004] who report a mean RFSW(TOA) efficiency of -35 ± 3 Wm^{-2} per unit of AOT at 550 nm in JJA and a lower efficiency for low-dust season (NDJ in their study) of about -26± 3 W m^{-2} based on satellite observations of dust over the Atlantic Ocean. Over the bright surface of the Sahara desert the magnitude of the TOA forcing is consistently reduced due to a high surface albedo and falls in the range of previous modelling estimates [e.g., *Miller et al.*, 2004]. The aggregate effect of the complex spatial structure in RFSW(TOA) simulated by RegCM3 is negative when averaged over the domain. The total space/time averaged RFSW(TOA) is -1.12W m^{-2} and -4.5 W m^{-2} for JFM and JJA periods respectively. The space/time average normalized RFSW(TOA) -1.61W m^{-2} and -3.22 W m^{-2} per unit for JFM and JJA respectively.The domain averaged normalized byAOT for the Bodélé Depression (15-20°E, 15-20°N) reaches -11 W m^{-2} for JFM and -15 W m^{-2} for JJA.

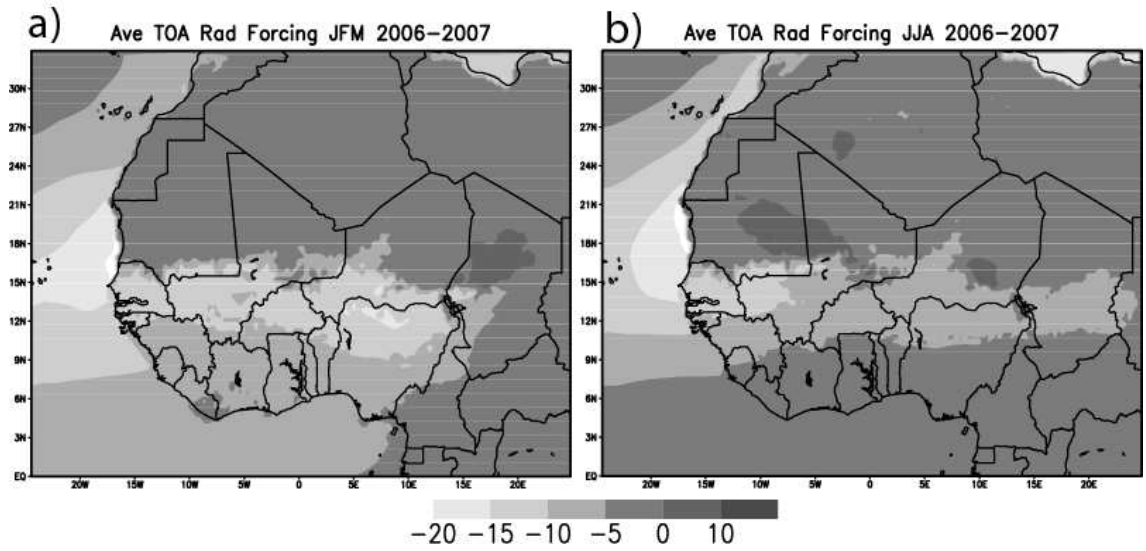

Figure 7.11: Average radiative forcing (W m^{-2}) at TOA. a-c) JFM 2006-07, b-d) JJA 2006-07.

Over parts of Niger and Chad in particular, as the dust aerosols produce an effective decrease in the planetary albedo over the bright desert surfaces (Figure 7.11). The effect of the higher aerosol *wo* results in a lower RFSW(TOA), i.e., more negative over dark surface and less positive over bright surfaces (Figure 7.11). In RegCM3 the albedo is typically around 0.33 over desert (Figure 17) similar to those observed from the ERBE (Earth Radiation Budget Experiment) satellite sensor obtained from the NASA Langley Research Center Atmospheric Science Data Center (not shown), in contrast to values of 0.2 from *Helmert et al.* [2007]. As such, the results of these modelling experiments illustrate how important it is to specify accurately not only the optical properties of aerosols but also the surface albedo. Over the darker land surfaces of the Central West African region between the borders of Algeria, Mali and Mauritania, the model simulated space average (15°W-5°E , 15°N-28°N) at midday RFSW(TOA) normalized by AOT are -21 and -13 W m-2 per unit AOT for both JFM and JJA, respectively (not shown).

The difference between surface and TOA forcing is proportional to the shortwave diabatic heating of the atmosphere due to the absorptive component of the dust. As previously mentione, an important limitation of this study is that the simulations does not take into account the LW emissivity and scattering of dust, which tends to counterbalance the short wave cooling effect over the dust source region mainly north of 17°N. There is not a particular agreement on the sign of net (SW + LW) radiative forcing at climatic timescale for this regions [*Konare et al.,* 2008]. Some modelling studies show positive net TOA forcing over the source region when long wave emissivity is accounted for

[*Balkanski et al.*, 2007]. However, the recent study of *Yoshioka et al*. [2007]still finds a dominant negative TOA even when taking into account the long wave forcing.

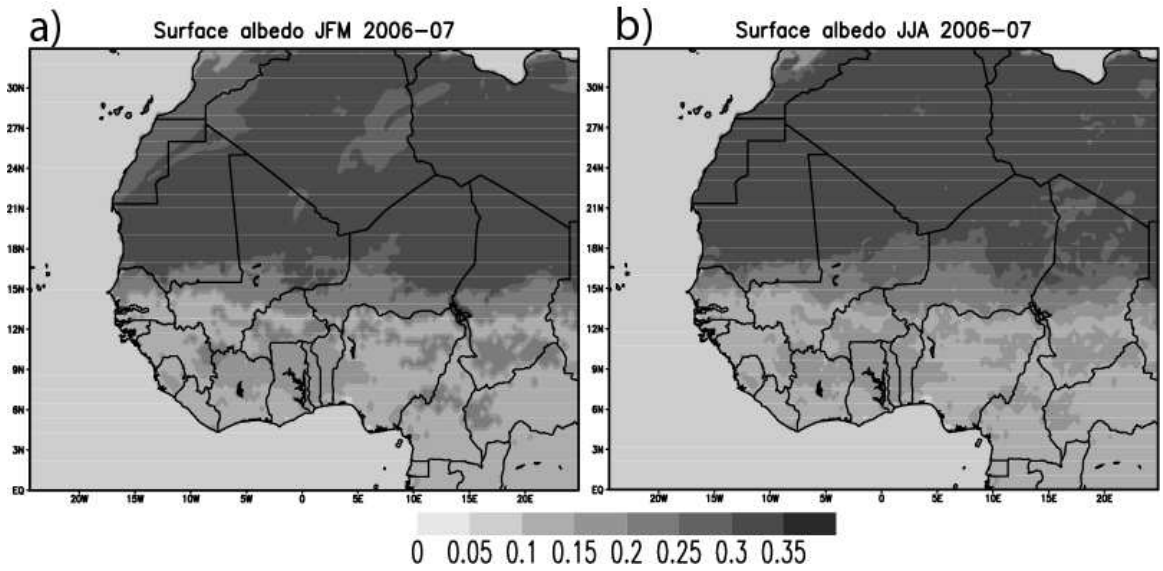

Figure 7.12: Time averaged surface albedo values. a) JFM and b) JJA

7.4. Summary

Observations and model simulations of dust emissions and long-term transport in the Sahara Desert in West Africa during a two years period analysis were evaluated. The analysis included a short climatology depicting winter months: January, February and March (hereafter JFM) and for the onset and peak of the monsoon season: June, July and August (hereafter JJA). The ability of the RegCM3 regional climate model with an implemented dust source activation frequency (DSAF) map defined from SEVIRI observations to define ‘‘potential’’ dust sources is tested. Estimates suggest that dust activity in preferential sources in the Sahara and transport patterns differs for the each period corresponding to winter (dry season) and summer (monsoon onset). The results show a good agreement of model estimates with MODIS observations in terms of the space/time structure of dust emission and transport particularly during the occurrence of several large dust events. Results also confirm that the Bodélé Depression accounts as the major dust source for the JFM period due to the strong dependence in topography and wind dynamics, which are represented adequately by the model. During the summer period, the highest values for the modeled AOT are congregated in a vast portion in the central region of the Sahara Desert. The large low-pressure system that drives the West African Monsoon and the dry, dusty air layers are closely related to the tropical cyclones, which form over the Atlantic Ocean which is one of the important implications of dust mobilisation during this season [*Dunion and Velden* 2004].

Dust emissions occur near the limits of the ITD close to the Saharan-Sahelian belt where the pressure gradient facilitates the formation of low-pressure centers or tropical troughs in the form of MCS’s. In turn, the development of these MCS favors the formation of density currents or cold pools, which occurs regularly in mountainous regions in northern Africa late sprint and early summer. These density currents generate the strong winds in front of MCS, which allows that dust particles to be pushed and lifted to the atmosphere. However, the dust concentrations in RegCM3 in zones close to MCS are not well represented. Behind a MCS a washout of particles behind leads to an increase in wet deposition, which suggests a residence time shorter that the dust generated during winter conditions. Also, the decrease of vertical stability due to the evaporation of cooled air related to deep moist convection in North Africa favours the development of density currents or *Haboobs* in high mountains during this summer [*Knippertz, et al,* 2006]. From previous studies during monsoon season, dust generated at the borderline of Algeria and

Mali follows a clockwise circulation just surrounding the Hoggar Mountains; these dust fronts are usually formed ahead of these cold pools. These plumes are then transported along the border of Algeria with Mauritania and Morocco to eventually either deposited just along the coastline or expelled to the Atlantic Ocean.

The SEVIRI imagery and the AOT retrievals from different instruments (MODIS, OMI, MISR) are helpful to determine the spatial structure of dust plumes. However, as shown in this chapter, products from different sources can show certain disagreements in the pattern and magnitude of dust emissions, hence these datasets must be used carefully. For this reason, moreground-base and aircraft observations are required (i.e. AERONET stations) to provide long-term information about dust distributions in areas and reduce the uncertainties shown to date by these instruments. The inclusion of the CALIPSO measurements makes possible to determine the vertical distribution and the height at which the dust is emitted and transported. Observations from CALIPSO also facilitate the evaluation of model performance and to measure the interactions with atmospheric column.

To estimate the contribution of the whole Sahara tothe mineral dust budget at the continental scale, it is necessary to evaluate on detailthe interactions between mineral dust and convective systems. Also it is necessary to implement more simulations representing different mechanisms that allow dust activation depending of the atmospheric regimes. Different authors have discussed the implications of the radiative forcing by dust in West Africa. *Konare et al.* [2008] suggest that RF shortwaveforcing of dust reduces the precipitation over the Sahel. Likewise, effects on the RF might include to strengthen the southernbranch of the AEJ and to weaken the Tropical Easterly Jet leading to the reduction in the strength of the West African Monsoon system [*Solmon et al.*, 2008]. To corroborate these arguments, a better arrangement in the simulated large dust activation sources requires a more detailed evaluation in dust scheme implemented in the model.

8 Conclusions and Perspectives

In this work, observational (satellite and ground-based) data and model simulations with the RegCM3 and WRF-Chem models with an incorporated dust scheme are used to determine impact of atmospheric dust in the Sahara Desert in North Africa. The combined use of both data sources is important to describe and evaluate the dust cycle and the atmospheric mechanisms interfering in dust emissions. Emphasis is given in very active source regions, including the Bodélé Depression and the West African sources in the heat low region of the Sahara.

As seen in the present work, several factors are acknowledged to limit the accuracy of modeling studies. The introduction of sensitivity analysis by approximating the most realistic representation in dust emissions occurrence results in a clear improvement in terms of the space/time structure of dust emission, transport and radiative forcing. On one hand, there is considerable qualitative and quantitative evidence that experiments with revised soil characteristics result in better estimates of Aerosol Optical Thickness (AOT). Likewise, the absolute magnitude of model simulated radiative forcing (RF) depends on AOT. Although the present research was merely focused on the direct effect of atmospheric dust particles, estimates of shortwave RF show the evidence of the substantial cooling effect dust events can produce at the surface. In addition, there is evidence of warming effect at TOA over desert surfaces even for highly reflective aerosols due to the high surface albedo in the model. In this work, the RF in the long wave spectrum was not estimated, therefore further analysis to determine the magnitude of the absorbing pattern on the infrared are required.

As seen in the results for both models (WRF-Chem and RegCM3), in the absence of truly accurate soil maps at high resolution, further refinements to the dust source activation maps and its implementation in dust models can lead to useful improvements in simulation of dust processes and forecast accuracy.

Furtherwork also requires the improvement of surface albedo configuration, boundary layer meteorology and the specification of dust physical and optical properties which would require additional numerical model simulations and the continuous reliability on satellite and ground-based for calibration and comparison purposes. Model inter-

comparisons are useful to quantify model uncertainties when we are able to partition model error associated with various sources within the model. This includes controlled model configurations such that the sensitivity of model estimates to individual factors such as meteorological model performance, model resolution, boundary conditions, soil characteristics, dust physical and optical properties and the various parameterizations within the emission schemes.

The analysis of long-term observations of dust mobilisation denotes a strong seasonal variability of atmospheric dust. As seen in this work, in general terms on a synoptic scale, dust transport is driven by the low level north-easterly*Harmattan* during winter whilst dust transport across the Sahara Desert is dominated by the south-westerly monsoon. However, there are still some uncertainties about dust mobilisation that must to be addressed in future work. In this matter, the progressing knowledge ofmeteorological conditions responsible for dust emission,transport and deposition, will help to understand the mechanisms implicated in the spatial-temporal distribution of dust emissions and the climate feedback. This question can be address throughout the application of more modelling studies as well as long-term observations (ground- and space-borne)particularly in regions with a very limited background of observations in the past (i.e. West Central Sahara). On the other hand, the interactions of atmospheric dust and monsoon circulationare a matter of intensescrutiny in modellingand observational studies. In order to improve forecast and climate projections within model studies, the knowledge on the dust interactions with tropical atmosphericelements (e.g. African Easterly Jet, the Saharan Heat Low, and West African Monsoon circulation), cloud development, convection or stability must be improved.

An other important issue to consider, is that while observations from space-borne instruments as those used in this work, i.e. the SEVIRI imagery and AOT retrievals from MODIS, OMI and MISR are helpful to evaluate spatial structure of dust plumes, some disagreements can be presented. Hence the aerosol products from these platforms must be used carefully. More ground-base (i.e. AERONET stations) and aircraft observations for calibration purposes would reduce the uncertainties shown to date by these instruments. The inclusion of the CALIPSO measurements makes possible to determine the vertical distribution and the height at which the dust is emitted and transported. Observations from CALIPSO also facilitate the evaluation of model performance and to measure the interactions with atmospheric column.

A final approach is to understand the role of dust in the climate system. It is necessary to quantify how dust emission and transport will change in the future and how these changes will affect the Earth's climate and environment will be an important topic in the aerosol studies in decades to come.

Annexes

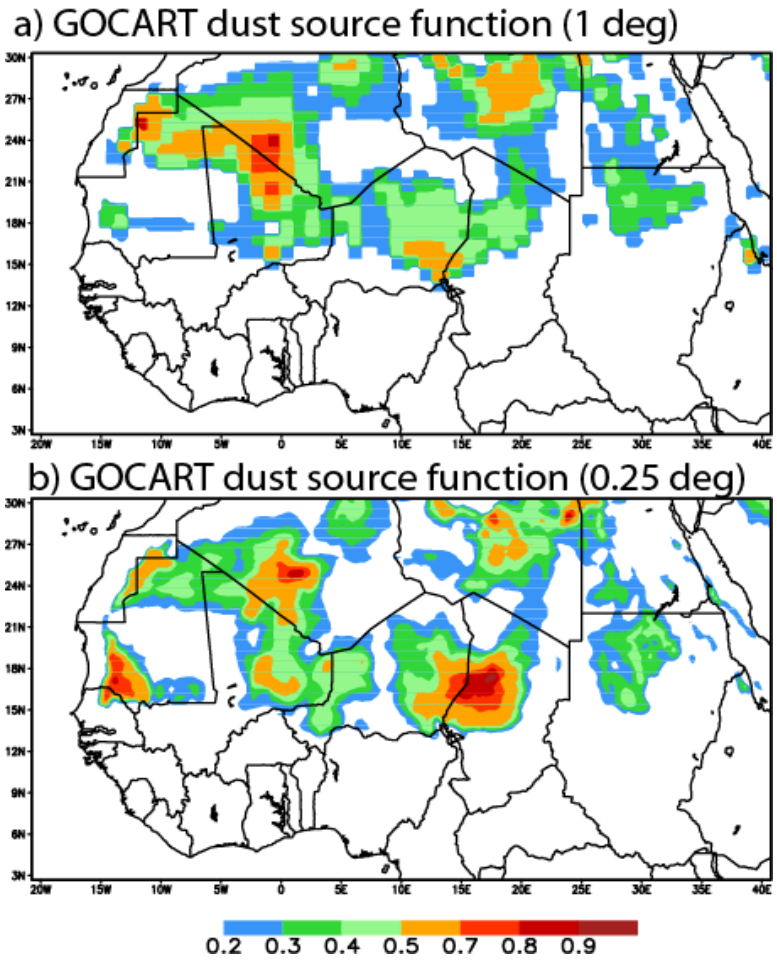

Annex A: The above figures represent the spatial distribution of the dust source function, calculated as a function of surface topographic depression, surface wetness and surface wind speed described in *Ginoux et al* [2001] used by the WRF-Chem with the GOCART scheme over North African. a) erodiility factor map using the bare soil surface map derived from the AVHRR at 1° X 1° spatial resolution used in the default configuration in the GOCART scheme b) The dust source function calculated implementing a new bare soil surface map from AVHRR at 0.25° X0.25° and use in the experiments included in this thesis work. The colorbar represents the probability of these sediments to erode and according to experiments done in the present work, it corresponds to the 30%.

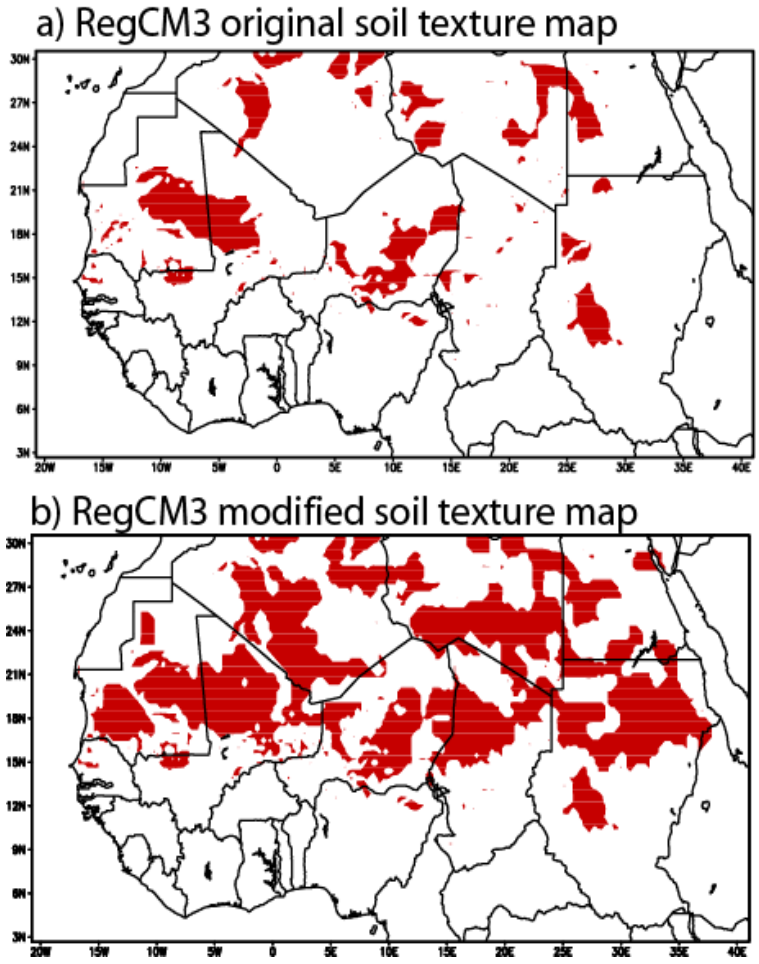

Annex B: The above figures represent the spatial distribution of text01 within the soil texture map. a) Default soil map in RegCM3 b) modified grid cells in which the DSAF is greater than 1% is prescribed as soil texture class of the sand type (100%) following *Schepanski, et al* 2007.

Bibliography

Ackerman, A. S., O. B. Toon and P. V. Hobbs. (1995). A Model for Particle Microphysics, Turbulent Mixing, and Radiative-Transfer in the Stratocumulus-Topped Marine Boundary-Layer and Comparisons with Measurements, *Journal of the Atmospheric Sciences,52*(8), 1204-1236.

Ackerman, A. S., O. B. Toon, J. P. Taylor, D. W. Johnson, P. V. Hobbs and R. J. Ferek. (2000). Effects of aerosols on cloud albedo: Evaluation of Twomey's parameterization of cloud susceptibility using measurements of ship tracks, *Journal of the Atmospheric Sciences,57*(16), 2684-2695.

Ajjaji, R., A. Al-Katheri and A. Danhani.(2008). Implementation and Preliminary Tests of an Air Quality Forecasting System Based on WRF-Chem over Middle East, Arabian Peninsula, and United Arab Emirates..

Albrecht, B. A. (1989). Aerosols, Cloud Microphysics, and Fractional Cloudiness, *Science,245*(4923), 1227-1230.

Alfaro, S. C., A. Gaudichet, L. Gomes and M. Maille. (1998). Mineral aerosol production by wind erosion: aerosol particle sizes and binding energies, *Geophysical Research Letters,25*(7), 991-994.

Alfaro, S. C. and L. Gomes. (2001). Modeling mineral aerosol production by wind erosion: Emission intensities and aerosol size distributions in source areas, *Journal of Geophysical Research-Atmospheres,106*(D16), 18075-18084.

Bagnold, R. A. (1935). The Movement of Desert Sand, *Geographical Journal,85*(4), 342-369.

Bagnold, R. A. (1937). The Transport of Sand by Wind, *Geographical Journal,89*(5), 409-438.

Balkanski, Y., M. Schulz, T. Claquin and S. Guibert. (2007). Reevaluation of Mineral aerosol radiative forcings suggests a better agreement with satellite and AERONET data, *Atmospheric Chemistry and Physics,7*, 81-95.

Barnum, B. H., N. S. Winstead, J. Wesely, A. Hakola, P. R. Colarco, O. B. Toon, P. Ginoux, G. Brooks, L. Hasselbarth and B. Toth. (2004). Forecasting dust storms using the CARMA-dust model and MM5 weather data, *Environmental Modelling & Software,19*(2), 129-140.

Bellouin, N., A. Jones, J. Haywood and S. A. Christopher. (2008). Updated estimate of aerosol direct radiative forcing from satellite observations and comparison against the Hadley Centre climate model, *Journal of Geophysical Research-Atmospheres,113*(D10)

Berthier, S., P. Chazette, P. Couvert, J. Pelon, F. Dulac, F. Thieuleux, C. Moulin and T. Pain. (2006). Desert dust aerosol columnar properties over ocean and continental Africa from Lidar in-Space Technology Experiment (LITE) and Meteosat synergy, *Journal of Geophysical Research-Atmospheres,111*(D21)

Bessagnet, B., A. Hodzic, R. Vautard, M. Beekmann, S. Cheinet, C. Honore, C. Liousse and L. Rouil. (2004). Aerosol modeling with CHIMERE - preliminary evaluation at the continental scale, *Atmospheric Environment,38*(18), 2803-2817.

Bey, I., D. J. Jacob, R. M. Yantosca, J. A. Logan, B. D. Field, A. M. Fiore, Q. B. Li, H. G. Y. Liu, L. J. Mickley and M. G. Schultz. (2001). Global modeling of tropospheric chemistry with assimilated meteorology: Model description and evaluation, *Journal of Geophysical Research-Atmospheres,106*(D19), 23073-23095.

Bian, H. S. and C. S. Zender. (2003). Mineral dust and global tropospheric chemistry: Relative roles of photolysis and heterogeneous uptake, *Journal of Geophysical Research-Atmospheres,108*(D21)

Bothwell, G. W., E. G. Hansen, R. E. Vargo and K. C. Miller. (2002). The Multi-angle Imaging SpectroRadiometer science data system, its products, tools, and performance, *Ieee Transactions on Geoscience and Remote Sensing,40*(7), 1467-1476.

Brindley, H. E. and A. Ignatov. (2006). Retrieval of mineral aerosol optical depth and size information from Meteosat Second Generation SEVIRI solar reflectance bands, *Remote Sensing of Environment,102*(3-4), 344-363.

Burpee, R. W. (1978). Comparison of the Structure of Easterly Wave Disturbances in Western Africa, the Eastern Atlantic, and the Caribbean During Gate, *Bulletin of the American Meteorological Society,59*(11), 1534.

Buseck, P. R. and M. Posfai. (1999). Airborne minerals and related aerosol particles: Effects on climate and the environment, *Proceedings of the National Academy of Sciences of the United States of America,96*(7), 3372-3379.

Catalisano, A. and B. Massa, The Sahara Desert, Raintree Publishers, 1989.

Cavazos, C., M. C. Todd and K. Schepanski. (2009). Numerical model simulation of the Saharan dust event of 6-11 March 2006 using the Regional Climate Model version 3 (RegCM3), *Journal of Geophysical Research-Atmospheres,114*

Chiapello, I., G. Bergametti, B. Chatenet, P. Bousquet, F. Dulac and E. S. Soares. (1997). Origins of African dust transported over the northeastern tropical Atlantic, *Journal of Geophysical Research-Atmospheres,102*(D12), 13701-13709.

Chiapello, I. and C. Moulin. (2002). TOMS and METEOSAT satellite records of the variability of Saharan dust transport over the Atlantic during the last two decades (1979-1997), *Geophysical Research Letters,29*(8)

Chin, M., P. Ginoux, S. Kinne, O. Torres, B. N. Holben, B. N. Duncan, R. V. Martin, J. A. Logan, A. Higurashi and T. Nakajima. (2002). Tropospheric aerosol optical thickness from the GOCART model and comparisons with satellite and Sun photometer measurements, *Journal of the Atmospheric Sciences,59*(3), 461-483.

Christensen, J. H. (1997). The Danish Eulerian hemispheric model - A three-dimensional air pollution model used for the Arctic, *Atmospheric Environment,31*(24), 4169-4191.

Christopher, S. A., P. Gupta, J. Haywood and G. Greed. (2008). Aerosol optical thicknesses over North Africa: 1. Development of a product for model validation using Ozone Monitoring Instrument, Multiangle Imaging Spectroradiometer, and Aerosol Robotic Network, *Journal of Geophysical Research-Atmospheres,113*

Claquin, T., M. Schulz, Y. Balkanski and O. Boucher. (1998). Uncertainties in assessing radiative forcing by mineral dust, *Tellus Series B-Chemical and Physical Meteorology,50*(5), 491-505.

Cook, K. H. (1999). Generation of the African easterly jet and its role in determining West African precipitation, *Journal of Climate,12*(5), 1165-1184.

Cooke, R., A. Warren and A. S. Goudie, Desert geomorphology, Taylor & Francis, 1993.

Cote, J., S. Gravel, A. Methot, A. Patoine, M. Roch and A. Staniforth. (1998). The operational CMC-MRB Global Environmental Multiscale (GEM) model. Part I: Design considerations and formulation, *Monthly Weather Review,126*(6), 1373-1395.

Cotton, W. R., R. A. Pielke, R. L. Walko, G. E. Liston, C. J. Tremback, H. Jiang, R. L. McAnelly, J. Y. Harrington, M. E. Nicholls, G. G. Carrio and J. P. McFadden. (2003). RAMS 2001: Current status and future directions, *Meteorology and Atmospheric Physics,82*(1-4), 5-29.

d'Almeida, G. A. and L. Schutz. (1983). Number, mass and volume distributions of mineral dust and soils of the Sahara, *Journal of Climate and Applied Meteorology,22*, 233-243.

Darmenova, K., I. N. Sokolik, Y. P. Shao, B. Marticorena and G. Bergametti. (2009). Development of a physically based dust emission module within the Weather Research and Forecasting (WRF) model: Assessment of dust emission parameterizations and input parameters for source regions in Central and East Asia, *Journal of Geophysical Research-Atmospheres,114*

DeFries, R. S. and R. G. Townshend. (1994). NDVI-derived land cover classification at a global scale, *International Journal of Remote Sensing,15*, 3567-3586.

Demott, P. J., K. Sassen, M. R. Poellot, D. Baumgardner, D. C. Rogers, S. D. Brooks, A. J. Prenni and S. M. Kreidenweis. (2003). African dust aerosols as atmospheric ice nuclei, *Geophysical Research Letters,30*(14)

Diaz, H. F. and R. S. Bradley, The Hadley circulation: present, past and future, Springer, 2004.

Dickinson, R. E., R. M. Errico, F. Giorgi and G. T. Bates. (1989). A Regional Climate Model for the Western United-States, *Climatic Change,15*(3), 383-422.

Diedhiou, A., S. Janicot, A. Viltard, P. de Felice and H. Laurent. (1999). Easterly wave regimes and associated convection over West Africa and tropical Atlantic: results from the NCEP/NCAR and ECMWF reanalyses, *Climate Dynamics,15*(11), 795-822.

Diongue, A., J. P. Lafore, J. L. Redelsperger and R. Roca. (2002). Numerical study of a Sahelian synoptic weather system: Initiation and mature stages of convection and

its interactions with the large-scale dynamics, *Quarterly Journal of the Royal Meteorological Society,128*(584), 1899-1927.

Drake, N. and C. Bristow. (2006). Shorelines in the Sahara: geomorphological evidence for an enhanced monsoon from palaeolake Megachad, *Holocene,16*(6), 901-911.

Dubovik, O., B. Holben, T. F. Eck, A. Smirnov, Y. J. Kaufman, M. D. King, D. Tanre and I. Slutsker. (2002). Variability of absorption and optical properties of key aerosol types observed in worldwide locations, *Journal of the Atmospheric Sciences,59*(3), 590-608.

Dubovik, O., A. Smirnov, B. N. Holben, M. D. King, Y. J. Kaufman, T. F. Eck and I. Slutsker. (2000). Accuracy assessments of aerosol optical properties retrieved from Aerosol Robotic Network (AERONET) Sun and sky radiance measurements, *Journal of Geophysical Research-Atmospheres,105*(D8), 9791-9806.

Duce, R. A. and N. W. Tindale.(1991). Atmospheric Transport of Iron and Its Deposition in the Ocean, *Limnology and Oceanography,36*(8), 1715-1726.

Dunion, J. P. and C. S. Velden. (2004). The impact of the Saharan air layer on Atlantic tropical cyclone activity, *Bulletin of the American Meteorological Society,85*(3), 353-+.

Engelstaedter, S., K. E. Kohfeld, I. Tegen and S. P. Harrison. (2003). Controls of dust emissions by vegetation and topographic depressions: An evaluation using dust storm frequency data, *Geophysical Research Letters,30*(6)

Engelstaedter, S., I. Tegen and R. Washington. (2006). North African dust emissions and transport, *Earth-Science Reviews,79*(1-2), 73-100.

Engelstaedter, S. and R. Washington. (2007). Atmospheric controls on the annual cycle of North African dust, *Journal of Geophysical Research-Atmospheres,112*(D3)

Falkovich, A. H., E. Ganor, Z. Levin, P. Formenti and Y. Rudich. (2001). Chemical and mineralogical analysis of individual mineral dust particles, *Journal of Geophysical Research-Atmospheres,106*(D16), 18029-18036.

Fink, A. H. and A. Reiner. (2003a). Spatiotemporal variability of the relation between African Easterly Waves and West African Squall Lines in 1998 and 1999, *Journal of Geophysical Research-Atmospheres,108*(D11)

Fink, A. H. and A. Reiner. (2003b). Spatiotemporal variability of the relation between African Easterly Waves and West African Squall Lines in 1998 and 1999, *Journal of Geophysical Research-Atmospheres,108*(D11)

Flamant, C., J. P. Chaboureau, D. J. Parker, C. A. Taylor, J. P. Cammas, O. Bock, F. Timouk and J. Pelon. (2007). Airborne observations of the impact of a convective system on the planetary boundary layer thermodynamics and aerosol distribution in the inter-tropical discontinuity region of the West African Monsoon, *Quarterly Journal of the Royal Meteorological Society,133*(626), 1175-1189.

Flamant, C., C. Lavaysse, M. C. Todd, J. P. Chaboureau and J. Pelon. (2009). Multi-platform observations of a springtime case of Bodele and Sudan dust emission,

transport and scavenging over West Africa, *Quarterly Journal of the Royal Meteorological Society,135*(639), 413-430.

Fontaine, B. and S. Bigot. (1993). West African Rainfall Deficits and Sea-Surface Temperatures, *International Journal of Climatology,13*(3), 271-285.

Forster, P., V. Ramaswamy, P. Artaxo, T. Berntsen, R. Betts, D. W. Fahey, J. M. Haywood, D. C. Lean, G. Lowe, G. Myhre, J. Nganga, R. Prinn, G. Raga, M. Schulz and R. Van Dorland, Changes in atmospheric constituents and in radiative forcing, in Climate Change 2007: The Physical Science Basis. Contribution of Working Group I to the Fourth Assessment Report of the Intergovernmental Panel on Climate Change, edited by S. Solomon, D. Qin, M. Manning, Z. Chen and M. Marquis, Cambridge University Press, Cambridge, United Kingdom; New York, NY, USA, 2007.

Fouquart, Y., B. Bonnel, G. Brogniez, J. C. Buriez, L. Smith, J. J. Morcrette and A. Cerf. (1987). Observations of Saharan Aerosols - Results of Eclats Field Experiment .2.Broad-Band Radiative Characteristics of the Aerosols and Vertical Radiative Flux Divergence, *Journal of Climate and Applied Meteorology,26*(1), 38-52.

Gamo, M. (1996). Thickness of the dry convection and large-scale subsidence above deserts, *Boundary-Layer Meteorology,79*(3), 265-278.

Ghan, S. J. and S. E. Schwartz. (2007). Aerosol properties and processes - A path from field and laboratory measurements to global climate models, *Bulletin of the American Meteorological Society,88*(7), 1059-+.

Gillette, D. A., B. Marticorena and G. Bergametti. (1998). Change in the aerodynamic roughness height by saltating grains: Experimental assessment, test of theory, and operational parameterization, *Journal of Geophysical Research-Atmospheres,103*(D6), 6203-6209.

Gillette, D. A. and R. Passi. (1988). Modeling Dust Emission Caused by Wind Erosion, *Journal of Geophysical Research-Atmospheres,93*(D11), 14233-14242.

Ginoux, P., M. Chin, I. Tegen, J. M. Prospero, B. Holben, O. Dubovik and S. J. Lin. (2001). Sources and distributions of dust aerosols simulated with the GOCART model, *Journal of Geophysical Research-Atmospheres,106*(D17), 20255-20273.

Giorgi, F., M. R. Marinucci and G. Visconti. (1990). Use of A Limited-Area Model Nested in A General-Circulation Model for Regional Climate Simulation Over Europe, *Journal of Geophysical Research-Atmospheres,95*(D11), 18413-18431.

Giorgi, F. and L. O. Mearns. (1999). Introduction to special section: Regional climate modeling revisited, *Journal of Geophysical Research-Atmospheres,104*(D6), 6335-6352.

Goudie, A. S. (2001). The global distribution of dust storms: Patterns and controls, *Annals of Arid Zone,40*(3), 303-315.

Goudie, A. S. and N. J. Middleton, Desert dust in the global system, Springer, 2006.

Greed, G., J. M. Haywood, S. Milton, A. Keil, S. Christopher, P. Gupta and E. J. Highwood. (2008). Aerosol optical depths over North Africa: 2. Modeling and model validation, *Journal of Geophysical Research-Atmospheres,113*

Grell, G. A. (1993). Prognostic Evaluation of Assumptions Used by Cumulus Parameterizations, *Monthly Weather Review,121*(3), 764-787.

Grell, G. A. and D. Devenyi. (2002). A generalized approach to parameterizing convection combining ensemble and data assimilation techniques, *Geophysical Research Letters,29*(14)

Grell, G. A., S. E. Peckham, R. Schmitz, S. A. Mckeen, G. Frost, W. C. Skamarock and B. Eder. (2005). Fully coupled "online" chemistry within the WRF model, *Atmospheric Environment,39*(37), 6957-6975.

Grini, A., G. Myhre, C. S. Zender and I. S. A. Isaksen. (2005). Model simulations of dust sources and transport in the global atmosphere: Effects of soil erodibility and wind speed variability, *Journal of Geophysical Research-Atmospheres,110*(D2)

Grini, A., P. Tulet and L. Gomes. (2006). Dusty weather forecasts using the MesoNH mesoscale atmospheric model, *Journal of Geophysical Research-Atmospheres,111*(D19)

Grini, A. and C. S. Zender. (2004). Roles of saltation, sandblasting, and wind speed variability on mineral dust aerosol size distribution during the Puerto Rican Dust Experiment (PRIDE), *Journal of Geophysical Research-Atmospheres,109*(D7)

Grini, A., C. S. Zender and P. R. Colarco. (2002). Saltation Sandblasting behavior during mineral dust aerosol production, *Geophysical Research Letters,29*(18)

Guerzoni, S., E. Molinaroli and R. Chester. (1997). Saharan dust inputs to the western Mediterranean Sea: Depositional patterns, geochemistry and sedimentological implications, *Deep-Sea Research Part Ii-Topical Studies in Oceanography,44*(3-4), 631-654.

Hall, N. M. J. and P. Peyrille. (2006). Dynamics of the west African monsoon, *Journal de Physique Iv,139*, 81-99.

Hansen, J., M. Sato, A. Lacis and R. Ruedy. (1997). The missing climate forcing, *Philosophical Transactions of the Royal Society of London Series B-Biological Sciences,352*(1350), 231-240.

Harries, J. E., J. E. Russell, J. A. Hanafin, H. Brindley, J. Futyan, J. Rufus, S. Kellock, G. Matthews, R. Wrigley, A. Last, J. Mueller, R. Mossavati, J. Ashmall, E. Sawyer, D. Parker, M. Caldwell, P. M. Allan, A. Smith, M. J. Bates, B. Coan, B. C. Stewart, D. R. Lepine, L. A. Cornwall, D. R. Corney, M. J. Ricketts, D. Drummond, D. Smart, R. Cutler, S. Dewitte, N. Clerbaux, L. Gonzalez, A. Ipe, C. Bertrand, A. Joukoff, D. Crommelynck, N. Nelms, D. T. Llewellyn-Jones, G. Butcher, G. L. Smith, Z. P. Szewczyk, P. E. Mlynczak, A. Slingo, R. P. Allan and M. A. Ringer. (2005). The geostationary Earth Radiation Budget Project, *Bulletin of the American Meteorological Society,86*(7), 945-+.

Hayward, D. and J. S. Oguntoyinbo, Climatology of West Africa, Rowman & Littlefield, 1987.

Haywood, J. and O. Boucher. (2000). Estimates of the direct and indirect radiative forcing due to tropospheric aerosols: A review, *Reviews of Geophysics,38*(4), 513-543.

Haywood, J., P. Francis, S. Osborne, M. Glew, N. Loeb, E. Highwood, D. Tanre, G. Myhre, P. Formenti and E. Hirst. (2003). Radiative properties and direct radiative effect of Saharan dust measured by the C-130 aircraft during SHADE: 1. Solar spectrum, *Journal of Geophysical Research-Atmospheres,108*(D18)

Haywood, J. M., R. P. Allan, I. Culverwell, T. Slingo, S. Milton, J. Edwards and N. Clerbaux. (2005). Can desert dust explain the outgoing longwave radiation anomaly over the Sahara during July 2003?,*Journal of Geophysical Research-Atmospheres,110*(D5)

Haywood, J. M. and K. P. Shine. (1995). The Effect of Anthropogenic Sulfate and Soot Aerosol on the Clear-Sky Planetary Radiation Budget, *Geophysical Research Letters,22*(5), 603-606.

Heinold, B., J. Helmert, O. Hellmuth, R. Wolke, A. Ansmann, B. Marticorena, B. Laurent and I. Tegen. (2007). Regional modeling of Saharan dust events using LM-MUSCAT: Model description and case studies, *Journal of Geophysical Research-Atmospheres,112*(D11)

Helmert, J., B. Heinold, I. Tegen, O. Hellmuth and M. Wendisch. (2007). On the direct and semidirect effects of Saharan dust over Europe: A modeling study, *Journal of Geophysical Research-Atmospheres,112*(D13)

Herman, J. R., P. K. Bhartia, O. Torres, C. Hsu, C. Seftor and E. Celarier. (1997). Global distribution of UV-absorbing aerosols from Nimbus 7/TOMS data, *Journal of Geophysical Research-Atmospheres,102*(D14), 16911-16922.

Hess, M., P. Koepke and I. Schult. (1998). Optical properties of aerosols and clouds: The software package OPAC, *Bulletin of the American Meteorological Society,79*(5), 831-844.

Hogan, T. F. and L. R. Brody. (1993). Sensitivity Studies of the Navy Global Forecast Model Parameterizations and Evaluation of Improvements to Nogaps, *Monthly Weather Review,121*(8), 2373-2395.

Holben, B. N., T. F. Eck, I. Slutsker, D. Tanre, J. P. Buis, A. Setzer, E. Vermote, J. A. Reagan, Y. J. Kaufman, T. Nakajima, F. Lavenu, I. Jankowiak and A. Smirnov. (1998). AERONET - A federated instrument network and data archive for aerosol characterization, *Remote Sensing of Environment,66*(1), 1-16.

Holtslag, A. A. and B. A. Boville. (1993). Local versus nonlocal boundary-layer diffusion in a global climate model, *Journal of Climate,6*, 1825-1842.

Hsu, N. C., S. C. Tsay, M. D. King and J. R. Herman. (2004). Aerosol properties over bright-reflecting source regions, *Ieee Transactions on Geoscience and Remote Sensing,42*(3), 557-569.

Huang, J. P., B. Lin, P. Minnis, T. H. Wang, X. Wang, Y. X. Hu, Y. H. Yi and J. K. Ayers. (2006). Satellite-based assessment of possible dust aerosols semi-direct effect on cloud water path over East Asia, *Geophysical Research Letters,33*(19)

Jacobson, M. Z. (2001). Global direct radiative forcing due to multicomponent anthropogenic and natural aerosols, *Journal of Geophysical Research-Atmospheres,106*(D2), 1551-1568.

Jickells, T. D., Z. S. An, K. K. Andersen, A. R. Baker, G. Bergametti, N. Brooks, J. J. Cao, P. W. Boyd, R. A. Duce, K. A. Hunter, H. Kawahata, N. Kubilay, J. laRoche, P. S. Liss, N. Mahowald, J. M. Prospero, A. J. Ridgwell, I. Tegen and R. Torres. (2005). Global iron connections between desert dust, ocean biogeochemistry, and climate, *Science,308*(5718), 67-71.

Jones, C., N. Mahowald and C. Luo. (2004). Observational evidence of African desert dust intensification of easterly waves, *Geophysical Research Letters,31*(17)

Kalu, A. E., The African dust plume: its characteristics and propagation across West Africa in Winter, in Saharan Dust: Mobilization, Transport, Deposition, edited by C. Morales, pp. 95-118, Wiley, New York, 1979.

Karam, D. B., C. Flamant, P. Knippertz, O. Reitebuch, J. Pelon, M. Chong and A. Dabas. (2008). Dust emissions over the Sahel associated with the West African monsoon intertropical discontinuity region: A representative case-study, *Quarterly Journal of the Royal Meteorological Society,134*(632), 621-634.

Karyampudi, V. M. and T. N. Carlson. (1988). Analysis and Numerical Simulations of the Saharan Air Layer and Its Effect on Easterly Wave Disturbances, *Journal of the Atmospheric Sciences,45*(21), 3102-3136.

Kaufman, Y. J., I. Koren, L. A. Remer, D. Rosenfeld and Y. Rudich. (2005a). The effect of smoke, dust, and pollution aerosol on shallow cloud development over the Atlantic Ocean, *Proceedings of the National Academy of Sciences of the United States of America,102*(32), 11207-11212.

Kaufman, Y. J., I. Koren, L. A. Remer, D. Tanre, P. Ginoux and S. Fan. (2005b). Dust transport and deposition observed from the Terra-Moderate Resolution Imaging Spectroradiometer (MODIS) spacecraft over the Atlantic ocean, *Journal of Geophysical Research-Atmospheres,110*(D10)

Kiehl, J. T., J. J. Hack, G. B. Bonan, B. A. Boville, D. L. Williamson and P. J. Rasch. (1998). The National Center for Atmospheric Research Community Climate Model: CCM3, *Journal of Climate,11*(6), 1131-1149.

King, M. D., Y. J. Kaufman, W. P. Menzel and D. Tanre. (1992). Remote-Sensing of Cloud, Aerosol, and Water-Vapor Properties from the Moderate Resolution Imaging Spectrometer (Modis), *Ieee Transactions on Geoscience and Remote Sensing,30*(1), 2-27.

King, M. D., Y. J. Kaufman, D. Tanre and T. Nakajima. (1999). Remote sensing of tropospheric aerosols from space: Past, present, and future, *Bulletin of the American Meteorological Society,80*(11), 2229-2259.

King, M. D., W. P. Menzel, Y. J. Kaufman, D. Tanre, B. C. Gao, S. Platnick, S. A. Ackerman, L. A. Remer, R. Pincus and P. A. Hubanks. (2003). Cloud and aerosol properties, precipitable water, and profiles of temperature and water vapor from MODIS, *Ieee Transactions on Geoscience and Remote Sensing,41*(2), 442-458.

Knippertz, P. (2007). Tropical-extratropical interactions related to upper-level troughs at low latitudes, *Dynamics of Atmospheres and Oceans,43*(1-2), 36-62.

Knippertz, P. (2008). Dust emissions in the West African heat trough - the role of the diurnal cycle and of extratropical disturbances, *Meteorologische Zeitschrift,17*(5), 553-563.

Knippertz, P., C. Deutscher, K. Kandler, T. Muller, O. Schulz and L. Schutz. (2007). Dust mobilization due to density currents in the Atlas region: Observations from the Saharan Mineral Dust Experiment 2006 field campaign, *Journal of Geophysical Research-Atmospheres,112*(D21)

Knippertz, P. and A. H. Fink. (2006). Synoptic and dynamic aspects of an extreme springtime Saharan dust outbreak, *Quarterly Journal of the Royal Meteorological Society,132*(617), 1153-1177.

Knippertz, P. and A. H. Fink. (2008). Dry-season precipitation in tropical West Africa and its relation to forcing from the extratropics, *Monthly Weather Review,136*(9), 3579-3596.

Knippertz, P. and J. E. Martin. (2005). Tropical plumes and extreme precipitation in subtropical and tropical West Africa, *Quarterly Journal of the Royal Meteorological Society,131*(610), 2337-2365.

Konare, A., A. S. Zakey, F. Solmon, F. Giorgi, S. Rauscher, S. Ibrah and X. Bi. (2008). A regional climate modeling study of the effect of desert dust on the West African monsoon, *Journal of Geophysical Research-Atmospheres,113*(D12)

Kondratyev, K. Y. (1996). Greenhouse warming versus aerosol cooling in the context of global climate change, *Energy Conversion and Management,37*(6-8), 763-768.

Koren, I., Y. J. Kaufman, R. Washington, M. Todd, Y. Rudich, J. V. Martins and D. Rosenfeld. (2006). The Bodélé depression: a single spot in the Sahara that provides most of the mineral dust to the Amazon forest, *Environmental Research Letters*,

Laing, A. G., J. M. Fritsch and A. J. Negri. (1999). Contribution of mesoscale convective complexes to rainfall in Sahelian Africa: estimates from geostationary infrared and passive microwave data, *Journal of Applied Meteorology,38*(7), 957-964.

Laurent, B., B. Marticorena, G. Bergametti, P. Chazette, F. Maignan and C. Schmechtig. (2005). Simulation of the mineral dust emission frequencies from desert areas of China and Mongolia using an aerodynamic roughness length map derived from the POLDER/ADEOS 1 surface products, *Journal of Geophysical Research-Atmospheres,110*(D18)

Lavaysse, C., C. Flamant, S. Janicot and P. Knippertz. (2010). Links between African easterly waves, midlatitude circulation and intraseasonal pulsations of the West African heat low, *Quarterly Journal of the Royal Meteorological Society,136*, 141-158.

Lavaysse, C., C. Flamant, S. Janicot, D. J. Parker, J. P. Lafore, B. Sultan and J. Pelon. (2009). Seasonal evolution of the West African heat low: a climatological perspective, *Climate Dynamics,33*(2-3), 313-330.

Le Treut, H., R. C. J. Somerville, U. Cubash, Y. J. Ding, C. Mauritzen, A. Mokssit, T. Peterson and M. Prather, Historical overview of climate change sciene, in Climate Change 2007: The Physical Science Basis., edited by S. Solomon, D. Qin, Z. Chen, M. Marquis, K. B. Averyt, M. Tignor and H. L. Miller, Cambridge University Press, Cambridge, United Kingdom and New York, NY. USA, 2007.

Lebel, T., B. Cappelaere, S. Galle, N. Hanan, L. Kergoat, S. Levis, B. Vieux, L. Descroix, M. Gosset, E. Mougin, C. Peugeot and L. Seguis. (2009). AMMA-CATCH studies in the Sahelian region of West-Africa: An overview, *Journal of Hydrology,375*(1-2), 3-13.

Legrand, M., A. Plana-Fattori and C. N'doume. (2001). Satellite detection of dust using the IR imagery of Meteosat 1. Infrared difference dust index, *Journal of Geophysical Research-Atmospheres,106*(D16), 18251-18274.

Levelt, P., E. Hilsenrath, G. W. Lepppelmeier, G. H. J. Van den Ooord, P. K. Bhartia, J. Taminnen, J. F. de Haan and P. Veefkind. (2006). Science objectives of the Ozone Monitoring Instrument, *IEEE Trans. Geosci.Remote Sens.,44*, 1093-1101.

Li, F., A. M. Vogelmann and V. Ramanathan. (2004). Saharan dust aerosol radiative forcing measured from space, *Journal of Climate,17*(13), 2558-2571.

Liao, H. and J. H. Seinfeld. (1998). Effect of clouds on direct aerosol radiative forcing of climate, *Journal of Geophysical Research-Atmospheres,103*(D4), 3781-3788.

Lin, S. J. and R. B. Rood. (1996). Multidimensional flux-form semi-Lagrangian transport schemes, *Monthly Weather Review,124*(9), 2046-2070.

Liou, K. N., An Introduction to Atmospheric Radiation, Academic Press, San Diego, 2002.

Liu, M., D. L. Westphal, S. G. Wang, A. Shimizu, N. Sugimoto, J. Zhou and Y. Chen. (2003). A high-resolution numerical study of the Asian dust storms of April 2001, *Journal of Geophysical Research-Atmospheres,108*(D23)

Liu, Z. Y., A. Omar, M. Vaughan, J. Hair, C. Kittaka, Y. X. Hu, K. Powell, C. Trepte, D. Winker, C. Hostetler, R. Ferrare and R. Pierce. (2008). CALIPSO lidar observations of the optical properties of Saharan dust: A case study of long-range transport, *Journal of Geophysical Research-Atmospheres,113*(D7)

Lohmann, U. (2006). Aerosol effects on clouds and climate, *Space Science Reviews,125*(1-4), 129-137.

Lohmann, U., J. Quaas, S. Kinne and J. Feichter. (2007). Different approaches for constraining global climate models of the anthropogenic indirect aerosol effect, *Bulletin of the American Meteorological Society,88*(2), 243-+.

Lu, H. and Y. P. Shao. (1999). A new model for dust emission by saltation bombardment, *Journal of Geophysical Research-Atmospheres,104*(D14), 16827-16841.

Mahowald, N. M., J. A. Ballantine, J. Feddema and N. Ramankutty. (2007). Global trends in visibility: implications for dust sources, *Atmospheric Chemistry and Physics,7*(12), 3309-3339.

Mahowald, N. M. and L. M. Kiehl. (2003). Mineral aerosol and cloud interactions, *Geophysical Research Letters,30*(9)

Marticorena, B. and G. Bergametti. (1995). Modeling the Atmospheric Dust Cycle .1. Design of A Soil-Derived Dust Emission Scheme, *Journal of Geophysical Research-Atmospheres,100*(D8), 16415-16430.

Mcgill, M. J., M. A. Vaughan, C. R. Trepte, W. D. Hart, D. L. Hlavka, D. M. Winker and R. Kuehn. (2007). Airborne validation of spatial properties measured by the CALIPSO lidar, *Journal of Geophysical Research-Atmospheres,112*(D20)

McGuffie, K. and A. Henderson-Sellers. (2001). Forty years of numerical climate modelling, *International Journal of Climatology,21*(9), 1067-1109.

Michalakes, J., D. Duhia, D. Gill, T. Henderson, J. Klemp and W. Wang, The Weather Research and Forecast Model: Software Architecture and Performance, paper presented at Eleventh ECMWF Workshop on the Use of High Performance Computing in Meteorology, 2005.

Middleton, N. J. (1986). Dust Storms in the Middle-East, *Journal of Arid Environments,10*(2), 83-96.

Middleton, N. J. and A. S. Goudie. (2001). Saharan dust: sources and trajectories, *Transactions of the Institute of British Geographers,26*(2), 165-181.

Miller, R. L. and I. Tegen. (1998). Climate response to soil dust aerosols, *Journal of Climate,11*(12), 3247-3267.

Miller, R. L., I. Tegen and J. Perlwitz. (2004). Surface radiative forcing by soil dust aerosols and the hydrologic cycle, *Journal of Geophysical Research-Atmospheres,109*(D4)

Milton, S. F., G. Greed, M. E. Brooks, J. Haywood, B. Johnson, R. P. Allan, A. Slingo and W. M. F. Grey. (2008). Modeled and observed atmospheric radiation balance during the West African dry season: Role of mineral dust, biomass burning aerosol, and surface albedo, *Journal of Geophysical Research-Atmospheres,113*

Myhre, G., A. Grini, J. M. Haywood, F. Stordal, B. Chatenet, D. Tanre, J. K. Sundet and I. S. A. Isaksen. (2003). Modeling the radiative impact of mineral dust during the Saharan Dust Experiment (SHADE) campaign, *Journal of Geophysical Research-Atmospheres,108*(D18)

Nickovic, S. and S. Dobricic. (1996). A model for long-range transport of desert dust, *Monthly Weather Review,124*(11), 2537-2544.

Nickovic, S., G. Kallos, A. Papadopoulos and O. Kakaliagou. (2001). A model for prediction of desert dust cycle in the atmosphere, *Journal of Geophysical Research-Atmospheres,106*(D16), 18113-18129.

O'Hara, S. L., M. L. Clarke and M. S. Elatrash. (2006). Field measurements of desert dust deposition in Libya, *Atmospheric Environment,40*(21), 3881-3897.

Palmen, E. and C. Newton, Atmospheric circulation systems: their structure and physical interpretation, Academic Press, 1969.

Parker, D. J., R. R. Burton, A. Diongue-Niang, R. J. Ellis, M. Felton, C. M. Taylor, C. D. Thorncroft, P. Bessemoulin and A. M. Tompkins. (2005a). The diurnal cycle of the West African monsoon circulation, *Quarterly Journal of the Royal Meteorological Society,131*(611), 2839-2860.

Parker, D. J., R. R. Burton, A. Diongue-Niang, R. J. Ellis, M. Felton, C. M. Taylor, C. D. Thorncroft, P. Bessemoulin and A. M. Tompkins. (2005b). The diurnal cycle of the West African monsoon circulation, *Quarterly Journal of the Royal Meteorological Society,131*(611), 2839-2860.

Penner, J. E., R. J. Charlson, J. M. Hales, N. S. Laulainen, R. Leifer, T. Novakov, J. Ogren, L. F. Radke, S. E. Schwartz and L. Travis. (1994). Quantifying and Minimizing Uncertainty of Climate Forcing by Anthropogenic Aerosols, *Bulletin of the American Meteorological Society,75*(3), 375-400.

Perez, C., S. Nickovic, G. Pejanovic, J. M. Baldasano and E. Ozsoy. (2006). Interactive dust-radiation modeling: A step to improve weather forecasts, *Journal of Geophysical Research-Atmospheres,111*(D16)

Peyrille, P., J. P. Lafore and J. L. Redelsperger. (2007). An idealized two-dimensional framework to study the West African monsoon. Part I: Validation and key controlling factors, *Journal of the Atmospheric Sciences,64*(8), 2765-2782.

Pilinis, C., S. N. Pandis and J. H. Seinfeld. (1995). Sensitivity of Direct Climate Forcing by Atmospheric Aerosols to Aerosol-Size and Composition, *Journal of Geophysical Research-Atmospheres,100*(D9), 18739-18754.

Power, H. C. (2003). The geography and climatology of aerosols, *Progress in Physical Geography,27*(4), 502-547.

Prasad, A. K. and R. P. Singh. (2007). Comparison of MISR-MODIS aerosol optical depth over the Indo-Gangetic basin during the winter and summer seasons (2000-2005), *Remote Sensing of Environment,107*(1-2), 109-119.

Prospero, J. M. (1979). Dust from the Sahara, *Natural History,88*(5), 53-&.

Prospero, J. M., K. Barrett, T. Church, F. Dentener, R. A. Duce, J. N. Galloway, H. Levy, J. Moody and P. Quinn. (1996). Atmospheric deposition of nutrients to the North Atlantic Basin, *Biogeochemistry,35*(1), 27-73.

Prospero, J. M., P. Ginoux, O. Torres, S. E. Nicholson and T. E. Gill. (2002). Environmental characterization of global sources of atmospheric soil dust identified with the Nimbus 7 Total Ozone Mapping Spectrometer (TOMS) absorbing aerosol product, *Reviews of Geophysics,40*(1)

Prospero, J. M., R. A. Glaccum and R. T. Nees. (1981). Atmospheric Transport of Soil Dust from Africa to South-America, *Nature,289*(5798), 570-572.

Prospero, J. M. and R. T. Nees. (1986). Impact of the North African Drought and El-Nino on Mineral Dust in the Barbados Trade Winds, *Nature,320*(6064), 735-738.

Pudykiewicz, J. (1989). An Application of A Supercomputer for the Simulation of Atmospheric Transport Processes, *Supercomputer,6*(3), 36-44.

Qian, Y. and F. Giorgi. (1999). Interactive coupling of regional climate and sulfate aerosol models over eastern Asia, *Journal of Geophysical Research-Atmospheres,104*(D6), 6477-6499.

Qian, Y., F. Giorgi, Y. Huang, W. Chameides and C. Luo. (2001). Regional simulation of anthropogenic sulfur over East Asia and its sensitivity to model parameters, *Tellus Series B-Chemical and Physical Meteorology,53*(2), 171-191.

Rahn, K. A., L. Schutz and R. Jaenicke. (1976). Elemental Composition of Sahara Aerosol and Sahara Soil, *Bulletin of the American Meteorological Society,57*(1), 146.

Ramanathan, V., P. J. Crutzen, J. T. Kiehl and D. Rosenfeld. (2001). Atmosphere - Aerosols, climate, and the hydrological cycle, *Science,294*(5549), 2119-2124.

Ramaswamy, V., O. Boucher, D. H. Haigh, J. Haywood, G. Myhre, T. Nakajima and et al.(2001). Radiative forcing of climate change, edited by J. T. Houghton and et al, pp. 349-416, Cambridge University Press, Cambridge, UK and New York, USA.

Randall, D. A. (1996). A university perspective on global climate modeling, *Bulletin of the American Meteorological Society,77*(11), 2685-2690.

Randall, D. A. and B. A. Wielicki. (1997). Measurements, models, and hypotheses in the atmospheric sciences, *Bulletin of the American Meteorological Society,78*(3), 399-406.

Randall, D. A., R. A. Wood, S. Bony, R. Colman, T. Fichefet, J. Fyfe, V. M. Kattsov, A. Pitman, J. Shukla, J. Srinivasan, R. J. Stouffer, A. Sumi and K. E. Taylor, Cilmate Models and Their Evaluation, in Climate Change 2007: The Physical Science Basis. Contribution of Working Group I to the Fourth Assessment Report of the Intergovernmental Panel on Climate Change, edited by F. Solomon, D. Qin, M. Manning, Z. Chen, M. Marquis, K. B. Averyt, M. Tignor and H. L. Miller, Cambridge University Press, Cambridge, United Kingdom and New York, NY, USA., 2007.

Redelsperger, J. L., C. D. Thorncroft, A. Diedhiou, T. Lebel, D. J. Parker and J. Polcher. (2006). African monsoon multidisciplinary analysis - An international research project and field campaign, *Bulletin of the American Meteorological Society,87*(12), 1739-+.

Rees, W. G., Physical Principles of Remote Sensing, Cambridge University Press, 1990.

Reid, J. S., J. E. Kinney, D. L. Westphal, B. N. Holben, E. J. Welton, S. C. Tsay, D. P. Eleuterio, J. R. Campbell, S. A. Christopher, P. R. Colarco, H. H. Jonsson, J. M. Livingston, H. B. Maring, M. L. Meier, P. Pilewskie, J. M. Prospero, E. A. Reid, L. A. Remer, P. B. Russell, D. L. Savoie, A. Smirnov and D. Tanre. (2003). Analysis of measurements of Saharan dust by airborne and ground-based remote sensing methods during the Puerto Rico Dust Experiment (PRIDE), *Journal of Geophysical Research-Atmospheres,108*(D19)

Rosenfeld, D., Y. Rudich and R. Lahav. (2001). Desert dust suppressing precipitation: A possible desertification feedback loop, *Proceedings of the National Academy of Sciences of the United States of America,98*(11), 5975-5980.

Saha, K., **Tropical Circulation Systems and Monsoons**, Springer, 2009.

Satheesh, S. K. and K. K. Moorthy. (2005). Radiative effects of natural aerosols: A review, *Atmospheric Environment,39*(11), 2089-2110.

Schepanski, K., I. Tegen, B. Laurent, B. Heinold and A. Macke. (2007). A new Saharan dust source activation frequency map derived from MSG-SEVIRI IR-channels, *Geophysical Research Letters,34*(18)

Schepanski, K., I. Tegen, M. C. Todd, B. Heinold, G. Bonisch, B. Laurent and A. Macke. (2009). Meteorological processes forcing Saharan dust emission inferred from MSG-SEVIRI observations of subdaily dust source activation and numerical models, *Journal of Geophysical Research-Atmospheres,114*

Schmetz, J., P. Pili, S. Tjemkes, D. Just, J. Kerkmann, S. Rota and A. Ratier. (2002). An introduction to Meteosat Second Generation (MSG), *Bulletin of the American Meteorological Society,83*(7), 977-+.

Schubert, S., M. Suarez, C. K. Park and S. Moorthi. (1993). Gcm Simulations of Intraseasonal Variability in the Pacific North-American Region, *Journal of the Atmospheric Sciences,50*(13), 1991-2007.

Schutz, L., Atmospheric mineral dust-properties and source markers, in Paleoclimatology and Paleometeorology: Modern and Past Patterns of Global Atmospheric Transport, edited by M. Leinen and M. Sarnthein, pp. 359-383, Kluwer Academic Publisers, 1989.

Schutz, L. and M. Sebert. (1987). Mineral Aerosols and Source Identification, *Journal of Aerosol Science,18*(1), 1-&.

Seinfeld, J. H., G. R. Carmichael, R. Arimoto, W. C. Conant, F. J. Brechtel, T. S. Bates, T. A. Cahill, A. D. Clarke, S. J. Doherty, P. J. Flatau, B. J. Huebert, J. Kim, K. M. Markowicz, P. K. Quinn, L. M. Russell, P. B. Russell, A. Shimizu, Y. Shinozuka, C. H. Song, Y. H. Tang, I. Uno, A. M. Vogelmann, R. J. Weber, J. H. Woo and X. Y. Zhang. (2004). ACE-ASIA - Regional climatic and atmospheric chemical effects of Asian dust and pollution, *Bulletin of the American Meteorological Society,85*(3), 367-+.

Shao, Y., Physics and modelling of wind erosion., Kluwer Academic, Dordrecht, 2000.

Shao, Y. (2001). A model for mineral dust emission, *Journal of Geophysical Research-Atmospheres,106*(D17), 20239-20254.

Shao, Y. P. (2004). Simplification of a dust emission scheme and comparison with data, *Journal of Geophysical Research-Atmospheres,109*(D10)

Shaw, W. J., K. J. Allwine, B. G. Fritz, F. C. Rutz, J. P. Rishel and E. G. Chapman. (2008). Evaluation of the wind erosion module in DUSTRAN, *Atmospheric Environment,42*(8), 1907-1921.

Sinclair, P. C. (1969). General characteristics of dust devils, *Journal of Applied Meteorology,8*, 32-45.

Slingo, A., T. P. Ackerman, R. P. Allan, E. I. Kassianov, S. A. McFarlane, G. J. Robinson, J. C. Barnard, M. A. Miller, J. E. Harries, J. E. Russell and S. Dewitte. (2006).

Observations of the impact of a major Saharan dust storm on the atmospheric radiation balance, *Geophysical Research Letters,33*(24)

Sokolik, I. N. and O. B. Toon. (1996). Direct radiative forcing by anthropogenic airborne mineral aerosols, *Nature,381*(6584), 681-683.

Sokolik, I. N., D. M. Winker, G. Bergametti, D. A. Gillette, G. Carmichael, Y. J. Kaufman, L. Gomes, L. Schuetz and J. E. Penner. (2001). Introduction to special section: Outstanding problems in quantifying the radiative impacts of mineral dust, *Journal of Geophysical Research-Atmospheres,106*(D16), 18015-18027.

Solmon, F., F. Giorgi and C. Liousse. (2006). Aerosol modelling for regional climate studies: application to anthropogenic particles and evaluation over a European/African domain, *Tellus Series B-Chemical and Physical Meteorology,58*(1), 51-72.

Stensrud, D. J. (1996). Importance of low-level jets to climate: A review, *Journal of Climate,9*(8), 1698-1711.

Stier, P., J. Feichter, S. Kinne, S. Kloster, E. Vignati, J. Wilson, L. Ganzeveld, I. Tegen, M. Werner, Y. Balkanski, M. Schulz, O. Boucher, A. Minikin and A. Petzold. (2005). The aerosol-climate model ECHAM5-HAM, *Atmospheric Chemistry and Physics,5*, 1125-1156.

Stier, P., J. H. Seinfeld, S. Kinne and O. Boucher. (2007). Aerosol absorption and radiative forcing, *Atmospheric Chemistry and Physics,7*(19), 5237-5261.

Stone, R.(1967). A desert glossary, pp. 211-268, Elsevier Publishing Company, Amsterdam, The Netherlands.

Sultan, B. and S. Janicot. (2000). Abrupt shift of the ITCZ over West Africa and intra-seasonal variability, *Geophysical Research Letters,27*(20), 3353-3356.

Sutton, L. J. (1931). Haboobs, *Quarterly Journal of the Royal Meteorological Society,57*, 143-161.

Swap, R., M. Garstang, S. Greco, R. Talbot and P. Kallberg. (1992). Saharan Dust in the Amazon Basin, *Tellus Series B-Chemical and Physical Meteorology,44*(2), 133-149.

Takemura, T., T. Nakajima, O. Dubovik, B. N. Holben and S. Kinne.(2002). Single-scattering albedo and radiative forcing of various aerosol species with a global three-dimensional model, *Journal of Climate,15*(4), 333-352.

Tanaka, T. Y. and M. Chiba. (2005). Global simulation of dust aerosol with a chemical transport model, MASINGAR, *Journal of the Meteorological Society of Japan,83A*, 255-278.

Tanaka, T. Y. and M. Chiba. (2006). A numerical study of the contributions of dust source regions to the global dust budget, *Global and Planetary Change,52*(1-4), 88-104.

Tanre, D., J. Haywood, J. Pelon, J. F. Leon, B. Chatenet, P. Formenti, P. Francis, P. Goloub, E. J. Highwood and G. Myhre. (2003). Measurement and modeling of the Saharan dust radiative impact: Overview of the Saharan Dust Experiment (SHADE), *Journal of Geophysical Research-Atmospheres,108*(D18)

Tao, W. K., J. D. Chern, R. Atlas, D. Randall, M. Khairoutdinov, J. L. Li, D. E. Waliser, A. Hou, X. Lin, C. Peters-Lidard, W. Lau, J. Jiang and J. Simpson. (2009). A Multiscale Modeling System Developments, Applications, and Critical Issues, *Bulletin of the American Meteorological Society,90*(4), 515-+.

Tegen, I. (2003). Modeling the mineral dust aerosol cycle in the climate system, *Quaternary Science Reviews,22*(18-19), 1821-1834.

Tegen, I. and I. Fung. (1994). Modeling of Mineral Dust in the Atmosphere - Sources, Transport, and Optical-Thickness, *Journal of Geophysical Research-Atmospheres,99*(D11), 22897-22914.

Tegen, I., S. P. Harrison, K. E. Kohfeld, S. Engelstaedter and M. Werner. (2002). Emission of soil dust aerosol: Anthropogenic contribution and future changes, *Geochimica et Cosmochimica Acta,66*(15A), A766.

Tegen, I., B. Heinold, M. Todd, J. Helmert, R. Washington and O. Dubovik. (2006). Modelling soil dust aerosol in the Bodele depression during the BoDEx campaign, *Atmospheric Chemistry and Physics,6*, 4345-4359.

Tegen, I., D. Koch, A. A. Lacis and M. Sato. (2000). Trends in tropospheric aerosol loads and corresponding impact on direct radiative forcing between 1950 and 1990: A model study, *Journal of Geophysical Research-Atmospheres,105*(D22), 26971-26989.

Teller, A. and Z. Levin. (2006). The effects of aerosols on precipitation and dimensions of subtropical clouds: a sensitivity study using a numerical cloud model, *Atmospheric Chemistry and Physics,6*, 67-80.

Thorncroft, C. D. and M. Blackburn. (1999). Maintenance of the African easterly jet, *Quarterly Journal of the Royal Meteorological Society,125*(555), 763-786.

Thorncroft, C. D. and H. A. Flocas. (1997). A case study of Saharan cyclogenesis, *Monthly Weather Review,125*(6), 1147-1165.

Todd, M. C., D. B. Karam, C. Cavazos, C. Bouet, B. Heinold, J. M. Baldasano, G. Cautenet, I. Koren, C. Perez, F. Solmon, I. Tegen, P. Tulet, R. Washington and A. Zakey. (2008a). Quantifying uncertainty in estimates of mineral dust flux: An intercomparison of model performance over the Bodele Depression, northern Chad, *Journal of Geophysical Research-Atmospheres,113*

Todd, M. C., R. Washington, J. V. Martins, O. Dubovik, G. Lizcano, S. M'Bainayel and S. Engelstaedter. (2007). Mineral dust emission from the Bodele Depression, northern Chad, during BoDEx 2005, *Journal of Geophysical Research-Atmospheres,112*(D6)

Todd, M. C., R. Washington, S. Raghavan, G. Lizcano and P. Knippertz. (2008b). Regional model simulations of the Bodele low-level jet of northern Chad during the Bodele Dust Experiment (BoDEx 2005), *Journal of Climate,21*(5), 995-1012.

Tompkins, A. M., C. Cardinali, J. J. Morcrette and M. Rodwell. (2005). Influence of aerosol climatology on forecasts of the African Easterly Jet, *Geophysical Research Letters,32*(10)

Torres, O., P. K. Bhartia, J. R. Herman, Z. Ahmad and J. Gleason. (1998). Derivation of aerosol properties from satellite measurements of backscattered ultraviolet radiation: Theoretical basis, *Journal of Geophysical Research-Atmospheres,103*(D14), 17099-17110.

Torres, O., A. Tanskanen, B. Veihelmann, C. Ahn, R. Braak, P. K. Bhartia, P. Veefkind and P. Levelt. (2007). Aerosols and surface UV products from Ozone Monitoring Instrument observations: An overview, *Journal of Geophysical Research-Atmospheres,112*(D24)

Tulet, P., M. Mallet, V. Pont, J. Pelon and A. Boone. (2008). The 7-13 March 2006 dust storm over West Africa: Generation, transport, and vertical stratification, *Journal of Geophysical Research-Atmospheres,113*

Twomey, S.(1977). Influence of Pollution on Shortwave Albedo of Clouds, *Journal of the Atmospheric Sciences,34*(7), 1149-1152.

Uno, I., Z. Wang, M. Chiba, Y. S. Chun, S. L. Gong, Y. Hara, E. Jung, S. S. Lee, M. Liu, M. Mikami, S. Music, S. Nickovic, S. Satake, Y. Shao, Z. Song, N. Sugimoto, T. Tanaka and D. L. Westphal. (2006). Dust model intercomparison (DMIP) study over Asia: Overview, *Journal of Geophysical Research-Atmospheres,111*(D12)

Vallis, G. K., Atmospheric and ocean fluid dinamics: fundamental circulation, Cambridge University Press, Cambridge, U.K., 2006.

Vaughan, M., S. A. Young, D. M. Winker, K. Powell, A. Omar, Y. Liu, Y. X. Hu and C. Hostetler. (2004). Fully automated analysis of space-based lidar data: An overview of the CALIPSO retrieval algorithms and data products, *Proc. SPIE,5575*, 16-30.

Wang, W. and N. L. Seaman.(1997). A comparison study of convective parameterization schemes in a mesoscale model, *Monthly Weather Review,125*(2), 252-278.

Warren, A., A. Chappell, M. C. Todd, C. Bristow, N. Drake, S. Engelstaedter, V. Martins, S. M'Bainayel and R. Washington. (2007). Dust-raising in the dustiest place on earth, *Geomorphology,92*(1-2), 25-37.

Washington, R., M. Harrison, D. Conway, E. Black, A. Challinor, D. Grimes, R. Jones, A. Morse, G. Kay and M. Todd. (2006a). African climate change - Taking the shorter route, *Bulletin of the American Meteorological Society,87*(10), 1355-+.

Washington, R., M. Todd, N. J. Middleton and A. S. Goudie. (2003). Dust-storm source areas determined by the total ozone monitoring spectrometer and surface observations, *Annals of the Association of American Geographers,93*(2), 297-313.

Washington, R. and M. C. Todd. (2005). Atmospheric controls on mineral dust emission from the Bodele Depression, Chad: The role of the low level jet, *Geophysical Research Letters,32*(17)

Washington, R., M. C. Todd, G. Lizcano, I. Tegen, C. Flamant, I. Koren, P. Ginoux, S. Engelstaedter, C. S. Bristow, C. S. Zender, A. S. Goudie, A. Warren and J. M. Prospero. (2006b). Links between topography, wind, deflation, lakes and dust: The case of the Bodele Depression, Chad, *Geophysical Research Letters,33*(9)

Wesely, M. L.(1989). Parameterization of Surface Resistances to Gaseous Dry Deposition in Regional-Scale Numerical-Models, *Atmospheric Environment,23*(6), 1293-1304.

Wetherald, R. T. and S. Manabe. (1988). Cloud Feedback Processes in A General-Circulation Model, *Journal of the Atmospheric Sciences,45*(8), 1397-1415.

Williams, N. R. (1948). Development of dust whirls and similar small-scale vortices, *Bulletin of the American Meteorological Society,29*, 106-117.

Winker, D. M., W. H. Hunt and M. McGill. (2007). Initial performance assessment of CALIOP, *Geophysical Research Letters,34*(L19803)

Woodward, S. (2001). Modeling the atmospheric life cycle and radiative impact of mineral dust in the Hadley Centre climate model, *Journal of Geophysical Research-Atmospheres,106*(D16), 18155-18166.

Yang, Z. L. and R. E. Dickinson. (1996). Description of the biosphere-atmosphere transfer scheme (BATS) for the soil moisture workshop and evaluation of its performance, *Global and Planetary Change,13*(1-4), 117-134.

Yoshioka, M., N. M. Mahowald, A. J. Conley, W. D. Collins, D. W. Fillmore, C. S. Zender and D. B. Coleman. (2007). Impact of desert dust radiative forcing on Sahel precipitation: Relative importance of dust compared to sea surface temperature variations, vegetation changes, and greenhouse gas warming, *Journal of Climate,20*(8), 1445-1467.

Yu, H., Y. J. Kaufman, M. Chin, G. Feingold, L. A. Remer, T. L. Anderson, Y. Balkanski, N. Bellouin, O. Boucher, S. Christopher, P. DeCola, R. Kahn, D. Koch, N. Loeb, M. S. Reddy, M. Schulz, T. Takemura and M. Zhou. (2006). A review of measurement-based assessments of the aerosol direct radiative effect and forcing, *Atmospheric Chemistry and Physics,6*, 613-666.

Zakey, A. S., F. Solmon and F. Giorgi. (2006). Implementation and testing of a desert dust module in a regional climate model, *Atmospheric Chemistry and Physics,6*, 4687-4704.

Zaveri, R. A., R. C. Easter, J. D. Fast and L. K. Peters. (2008). Model for Simulating Aerosol Interactions and Chemistry (MOSAIC), *Journal of Geophysical Research-Atmospheres,113*(D13)

Zender, C. S., H. S. Bian and D. Newman. (2003a). Mineral Dust Entrainment and Deposition (DEAD) model: Description and 1990s dust climatology, *Journal of Geophysical Research-Atmospheres,108*(D14)

Zender, C. S., R. Miller and I. Tegen. (2004). Quantifying Mineral Dust Mass Budgets: Terminology, Constraints, and Current Estimates, *EOS,85*(45), 509-512.

Zender, C. S., D. Newman and O. Torres. (2003b). Spatial heterogeneity in aeolian erodibility: Uniform, topographic, geomorphic, and hydrologic hypotheses, *Journal of Geophysical Research-Atmospheres,108*(D17)

Zhang, Y. (2008). Online-coupled meteorology and chemistry models: history, current status, and outlook, *Atmospheric Chemistry and Physics,8*(11), 2895-2932.

Zobler, L.(1986). A World Soil File for Global Climate Modelling, NASA Goddard Institute for Space Studies.